IAEA Nuclear Energy Series

No. NF-T-4.1

Basic
Principles

Objectives

Guides

Technical
Reports

Status and Trends of Nuclear Fuels Technology for Sodium Cooled Fast Reactors

IAEA

International Atomic Energy Agency

IAEA NUCLEAR ENERGY SERIES PUBLICATIONS

STRUCTURE OF THE IAEA NUCLEAR ENERGY SERIES

Under the terms of Articles III.A and VIII.C of its Statute, the IAEA is authorized to foster the exchange of scientific and technical information on the peaceful uses of atomic energy. The publications in the **IAEA Nuclear Energy Series** provide information in the areas of nuclear power, nuclear fuel cycle, radioactive waste management and decommissioning, and on general issues that are relevant to all of the above mentioned areas. The structure of the IAEA Nuclear Energy Series comprises three levels: **1 — Basic Principles and Objectives; 2 — Guides; and 3 — Technical Reports.**

The **Nuclear Energy Basic Principles** publication describes the rationale and vision for the peaceful uses of nuclear energy.

Nuclear Energy Series Objectives publications explain the expectations to be met in various areas at different stages of implementation.

Nuclear Energy Series Guides provide high level guidance on how to achieve the objectives related to the various topics and areas involving the peaceful uses of nuclear energy.

Nuclear Energy Series Technical Reports provide additional, more detailed, information on activities related to the various areas dealt with in the IAEA Nuclear Energy Series.

The IAEA Nuclear Energy Series publications are coded as follows: **NG** — general; **NP** — nuclear power; **NF** — nuclear fuel; **NW** — radioactive waste management and decommissioning. In addition, the publications are available in English on the IAEA's Internet site:

http://www.iaea.org/Publications/index.html

For further information, please contact the IAEA at PO Box 100, Vienna International Centre, 1400 Vienna, Austria.

All users of the IAEA Nuclear Energy Series publications are invited to inform the IAEA of experience in their use for the purpose of ensuring that they continue to meet user needs. Information may be provided via the IAEA Internet site, by post, at the address given above, or by email to Official.Mail@iaea.org.

STATUS AND TRENDS OF
NUCLEAR FUELS TECHNOLOGY
FOR SODIUM COOLED FAST REACTORS

The following States are Members of the International Atomic Energy Agency:

AFGHANISTAN	GHANA	NORWAY
ALBANIA	GREECE	OMAN
ALGERIA	GUATEMALA	PAKISTAN
ANGOLA	HAITI	PALAU
ARGENTINA	HOLY SEE	PANAMA
ARMENIA	HONDURAS	PARAGUAY
AUSTRALIA	HUNGARY	PERU
AUSTRIA	ICELAND	PHILIPPINES
AZERBAIJAN	INDIA	POLAND
BAHRAIN	INDONESIA	PORTUGAL
BANGLADESH	IRAN, ISLAMIC REPUBLIC OF	QATAR
BELARUS	IRAQ	REPUBLIC OF MOLDOVA
BELGIUM	IRELAND	ROMANIA
BELIZE	ISRAEL	RUSSIAN FEDERATION
BENIN	ITALY	SAUDI ARABIA
BOLIVIA	JAMAICA	SENEGAL
BOSNIA AND HERZEGOVINA	JAPAN	SERBIA
BOTSWANA	JORDAN	SEYCHELLES
BRAZIL	KAZAKHSTAN	SIERRA LEONE
BULGARIA	KENYA	SINGAPORE
BURKINA FASO	KOREA, REPUBLIC OF	SLOVAKIA
BURUNDI	KUWAIT	SLOVENIA
CAMBODIA	KYRGYZSTAN	SOUTH AFRICA
CAMEROON	LATVIA	SPAIN
CANADA	LEBANON	SRI LANKA
CENTRAL AFRICAN	LESOTHO	SUDAN
REPUBLIC	LIBERIA	SWEDEN
CHAD	LIBYAN ARAB JAMAHIRIYA	SWITZERLAND
CHILE	LIECHTENSTEIN	SYRIAN ARAB REPUBLIC
CHINA	LITHUANIA	TAJIKISTAN
COLOMBIA	LUXEMBOURG	THAILAND
CONGO	MADAGASCAR	THE FORMER YUGOSLAV
COSTA RICA	MALAWI	REPUBLIC OF MACEDONIA
CÔTE D'IVOIRE	MALAYSIA	TUNISIA
CROATIA	MALI	TURKEY
CUBA	MALTA	UGANDA
CYPRUS	MARSHALL ISLANDS	UKRAINE
CZECH REPUBLIC	MAURITANIA	UNITED ARAB EMIRATES
DEMOCRATIC REPUBLIC	MAURITIUS	UNITED KINGDOM OF
OF THE CONGO	MEXICO	GREAT BRITAIN AND
DENMARK	MONACO	NORTHERN IRELAND
DOMINICAN REPUBLIC	MONGOLIA	UNITED REPUBLIC
ECUADOR	MONTENEGRO	OF TANZANIA
EGYPT	MOROCCO	UNITED STATES OF AMERICA
EL SALVADOR	MOZAMBIQUE	URUGUAY
ERITREA	MYANMAR	UZBEKISTAN
ESTONIA	NAMIBIA	VENEZUELA
ETHIOPIA	NEPAL	VIETNAM
FINLAND	NETHERLANDS	YEMEN
FRANCE	NEW ZEALAND	ZAMBIA
GABON	NICARAGUA	ZIMBABWE
GEORGIA	NIGER	
GERMANY	NIGERIA	

The Agency's Statute was approved on 23 October 1956 by the Conference on the Statute of the IAEA held at United Nations Headquarters, New York; it entered into force on 29 July 1957. The Headquarters of the Agency are situated in Vienna. Its principal objective is "to accelerate and enlarge the contribution of atomic energy to peace, health and prosperity throughout the world''.

STATUS AND TRENDS OF NUCLEAR FUELS TECHNOLOGY FOR SODIUM COOLED FAST REACTORS

FOREWORD

From the inception of nuclear energy, the important role of the sodium cooled fast reactor (SFR) and its fuel cycle has been recognized for the long term sustainability of nuclear power. The two recent international projects on the development of advanced and innovative nuclear energy systems, namely, the IAEA initiated International Project on Innovative Nuclear Reactors and Fuel Cycles (INPRO) and the US Department of Energy initiated Generation IV International Forum (GIF) have also identified the importance of fast reactors and their fuel cycle in the 21st century. The IAEA's Technical Working Group on Nuclear Fuel Cycle Options and Spent Fuel Management (TWGNFCO) reviews available information on fast reactor fuels and fuel cycle and prepares publications. Accordingly, actions were initiated for preparation of the following: (a) Status and trends of nuclear fuels technology for sodium cooled fast reactors (SFRs); (b) Status and trends of SFR fuel cycle technology — aqueous and pyro-chemical techniques of reprocessing; and (c) Structural materials for SFR fuel assembly — fabrication, properties and irradiation behaviour.

The present publication covers the status and trends of fuels technology for SFRs, highlighting the manufacturing processes, out of pile properties and irradiation behaviour of mixed uranium plutonium oxide (MOX), monocarbide (MC), mononitride and metallic fuels. To the extent possible, minor actinide (MA: Np, Am and Cm) bearing fuels are also covered.

This report has been prepared on the basis of contributions of leading experts from Member States who participated in three consultants meetings and one technical committee meeting. In addition, feedback was received from the experts of the INPRO Joint Study on Fast Reactor and Closed Fuel Cycle.

The IAEA wishes to express its gratitude to all contributors and reviewers of this publication. The IAEA officer responsible for this publication was C. Ganguly of the Division of Nuclear Fuel Cycle and Waste Technology.

CONTENTS

1. INTRODUCTION

1.1. BACKGROUND

Natural uranium and thorium are the basic raw materials for nuclear fuels. Natural uranium contains two main isotopes, namely, ^{238}U, a fertile isotope, which accounts for ~99.3% and the balance ~0.7% is ^{235}U, the only 'fissile' isotope in nature. Thorium occurs in nature only as ^{232}Th, which is a fertile isotope. The fertile isotopes ^{238}U and ^{232}Th could be transmuted to human-made 'fissile' isotopes ^{239}Pu and ^{233}U, respectively, by neutron capture reactions in a reactor. In the case of ^{238}U, a series of neutron capture and beta decay reactions also lead to the formation of other isotopes of plutonium (^{238}Pu, ^{240}Pu, ^{241}Pu and ^{242}Pu) and minor actinides (MAs), namely, Np, Am and Cm as shown in Fig. 1. ^{241}Pu is also a fissile isotope. The important nuclear properties of uranium, plutonium and MA isotopes are summarized in Table 1.

The potential of fast reactors for exploiting the virtually inexhaustible energy locked in natural uranium and thorium was realized in the mid-1940s. In a fast reactor, the average neutron energy is >0.1 MeV. The average number of neutrons emitted in the fission process per neutron absorbed, known as η, is higher in a fast reactor compared to thermal reactor, where the average neutron energy is in the range of 0.025 eV. The value of η in the fast neutron spectrum for ^{239}Pu is higher than that of ^{235}U and ^{233}U, and are 2.45, 2.10 and 2.31, respectively, implying that more neutrons are available for breeding ^{239}Pu from ^{238}U in a ^{238}U–^{239}Pu fuel system. In addition, in the fast neutron spectrum, the ratio of fission to capture-neutron cross-sections favours fission for almost all of the actinide isotopes, including ^{238}U and MAs. Hence, ^{239}Pu is the best fissile material in the fast neutron spectrum and ^{238}U–^{239}Pu fuel cycle is ideally suited for breeding and or burning plutonium and burning MAs. Breeding is also possible in the ^{232}Th–^{233}U fuel cycle in the fast neutron spectrum but the breeding ratio would be much lower than that of the ^{238}U–^{239}Pu fuel cycle. The thorium fuel cycle has not been tried so far in fast reactors anywhere in the world. Thorium based fuels and fuel cycle options are not covered in this report.

The first fast reactor in the world was Clementine at Los Alamos, USA. The reactor was commissioned in 1946 and used ^{239}Pu in metal form as fuel. The Experimental Breeder Reactor I (EBR-I) in Idaho, USA, another fast reactor, was the first reactor in the world to demonstrate generation of electricity from the fission process on 20 December 1951. EBR-I used high enriched uranium (HEU: >20% ^{235}U) metal containing >90% ^{235}U as fuel. Later, in 1962, EBR-I demonstrated breeding of ^{239}Pu from ^{238}U, for the first time in the world.

The former Soviet Union started its fast reactor activities in the early 1950s, soon after the commissioning of Clementine and EBR-I in the USA. Its first major achievement was the commissioning of the BR-5 (5 MW(th)) experimental fast reactor in 1958 with a plutonium oxide core. Subsequently, an HEU carbide core was used in BR-5, following which the reactor was upgraded to the BR-10 (8 MW(th)) with an HEU nitride core. In the UK, fast reactor technology started with commissioning of the Dounreay experimental Fast Reactor (DFR) with HEU metal alloy (U–Mo) fuel in 1959. In France, the first fast reactor, Rapsodie, became operational in 1967 with MOX fuel. In Germany, the sodium cooled thermal reactor KNK was converted to the fast reactor KNK II during 1975–1977 with a MOX core. In Japan, the first experimental fast reactor, JOYO, attained criticality in 1977 with a MOX core. India commissioned the Fast Breeder Test Reactor (FBTR) with a hitherto untried plutonium rich mixed uranium plutonium carbide core in 1985. The largest commercial fast reactor, Superphenix (1240 MW(e)), in France, attained criticality in 1985 with a MOX core. Presently, three fast reactors are under construction, namely the China Experimental Fast Reactor (CEFR), the Prototype Fast Breeder Reactor (PFBR, 500 MW(e)) in India, and the commercial reactor BN-800 (MW(e)) in the Russian Federation.

Table 2 summarizes the major features of liquid metal cooled fast reactors (LMFRs) constructed and operated and under construction in the world. The details of these reactors and their major design features are summarized in IAEA publications [1, 2]. Except the Clementine reactor in the USA, all LMFRs are SFRs. The four prototype SFRs include the BN-350 in Kazakhstan (as part of the former Soviet Union), the prototype fast reactor (PFR) of 250 MW(e) in the UK, the Phenix 250 MW(e) in France and MONJU 250 MW(e) in Japan. Of the two, commercial SFRs that have been constructed and operated successfully, the BN-600 (MW(e)) in the Russian Federation has been in operation since 1980 but the Superphenix was shut down in 1996. The Phenix 250 MW(e) was shut down in March 2009. In Japan, the MONJU reactor is likely to restart at the end of 2009. So far, more than 300 reactor-years of operating experience have been accumulated worldwide.

Nuclear reaction chain for formation of plutonium and minor actinide isotopes in uranium fuel cycle

[Natural uranium ÷ ^{238}U : 99.284% + ^{235}U : 0.711% + ^{234}U : 0.0058%]
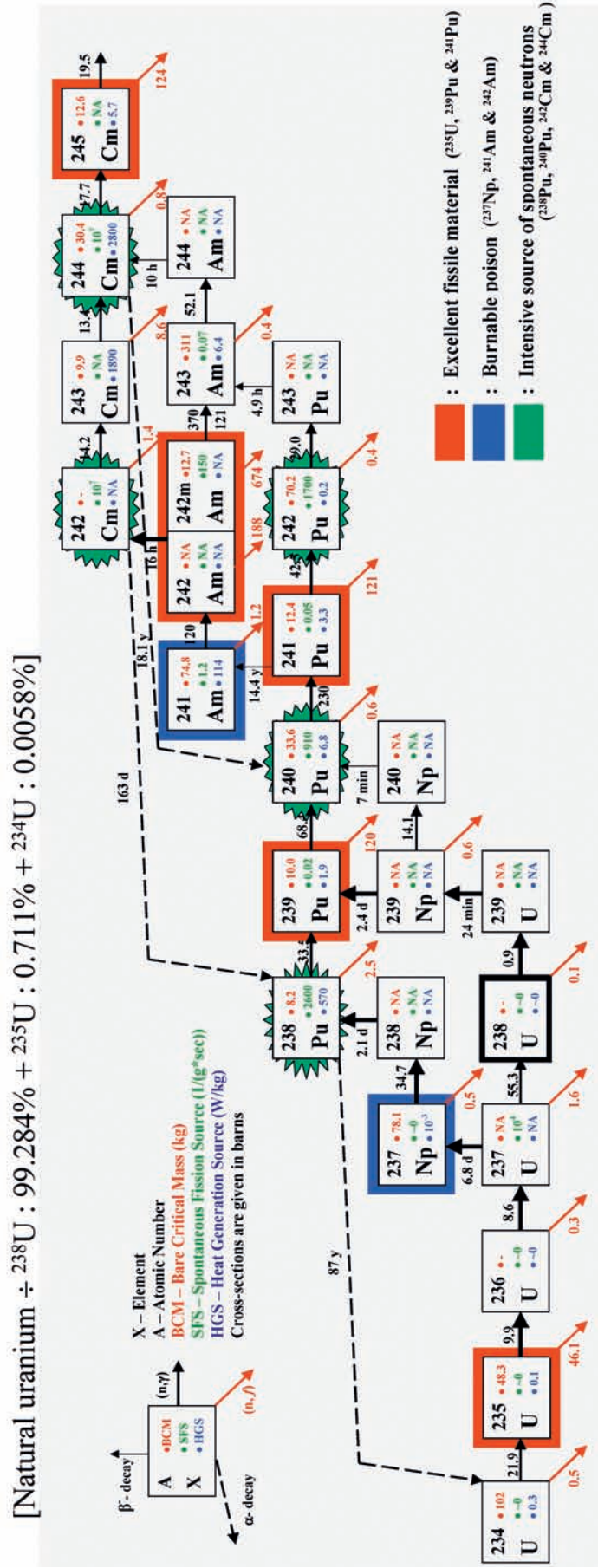
FIG. 1. *Formation of plutonium and MA isotopes in a reactor fuelled with natural or low enriched uranium (LEU: <20% ^{235}U) by neutron capture reactions.*

TABLE 1. HALF-LIFE, NEUTRON YIELD, DECAY HEAT AND CRITICAL MASS OF NATURAL AND HUMAN-MADE 'FISSILE' AND 'FERTILE' ACTINIDE ISOTOPES RELEVANT FOR NUCLEAR REACTORS

Isotope	Half-life (a)	Neutron yield (neutrons/sec-kg)	Decay heat (W/kg)	Critical mass (kg)
^{231}Pa	32.8×10^3	nil	1.3	162
^{232}Th	14.1×10^9	nil	nil	infinite
^{233}U	159×10^3	1.23	0.281	16.4
^{235}U	700×10^6	0.364	6×10^{-5}	47.9
^{238}U	4.5×10^9	0.11	8×10^{-6}	infinite
^{237}Np	2.1×10^6	0.139	0.021	59
^{238}Pu	88	2.67×10^6	570	10
^{239}Pu	24×10^3	21.8	2.0	10.2
^{240}Pu	6.54×10^3	1.03×10^6	7.0	36.8
^{241}Pu	14.7	49.3	6.4	12.9
^{242}Pu	376×10^3	1.73×10^6	0.12	89
^{241}Am	433	1540	115	57
^{243}Am	7.38×10^3	900	6.4	155
^{244}Cm	18.1	11×10^9	2.8×10^3	28
^{245}Cm	8.5×10^3	147×10^3	5.7	13
^{246}Cm	4.7×10^3	9×10^9	10	84
^{247}Bk	1.4×10^3	nil	36	10
^{251}Cf	898	nil	56	9

For the first generation of experimental, prototype and commercial SFRs, high enriched uranium (HEU: >20% ^{235}U) oxide and mixed uranium plutonium oxide (MOX) have been the undisputed choice for the driver fuel. Mixed uranium plutonium monocarbide (MC), mononitride (MN) and the U–Zr and U–Pu–Zr alloys are considered as advanced SFR fuels on the basis of their higher breeding ratio, better thermal conductivity and excellent chemical compatibility with sodium coolant as compared to the oxide fuel.

The SFR fuel development activities were most intense in the 1970s and continued until the mid 1980s. The EBR-II and FFTF in the USA, the DFR and PFR in the UK, the BR-10 and BOR-60 in the Russian Federation, the Rapsodie and Phenix in France, the KNK II in Germany, the JOYO in Japan and FBTR in India were extensively utilized for irradiation testing of oxide, carbide, nitride, and metallic fuel compositions containing uranium and mixed uranium plutonium. Though several types of austenitic stainless steels have been used, ferritic–martensitic steels and oxide dispersion strengthened (ODS) steels are also being developed for use as fuel cladding and fuel assembly components to withstand radiation damage to high fast neutron fluence (~3×10^{23} n/cm^2). The two principal types of fuel design were the helium bonded rods and the sodium bonded rods. The MOX fuel rods use He-bonding only, whereas the MC and MN fuel rods could be either He-bonded or have sodium in the gap between the pellets and the inner wall of cladding tubes. The metallic fuel rods are mostly sodium bonded. In sodium bonded fuel rods, a large gap is kept between the fuel and cladding. In sodium bonded MC/MN fuel pins, a shroud tube is sometimes used in the gap between the fuel and cladding to contain any fuel chips that might be dislodged from the fuel. The manufacturing details, properties and irradiation behaviour of SFR fuels have been well documented in

TABLE 2. IMPORTANT FEATURES OF SOME MAJOR LMFRs CONSTRUCTED AND OPERATED AND UNDER CONSTRUCTION IN THE WORLD

Country	Reactor name (Loop or Pool type)	Location	First criticality/ Shutdown date	Thermal/electric capacity (MW)	Fuel
China	CEFR -Pool	Beijing	under construction	65/23.4	UO_2 (HEU)
France	Rapsodie-Loop	Cadarache	1966/1982	20/40/0	MOX
	Phénix -Pool	Marcoule	1973/2009	563/255	MOX
	Superphénix-Pool	Creys-Malville	1985/1996	2990/1242	MOX
Germany	KNK-II-Loop	Karlsruhe	1977/1991	58/20	MOX/UO_2(HEU)
India	FBTR-Loop	Kalpakkam	1985/In operation	40/13	(U, Pu)C
	PFBR-Pool	Kalpakkam	under construction	1250/500	MOX
Japan	JOYO-Loop	O-arai	1977 (Mark-I)/In operation	140 (Mark-II)/0	MOX
	MONJU-Loop	Tsuruga	1994/Interrupted since 1995 likely to restart in 2009	714/280	MOX
Kazakhstan	BN-350-Loop	Chevenko	1972/1999	750/130 and desalination	UO_2
Russian Federation	BR-5 -Loop	Obninsk	1959/1971	5	PuO_2/UC
	BR-10 -Loop	Obninsk	1959/1971	8/0	MOX/UN
	BOR-60-Loop	Dimitrovgrad	1969/In operation	55/12	UO_2(HEU)/MOX
	BN-600-Pool	Beloyarsk	1980/In operation	1 470/600	UO_2(HEU)
	BN-800-Pool	Beloyarsk	Under construction	2 100/880	UO_2 (HEU)
UK	DFR-Loop	Dounreay	1959/1977	60/15	U-Mo
	PFR-Pool	Dounreay	1974/1994	650/250	MOX
USA	Clementine-Pool (mercury-cooled)	Los Alamos	1946/1953	0.025	Pu metal
	EBR-I-Pool	Idaho	1951/1963	1.4/0.2	U (HEU)
	EBR-II-Pool	Idaho	1963/1994	62.5/20	U-Fs*, U-Zr (HEU)
	Enrico Fermi-Loop	Detroit	1963/1972	200/61	U-Mo (HEU)
	FFTF-Loop	Hanford	1980/1994	400/0	MOX

Fs (wt%) = 2.4% Mo, 1.9% Ru, 0.3% Rh, 0.2% Pd, 0.1% Zr and 0.01% Nb.

Refs [3–11]. Tables 3 and 4 give an intercomparison of the important properties and behaviour of MOX, MC, MN and metallic fuels for SFRs.

The R&D and industrial activities on SFR and its fuel cycle began to decline from the late 1980s for a number of reasons. Firstly, the nuclear incidents at Three Mile Island and Chernobyl nuclear power plants, in quick succession, slowed down the growth of nuclear power. As a result, the demand and spot price of uranium started to fall rapidly and instead of the projected shortage, uranium remained abundantly available and relatively cheap. Secondly, fast reactors were not found to be economically competitive with thermal reactors. Thirdly, opposition to breeding and recovery of plutonium from spent fuel, from a weapons proliferation viewpoint, forced some countries to suspend their fast reactor fuel development programme.

TABLE 3. INTERCOMPARISON OF SOME MAJOR PROPERTIES AND EXPERIENCE OF MOX, MC, MN AND METALLIC FUELS FOR SFRs

Properties	$(U_{0.8} Pu_{0.2})O_2$	$(U_{0.8} Pu_{0.2})C$	$(U_{0.8} Pu_{0.2})N$	$U-^{19}Pu-^{10}Zr$
Theoretical density g/cc	11.04	13.58	14.32	15.73
Melting point ºK	3023	2750	3070	1400
Thermal conductivity (W/m ºK) 1000 K	2.6	18.8	15.8	25
2000 K	2.4	21.2	20.1	
Crystal structure (Type)	Fluorite	NaCl	NaCl	γ (>973 K)
Breeding ratio	1.1–1.15	1.2–1.25	1.2–1.25	1.35–1.4
Swelling	Moderate	High	High	High
Handling	In air	Inert atmosphere	Inert atmosphere	Inert atmosphere
Compatibility-clad coolant	Average Average	Carburization Good	Good Good	Eutectics Good
Dissolution and reprocessing amenability	Demonstrated on industrial scale for aqueous and pilot scale for pyro-processes	Process not yet demonstrated on industrial scale	Dissolution easy but risk of C^{14} in reprocessing	Pyro-processing demonstrated on pilot plant scale
Fabrication/irradiation experience	Large Good	Limited	Very little	Limited

However, from the beginning of the 21st century, there have been 'rising expectations' from nuclear power worldwide based on the low cost of nuclear electricity generation, the excellent safety and performance records of nuclear power plants since the late 1980s and the important role of nuclear energy in mitigating global warming and climate change. Two international projects are under way from the beginning of this century. One is the International Project on Innovative Nuclear Reactors and Fuel Cycles (INPRO) sponsored by the IAEA and the other the Generation IV International Forum (GIF) — Technology Roadmap for Generation IV Nuclear Energy Systems initiated by the US Department of Energy [12, 13]. Both projects are aimed at the selection of design concepts and promotion of development of advanced nuclear power technologies, which may set the basis for sustainable growth of the power industry and make it possible to develop nuclear power in the 21st century. Different fast breeder reactor systems such as SFRs, lead cooled fast reactors and gas cooled fast reactors are considered under Generation IV as the promising options for development and deployment around 2030–2050. In 2007, five GIF Members (Euratom, France, Japan, the Republic of Korea and the USA) signed the project arrangement of advanced fuel for SFR. Under the INPRO project, a Joint Case Study on Closed Nuclear Fuel Cycle with Fast Reactors (CNFC-FR) has identified the broad parameters of innovative SFR that could meet the objectives of sustained nuclear energy growth. Currently, SFR and its fuel cycle are being considered as part of the innovative nuclear energy system for long term sustainability of nuclear power.

TABLE 4. RELATIVE ADVANTAGES AND DISADVANTAGES OF OXIDE, CARBIDE, NITRIDE AND METAL ALLOY FUELS, WITH AND WITHOUT MINOR ACTINIDES, FOR LMFR

Fuel	Advantage	Disadvantage
Oxide	— Proven burnup >25 at.% — Industrial scale fabrication and irradiation experience — High creep rate, negligible PCMI — High melting temperature — Good stability at high temperature for Am_2O_3 and Cm_2O_3 (up to 5%)	— Very low dissolution rate of pure PuO_2 and plutonium rich MOX in nitric acid — Likelihood of chemical interaction with Na/cladding material — Poor thermal conductivity — Powder processing route of fuel fabrication is associated with the problem of radio toxic dust hazard
Carbide	— Hard spectrum (small fraction of Pu required for reactivity balance) — High thermal conductivity favouring high linear rating of fuel rod — Proven to 18 at.%	— Pyrophoric (must be handled and fabricated in inert gas atmosphere) — Powder processing route of fuel fabrication is associated with the problem of radio toxic dust hazard — High vapour pressure of AmC (vaporizes at <1500 K in vacuum)
Nitride	— Hard spectrum (small fraction of Pu required for reactivity balance) — High thermal conductivity — Test fuel pins have demonstrated proven burnup of 20 at% — High solubility rate in nitric acid	— Pyrophoric (must be handled and fabricated in inert gas atmosphere) — Powder processing route of fuel fabrication is associated with the problem of radio toxic dust hazard — Small creep rate leading to: pellet — clad mechanical interaction (PCMI) — Production of ^{14}C by $^{14}N(n,p)$ reaction — To avoid ^{14}C formation, ^{15}N enrichment in necessary — To avoid dissociation of AmN, temperature of fuel fabrication should be below 1800 K
Metallic Fuel (U–Zr and U–Pu–Zr)	— Hard spectrum (small fraction of Pu required for reactivity balance) — High thermal conductivity — Proven to 20 at% in EBR-II — Simplified fabrication, involving melting and casting which avoids the problem of radiotoxic dust hazard	— Low melting temperature (Pu must be alloyed with Zr) — Volatility of Am (rapid cooling of molten alloy during fabrication) — Large swelling rate requires large sodium bonded pellet clad gap — Alpha contaminated Na waste — Pyro processing

1.2. OPERATING POWER REACTORS AND THE ROLE OF FAST REACTORS IN THE 21st CENTURY

The fast neutron reactor is the only energy source which generates electricity and breeds its own fuel. In spite of these attractive features, LMFR was not economically competitive with thermal neutron reactors, using water or gas as coolant. The light water cooled reactor (LWR) emerged as the most popular reactor system for the generation of electricity in the 1970s. A large number of LWRs, consisting of pressurized water reactors (PWRs) of the Western type and the Russian design (WWER) and boiling water reactors (BWRs), were constructed all over the world in the 1970s and 1980s. The pressurized heavy water reactor (PHWR) was also constructed in some countries, though they were fewer in numbers. The gas cooled reactors, namely, MAGNOX and advanced gas cooled reactors (AGRs) were commercially exploited only in the UK and the light water cooled graphite moderated reactors, namely the RBMK, were constructed in the Russian Federation and a few other countries in the former Soviet Union. Since ^{235}U is the only fissile material in nature, it was the obvious choice as fuel for all types of nuclear power reactors. The LWRs, RBMKs and AGRs use low enriched uranium (LEU), containing up to 5% ^{235}U as fuel in the form of high density uranium oxide pellets. The PHWRs and MAGNOX use natural uranium fuel (~0.7% ^{235}U) in the form of high density uranium oxide and uranium metal, respectively. Currently, 439 nuclear power reactors are in operation in 30 countries, with installed capacity of 371 GW(e) and generating ~15% of the world's electricity. The LWRs account for 87% (56% PWRs, 22% BWRs and 9% WWERs) of installed nuclear power today and would continue to dominate global nuclear power at least until the middle of the century. The PHWRs contribute to ~5% of installed nuclear power. The MAGNOX reactors are being phased out and AGRs and RBMKs are not constructed anymore.

Presently, the operating thermal neutron power reactors discharge some 10 500 t HM of spent nuclear fuel (SNF) annually, of which only ~15% is reprocessed. The balance is stored in interim facilities, awaiting a decision on whether to dispose of them directly in repositories or subject them to reprocessing and recycling. The spent LWR fuel contains 95–96% uranium, 3–4% fission product, ~1% plutonium and ~0.1% MA.

In the operating uranium fuelled thermal reactors, the ratio of the quantity of the fissile material (^{239}Pu) formed to the primary fissile material (^{235}U) consumed, known as 'conversion ratio' is in the range of 0.4–0.6. The plutonium formed could be recycled in these thermal reactors along with uranium but even after recycling several times, the total uranium resource utilization does not exceed 1% of the mined uranium. Because of this low uranium utilization factor, it is quite understandable that nuclear energy, when solely based on thermal neutron reactors, will not be able to play a long term role in the world's energy supply. However, if plutonium, a by-product from thermal reactors, is utilized as the primary fuel in SFR in combination with ^{238}U, the 'breeding ratio' could be >1.0, implying that more Pu is formed from ^{238}U than is consumed during fission. On recycling several times Pu and ^{238}U in SFR, at least 60% of the entire natural uranium resource could be utilized, thereby, meeting the long term energy demand of the world. Further, the SFRs could also be used for converting another naturally occurring fertile isotope ^{232}Th, which is three times more abundant than uranium, into the fissile isotope ^{233}U, thereby further increasing the potential of nuclear fission energy. For the long term sustainability of nuclear power, it is therefore generally agreed that the plutonium produced in operating thermal reactors should be utilized in SFRs in combination with natural uranium (Nat.U)/reprocessed uranium (RepU) from spent thermal reactor fuel reprocessing plant or depleted uranium (DU) from ^{235}U enrichment plant.

1.3. SFR CORE AND FUEL ASSEMBLY

The core of an SFR is smaller than that of a water cooled reactor of comparable power and consists of a 'central core', containing the fuel assemblies in triangular or hexagonal array and an 'outer region' with radial blankets, radial shields as shown in Fig. 2. SFR fuel elements have a fissile material enrichment that is much higher than in a thermal reactor. The small experimental reactor like EBR I and II, BR 10 and DFR have fissile material enrichment as high as 90% or more, while medium and large cores like Phenix and Superphenix respectively would have fuel with fissile material in the range of 20–25% and 15–20% respectively. The high fissile material investment necessitates the fuel to operate at a much higher burnup level compared to that of LWR. Accordingly, refuelling times are longer.
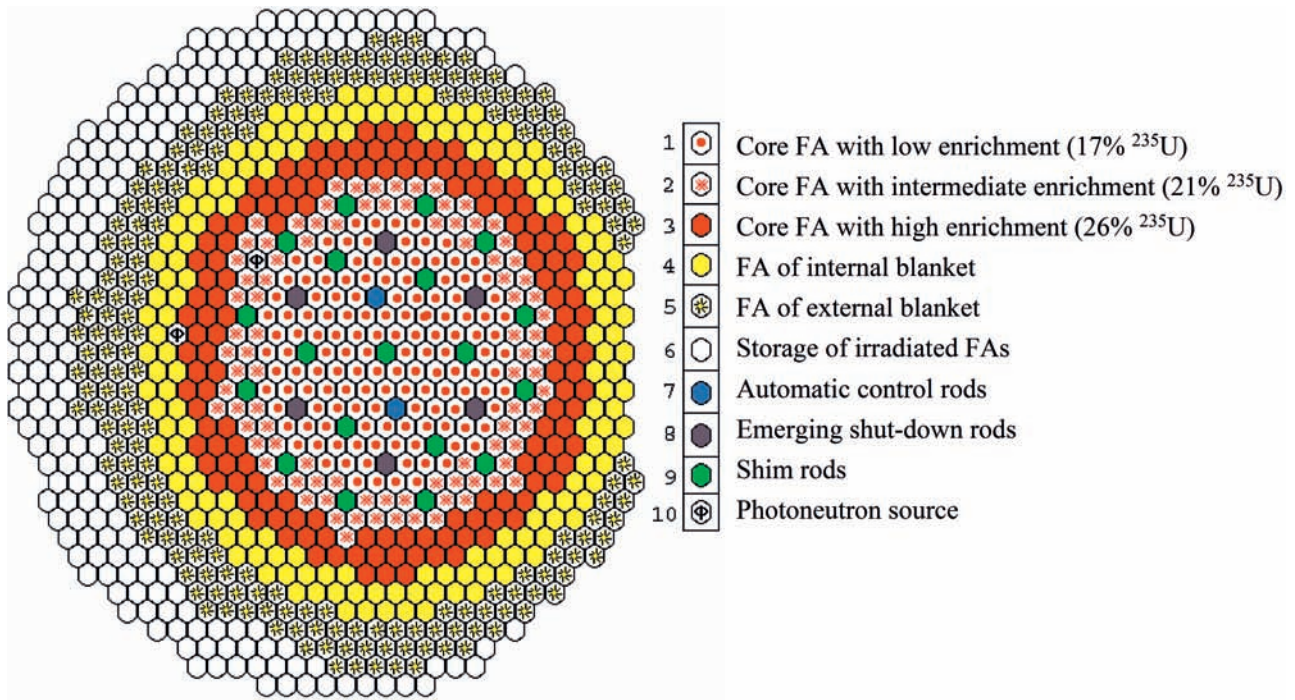
FIG. 2. Core configuration of the BN-600 in operation in the Russian Federation.

The sodium coolant in the primary heat transport system of an SFR becomes radioactive (by neutron activation) and hence a secondary sodium coolant circuit is needed. The fission heat energy is transferred by primary sodium in an intermediate heat exchanger (IHX) to a secondary sodium coolant in either a 'loop' or a 'pool' configuration. The hot non-radioactive secondary sodium is used to generate steam in another heat exchanger. The temperature of sodium leaving the reactor is ~550°C, which is substantially higher than that of water cooled reactors (300–330°C). Unlike water cooled reactors, SFRs do not require pressurization to keep the coolant in a liquid state because of the high boiling point of sodium (882°C). The outlet coolant pressure in the SFR is near atmospheric and consequently the reactor vessel need not be as thick as that for a typical LWR.

Figure 3 shows the representative SFR fuel assembly consisting of cluster of stainless steel clad, wire wrapped fuel rods within the assembly duct. SFR fuel rods are smaller than thermal reactor fuel rods with smaller rod diameter and shorter fuel column. The fuel usually consists of a mixture of fissile and fertile materials encapsulated in stainless steel cladding tubes. The oxide, carbide and nitride fuels are mostly in the form of a stack of cylindrical 'pellets' of diameter in the range of 4–8 mm, with or without a central hole and a pellet length to diameter ratio in the range of 1–1.5. In some cases, the ceramic fuels are used in the form of irregular shaped tiny (10–1 000 µm) 'particles' or 'microspheres' vibro-compacted in the cladding tube. The metallic fuel is cast in the form of long single 'pin'. The cladding tube has fission gas plenum located at either the bottom or top or both ends. The SFR fuel is designed to accommodate all released fission gases. The blanket fuel assembly is made of fertile ^{238}U in the form of DU, NatU or RepU, in the form of oxide pellets or metallic pins. Both axial and radial blankets have been used in an SFR core. The axial blanket could be an integral part of the fuel rod on both ends of the fuel stack or as separate axial blanket assembly. In India, ThO_2 has been used as radial blanket in the FBTR.

The fissile material concentration and in turn the burnup of the SFR fuel is much higher than that of the LWR fuel and depends mainly on the extent of radiation damage of the fuel assembly structural materials, including the cladding tube and duct tube, due to the high fast neutron flux (10^{16} n/cm²/s) and fluence (~10^{23} n/cm²).

Figure 4 shows the different stages of 'closed' fuel cycle for the SFR, highlighting multiple recycling of plutonium and MA with fertile materials. In the first few cycles, plutonium obtained by reprocessing spent uranium fuels from thermal reactors are used but subsequently after reaching a breeding ratio of 1, the ^{238}U–^{239}Pu fuel cycle becomes self-sustaining.
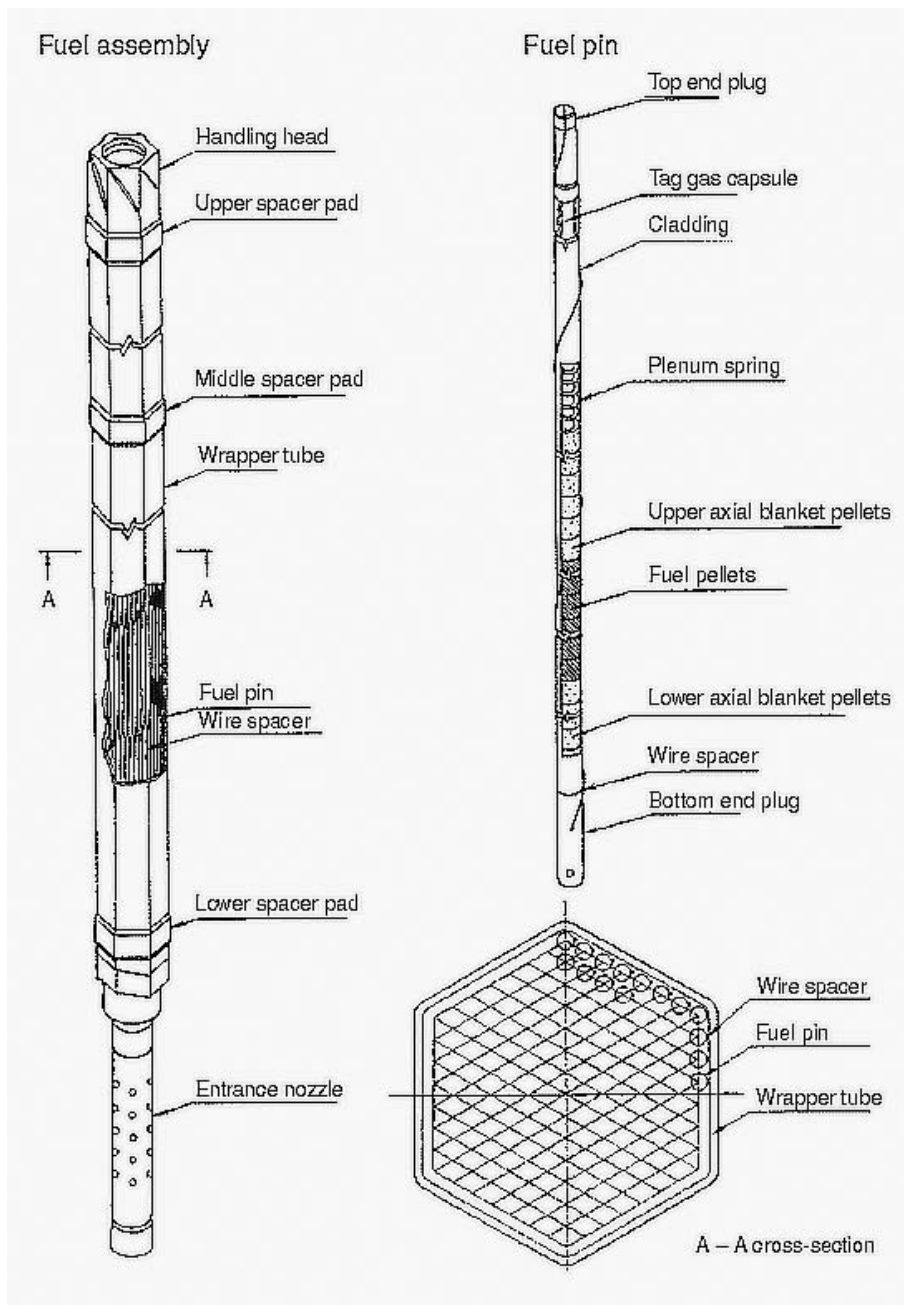
FIG. 3. Representative fuel rod and assembly for MONJU, Japan.

The key to the commercial success of the SFR fuel cycle lies in developing plutonium based fuels that would:

(a)   Operate safely to high burnup (up to 20 at.% or more) without failure;
(b)   Be simple and safe to manufacture economically on an industrial scale;
(c)   Be easy to reprocess, adapting the established aqueous or pyro-electrolytic processes;
(d)   Breed and burn plutonium efficiently from ^{238}U and burn MA;
(e)   Breed ^{233}U if ^{232}Th is used in blanket;
(f)   Be amenable to 'proliferation resistance'.

For manufacturing and handling plutonium, MAs and fissile uranium isotope bearing fuels, the issues related to radiological safety, criticality hazard, proliferation resistance and in turn nuclear security are of paramount importance. The isotopes of plutonium, in particular, ^{238}Pu, ^{240}Pu, ^{241}Pu and ^{242}Pu and MAs are highly radiotoxic and associated with emission of health hazardous beta-gamma and neutron radiation. Hence, adequate radiation

[DU, RepU & NatU could be used as fertile materials in fuel and blanket assemblies]
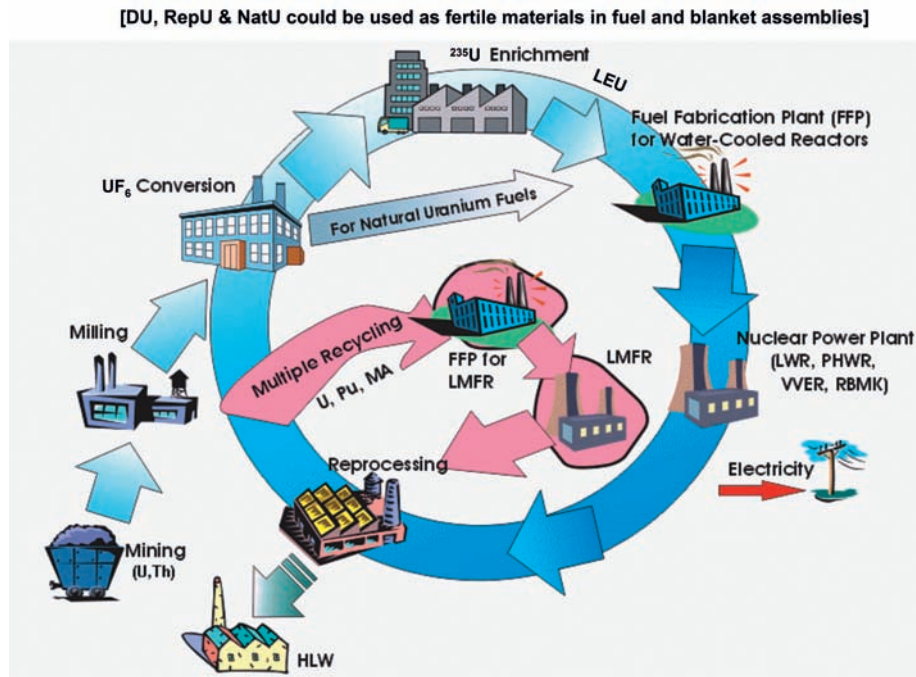
FIG. 4. ^{238}U–^{239}Pu closed fuel cycle for SFRs with multiple recycling of U, Pu and MA.

shielding, remote handling and automation are essential for SFR fuel fabrication plants. The critical mass of ^{235}U, ^{233}U, plutonium and some of the minor actinide isotopes are small as shown in Table 1. It would be desirable to avoid use of separated fissile material as feed material for fuel fabrication in order to ensure adequate proliferation resistance.

1.4. OBJECTIVES OF THE PUBLICATION

Initially, the objective for developing SFRs was 'breeding' in order to use fertile isotopes ^{238}U and ^{232}Th efficiently and conserve uranium and thorium resources. However, the motivation for building the SFR has changed over the years in some countries. Today, SFRs are expected to play the following additional roles: (a) burning plutonium stockpiled over the years from civil and military programmes; and (b) reducing the volume, radio toxicity and decay heat of spent fuel by reprocessing, multiple recycling of plutonium and burning minor actinides. The renewed realization that fast reactors can greatly reduce the nuclear waste burden has created new fuel development initiatives worldwide. However, most of the new fuels are extensions of what is already known and what has been extensively tested.

The present publication is a compilation of updated information on manufacturing technology, properties and irradiation behaviour of the conventional mixed uranium plutonium oxide (MOX) fuel and advanced SFR fuels, namely, mixed uranium plutonium monocarbide (MC), mononitride (MN) and the metallic U–Pu–Zr fuel. This report has seven sections. Section 1 gives a brief historical review of LMFRs and uranium and plutonium-bearing fuels for SFRs. Section 2 briefly describes the SFR programme and fuel cycle activities in IAEA Member States. Sections 3, 4 and 5 cover the manufacturing and irradiation behaviour of uranium plutonium oxide, non-oxide (carbide and nitride) and metallic fuels, respectively for SFR. Section 6 summarizes the important thermo physical properties of SFR fuels. Section 7 gives the summary and recommendations for future activities. To the extent possible, the report has covered the emerging knowledge base for minor actinide bearing SFR fuels.

2. SFR AND ITS FUEL CYCLE ACTIVITIES IN MEMBER STATES

2.1. CHINA

As the first major step in developing SFR technology, China is constructing the 20 MW(e) China experimental fast reactor (CEFR). The reactor is expected to be in operation in 2009. China is focusing on sodium cooled, pool type, inherently safe SFR with UO_2 (HEU) as reference and MOX and U-Pu-Zr as advanced fuels. In the next phase, China prototype fast reactor (CPFR) of 600 MW(e) has been planned by 2020. The possibility of China modular fast reactor (CMFR) of 300 MW(e) is also being considered. In the third phase, China demonstration fast reactor (CDFR) of 1 000–1 500 MW(e) is likely to be constructed in 2025. The China Commercial Fast Reactor (CCFR) is likely to be operational by 2035. In the area of the SFR fuel cycle activities, China is constructing a medium size reprocessing plant and a laboratory-size MOX fuel production line. Later, there are plans to build industrial size reprocessing and MOX fuel fabrication plants. Table 5 summarizes the engineering development in SFR fuels technology in China.

2.2. FRANCE

France is firmly committed to nuclear power. Figure 5 shows a sample long term scenario of the French nuclear power system. The scenario shows a constant nuclear power production of the current fleet of thermal reactors (PWRs) until about 2025, and thereafter a possible slight decrease (of about 15%) until 2040, followed by a constant supply of power. A licence extension of current plants is taken into account, Generation III (Gen. III) reactors (advanced PWRs) would replace retired plants of the current generation in 2025, and finally by around 2040 Generation IV (Gen IV) reactors, i.e. fast reactors, would be added.

During the last four decades, France has gained extensive industrial scale experience in SFR fuel cycle with MOX fuel including fuel design, fabrication, in-reactor performance, reprocessing and refabrication based on the lessons learned from Rapsodie, Phenix and Superphenix. So far, some 427 000 MOX fuel pins have been fabricated in France, in the Cadarache facility for the Rapsodie, Phenix, Superphenix and PFR (UK). The MOX fuel has performed satisfactorily to high burnup (150 GW·d/t) and modified austenitic stainless steel used for fuel assembly has also withstood a high neutron dose level (155 dpa) without failure. In the Rapsodie-Fortissimo core, some MOX experimental fuel pins have been successfully irradiated to burn up of 27 at.%. The MOX fuel in prototype fast reactor Phenix achieved a maximum burnup of 17.5 at.% with 8 cores of fuel consisting of 166 000 MOX fuel pins. Phenix is also the first reactor to demonstrate a breeding ratio of 1.16, which enabled loading of the first fuel assembly made with reprocessed plutonium in 1980. For the Superphenix reactor, some 208 000 MOX fuel pins

TABLE 5. THE SFR PROGRAMME IN CHINA

|	CEFR	CPFR	CDFR
Power (MW(e))	25	600	1 000–1 500
Coolant	Sodium	Sodium	Sodium
Fuel	UO_2	MOX and Metal	MOX and Metal
Cladding	Cr-Ni	Cr-Ni, ODS	Cr-Ni, ODS
Core outlet temp., C	530	500–550	500
Linear power, W/cm	430	450–480	450
Burnup GW·d/t	60–100	100–120	120–150
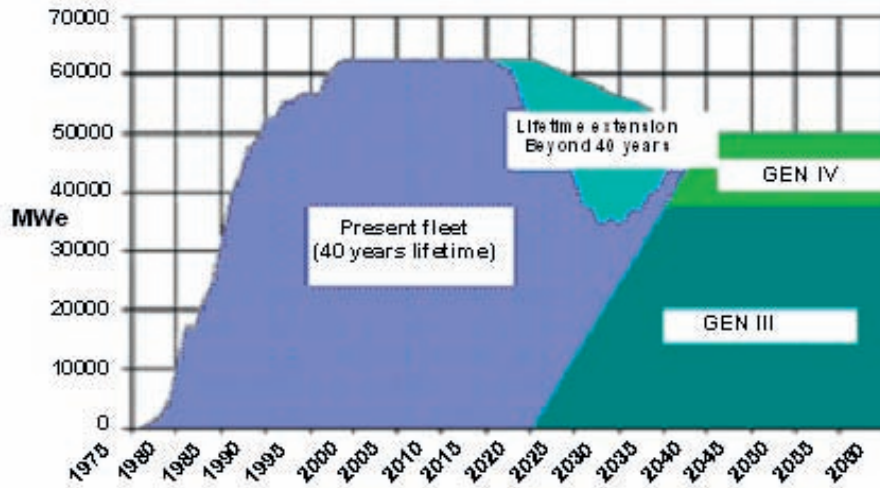
FIG. 5. Transition scenario from present fleet and Gen. III light water reactors to Gen. IV fast reactors in France.

containing ~22 tonnes of plutonium, have been fabricated. France had also developed, fabricated and irradiated (U, Pu)C fuel assemblies in the RAPSODIE reactor.

2.3. GERMANY

The fast reactor programme in Germany started with a compact sodium cooled loop type reactor, KNK-II in the Research Centre Karlsruhe, with a gross electrical output of 21 MW(e). KNK-II began operation in October 1977 with MOX fuel. A prototype fast reactor SNR-300 was constructed and manufacturing of MOX fuel for the core was completed in 1985. However, owing to a political impasse, SNR-300 was never allowed to start. Germany has discontinued its programme on SFR and its fuel cycle.

2.4. INDIA

India is pursuing a three stage, self-reliant and indigenous nuclear power programme, linking the fuel cycles of PHWR, SFR and self-sustaining ^{232}Th–^{233}U reactor systems for judicious utilization of modest uranium but vast thorium resources. SFR is the centre stage of the nuclear power programme. A fast breeder test reactor (FBTR) with plutonium rich mixed uranium plutonium carbide fuel core has been in operation since October 1985. The present core configuration for the FBTR, described in Fig. 6, shows the position of Mark I and Mark II mixed carbide fuel assemblies and the MOX fuel assembly recently introduced. The main characteristics of the FBTR are summarized in Table 6. The Mark I carbide core with composition 70% PuC + 30% UC has reached the burnup of 160 GW·d/t without any failure. A prototype fast breeder reactor of 500 MW(e) (PFBR-500) is under construction at Kalpakkam. The PFBR-500 would use MOX fuel with 2 enrichments (21% and 28% PuO$_2$). The target burnup is 100 GW·d/t, which is likely to be increased to 150 GW·d/t subsequently, 20% cold worked stainless steel type D9 would be used as fuel cladding and fuel assembly structural material. A dedicated fast reactor fuel cycle facility (FRFCF), comprising fuel fabrication, reprocessing and waste management plants, is also being co-located with PFBR with sharing of common facilities in order to reduce fuel cycle cost. The next four SFRs to be constructed after PFBR would also use mixed oxide as the fuel.
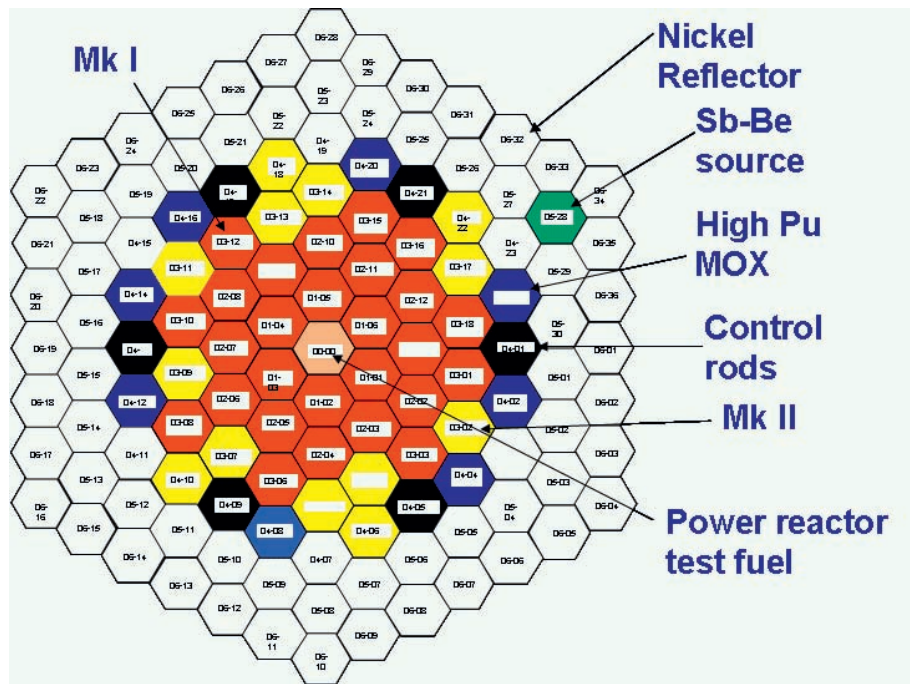
FIG. 6. Present core configuration of FBTR showing MARK-I, MARK-II, mixed carbide and mixed oxide fuel assembly locations.

TABLE 6. MAIN CHARACTERISTICS OF THE FBTR

Reactor power	40 MW(th)/13.2 MW(e)
Reactor coolant	Sodium
Concept of primary circuit	Loop (2)
Fuel Mark I Mark II	70%PuC + 30%UC 55%PuC + 45%UC
Fuel pin diameter	5.1 mm
No. of pins in a subassembly	61
Control rod material	B_4C (90% enriched in B^{10})
Neutron flux	3×10^{15} n/cm^2/s
Core height	320 mm
Reactor inlet sodium temperature	380ºC
Reactor outlet sodium temperature	515ºC

2.5. JAPAN

The SFR programme in Japan was initiated with the commissioning of the experimental fast reactor JOYO that attained criticality in 1977. In 1982, the reactor core was upgraded to 100 MW(th) (MK-II), and finally to 140 MW(th) (MK-III) in 2004. Since the 3rd cycle, oxide dispersion strengthened ferritic steel (ODS) and MOX fuel with the addition of 5% americium and neptunium have been irradiated.

The 250 MW(e) prototype, sodium cooled MONJU reactor, fuelled with Pu-U mixed oxide, successfully achieved its first criticality in April 1994, and supplied electricity to the grid initially in August 1995. However, the

pre-operational test of the plant was interrupted by a sodium leak inident in the secondary heat transport system in December 1995 during a 40% power operation test. The restart is expected to be achieved by the end of 2009.

To investigate a wide range of technical options for fast reactors and the related fuel cycle technologies, a feasibility study on Commercialized Fast Reactor Cycle Systems (FRCS) has been launched by a joint team of Japan Nuclear Cycle Development Institute (JNC), which has been reorganized into the Japan Atomic Energy Agency (JAEA). The key specifications of the fast reactor fuel cycle system are high average core burnup (>150 GW·d/t), low decontamination reprocessing process, and MA bearing fuel (<5 wt%). These issues contribute to achieve economic competitiveness, reduction of environmental burden, enhancement of nuclear non-proliferation, etc.

At the end of phase I, representative fast reactor fuels, namely, oxide, nitride and metallic fuels and their reprocessing methods such as advanced aqueous, oxide electro winning and metal electro refining and fuel fabrication methods such as simplified pelletizing, sphere-packing, vibro-packing, coated particle and injection casting were selected.

Recently, a feasibility study on commercializing fast reactor and associated fuel cycle has been completed. A loop type SFR of 1 500 MW(e) has emerged with MOX as reference fuel. An advanced aqueous reprocessing and a simplified process based on cold pelletization of MOX fuel are considered most promising. Metallic fuel is considered to have potential merit to improve the core performance of the SFR.

The past, on-going and future SFR development programme in Japan is shown in Fig. 7. The switchover from the LWR to the SFR will be completed only by the end of this century as shown in Fig. 8. With the sodium cooled reactor cycle, it will take about 60 years to complete the switchover from the LWR to the SFR cycle, which is almost the same period of LWR plant life.

2.6.   REPUBLIC OF KOREA (ROK)

The ROK government launched a 10 year programme in 2007 for the development of a conceptual design of a Gen IV SFR. The programme is being conducted by the Fast Reactor Technology Development Group at KAERI under the third national mid- and long term nuclear R&D programme. The basic R&D efforts have been directed towards the development of the advanced fast reactor concept called KALIMER-600 (Korea advanced liquid metal reactor — 600 MW(e)).

The KALIMER-600 features a proliferation resistant core without blanket, and a decay heat removal circuit using natural sodium circulation cooling for a large power system. The KALIMER-600 conceptual design, which evolved on the basis of the KALIMER-150 (150 MW(e)) design, was selected as one of the promising Gen-IV SFR
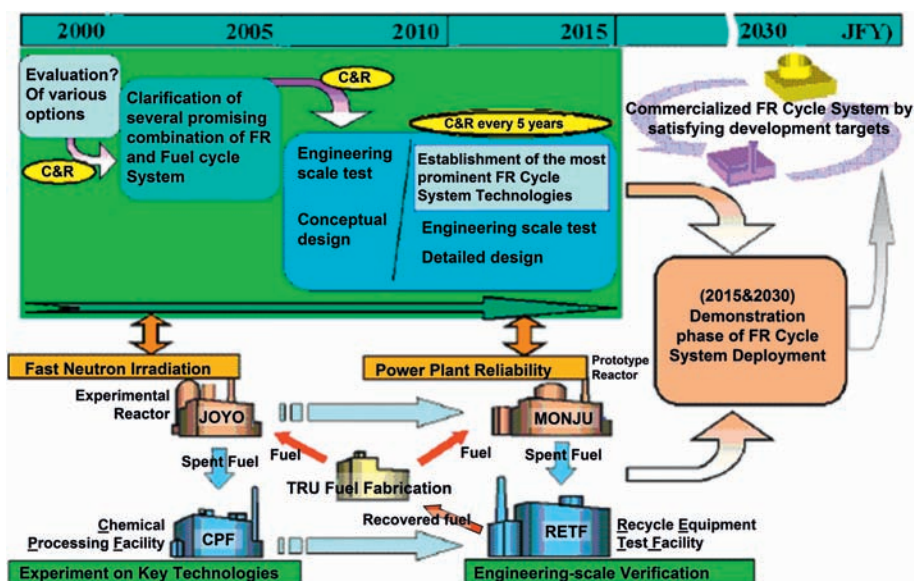

*FIG. 7. Past, present and future SFR programme in Japan.*
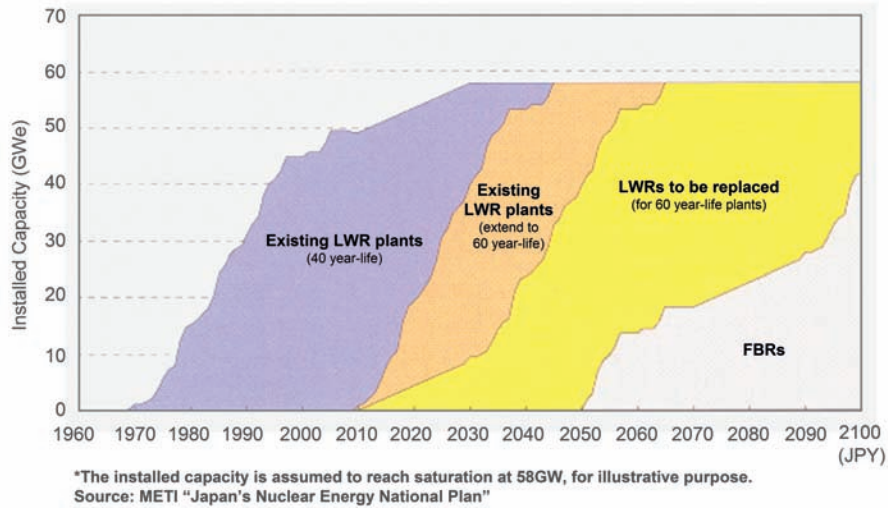
FIG. 8. Long term framework for nuclear energy in Japan (basic projection as visual image) [14].
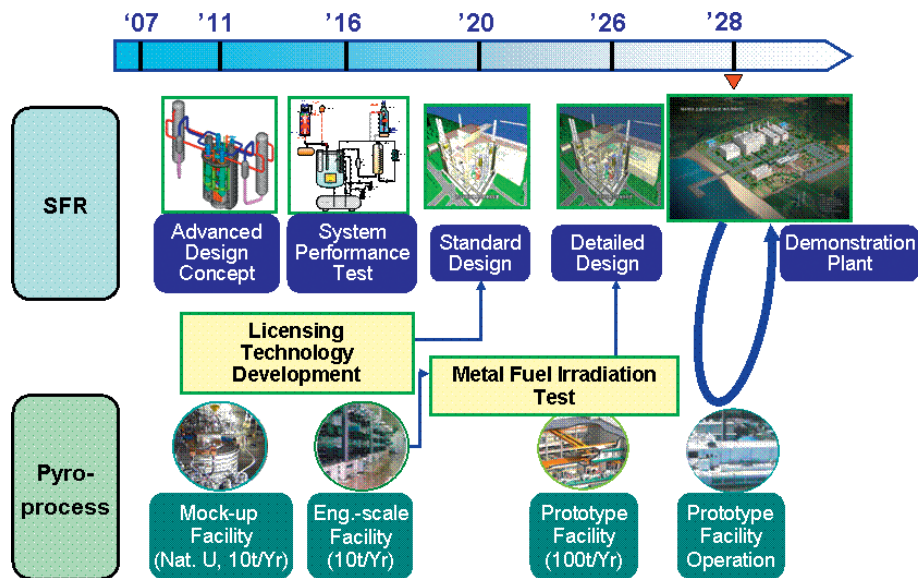

FIG. 9. Long term plan for the SFR and pyroprocess development in the Republic of Korea.

candidates. The KALIMER-600 design will serve as a starting point for meeting the Gen IV technology goals of sustainability, safety and reliability, economics, proliferation resistance and physical protection.

In December 2008, the government of the ROK authorized the long term Gen-IV SFR development plan, the construction of an advanced Gen IV SFR demonstration plant by 2028 in association with the pyroprocess technology development in three phases (Fig. 9):

— First phase (up to–2011): development of an advanced Gen IV SFR design concept;
— Second phase (2012–2017): standard design of an advanced Gen IV SFR demonstration plant;
— Third phase (2018–2028): construction of an advanced Gen IV SFR demonstration plant.

The Gen IV SFR development will be extended to the commercialization phase with its initialization around 2050.

2.7. RUSSIAN FEDERATION

According to the energy strategy of the Russian Federation, electricity generation by nuclear power plants would be increased from 140 billion kW·h in 2002 to 195 billion kW·h in 2010 and up to 300 billion kW·h in 2025. The share of electricity generation by nuclear power plants will rise from 16% in 2000 to nearly 25% by 2025. For this, the target is to commission ~2 GW(e) per year. Taking into account planned lifetime extension of existing operating nuclear power units by 15 years (average), the total installed capacity of NPPs in the Russian Federation should reach 51 GW(e) by 2030. Figure 10 shows the planned transition from the present water cooled thermal reactors (WWER and RBMK) to fast reactors with a closed fuel cycle in the Russian Federation. In addition to SFR, lead–bismuth cooled fast reactor, namely BREST 300 and BREST 1200 are being studied. The Russian Federation has accumulated nearly four decades of experience in nuclear submarine reactors cooled with Pb and Pb-Bi alloy.

The Russian Federation has more than 125 reactor years operating experience with SFR. The experimental reactors BR-10 and BOR-60 and the commercial reactor BN-600 have been extensively used to lay the foundation of SFR and its fuel cycle technology. BN-600, the only operating commercial SFR in the world today, is in operation since 1982 with a capacity factor exceeding 74%. The design of BN-800 is based on the design features proven in the course of construction and operation of the previous reactor BN-600. The parameters of the NPP with BN-600 and BN-800 are summarized in Table 7.

The driver fuel of the SFRs in the Russian Federation has mostly been HEU oxide pellets clad in stainless steel. However, development activities are under way for manufacturing experimental Vibro MOX fuel assemblies, using $(U, Pu)O_2$ granules as feed material and also by the novel DDP/DOVITA (Dimitrovgrad dry process/**d**ry reprocessing, **o**xide fuel, **v**ibro-pack, **i**ntegral, **t**ransmutation of **a**ctinides) process, described in detail in Section 3. Weapons grade plutonium is planned to be used as MOX fuel in Russian fast reactors including BN-800.

2.8. UNITED KINGDOM

The Dounreay Nuclear Power Development Establishment was started in 1955 primarily to pursue the UK Government policy of developing FBR technology. The Dounreay experimental fast reactor (DFR) came on-line in November 1959. The prototype fast reactor (PFR) of 250 MW(e) achieved criticality in 1974 and began supplying power in January 1975. The output of PFR was in operation up to 1994 and served as an invaluable test facility for
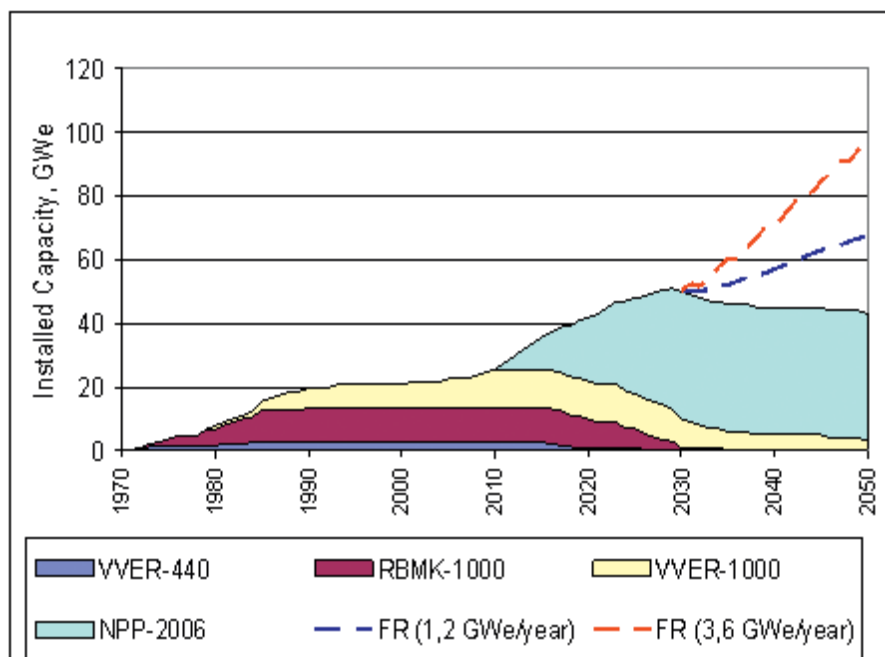

FIG. 10. Transition from thermal reactors to fast reactors in the Russian Federation.

TABLE 7. CHARACTERISTICS OF BN-600 AND BN-800 REACTORS

Characteristic	BN-600	BN-800
Thermal power, MW(th)	1470	2100
Electric power, MW(e)	600	880
Fuel	UO$_2$	MOX
Primary sodium temperature, ˚C:		
core inlet	377	354
core outlet	550	547
Steam parameters:		
temperature, ˚C	505	490
pressure, MPa	142	137
Intermediate steam superheating by:	Sodium	Steam
Reactor vessel overall dimensions, m		
diameter	12.86	13.4
height	14.70	15.0
Reactor vessel material	09Cr118Ni9 steel	
Reactor plant materials intensity per MW(e)/t	13	9.7
Equipment seismic stability (points on MSK-64 earthquake scale)	6	7
Service life, years	30	30–40

developing advanced fuel and cladding materials that performed satisfactorily up to high burnup and withstood high neutron dose. Both DFR and PFR have been shut down.

With regard to the future programme related to fast reactor and accelerator driven systems, the UK has been participating in the CEA-led CAPRA and CADRA programme. The focus of these programmes is on the incineration of Pu in a fast reactor core and the incineration of minor actinides and long lived fission products. The UK covers the domain of core physics, fuel performance modeling, and fuel cycle modeling.

2.9. UNITED STATES OF AMERICA

In the USA, a very active R&D programme was under way on LMFR and its fuel cycle for nearly three decades during the 1950s and 1980s. Five fast neutron reactors were in operation in the past, which generated extensive experience and several more have been designed. Presently, there are no operating LMFRs in the USA.

The experimental breeder reactor II (EBR-II) and the 400 MW(th) fast flux test facility (FFTF) were extensively used in the 1980s for development of LMFR fuels technology. More than 130 000 metallic fuel rods, over 50 000 MOX rods and some 600 mixed uranium and plutonium carbide and nitride fuels have been irradiated in these two reactors. The FFTF was not a breeder, but rather a sodium cooled fast neutron reactor to test advanced nuclear fuels, materials, components, nuclear power plant operations and maintenance protocols, and reactor safety designs. The FFTF operated between 1982 and 1992 at the Hanford Site, Washington, as a major national research reactor. It was closed down at the end of 1993, and has been in a decommissioned state since 2001. The EBR-II was shut down in 1994.

The key achievement in the US programme on SFR technology is the demonstration of an inherently safe, integral fast reactor (IFR) concept at the EBR-II site with colocation of metal fuel fabrication, EBR-II reactor and pyro-electrolytic reprocessing plants. The IFR design has inherent safety features through a combination of metal fuel (U-Zr and U-Pu-Zr) and sodium cooling. By providing a fuel which readily conducts heat from the fuel to the

coolant, and which operates at relatively low temperatures, the IFR takes maximum advantage of expansion of the coolant, fuel, and structure during off-normal events which increase temperatures. The expansion of the fuel and structure in an off-normal situation causes the system to shut down even without human operator intervention.

The goals of the IFR project were to increase the efficiency of uranium usage by breeding plutonium and eliminating the need for transuranic isotopes to ever leave the site. The reactor was an unmoderated design running on fast neutrons, designed to allow any transuranic isotope to be consumed. IFR had a very efficient fuel cycle. The basic scheme used electrolytic separation to remove transuranics and actinides from the wastes and concentrate them. These concentrated fuels were then reformed, on-site, into new fuel elements. From the available fuel metals, plutonium was never separated and therefore there was no direct way to use the fuel metals in nuclear weapons. Also, plutonium never had to leave the site and thus it was not amenable for any unauthorized diversion. Another important benefit of removing the long half-life transuranics from the waste cycle is that the remaining waste becomes a much shorter term hazard. The goal was demonstrating a proliferation resistant closed fuel cycle, with plutonium being recycled with other actinides.

In recent years, there has been renewed interest in the USA in fast reactors, in general and SFR in particular. The priority for fast reactors is in response to the sustainability goals of the Gen IV roadmap, and reflects their excellent potential to burn plutonium and minor actinides thus reducing the volume, radio toxicity and decay heat load of spent LWR fuels and the need for a second geological repository for many decades. As part of the recent Advanced Fuel Cycle Initiative (AFCI) in the USA an advanced burner reactor (ABR) has been planned. The ABR is an advanced fast reactor for burning plutonium and MA recovered from reprocessing spent nuclear fuel from operating thermal neutron reactors. Thus, the volume, radio toxicity and decay heat of the high level waste for disposal in the geologic repository at Yucca Mountain, Nevada, would be significantly reduced.

Fuel loading for such reactors may consist of either MOX or metal fuel based on U-Pu-Zr alloy with fuel burnup in the range of 150–200 GW·d/t. Efforts are under way under AFCI to develop aqueous and pyrochemical processing. Both technologies ensure that there is no separated plutonium stream at all stages of processing.

3. OXIDE FUEL

3.1. INTRODUCTION

For the first generation of experimental, prototype and commercial SFRs, oxide has been the undisputed choice for the driver fuel. In France, Germany and Japan, mixed uranium plutonium oxide (MOX), containing up to 30% PuO_2 has been the driver fuel. In the Russian Federation, high enriched uranium (HEU: >20% ^{235}U) oxide has been used as the fuel for BOR-60, BN-350 and BN-600. The UK and USA have used both metallic and MOX fuels in their experimental and prototype fast reactors and test facilities. The oxide fuel continues to be the reference fuel for SFRs based on the following reasons:

— Simplicity and less number of process steps in fabrication, and maturity of UO_2 and MOX fuels fabrication industry;
— High melting point and good chemical stability of UO_2 and MOX fuels;
— Satisfactory chemical compatibility of UO_2 and MOX with sodium coolant and stainless steel cladding;
— Considerable and satisfactory irradiation database of UO_2 and MOX fuels to high burnup in thermal and fast reactors;
— Well advanced safety analysis based on large number of out-of-pile and in-pile experiments world wide, simulating incidental and accidental conditions;
— Industrial scale experience in reprocessing of spent UO_2 and MOX fuels.

In France and the UK, all the steps of the SFR fuel cycle including fabrication, irradiation, reprocessing and re-fabrication have been demonstrated on an industrial scale with MOX fuel. Japan also has industrial scale manufacturing experience of MOX fuel for JOYO and MONJU. The Russian Federation has industrial scale

manufacturing and high burnup irradiation experience of UO_2 fuel containing HEU in BOR-60, BN-350 and BN-600. The Indian PFBR-500 will also use MOX as the driver fuel.

3.2. FABRICATION

UO_2 and PuO_2 are iso-structural (CaF_2 type FCC), completely solid soluble at stoichiometric composition and have very similar thermodynamic and thermo physical properties. Hence, the manufacturing processes of UO_2 and $(U, Pu)O_2$ are similar. The oxide fuels are generally used in the form of 'pellets' and manufactured by powder metallurgy (P/M) processes. The main process steps in 'powder–pellet' routes are:

— Preparation of oxide powder;
— Granulation of oxide powder in some cases;
— Cold — pelletization;
— High temperature sintering in hydrogen atmosphere.

The major challenges in the P/M route are 'radiotoxic dust hazard' associated with the generation and handling of large quantities of very fine powders of UO_2, highly radioactive PuO_2 and oxides of minor actinides and the poor flowability of the powder. The isotopes of plutonium, in particular, [238]Pu, [240]Pu, [241]Pu and [242]Pu are highly radiotoxic and are associated with emission of beta-gamma radiations and neutrons. Hence, fabrication processes, which avoid milling and grinding operations and deal with dust free and free flowing fuel materials are attractive. This would, in turn, facilitate remote and automated fuel fabrication.

3.2.1. Industrial processes for fabrication of UO2 and (U, Pu)O2 fuel pellets

The major steps in manufacturing UO_2 and $(U, Pu)O_2$ fuel are preparation of oxide powder, sintered pellets of controlled diameter, length to diameter ratio, density and microstructure (in terms of grain size, pore size, shape and distribution), inspection and loading of accepted fuel pellets in one end welded stainless steel cladding tubes followed by welding of the other end plug and encapsulation with helium as filler gas. In most cases, the UO_2 axial blanket is part of the fuel rod and loaded in both ends of the fuel pellet stack. The fuel rods are then wire wrapped and assembled in the hex can or wrapper tubes to form the fuel assembly.

Figure 11 summarizes the industrial processes for producing UO_2, PuO_2, and $(U, Pu)O_2$ powders using UF_6, uranium nitrate hexahydrate (UNH) and plutonium nitrate as feed materials. In the integrated dry route (IDR), only UF_6 can be used as starting material. The wet chemical processes adapting the ammonium diuranate (ADU) and ammonium uranium carbonate (AUC) processes use either UF_6 or UNH as feed material. UO_2 powder prepared by IDR and ADU processes is extremely fine and not free flowing, needing a granulation step for producing press feed material. Only the AUC route leads to relatively coarse and free flowing UO_2 powder, which could be directly pelletized.

Figure 12 summarizes the industrial methods followed for production of $(U, Pu)O_2$ fuel pellets on an industrial scale. So far, five processes have been utilized, namely, the **co**broyage **ca**darche (COCA) process of France, the **m**icronized **m**aster **m**ix (MIMAS) process of Belgium and France, the **s**hort **b**inder less **r**oute (SBR) of the UK and the **o**xide **c**omilling (OCOM) and **a**mmonium **u**ranium **p**lutonium **c**arbonate (AUPuC) processes of Germany. COCA, SBR, OCOM and AUPuC have been used for fabrication of MOX fuel pellets for fast reactors. MIMAS is mostly used for fabrication of MOX fuel for thermal reactors. The PuO_2 powder is prepared by the oxalate route using plutonium nitrate as feed material. On calcination of plutonium oxalate at ~600°C, very fine particles of PuO_2 powder is produced which requires granulation. The conventional route uses mechanical blending of the feed powders; namely UO_2, PuO_2 or co-precipitated $(U, Pu)O_2$ followed by granulation, cold pelletization and sintering. The challenges in these processes are to obtain fuel pellets with controlled density, oxygen to metal ratio and a single phase microstructure with uniform distribution of plutonium.

The MOX plant of CEA, France at Cadarache had followed the COCA process for fabrication of MOX fuel for the Rapsodie, Phenix and Superphenix reactors. The COCA process consists of optimized ball milling and blending of UO_2 and PuO_2 powders, followed by forced extrusion of lubricated micronized powder through a sieve leading to free flowing granules which are directly pelletized and sintered.
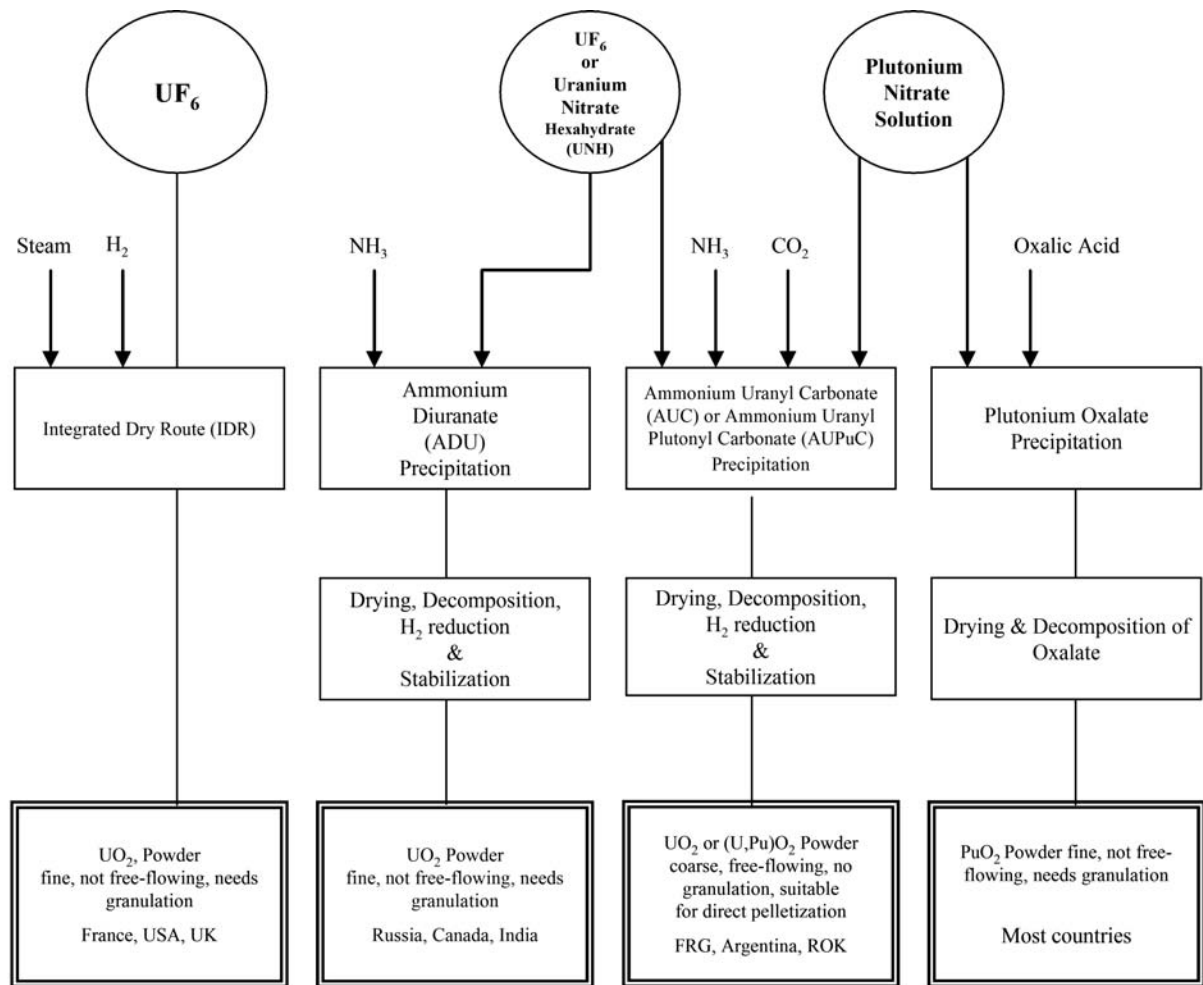
FIG. 11. Industrial processes for producing UO_2, PuO_2 and $(U, Pu)O_2$ powders.

The MIMAS process, developed by Belgo Nucleaire (BN) in the early 1980s, has been followed for manufacturing MOX fuels in Belgium and France (in the MELOX plant) for both LWRs and LMFRs. In the MIMAS process, the single blending step is replaced by a two step blending approach, where in the first step, the pure PuO_2 feed and some UO_2 are co-milled resulting in a master mix of $UO_2 \sim 30\%$ PuO_2, which is the fundamental principle of the MIMAS process; in the second step, the master mix is blended down with free flowing UO_2 obtained from AUC, to the specified plutonium content of the MOX fuel. The very close contact between the milled UO_2 and PuO_2 particles provides for adequate inter-diffusion during sintering and therefore the required solubility in HNO_3.

The UK developed the SBR for manufacturing MOX fuel pellets for LMFR in their MOX demonstration facility (MDF) in Sellafield with a capacity of 8 tHM/a. Some 13 tonnes of MOX fuel was manufactured for the PFR. The SBR process is based on attrition of oxide powders followed by spheroidization of mixed oxide powder agglomerates, cold-pelletization and sintering. The attritor provides the desired micro-homogeneity in the UO_2-PuO_2 powder mixture. The SBR process was adapted for the Sellafield MOX Plant (SMP) with a capacity of 120 tHM/a for manufacturing MOX fuel for LWRs. The MDF was also used for MOX fuel fabrication for LMFR.

In Germany, the OCOM and AUPuC processes were developed by Alkem in Hanau as part of a MOX fuel fabrication campaign for SNR-300. The MOX core was manufactured for SNR 300 but the reactor was not commissioned. Subsequently the MOX fuel fabrication plant at Hanau was shut down. The AUPuC process is an extended version of AUC process, in which free flowing $(U, Pu)O_2$ powder, suitable for direct pelletization, could be co-precipitated from mixed uranium plutonium nitrate solution. Thus, the separation of the plutonium stream in the reprocessing plant is not needed. The AUPuC process is, therefore, very attractive from the point of view of:

Process	Conventional	MIMAS	COCA	SBR		AUPuC
Plant	PFPF (Japan)	BN (Belgium), CFG&MELOX (France)	CFCa (France)	MDF (UK)	SMP (UK)	Alkem (Germany)
Feed	UO$_2$; U-50% Pu)O$_2$	UO$_2$; PuO$_2$	UO$_2$; PuO$_2$	UO$_2$; PuO$_2$	UO$_2$; PuO$_2$	Uranyl nitrate & Plutonium nitrate solution → (NH$_4$OH + CO$_2$ Dosing) → AUPuCl
Dispensing	Dosing ; Dosing	Dosing	Dosing ; Dosing	Dosing ; Dosing	Dosing ; Dosing	(U, Pu)O$_2$
Blending	Blendingr → Ball milling → Addition of binder & pore former	Ball milling	Ball milling	Attritor milling	Attritor milling → Homogenization	
Conditioning	Slug pressing → Granulation → Addition of Lubricant	Forced sieving → Secondary blending	Forced sieving → Mixing Additives	Spheroidization	Spheroidization	Direct-pelletization

FIG. 12. Industrial process flow sheets for fabrication of MOX fuel.

— Proliferation resistance;
— Minimizing the problem of radiotoxic dust hazard to some extent;
— Ensuring homogenous distribution of Pu in (U, Pu)O$_2$ powder.

For MOX fuel fabrication, Japan has a laboratory facility known as the Plutonium Fuel Development Facility (PFDF), a pilot plant known as Plutonium Fuel Fabrication Facility (PFFF) and a fully automated Plutonium Fuel Production Facility (PFPF), with sufficient capacity to manufacture MOX fuel for MONJU and JOYO. In PFFF and PFPF, the feed material is microwave denitrated MOX powder containing some 50% PuO$_2$. The MOX powder from the reprocessing plant is down blended with UO$_2$ to obtain MOX of the as-desired PuO$_2$ content. In recent years, Japan has further simplified the manufacturing process of MOX fuel pellet based on microwave de-nitration of mixed uranium plutonium nitrate solutions followed by direct pelletization and sintering as shown in Fig. 13. The process has the following attractive and unique features:

— Plutonium enrichment adjustment in solution (Pu EAS);
— The plutonium is not separated from uranium, making the process attractive from the point of view of proliferation resistance.

Apart from the above industrial MOX fuel fabrication plant facilities, five pilot plants were set-up in the USA, where MOX fuel for EBR II and FFTF cores were manufactured. More than 125 000 MOX fuel pins were manufactured in some of these facilities for FFTF, by the classical powder pellet process employing co-milling UO$_2$ and PuO$_2$ powders, granulation, cold-pelletization and sintering. Likewise, in the Russian Federation, the Paket/Chelyabinsk small scale facility was in operation for manufacturing experimental MOX pellets using
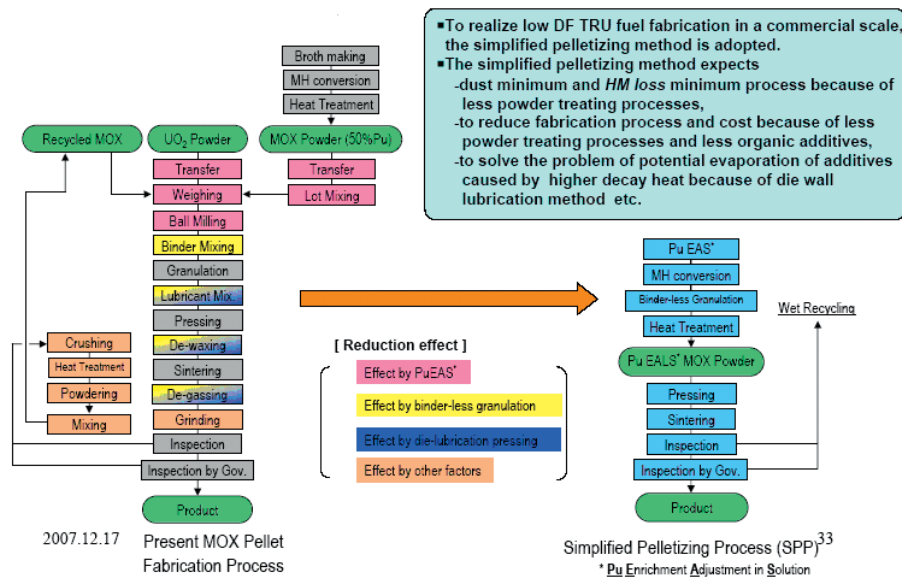
FIG. 13. Schematic flow sheet of a simplified process under development in Japan for fabrication of MOX fuel pellets, involving microwave de-nitration.

classical P/M route as well as co-precipitated granules (Granat process) as feed materials for irradiation in BOR 60 and BN 600. The Paket facility mostly used UO_2 and PuO_2 powders as feed materials, a high energy mixer for milling and blending and the conventional powder-pellet route. However, in Granat process, some MOX fuel pellets were also prepared by ammonia co-precipitation of MOX powder followed by pelletization and sintering. In India, a MOX pilot plant has been set up based on attritor co-milling of UO_2 and PuO_2 powder, followed by pelletization. An experimental MOX fuel assembly of PFBR 500 fuel composition has been manufactured in this facility and is undergoing irradiation testing in FBTR. The facility has also been utilized for manufacturing a few MOX fuel assemblies containing ~45% PuO_2 for use in FBTR.

3.2.2. Sol–gel processes

The 'vibro-sol' and 'sol-gel microsphere pelletization (SGMP)' are dust free processes for manufacturing UO_2 and homogeneous MOX fuel pellets. These processes have so far been utilized only on a pilot plant scale in a limited number of countries [15, 16]. In these processes, first, free flowing hydrated gel-microspheres of the mixed oxide are prepared by 'ammonia external/internal gelation process' starting from the nitrate solutions of the heavy metals. The 'ammonia gelation' is achieved either 'externally' via NH_3 gas and NH_4OH or 'internally' via an added ammonia generator, namely hexa methylene tetra amine (HMTA). Figures 14 and 15 show the ammonia external gelation of uranium (EGU) and ammonia internal gelation of uranium (IGU) processes, respectively for preparation of hydrated gel microspheres of uranium oxide [17, 15]. The EGU and IGU processes could be extended for mixed uranium plutonium oxide. The major steps in EGU and IGU processes are:

— Preparation of sol or broth from nitrate solutions of uranium and plutonium;
  • In the EGU process, the broth is prepared by mixing uranium plutonium nitrate solutions with urea and ammonium nitrate in the proportion of 1.0 mole per liter, 4.0 moles per liter and 2.5 moles per liter respectively followed by boiling for ~30 minutes. A small amount of polyvinyl alcohol (5 g/l) could be added to the mixed solution for mechanical stability of the gel.
  • In the IGU process, uranium and plutonium nitrate solutions are mixed with HMTA and urea in mole proportions of 1.25 and 1.75 respectively and cooled to 0ºC. Urea prevents premature gelation of the solution.
— Droplet formation by vibrating nozzle.
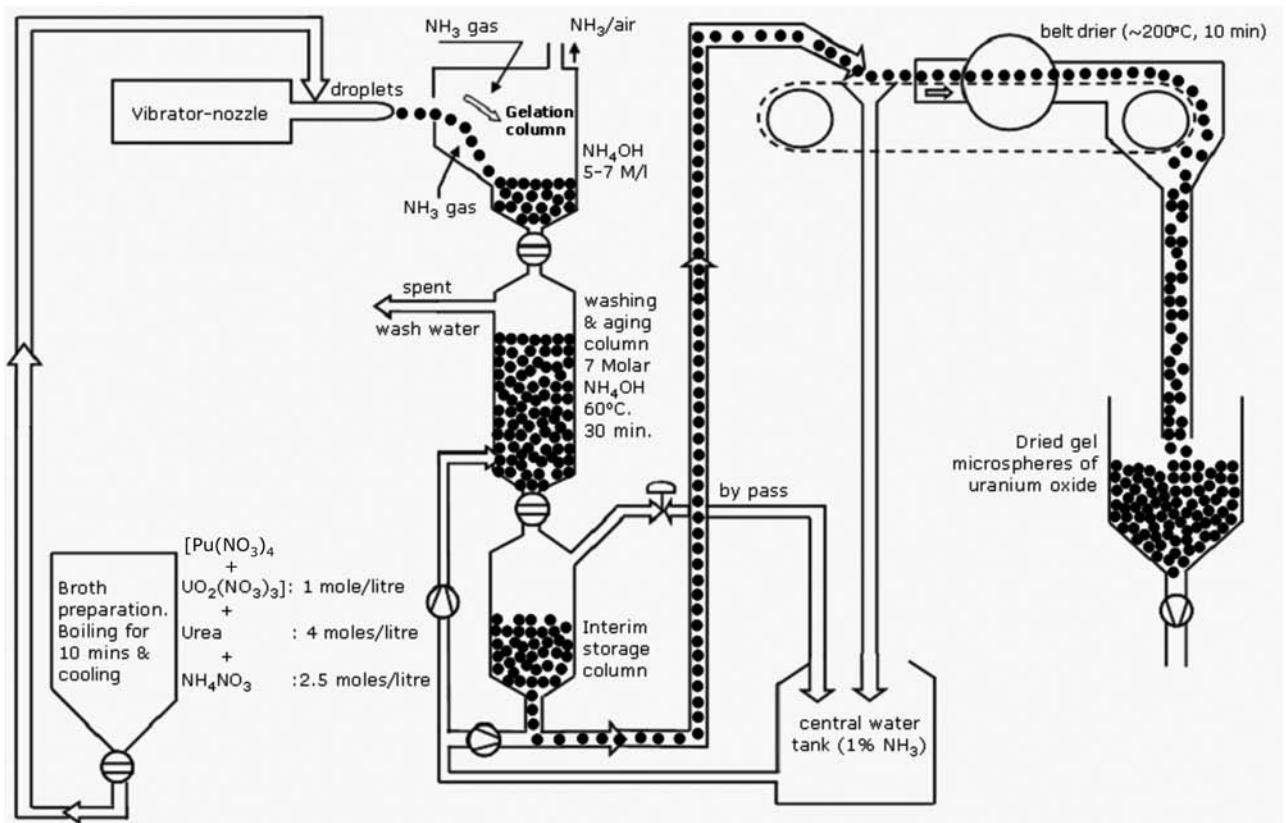
FIG. 14. External gelation of uranium (EGU) process for preparation of hydrated gel-microspheres of uranium oxide or mixed uranium plutonium oxide.
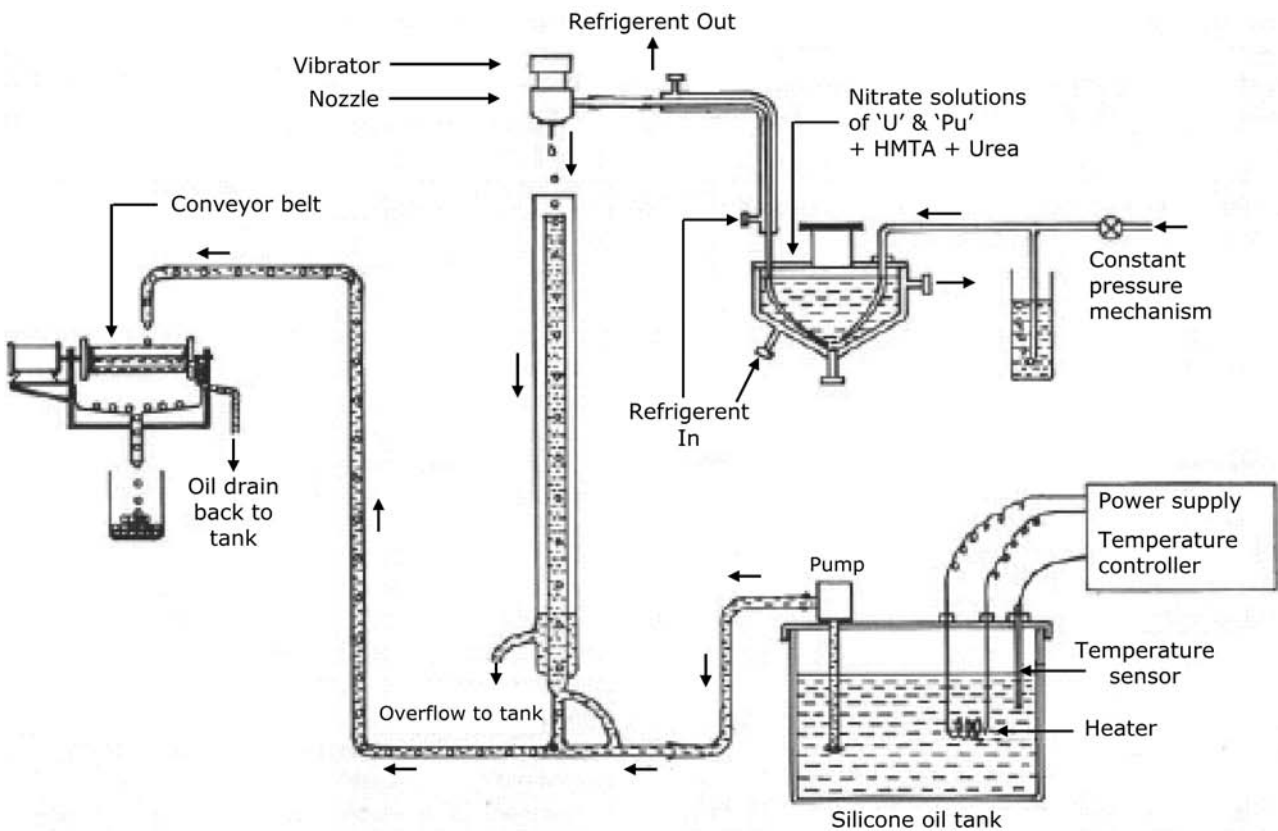

FIG. 15. Ammonia internal gelation of uranium process for preparation of hydrated gel-microspheres of uranium oxide and mixed uranium plutonium oxide.

— Droplet gelation in NH_3 gas and NH_4OH bath (for EGU) or silicon oil bath at 90 ± 1^oC which decomposes HMTA to release ammonia for conversion of the droplets into hydrous gel-microspheres; in the IGU process, microwave heating could also be used in place of silicon oil.
— Washing of gel-microspheres; in the EGU process, the microspheres are washed in 1% ammonia solution for removal of NH_4NO_3; in the IGU process, the gel-particles are washed with CCl_4 to remove oil and in 3M NH_4OH solution to remove ammonium nitrate.
— Drying of gel-microspheres on a continuous belt dryer at 200–250^oC.
— Controlled sintering at ~1600^oC in hydrogen atmosphere to produce very high density (>99% TD) 'non-porous' UO_2 or $(U, Pu)O_2$ microspheres.

In order to produce 'porous' microspheres, carbon black pore former is added to the sol or solution prior to gelation and later removed by controlled calcination of the gel-microspheres at ~700^oC in air followed by hydrogen [16].

The gel-microspheres are subjected to controlled calcination and sintering, after which they are 'vibro-compacted' in fuel tubes. The porous microspheres are directly pelletized and sintered to obtain fuel pellets. The 'vibro-sol' and SGMP processes are amenable to automation and remotization and well suited for manufacturing highly radiotoxic plutonium and minor actinide bearing mixed oxide fuels.

The advantages of sol-gel processes are:

— A high degree of microhomogenity is attained in MOX fuel because uranium and plutonium nitrate solutions are mixed prior to gelation;
— Generation and handling of fine powders of UO_2 and PuO_2 are avoided, thereby, minimizing the problem of radiotoxic dust hazard associated with the conventional 'powder-pellet' route;
— Dust free and free flowing microspheres facilitate remote and automated manufacturing of fuel rods by 'vibro-sol' or SGMP processes;
— The sol-gel plant could be easily integrated with the spent fuel reprocessing plant and could be utilized for preparation of MOX containing minor actinide oxides.

One of the major limitations of the sol-gel processes is the generation of large volume of high level of liquid wastes containing organic chemicals. However, this problem could be significantly minimized if the sol-gel plant is integrated with the spent fuel reprocessing plant.

The sol-gel derived oxide, carbide or nitride fuel microspheres have been used for manufacturing fuel rods of the following types on a pilot plant scale:

'Vibro–Sol' fuel

In this process, high density oxide, carbide or nitride fuel microspheres of two or three size fractions (800–1 000, 80–100 and ~10 micron) are loaded in one end welded fuel cladding tubes and subjected to vibratory compaction. It is possible to prepare fuel rods of smear density in the range of 70–85% by this process [18, 19]. In the UK, several MOX fuel assemblies manufactured for PFR by the vibro-sol route were initially irradiated through the programme, which was given up later. The limitation of vibro-sol elements are lower operating limits on the linear power of fuel elements at beginning of life (BOL), concern about the fine fraction segregation in the fuel elements and fuel dispersion in the case of clad breach [20]. The Russian Federation opted for the DDP/DOVITA process which produces irregular particles and overcame some of the problems in vibro-sol fuel experienced with sol-gel derived microspheres.

Sol-Gel microsphere pelletization (SGMP)

In the SGMP process sol-gel derived porous or non-porous microspheres are directly compacted to pellets and sintered at ~1 700^oC in hydrogen atmosphere. The 'non-porous' microspheres retain their individual identity even after pelletization at high pressure (~840 MPa) and sintering at high temperature (1700^oC), resulting in 'blackberry' structures with microsphere boundaries and 'open' porosity. This is because of densification within the microspheres and not between them during the sintering process. The 'porous' microspheres have low crushing
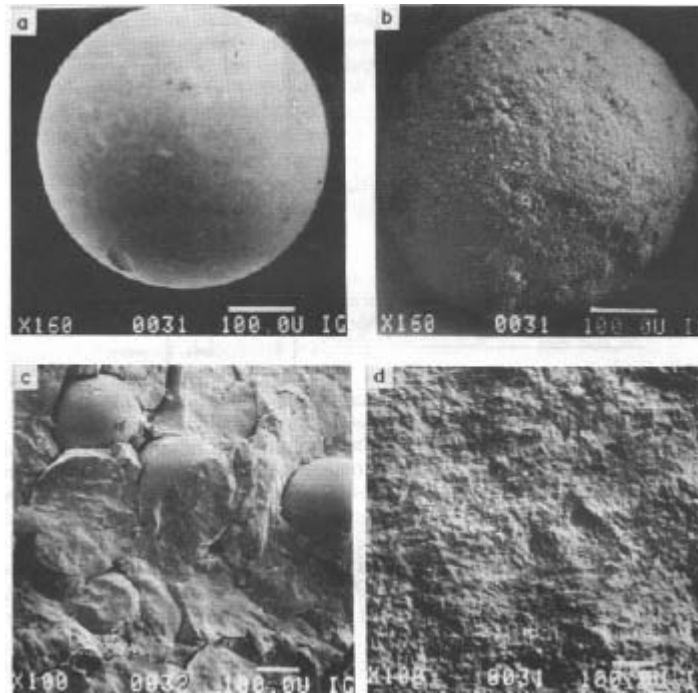
FIG. 16. SEM pictures of: (a) 'non-porous' microsphere,(b) 'porous' microsphere, (c) sintered pellets from 'non-porous' microspheres (showing black-berry structure) and (d) sintered pellets from 'porous' microspheres showing no-microsphere boundaries.

strength, disintegrate easily during pelletization at ~350 MPa and yield sintered pellets without microsphere boundaries. Figure 16 shows SEM pictures of non-porous and porous microspheres and sintered pellets made from these microspheres [21].

3.2.3. DDP/DOVITA (Dimitrovgrad Dry Process/Dry reprocessing, Oxide fuel, Vibro-pack, Integral, Transmutation of Actinides) process in the Russian Federation

The Research Institute of Atomic Reactor (RIAR) in the Russian Federation has developed novel methods, DDP/DOVITA, for production of UO_2, PuO_2 and $(U, Pu)O_2$ fuels, with and without minor actinides, from fresh/spent UO_2 and $(U, Pu)O_2$ fuels. The initial fuel product (fresh/spent UO_2 or $(U, Pu)O_2$ fuel) is subjected to molten salt dissolution in a 'chlorinator–electrolyzer' made of pyrolitic graphite [22]. Next, the electro refined UO_2 and/or MOX is deposited on the cathode as a loose crust that is crushed and sized to produce the required size fractions which are fed into the fuel rod by vibro-compaction. Figure 17 shows the schematic of pyrochemical production/reprocessing of spent oxide fuel for co-depositing $(U, Pu)O_2$ on cathode. The main chlorinator-electrolyzer equipment in the pilot plant at RIAR has a diameter of ~380 mm which could co-deposit 30 kg MOX fuel in a batch. Figure 18 shows a picture of the main equipment, co-deposited MOX and characteristics of the granulated MOX particles used for vibratory compaction. Several MOX fuel pin assemblies have been prepared by the DDP/DOVITA process and successfully irradiated in BOR-60 and BN-600.

3.3. IRRADIATION EXPERIENCE

Mixed uranium plutonium oxide has been the driver fuel for most of the demonstration, prototype and commercial SFRs. Hence, the irradiation experience of MOX fuel in fast reactor has been way above the other type of SFR fuels. So far, more than 265 000 pins containing MOX have been irradiated in European fast reactors [23]. In the Russian BN-350 and BN-600 reactors 1500 and 2500 MOX fuel rods, respectively, have been irradiated. In addition, approximately 1000 rods with vibro-pack MOX fuel were irradiated in BN-350 and BN-600 at burnup up to 130 GW·d/(t HM), and more than 16 000 rods with vibropack MOX fuel were irradiated in the BOR-60 reactor at even higher burnup. Further, about 54 000 pins have been irradiated in Japan. Of these, 61 pins have reached
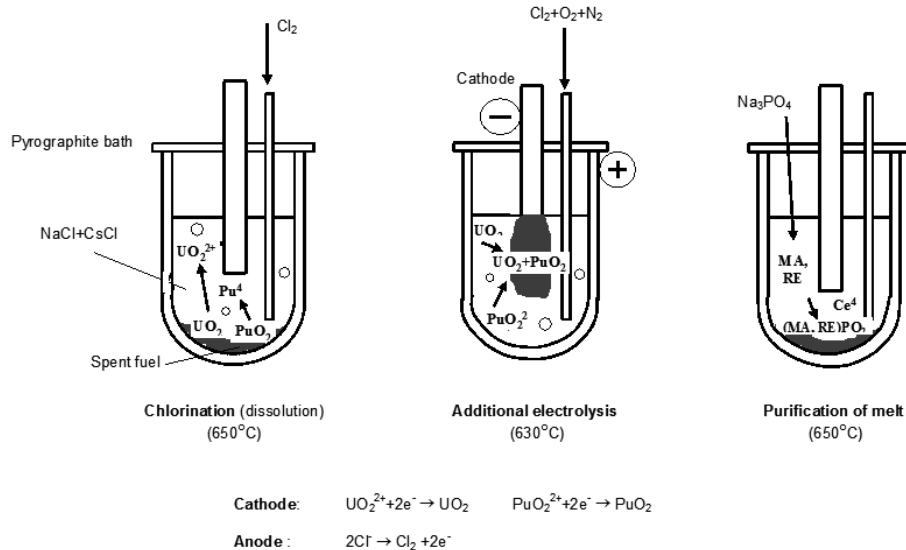
FIG. 17. Oxide electrowinning process steps.
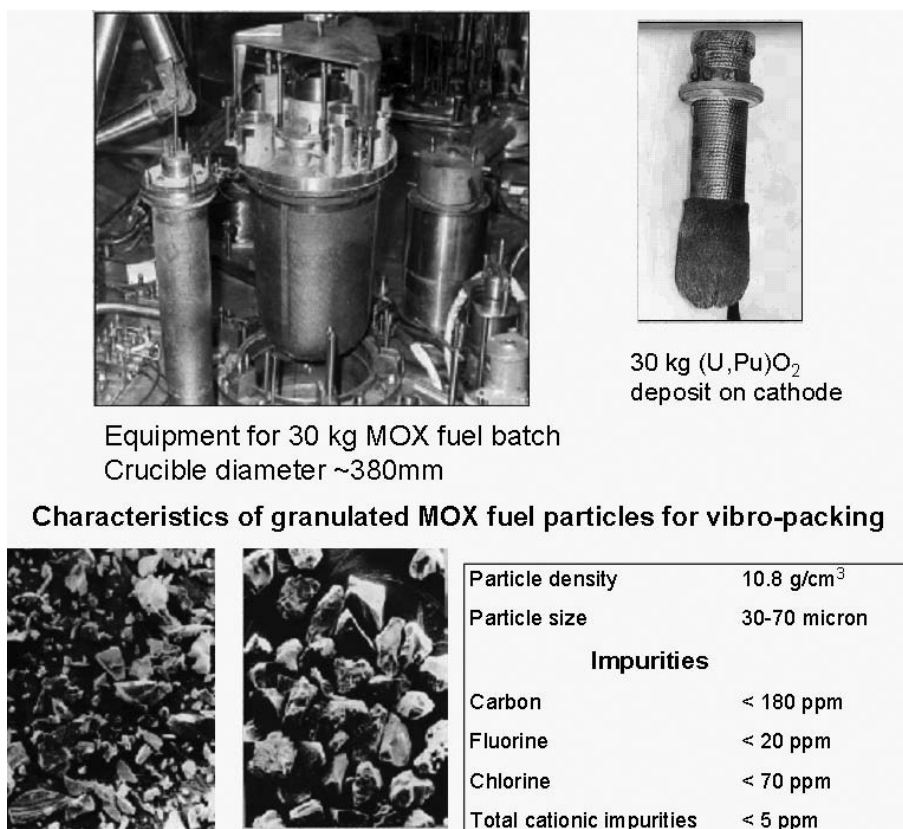
FIG. 18. The chlorinator electrolyzer facility with 30 kg MOX fuel batch, co-deposited MOX and characteristics of the granulated MOX particles for vibratory compaction.

burnup values of 130 GW·d/(t HM), though none have exceeded 150 GW·d/(t HM). In addition, some experimental pins irradiated in test and prototype reactors throughout the world have attained burnup levels greater than 210 GW·d/(t HM).

Conditions in fast reactor cores cause restructuring of the MOX fuel. Four distinct regions at linear heat generation rates of 40 kW/m and above have been formed. The innermost region is a central void that results from transport of as-fabricated porosity and some of the fuel cladding gap up the temperature gradient to the fuel centre.

The fuel surrounding this void consists of dense grains, of at least 98% theoretical density (TD), that are elongated radially. These grains form lenticular voids that move inwards by fuel vaporizing from the hotter (inner) side of the voids and condensing on the cooler (outer) side, giving a net outward movement of fuel. The lenticular voids develop from large (>5 µm) fabrication pores or startup cracks in the fuel, which heal in the process. Zones of increased plutonium content may be observed within this columnar grain region as well. Outside the columnar grains is a region where temperatures are sufficiently high for grain growth to take place by bulk diffusion. The enlarged fuel grains in this region, although normally termed 'equiaxed', are slightly elongated in the direction of the temperature gradient with their boundaries invariably decorated with gas bubbles and fission product inclusions.

The fuel between the equiaxed grain growth region and the cladding retains its original microstructure and density and is simply labeled the unrestructured region. Fuel in this region operates at temperatures below about 1200°C, where mobilities are low and where, therefore, the fuel tends to retain most of its original characteristics.

3.3.1. Fuel failure and irradiation behaviour

It is important that, for safe operation, the integrity of the cladding be maintained during irradiation. There are four main threats to the cladding integrity in FBR pins [24]:

— Manufacturing defects;
— Mechanical interaction between pin, spacer and wrapper;
— Fuel cladding mechanical interaction (FCMI);
— Fuel cladding chemical interaction (FCCI).

Fuel cladding mechanical interaction has been largely overcome by suitable fuel pin design such as lower smear density, annular pellet, etc. However, it could be an issue at higher burnup (>200 GW·d/t) for structural materials even with large incubation doses.

Among the defects mentioned above, the first two have been identified as the cause in over 40% of the failures in European fast reactors. FCCI in FBR pins is caused by the migration of oxygen and volatile fission products to the fuel surface due to the severe operating conditions and generally low density of the oxide fuel. FCCI consists mainly of the oxidation of constituents of the cladding material, particularly chromium, in the presence of caesium, molybdenum, tellurium and iodine.

FCCI has been observed in a number of forms, with broad front oxidative attack being the most commonly observed mode. The extent of this type of attack is influenced by fuel and cladding temperature and oxygen potential but is not related to stress. The mechanism is generally believed to be a fission product assisted oxidation process with caesium the main catalyst, although the presence of tellurium has been identified in some cases. The extent of FCCI increases progressively with burnup but is not considered a life limiting feature since pin designs have taken the anticipated clad wastage into account. It should be noted that the experience gained with fuel in Phénix, PFR, JOYO and FFTF since the 1970s, in which there have been only two failures attributed specifically to FCCI. This lower than expected incidence of failure has been attributed to the ability of the volatile fission products to buffer the oxidation of the cladding by absorbing the excess oxygen and forming oxides in the fuel–cladding gap [25, 26].

3.3.2. Irradiation capabilities of MOX fuel

The experience gained from irradiation experiments and post-irradiation examination has led to the conclusion that the behaviour of MOX fuel is not a life limiting factor for fuel pins, even under the stringent high burnup requirements. The main observations confirming this point are:

— A moderate fuel swelling rate, even at very high burnup, and no dramatic degradation of heat transfer properties;
— Problems of mechanical and chemical interaction between the fuel and cladding can be overcome with adequate pin design. Recommended variations include using a moderate linear heat rating and increased pin diameter, resulting in a lower fuel surface temperature, a greater cladding thickness and lower initial oxygen to metal (O/M) ratio;

— In the case of pin failure, no major reaction of fuel with coolant, which might lead to a great loss of fissile material or to a rapid development of secondary failures, or to failure propagation within the assemblies, has been observed.

On the basis of the excellent results obtained with MOX, it is currently believed that the target burnup for future large FBRs of 200 GW·d/(t HM) can be reached with this fuel type.

3.3.3. Fuel behaviour in transient and accident conditions

A number of experimental investigations into the behaviour of FBR fuel in accident or off-normal conditions have been carried out. The safe and reliable performance of MOX fuel was demonstrated in an extensive and broad based testing programme in EBR-II in the Argonne National Laboratory (West) facility in Idaho [27]. A total of 57 tests were completed including 100% overpower transients, long term operation with multiple fuel failures and power to melt tests. These tests showed that MOX fuel pins can survive such off normal conditions with little or no effect on their performance — in particular, breached blanket pins had no definitive effect on plant operations and the most limiting parameter for reliability was shown to be the integrity of the cladding properties.

Fuel pin diameter should be looked at first when considering core optimization because it dominates most of the other design parameters including fissile content, breeding ratio, specific power and fissile specific inventory. If the design requirement is higher breeding ratio, then the pin diameter has to be larger. However, the specific power of the reactor will go down and requires larger fuel inventory. From the economic point of view, a large diameter fuel pin has many advantages because it reduces fuel fabrication cost per unit weight of fuel and because it is effective in lowering any power mismatch due to the burnup extension. It is assumed that the economically optimum outer diameter of high burnup fuel is much greater than those designed in the past. Design studies from this viewpoint are being conducted on high burnup cores with large diameter fuel pins [28].

While a number of countries have postponed their fast reactor development programmes, countries like Japan in particular, continue with new work programmes. Examples include:

— A development programme on a simplified and shortened pellet fabrication process, the 'SPP', is under way at JNC, the aim of which is to reduce the cost of MOX fuel fabrication markedly [29];
— Long life materials for structural components are essential for extending the fuel discharge burnup; oxide dispersion strengthened steels are being developed to endure a fast neutron exposure of 250 dpa at 700°C [30];
— Feasibility studies on a commercial FBR cycle system are also being conducted in Japan;
— In the Russian Federation, construction of a BN-800 reactor has started in which it is planned to use MOX fuel.

It is generally considered that melting temperature and thermal conductivity of irradiated mixed oxide fuel decrease with increasing burnup due to the buildup of fission products in a fuel matrix. However, few post irradiation examination data that make possible a detailed discussion of such irradiation effects have been reported because of large uncertainties of measured values. A more detailed description of irradiation behaviour of MOX fuels is available in Refs [2, 31].

4. CARBIDES AND NITRIDES

4.1. INTRODUCTION

Mixed uranium plutonium monocarbide (MC) and mononitride (MN) have been identified as advanced LMFR fuels, nearly three decades back, on the basis of their high heavy metal density, high breeding ratio (and in turn short doubling time), high thermal conductivity and excellent chemical compatibility with sodium coolant

[32]. MC and MN belong to the same family on the basis of their crystal structure (F.C.C, NaCl type) and similar physical and chemical properties. The monocarbides and mononitrides of uranium and plutonium have complete solid solubility. However, compared to mixed oxide fuel, the experience on monocarbide and mononitride fuels, although significant, remains very limited [5, 33, 11].

The research and development programmes on carbide and nitride fuels for FR were actively pursued in the USA, France, Germany, the United Kingdom and the Russian Federation during the 1960s and 1970s and a little later in India and Japan. The investigations were, however, restricted to UC, UN, (U, Pu)C, and (U, Pu)N fuels with a maximum plutonium content of 20%. Both helium bonded and sodium bonded carbide and nitride fuel have been developed and irradiated successfully to high burnup (up to 20 at.%).

Carbide fuels can be operated under ideal heat transfer condition at linear heat ratings ~1000 W/cm due to its high thermal conductivity. However, its high swelling rate necessitates provision of a large fuel clad gap resulting in poor gap conductance with helium as bond gas. To extract the full potential of the carbide fuel, sodium can also be employed as the bonding medium between fuel and the clad improving the gap conductance enabling high linear power operation. However due to the cumbersome handling of sodium during fuel fabrication and increased probability of clad carburization through transport of carbon from fuel to the clad through sodium and the degradation of quality of the bond due to voids, helium bonded fuel pins have been preferred over sodium bonded fuel pins. The fuel pin failure rate has been significantly lower in helium bonded fuel pins as compared to sodium bonded fuel pins. However, the helium bonded fuel pins cannot be operated at linear powers >600 W/cm. In the Russian Federation, a uranium monocarbide core was in operation in the BR-5 reactor from 1965 to 1971 and achieved a maximum burnup of 6.2 at.%. Mixed uranium plutonium monocarbide of plutonium rich composition (70% and 55% PuC), has been used as the driver fuel in the FBTR in India. The initial mixed carbide core (Mark I) with 70% PuC as the reference fuel is in operation since 1985 and has reached a peak burnup of 18 at.% without any fuel failure. An expanded mixed carbide fuel core (Mark II) with 55% PuC content is under irradiation [34].

A large number of UN sub-assemblies were also successfully irradiated in BR-10 core up to a burnup of 9 at%. In the BOR-60 reactor too, several UC, U(C, N), (U, Pu)C and (U, Pu)N test sub-assemblies were successfully irradiated to high burnup. In the USA, nearly 700 helium bonded and sodium bonded fuel pins containing MC and MN pellets were successfully irradiated in EBR II and FFTF to high burnup in the range of 10–20 at.%. Most of these pins were He bonded containing MC pellets. A limited number of test-irradiations were also carried out using 'vibro-packed' MC pins.

Irradiation-testings of monocarbide and mononitride fuel pins have also been carried out in thermal reactors, Rapsodie/Fortissimo and Phenix reactors in France, DFR in UK, BR-2 in Belgium, KNK-II in Germany, HFR (Petten), Netherlands and JRR-2 and JMTR in Japan. In none of these reactors has mixed carbide or mixed nitride been used as driver fuel.

Having equivalent densities and thermo physical properties, MC and MN behave basically the same way under irradiation. From the point of view of fabrication, nitride fuel has the following advantages: (a) it is not as reactive and as pyrophoric as MC, (b) it is relatively easier to fabricate single phase MN since plutonium forms only the mononitride and the higher nitrides of uranium (UN_2 and U_2N_3) are unstable and easy to dissociate to UN by high temperature ($\geq 1\,673$ K) treatment in vacuum or argon. The major problem of MN fuel is the formation of radioactive ^{14}C by (n,p) reaction with ^{14}N and the high parasitic absorption of fast neutrons by ^{14}N. The problem of ^{14}C could be avoided by using ^{15}N. However, the process of ^{15}N enrichment is expensive.

4.2. FABRICATION EXPERIENCE

The different techniques of synthesis and consolidation of MC and MN are similar because these non-oxide actinide compounds are isostructural, completely solid soluble and have very similar physical, chemical and thermodynamic properties. UC, PuC, (U, Pu)C, UN, PuN and (U, Pu)N are difficult and expensive to fabricate because of the following main reasons:

— Firstly, the numbers of process steps are more compared to that of oxide fuel;

— These actinide compounds are highly susceptible to oxidation and hydrolysis and are pyrophoric in powder form. The entire fabrication is, therefore, required to be carried out inside leak tight glove boxes maintained in an inert cover gas (N_2, Ar, He etc) atmosphere containing minimal amounts of oxygen and nitrogen (<20 ppm each);

— The stringent control of the carbon contents is needed during the different stages of fabrication in order to avoid the formation of the unwanted metallic phase and for keeping higher carbides (M_2C_3 and MC_2) within acceptable limits. Higher nitrides (M_2N_3 and MN_2) dissociate to MN at elevated temperature ($\geq 1400^{\circ}$C) in inert atmosphere and pose no problem.

Table 8 summarizes the basic differences in the manufacturing of carbide and nitride fuel with the oxide fuel.

The two main steps for fabrication of UC, UN, PuC, PuN, MC and MN fuels comprise; (a) preparation of buttons, powders, clinkers, or sol-gel microspheres of the monocarbide or mononitride, starting either from the oxide or from the metal; (b) fabrication of fuel pellets, followed by loading of the fuel pellet stack in cladding tube and encapsulation or vibro-packing of granules or microspheres in fuel cladding tube followed by encapsulation [10].

4.2.1. Synthesis of MC and MN

The following are the principal methods of synthesis of MC and MN [10, 35, 36]:

— Direct synthesis by arc-melting;

— Hydriding-dehydriding of bulk metal (to form fine metal powder) followed by carburization and nitridation with methane/propane and nitrogen for obtaining fine powders of MC and MN respectively;

— Carbothermic reduction of oxide-carbon mixture in vacuum/argon and flowing nitrogen for preparation of MC and MN respectively.

TABLE 8. COMPARISON OF MIXED URANIUM PLUTONIUM OXIDE, CARBIDE AND NITRIDE FUEL FABRICATION USING UO_2 AND PuO_2 POWDERS AS FEED MATERIALS [M = U, Pu OR (U, Pu)]

	Basis	Oxide	Carbide/Nitride
1.	Principal steps in fabrication	(a) Co-milling of UO_2 and PuO_2 (b) Compaction (c) Sintering	(a) Mixing of UO_2, PuO_2 and Carbon (b) Tableting (c) Carbothermic reduction (d) Crushing (e) Milling (f) Compaction (g) Sintering
2.	Glove box atmosphere	Air	Inert gas: Ar or N_2 containing < 20 ppm each of O_2 and moisture
3.	Process controls	(a) O/M (b) Pellet density	(a) C/M or N/M (b) O, C & N contents of powder and pellet (c) MO_2, M_2C_3 & MC_2 or MO_2, MN_2 and M_2N_3 contents of powder and pellets (d) Pellet density
4.	Additional equipment for (U, Pu)C fabrication		(a) High temperature furnace for carbothermic reduction (b) O, N and C analysers (c) Trace oxygen and moisture monitors (d) Personnel safety oxygen monitors (e) Inert gas system — once through or recirculation — purification

Among these methods, the carbothermic reduction of oxides is the most attractive route for large scale production and has, therefore, been studied extensively in all the laboratories associated with the development of MC and MN fuels. In the carbothermic reduction of oxide, a high degree of microhomogeneity of the starting oxide-carbon mixture is necessary. Otherwise, localized deficiencies and excesses of carbon will lead to the formation of unwanted phases. The requisite homogenization is achieved either by a 'dry method' involving prolonged milling and blending of the oxide-carbon powder-mixture followed by pelletizing or alternatively by a 'wet chemical route', popularly known as the 'sol-gel' process. In the 'sol-gel' route, gelled microspheres (100–200 µm) of oxide plus carbon are prepared from the nitrate solution of uranium and plutonium by ammonia external or internal gelation processes.

Figure 19 shows the sol-gel process adapted by the Paul Scherrer Institute (PSI), Switzerland, for fabrication of high density (U, Pu)C and (U, Pu)N microspheres for manufacturing 'vibro-sol' fuel pins. The ammonia 'internal gelation' was followed for preparation of the hydrated gel-microspheres.
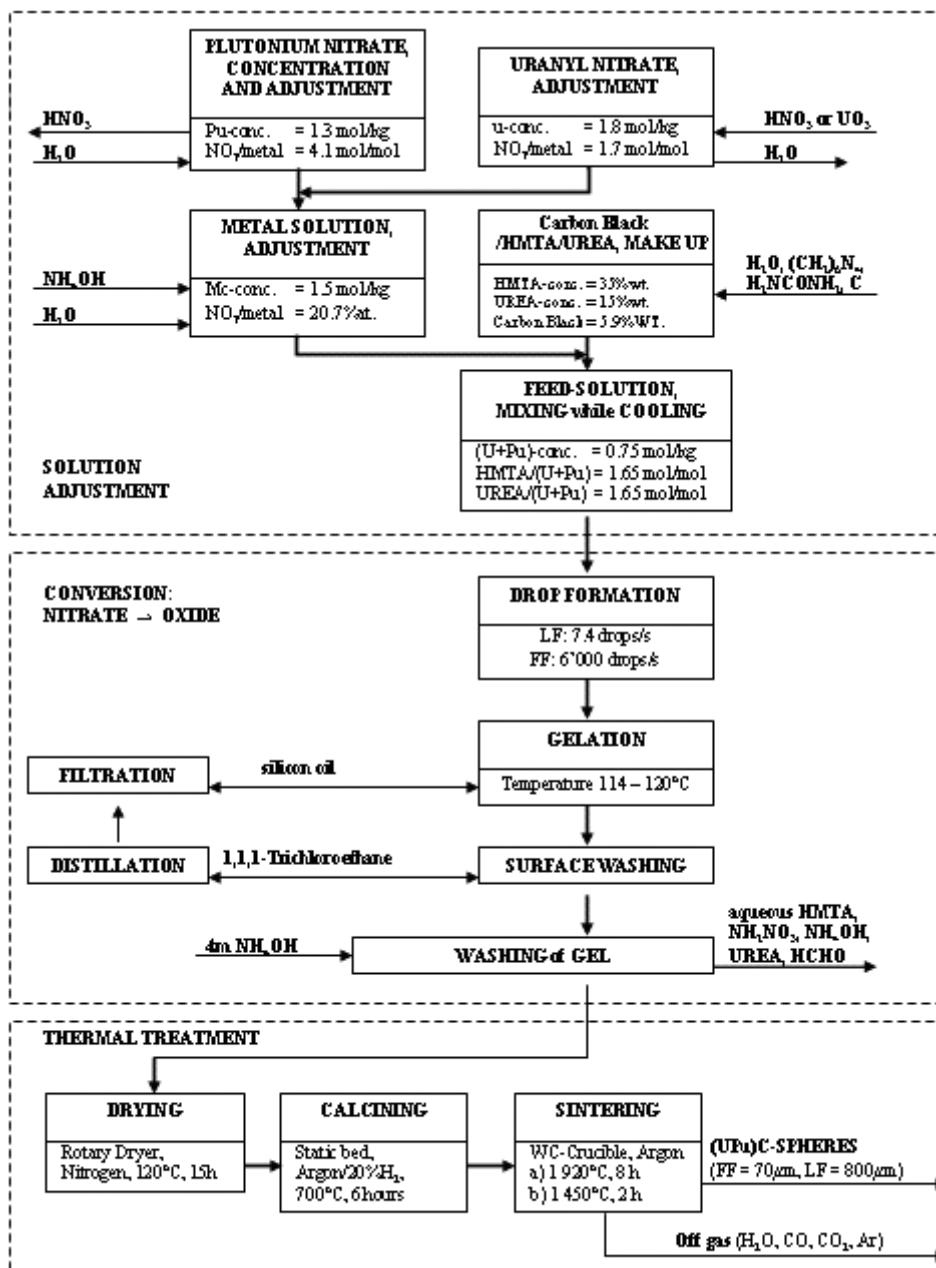

FIG. 19. Vibro-sol process, using ammonia internal gelation, for manufacturing (U, Pu)C and (U, Pu)N fuel pins in PSI, Switzerland.

4.2.2. Carbothermic synthesis of (U, Pu)C from oxide

The overall simplified chemical equation for the production of monocarbide by carbothermic reduction of oxide can be represented by the following reaction [10, 35] :

$$MO_2 + 3\,C = MC + 2\,CO \uparrow \tag{4.1}$$

where MO_2 is either a mechanical mixture or a solid solution of UO_2 and PuO_2.

Figure 20 summarizes the various carbothermic reduction techniques developed for the synthesis of MC. During carbothermic reduction, the control of the partial pressure of carbon monoxide is very important since the evolution of this gas not only constitutes the primary reduction mechanism but also controls the kinetics of this reaction.

'Single-step, solid state synthesis in a static bed' is the simplest technique for preparation of MC. In this method, the MC end product will always contain M_2C_3 second phase and residual oxygen and nitrogen impurities. This is because oxygen and nitrogen act as carbon equivalents and replace 'C' in the MC lattice to form the compound $(U, Pu)(O_xN_zC_{1-x-z})$, where 'x', z and their summation is less than 1.0.

Figure 21 illustrates the process steps followed in India for preparation of plutonium rich (U, Pu)C pellets for FBTR by the single step 'carbothermic synthesis' route in a static bed.

'Two-step solid state synthesis in a static bed' is an improvement over the single-step synthesis and aims at the preparation of single-phase MC with very low oxygen and nitrogen contents and with practically no losses of plutonium by volatilization. M_2C_3, unlike MC, has very little oxygen and nitrogen solid-solubility and can be easily formed at a lower carbothermic temperature, thereby, minimizing plutonium volatilization loss. In the first step, carbothermic reduction at a relatively low temperature with excess carbon ensures that only M_2C_3 is formed. In the
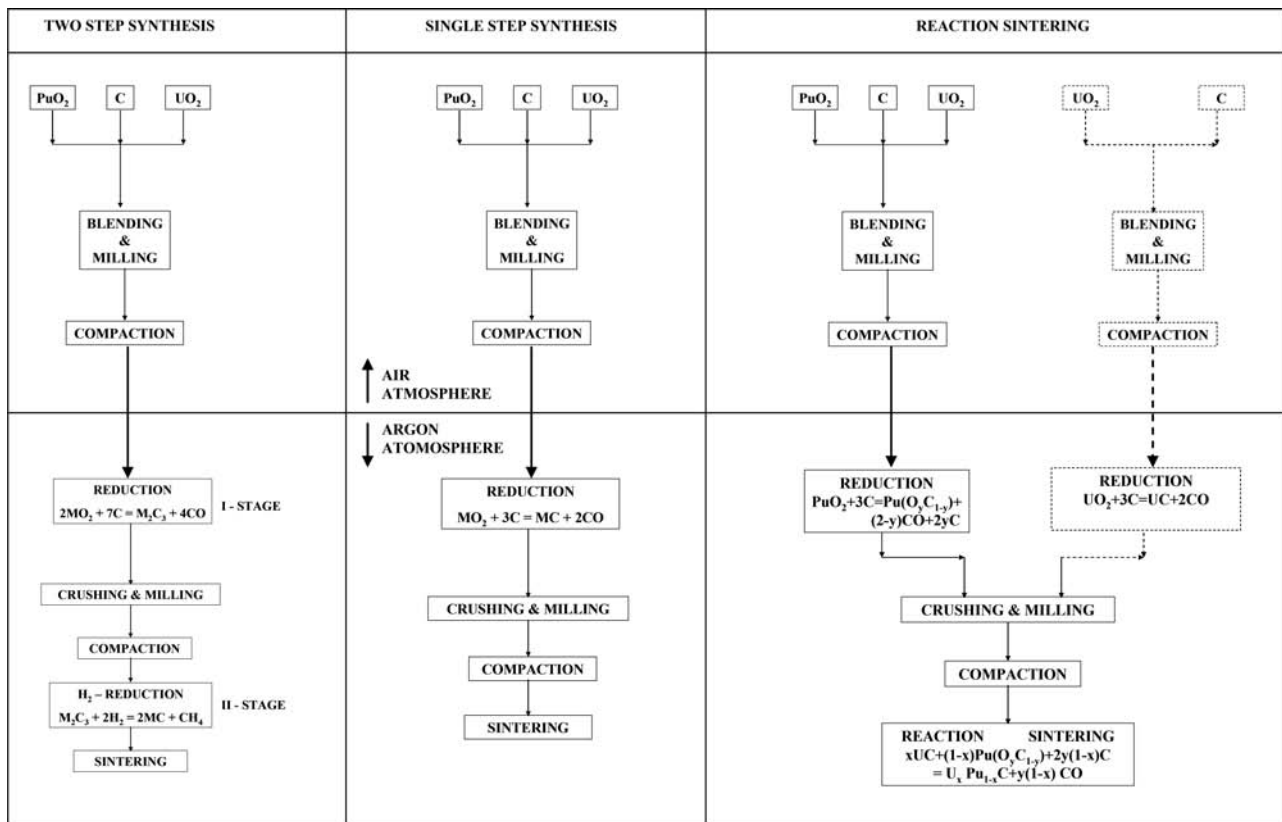

FIG. 20. Different carbothermic reduction processes for synthesis of (U, Pu)C starting from UO2 and PuO2 powders (single step synthesis of oxide + graphite mixture is most common).
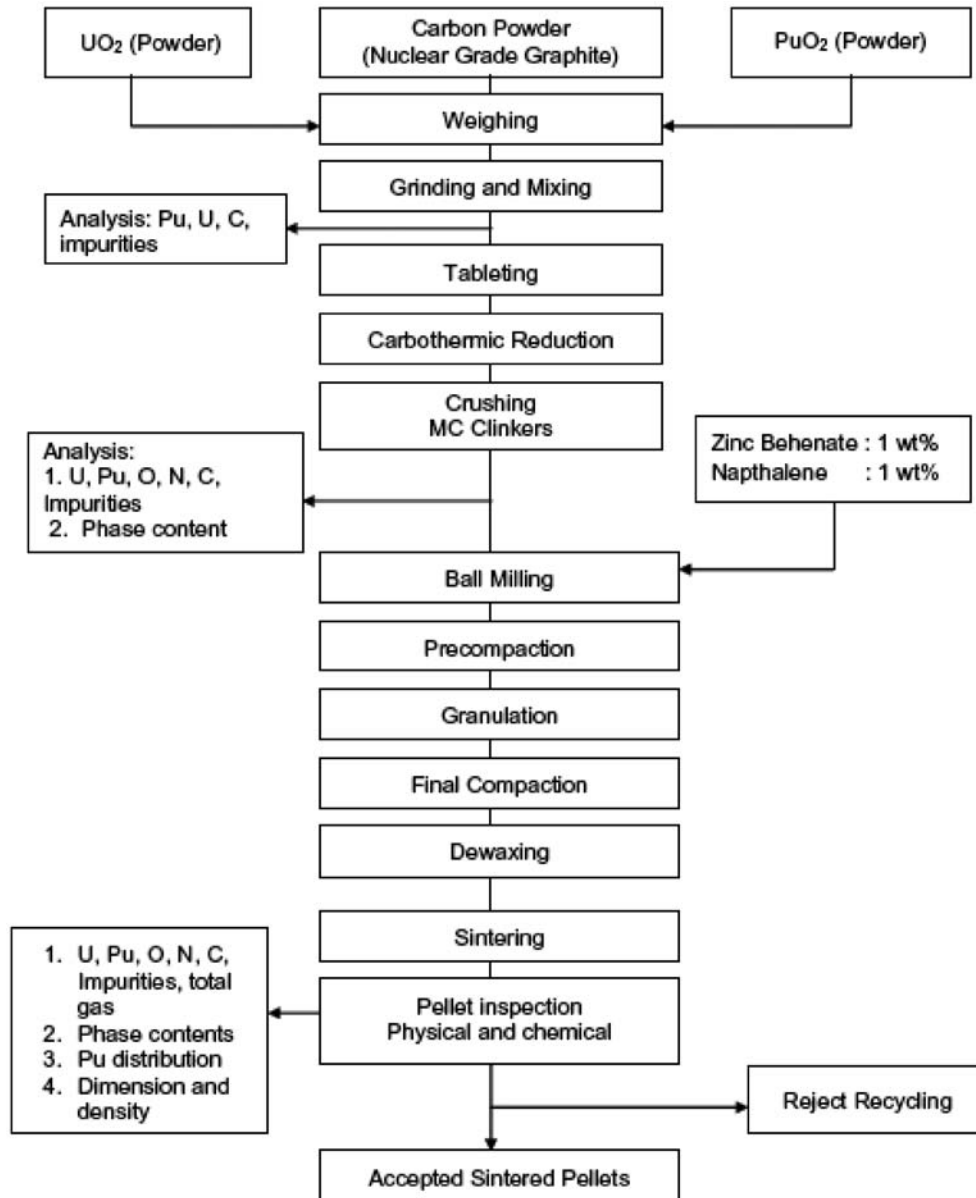
FIG. 21. Process steps followed in India for preparation of plutonium rich (U, Pu)C pellets for FBTR by the 'single step 'carbothermic synthesis' route in a static bed.

second step, the M_2C_3 is crushed, milled and treated with hydrogen at ~1 123 K in order to reduce it to MC and remove free carbon as methane.

The three-step 'reaction-sintering' process involves separate preparation of UC and plutonium oxycarbide by carbothermic synthesis of the respective oxides. The low temperature of plutonium oxycarbide formation minimizes the plutonium volatilization loss. In the third step, the uranium carbide and plutonium oxycarbide powders are blended, compacted and subjected to reaction sintering.

4.2.3. Carbothermic synthesis of (U, Pu)N from oxide

The overall chemical reaction for carbothermic synthesis of MN starting from the oxide can be represented by the following equation [32]:

$$MO_2 + 2C + 1/2\ N_2 = MN + 2CO \uparrow \tag{4.2}$$

In the carbothermic synthesis of MN, N_2 plays the dual role of the reactant and the carrier for the removal of CO. The reaction product will have the general formula ($MN_{1-x-y}C_xO_y$). The oxygen and carbon retained in MN will depend on the partial pressures of nitrogen and carbon monoxide, flow rate of reacting gas (N_2, $N_2 + H_2$), the oxide to carbon mole-ratio of the starting MO_2-C mixture and whether hydrogen is used for removing the excess carbon [38, 39]. The ideal way to obtain nearly single phase MN with very low oxygen, carbon and higher nitride is to use around 10% excess carbon in the oxide-carbon mixture, a synthesis temperature of 1500–1600°C in flowing N_2, followed by $N_2 + H_2$ and Ar. The CO in the exhaust gas should be closely monitored.

The process flow sheets followed for synthesis of (U, Pu)N fuel by 'powder-pellet', SGMP and vibro-sol processes are shown in Fig. 22.

The initial oxides and carbon are mixed up in ball mill/attritor and are pressed at a pressure of 75–150 MPa. The tablets are loaded in the furnace and heated up in a flow of nitrogen for nitriding and followed by nitrogen-hydrogen mixture for removal of excess carbon. Temperature of uranium nitride production is from 2020 to 2220 K, and mixed uranium-plutonium nitride is from 1820 to 1920 K. At the end of nitriding process the product is cooled in argon atmosphere to avoid formation of U_2N_3.

4.2.4. Consolidation of MC and MN

The principal methods of consolidation of MC and MN microspheres or powders in the form of small diameter fast reactor fuel pins are:

— Cold pelletization of the powder into pellets followed by sintering;
— Direct pressing;
— Vibratory compaction of the granules, microspheres or crushed clinkers in cladding tubes;
— Sol-gel microsphere pelletization.

In the fabrication process involving cold pelletization followed by sintering, suitable binders and sintering aids (if any) are added to the milled powder and the milling is continued for several hours for proper homogenization. However, the use of attritor instead of ball mill reduces the milling time for powder homogenization significantly. The powder is then compacted into pellets (length to diameter ratio ~1.6), preferably in a double action press at 60–200 MPa, followed by sintering in argon – hydrogen gas or vacuum in the temperature range 1400–1900 °C. Pellets of MN with density 88–95% of theoretical are produced by pressing at 100–300 MPa and sintering in vacuum or in an atmosphere in argon and hydrogen mixture at ~1600 °C.

In the 'direct pressing' route, [1] the MC or MN clinkers after carbothermic synthesis are directly compacted and sintered thus avoiding the crushing and milling steps. This process generates fuel pellets with densities in the range of 80–88% TD, reduces oxygen contamination, risk of self-ignition, dust generation, radiation exposure to personnel, concentration of metallic impurities, etc.

The vibratory compaction or vibro-sol route has several advantages over the 'powder-pellet' route. First, the number of fabrication steps is less and there is maximum flexibility of operation. Given two or three different sizes of particles, fuel cladding tubes of any internal dimensions can be vibro-filled to a wide range of smear densities (60–90% TD). Unlike the other methods, the questions of surface grinding of rods, centreless grinding of pellets and die or mold sizing for particular pins do not arise at all [1]. The vi-pack route is amenable to automation and remotization and avoids handling and generation of fine MC and MN powders, which are highly radiotoxic and pyrophoric.

The SGMP process is a hybrid of the 'vibro-sol' and the 'powder-pellet' routes, where the fabrication advantages of sol-gel process is combined with the in-pile performance advantages of 'pellet-pin' design [43]. The advantages of SGMP process are as follows:

— 'Radiotoxic dust hazard' and pyrophoricity hazard are minimized;
— Dust free and free flowing microspheres facilitate automation and remotization;
— Fabrication steps for monocarbide and mononitride fuel pellets are significantly reduced;
— Excellent microhomogenity is ensured in fuel pellets because U and Pu are mixed as nitrate solutions;
— Fabrication of relatively low-density pellets (~85% T.D.) with 'open' pore structure specified for He-bonded FR fuel pins is possible without addition of pore former.
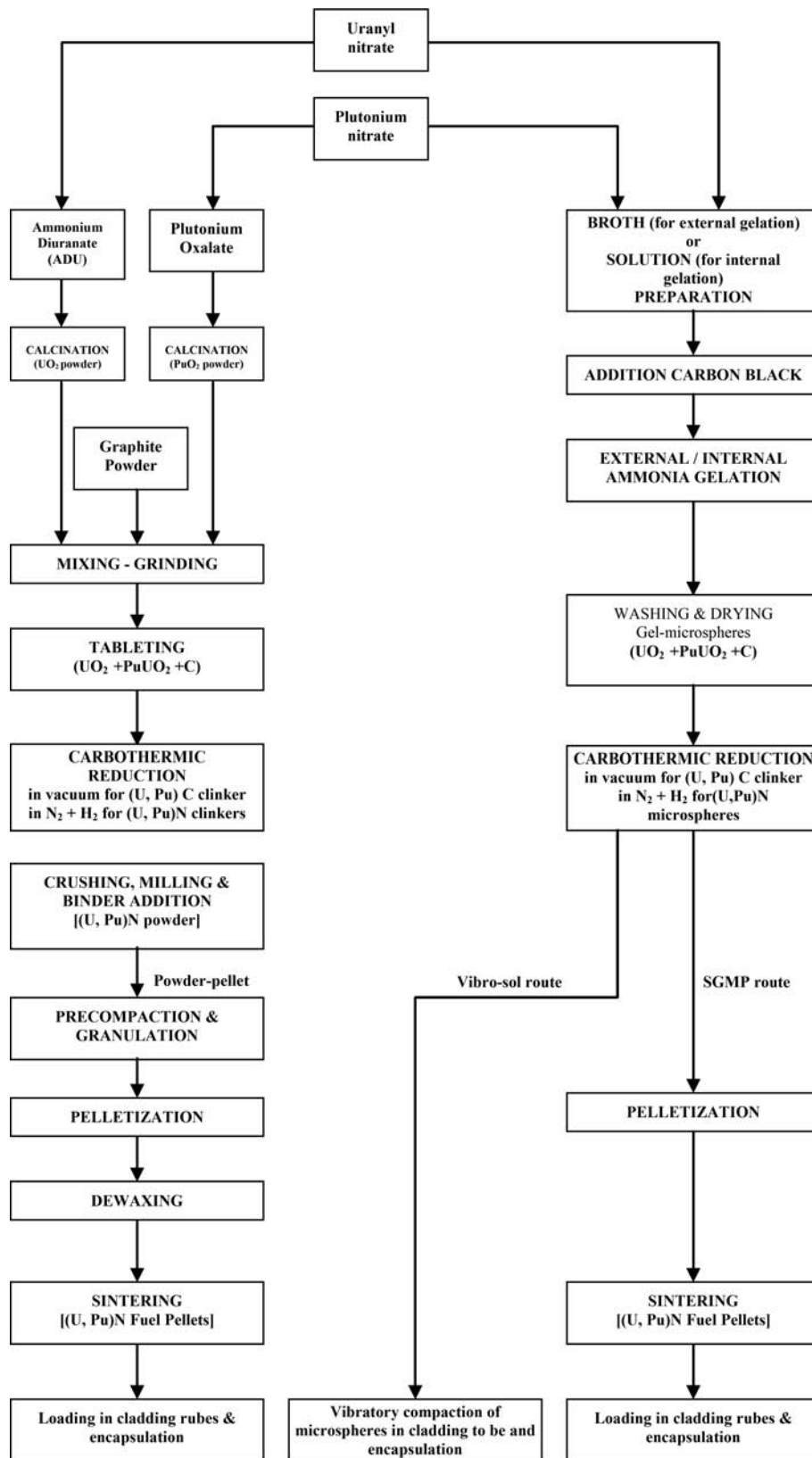
FIG. 22. *Process flow sheet generally followed for synthesis of (U, Pu)N from UO$_2$ and PuO$_2$ powders.*

The process flow sheet developed in India consists of the following major steps:

— Preparation of hydrated gel-microspheres of $UO_3 + PuO_2$ and $UO_3 + PuO_2 + C$ by 'ammonia internal gelation' process, using hexamethylene tetra amine (HMTA) as ammonia generator, urea as a buffer and silicone oil at 90°C as gelation bath;
— Carbothermic synthesis in vacuum and flowing $N_2/N_2 + H_2$ for preparation of press-feed microspheres of (U, Pu)C and (U, Pu)N respectively;
— Cold-pelletization and sintering.

The dust free and free flowing MC and MN microspheres are directly cold-pelletized at around 1200 MPa and sintered at 1700°C in Ar + 8% H_2 atmosphere.

4.3. IRRADIATION EXPERIENCE

4.3.1. EBR-II and FFTF, USA

During the 1970s and early 1980s a substantial development effort was directed towards irradiation testing of mixed carbide fuel in EBR-II and FFTF. Some 470 MC fuel rods were irradiated in EBR-II and another 200 fuel rods were irradiated in FFTF. The parameters explored included: sodium or helium bond, variation in cladding type, (316, D9, 321 stainless steels and ferritic HT-9 and nickel based PE-16), variation in pellet density (84% TD for solid fuel pellets and 97% TD for annular pellets), variation in pellet cladding gap size (0.13–0.2 mm) and both pellet and sphere-pac fuel. In most cases, all the high density pellet pins failed whereas all low density pellet pins survived. The main conclusion was that the fuel cladding mechanical interaction (FCMI) is too severe for pellet densities in excess of 85 % T.D.

During the course of irradiating MC fuel in EBR-II, 21 fuel breaches occurred. Fifteen of the breaches occurred with PE-16 clad fuel. The failures were due to the embrittlement of the cladding where the failures tended to occur under the wire wrap. The remaining six were observed to be in Na-bonded rods, but those results were deemed less relevant because emphasis was placed on He-bonded MC fuel [44]. One rod breached in FFTF, but there was no post-irradiation examination of that rod. The FC-1 FFTF experiment (a full-size, 91-rod FFTF assembly) attained goal burnup with breach. A peak fuel burnup of 20 at.% was achieved in EBR-II for 10 MC fuel rods clad in Type 316 stainless steel [10, 45]. Of those rods, 5 had experienced a 15% transient-overpower test in EBR-II after attaining 12 at.% burnup. Thirteen other He-bonded rods and 3 Na-bonded rods attained 16 at.% burnup in EBR-II without breach. The FFTF AC-3 experiment results showed that, for the relatively low temperature conditions used for the test, the pellet fuel and sphere-pac exhibited only minor differences in behaviour, and both performed in a manner consistent with the rest of the MC fuel database [46].

MC fuel tends to crack because the relatively high thermal conductivity of carbide fuel allows the fuel to operate at a low temperature where its brittle properties cannot withstand even the modest tensile stresses formed under a thermal gradient. Such cracking and resulting fuel relocation has not been observed to cause premature pin failure. Carbide fuel failures typically result from FCMI, owing to the fact that fuel swelling is greater than that of the oxide which leads to early fuel/cladding gap closure, and since it generally operates at relatively low temperature, fuel creep is not effective at relieving cladding stress [44]. For this reason, MC fuel pin design must incorporate a large fuel/cladding gap and make use of a low density fuel in order to delay the onset of FCMI. While cladding carburization has been a historical concern for MC fuels, and was observed in the Type 316SS-clad rods irradiated in EBR-II, no fuel failures have been attributed to this phenomenon [44, 47].

Ten transient-overpower tests involving MC fuels were conducted in TREAT using fuel irradiated in EBR-II to burnup ranging from 0 to 12 at.%, primarily for the purposes of establishing that cladding breach would occur at a margin above that of the FFTF plant protection system settings (at 115% and 125% overpower). The results suggested FCMI-induced breaches, but most importantly indicated comfortable margins to failure (roughly 3 times nominal linear heat generation rate in a MC fuel and up to 6 times the nominal linear heat generation rate typical of oxide fuel cores). The rods indicated only small cladding strains and small amounts of liquid-phase penetration of the cladding. The conclusion of the test series was a determination that nothing in fuel transient-overpower response would prevent or limit application of MC fuels to fast reactors [10, 47].

The EBR-II tests also included rods irradiated beyond goal burnup to breach and one intentionally defected rod irradiated for 100 days beyond cladding breach. The intentionally defected rod exhibited a reaction between the fuel and the coolant (presumed to be the oxygen within the coolant) that resulted in a higher specific volume reaction product that caused expansion and widening of the defect. However, it was observed that little fuel was released from the cladding into the coolant. Other rods irradiated to natural breach in EBR-II did not exhibit that phenomenon. MC fuels appear to operate benignly after cladding breach [16, 44]. Another experiment in EBR-II irradiated a MC fuel rod with a purposely induced Na-bond void intended to simulate a Na bond void resulting from Na expulsion during irradiation, and although the fuel rod exhibited microstructural changes reflecting a local high fuel temperature, there was no loss of cladding integrity. This experiment indicated that MC fuel would withstand a Na bond expulsion of some magnitude. A detailed presentation of MC characteristics and performance is given in [32, 10].

The irradiation performance database for MN fuels is substantially smaller than that for MC fuels. Compared to MC fuels, MN fuels exhibit less fuel swelling, lower fission gas release, and are considerably easier to reprocess; however, the problem of the production of biologically hazardous ^{14}C in nitride fuels fabricated using natural nitrogen poses a considerable concern for the reprocessing of MN fuels [48].

MN fuels were found to exhibit extensive cracking and fragmentation during simple startup and shutdown transients if operated at high temperatures. This cracking phenomenon was considered to be the reason for the early fuel failures seen in US irradiation tests [49]. Use of a metallic shroud around the fuel column to prevent fuel relocation subsequent to fragmentation provided an engineering solution to this problem to some extent. Nevertheless, the US specifications for MN fuels recommended that their peak fuel temperatures be restricted to as low as 1200°C to mitigate fragmentation and eliminate the need for the use of shrouds. A further issue of concern regarding MN fuels was that they dissociate at temperatures substantially lower than their congruent melting point if a nitrogen overpressure is not maintained. A more detailed description of MN fuel characteristics and performance is given in [32].

4.3.2. FBTR, India

The fast breeder test reactor (FBTR) in India uses a unique mixed carbide of high plutonium content $(U_{0.3} Pu_{0.7})C$ as the driver fuel and 20% cold worked austenitic stainless steel SS316 as the core structural material. A design limit of 50 GW·d/t burnup and linear heat rating of 320 W/cm was arrived for this fuel composition based on out of pile experiments, physiochemical characterization and theoretical studies. However, the burnup of this fuel has been progressively increased to about 160 GW·d/t at a peak linear heat rating of 400 W/cm aided by stage-wise post irradiation examination (PIE) carried out after 25, 50, 100 and 155 GW·d/t burnup and thermo-mechanical modelling. No fuel pin failure has occurred so far indicating the excellent performance of mixed carbide fuel.

Swelling of the fuel was studied at different burnups using non-destructive techniques like X radiography and neutron radiography and destructive techniques like ceramography. The lower operating temperatures with higher Pu content of the fuel resulted in lower swelling rates even at high burnup. Ceramography of fuel cross sections at lower burnups indicated free swelling regime as evident from the radial cracking patterns and observed post-irradiation fuel-clad gap. The free swelling rates of the carbide fuel were in the range of 1–1.2% per at% burnup. Figure 23 shows the comparison of photo-mosaics of fuel-clad cross sections at the centre of the fuel column at different burnups. With increasing burnup beyond 50GW·d/t, the cracking pattern changed to circumferential with the closure of fuel-clad gap indicating a restrained swelling phase. A progressive reduction in the porosities was observed on the fuel microstructure with increasing burnups. At the burnup of 155 GW·d/t, distinct porosity free peripheral zones were observed in the fuel. This indicated that Pu rich carbide fuel on account of its lower melting point exhibited sufficient plasticity to accommodate the swelling in fuel clad mechanical interaction (FCMI) regime by creeping (the melting temperature of mixed carbide with 70% PuC is 2 148 K and that of the fuel with 20% PuC is 2 750 K). The clad microstructure did not indicate any evidence of carburization even at high burnup. A maximum gas release of 16% and an internal pressure of 2.09 MPa in the fuel pin due to fission gas release indicate a low fission gas release in carbide fuel even at 155 GW·d/t burnup [50].

The major concern was the significant increase in dimensions of SS316 hexagonal wrapper and fuel pins and degradation in their mechanical properties. Dimensional changes were significant beyond 100 GW·d/t burnup (56 dpa) with a faster rate of increase at 155 GW·d/t (83 dpa) as compared to the trends at lower burnups. The

| 25 GWd/t BURN- | 50 GWd/t BURN- | 100 GWd/t BURN- | 155 GWd/t BURN- |
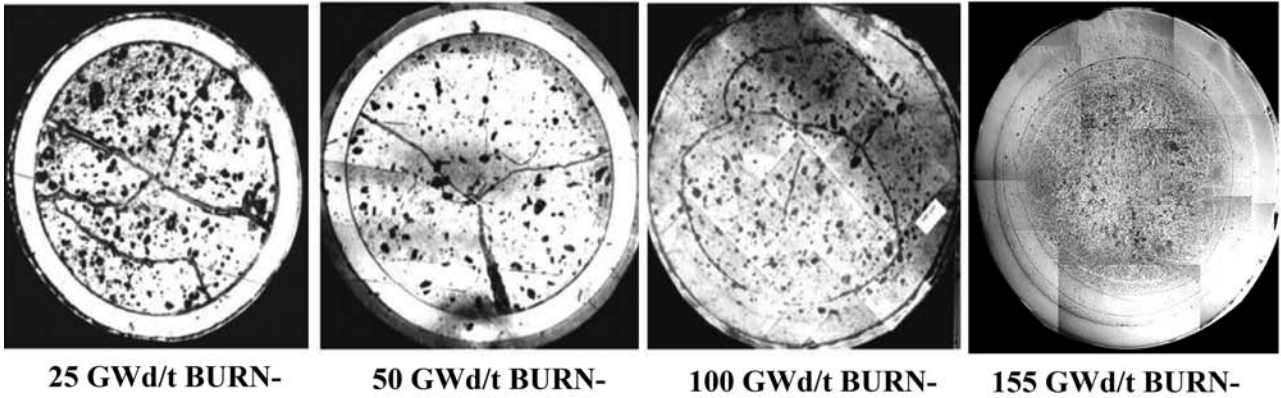
FIG. 23. Comparison of ceramographs of FBTR fuel-clad cross-section at various burnup.

measured strains were found to be predominantly from the void swelling of the SS316. While cladding operating at 723 K-803 K showed reduction in strength and ductility with increasing neutron displacement damage, the wrapper at 673 K-703 K indicated increase in strength (hardening) and reduction in ductility. Transmission electron microscopy (TEM) studies of irradiated SS316 showed extensive void formation beyond 40 dpa and precipitation of type Si rich M_6C (η) and cubic G phases at higher displacement damages.

4.3.3. Experience in France, Germany, the UK and the Russian Federation

In France, the (U, Pu)C fuel pins with 71% T.D. smear density reached a burnup of 12 at.% with clad deformation of 1 to 3%. The German mixed carbide fuel irradiation programme (75% TD smear density, 800 W/cm) was successfully tested under power cycling and transient conditions.

The mixed carbide pin irradiation programme in the UK was successful with low smear density (70% T.D.) vibro-packed fuel of about 1000 W/cm, with target burnup of 100 GW·d/t. From the analysis of the failed pins performed by the programmes mentioned above, the following conclusions can be made:

— The performance of He-bonded (U, Pu)C pins is strongly influenced by design parameters, in particular, smear and fuel pellet density and the pin diameter play a primordial role;
— Cladding breaches are due to fuel swelling and loss of clad ductility due to carburization. FCMI is tolerable only when the hoop stress exerted on the cladding is circumferential and of near-cylindrical symmetry. Localized stresses for long periods of time often lead to clad fracture.

Clad carburization in hyperstoichiometric fuel has been recognized as a problem, less in He-bonded pins but more in Na-bonded pins, where excessive carburization can occur with hyperstoichiometric (U, Pu)C$_{1+x}$. The carburization is generally characterized by the formation of $M_{23}C_6$ type carbide. The transfer of carbon from fuel to cladding could lead to serious clad carburization problem. The major driving force for the reaction between carbon and stainless steel is provided by the very low free energy of formation of various carbides among which those of the type (FeCr)$_{23}$C$_6$ are found to play the major role in the carburization processes; the equilibrium carbon activity of $Cr_{23}C_6$ is lower than the carbon activity of a hyperstoichiometric uranium carbide by several orders of magnitude. The dissociation reaction:

$$M_2C_3 \rightarrow 2\ MC + C \tag{4.3}$$

can therefore be thought to control carburization of steel cladding.

The problem of clad carburization in case of MN fuel has not been studied to the same extent as MC. In the case of He-bonded MN fuel pins, wherever the starting fuel contained about 3000 ppm O and C, the proposed transfer mechanism of C is either by diffusion through the fuel after contact with the clad or by CO/CO$_2$ transfer. The eradication of the clad carburization problem is possible only if the MN fuel contains very low residual oxygen

and carbon impurities. This could be achieved only if the MN powder is prepared by the hydriding-dehydriding followed by nitridation route and hot carbothermic nitridation of the oxide in the case of MN fuels.

Russian experience shows that carburization of austenitic stainless steel cladding in case of pure MN (content of O and C less than 0.2% of each) is 2.5 times lower than that of low purity MN. For MN with 0.2–0.5% O and 0.3–0.5% C, the depth of corrosion attack (carburization) was ~50 µm for He-bonded fuel at burnup of 8.2 at%.

4.3.4. Advanced fuels with minor actinides (MA)

Nitride is a candidate material of advanced fuels for fast reactors and for transmutation of minor actinide elements such as Np, Am and Cm because of its advantageous thermal and neutronic properties [52]. Nitride fuels are attractive primarily due to high thermal conductivity relative to actinide oxides, high actinide density, and simple phase equilibria — only a rock salt (face-centered cubic) phase is known to form in the Np, Pu, Am, and Cm systems. The major issue confronting the use of this fuel is the need to enrich nitrogen in the ^{15}N isotope in order to avoid production of large amounts of ^{14}C in reactor through the ^{14}N(n,p)^{14}C reaction.

Typically, ZrN, TiN, YN, or AlN are proposed as the inert matrix phase for nitride fuels. Recent emphasis has been on fabrication of these inert matrix fuels (IMF) of specimens for irradiation testing. NpN, (Np,Pu)N, (Np,U)N, AmN, (Am,Y)N, (Am,Zr)N, and (Cm,Pu)N have been recently prepared by JAERI by the carbothermic reduction of oxides [55]. For the heterogeneous recycling of Am and Cm without U, solid solution or dispersed fuels, so-called U-free fuels, can be used in order to attain the requirements of the target for ADS such as chemical and physical stabilities at high temperature and high radiation dose. Nitrides containing MAs such as AmN, (Am,Y)N, (Am,Zr)N and (Pu,Cm)N have already been synthesized by the carbothermic reduction technique using their oxide powders as starting materials, where a carbon-rich condition was chosen from the properties that MA elements reduce the stability of carbides and increase the stability of oxides. Pellets of (Pu,Zr)N and two-phased TiN + PuN have been fabricated and these pellets are undergoing irradiation testing. Activities on (Pu,Zr)N fuel fabrication are also conducted in Switzerland as part of the CONFIRM programme and in the USA as part of the AFCI programme [54].

5. METALLIC FUELS

5.1. INTRODUCTION

Metallic fuel was the first to be selected for the experimental fast reactors in the USA and the UK, in the 1950s, based on the ease of its fabrication, high thermal conductivity and high fissile and fertile atom densities, which facilitates higher breeding and the use of smaller cores. The EBR-I in the USA used unalloyed uranium, U-Zr and Pu-Al and the Enrico Fermi reactor was fuelled with U-Mo alloy. The DFR in the UK utilized the U-Mo alloy fuel and also tried the U-Cr alloy. The major drawbacks of metallic uranium and plutonium and some of their alloys are unusual irradiation growth and swelling attributed to anisotropic crystal structure and formation of low melting eutectic with the cladding material. With the addition of proper alloying elements, and following proper heat treatment, the isotropic phases are made predominant which enhanced the dimensional stability. The EBR-II initially operated with U-5% Fs (Fs is fissium, a simulated mixture of noble metal fission products of composition (wt%): 2.4% Mo, 1.9% Ru, 0.3% Rh, 0.2% Pd, 0.1% Zr and 0.01% Nb) cores and later used U-Zr as driver fuel. Later, an integral fast reactor (IFR) concept was developed in the USA, for which the choice of fuel was U-19 wt%Pu-10 wt%Zr. Zirconium was added to increase the solidus temperature of the fuel and to enhance the chemical compatibility between fuel and stainless steel cladding. A number of U-Pu-Zr fuel pins were irradiated in EBR-II and FFTF to high burnup (20 at.%) [57].

The closed fuel cycle, with the reprocessed product always remaining highly radioactive, was the key to proliferation resistance. This fuel cycle made use of, through fissioning, the minor actinides (americium, neptunium, curium) and as well the bred plutonium. During the 1990s to the present, the direct disposal of spent light water reactor (LWR) fuel in a permanent repository became an obstacle for the further use of nuclear power.

The actinides in the spent fuel, with their several thousand year half-lives and high heat loads, made licensing the repositories a difficult task, with many adversaries. If the actinides could be removed from the fuel and fissioned then the radioactive half-life of the spent fuel would be reduced to hundred year half-lives of the fission products in the fuel. The rationale for the repository would then be more credible, the heat load would be much less, and the capacity of the repository would increase.

The integral fast reactor (IFR) concept and its fuel cycle were developed in the USA, based on the actinide recycle Programme (ARP). The IFR fuel cycle, shown in Fig. 24, is based on reprocessing of its spent U-Pu-Zr alloy fuel using molten salt electro refining process.

The molten salt electro refining operation involves the following steps:

— Chopping of fuel pin containing spent fuel into pieces and loading into the electro refining cell in a basket;
— Addition of $CdCl_2$ to the electro refining cell at a temperature of 773 K to transfer most of the actinides, sodium and fission products as chlorides to the electrolyte (eutectic mixture of KC1 and LiCl);
— Deposition of U on a solid cathode (dendritic deposit);
— Introduction of cadmium cathode in the cell as the pre-determined concentration of Pu is reached in the electrolyte to deposit Pu and the remaining actinides, including an approximately equal amount of uranium on the cadmium cathode.

A cylindrical rod of low carbon steel (zirconium, molybdenum or uranium also may be used) is used as the cathode for selective deposition of uranium. The higher thermodynamic stability of $PuCl_3$ compared to UCl_3 renders the deposition of plutonium on solid cathode impossible, unless the $PuCl_3$ to UCl_3 ratio is >2 which is not realizable under normal process conditions. However, co-deposition of uranium and plutonium on liquid cadmium cathode is enabled by the lower activity coefficient of Pu in cadmium compared to that of uranium. Liquid cadmium cathode (liquid cadmium in a beryllia crucible) is used in the IFR reactor fuel cycle pyroprocess.

The deposit of uranium and plutonium on the cadmium cathode tends to grow and short the electrodes and hence a rotating cathode is used to compress the salt/cadmium surface to produce a deposit without dendrites. Cathode deposits are removed from the electrorefining cell after the process is completed. Uranium is separated from the salt (in case of solid cathode) and U-Trans-Uranium Elements (TRU) from cadmium (in case of molten cadmium) through distillation in a retort and then melted. Ingots of materials are used for fabrication of fuel elements by injection casting process [58, 59].

The R&D on fabrication of metal fuel has been performed at the plutonium facility in JAERI/JAEA under the collaboration of CRIEPI and JAERI/JAEA. A small amount of U-Pu-Zr alloy is now being fabricated at the plutonium facility in JAEA, and the alloy will be used for pin irradiation test in JOYO. The compatibility test between metal fuel and sodium was done. A very small scale irradiation test of metal fuel was done in Phenix, France and PIE was done mainly in ITU, Germany under collaboration between CRIEPI and ITU. The metal fuel pin irradiation test is planned in JOYO in near future.

Since 2007, fabrication technology of metallic fuel for the SFR is being developed in the Republic of Korea (ROK) as a national nuclear R&D programme.. Various casting technologies have been tested in laboratory scale. Rod-type samples of U-Zr and U-Zr-Ce (Cerium as Am surrogate) were fabricated by vacuum injection casting and vacuum-assisted gravity casting. Alternate fabrication techniques such as continuous casting which was used for fabrication of U rods and centrifugal atomization for the preparation of spherical powder of U-Zr are being developed.

5.2. FABRICATION

Metal fuel was fabricated with a variety of techniques. Many techniques were deficient in that they did not lend themselves to remote fabrication in a hot cell and special heat treatments and alloying were required to avoid excessive irradiation induced growth due to the preferred orientation of the alpha uranium.

Injection casting of the uranium alloyed fuel was developed early and proved to be the best method to fabricate the fuel in a remote environment. Figure 25 shows the principal components of a metal fuel pin. The fuel slug is cast such that a gap exists initially between fuel and cladding. The gap is sized to allow enough fuel swelling for interconnected porosity and gas release to occur. This phenomenon will be discussed further in the performance
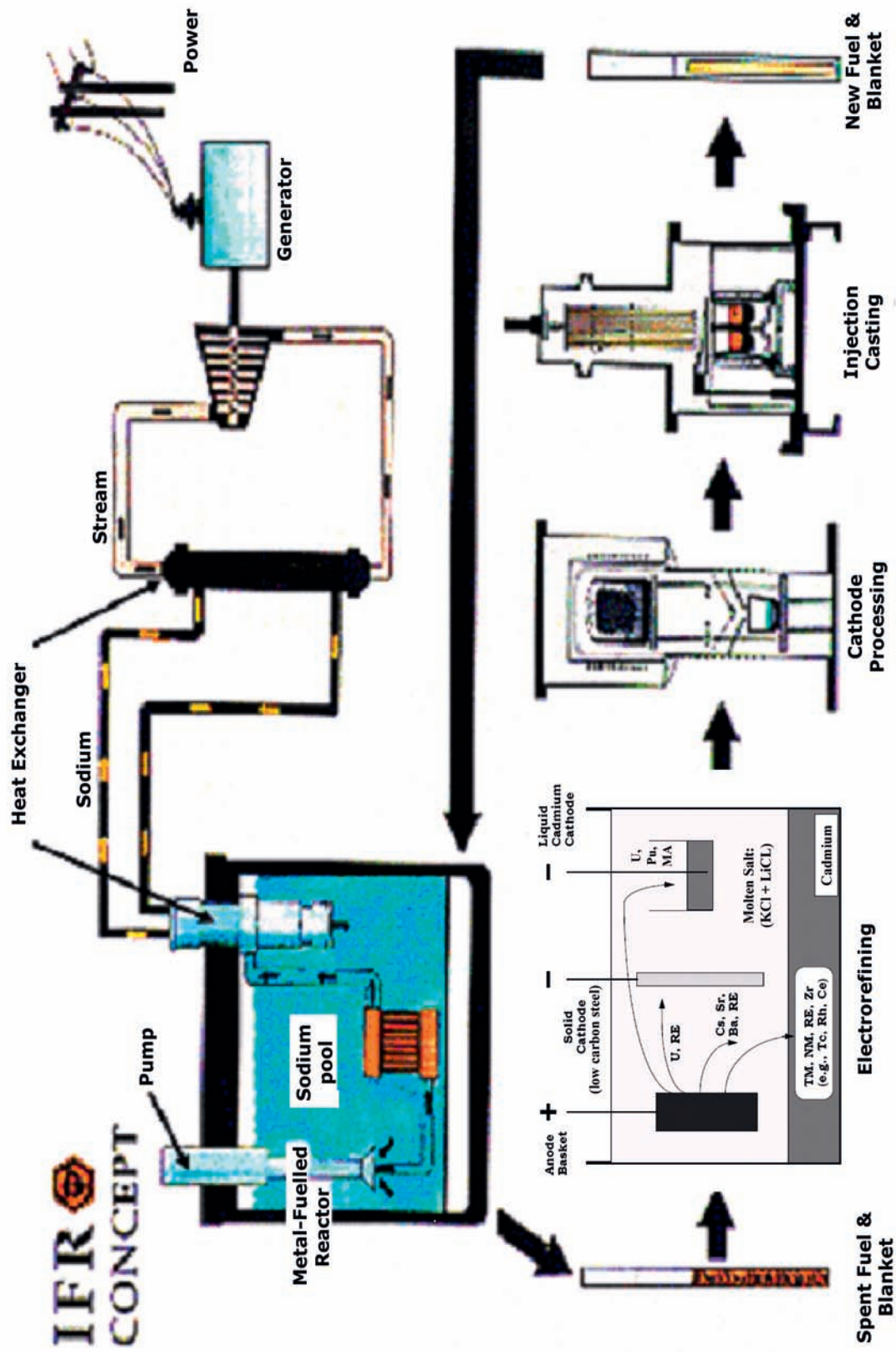
FIG. 24. Schematic of IFR with metallic fuel showing co-location of reactor spent fuel electro refining and fuel Re-fabrication plants. The metallic fuel is fabricated by vacuum melting followed by injection casting.
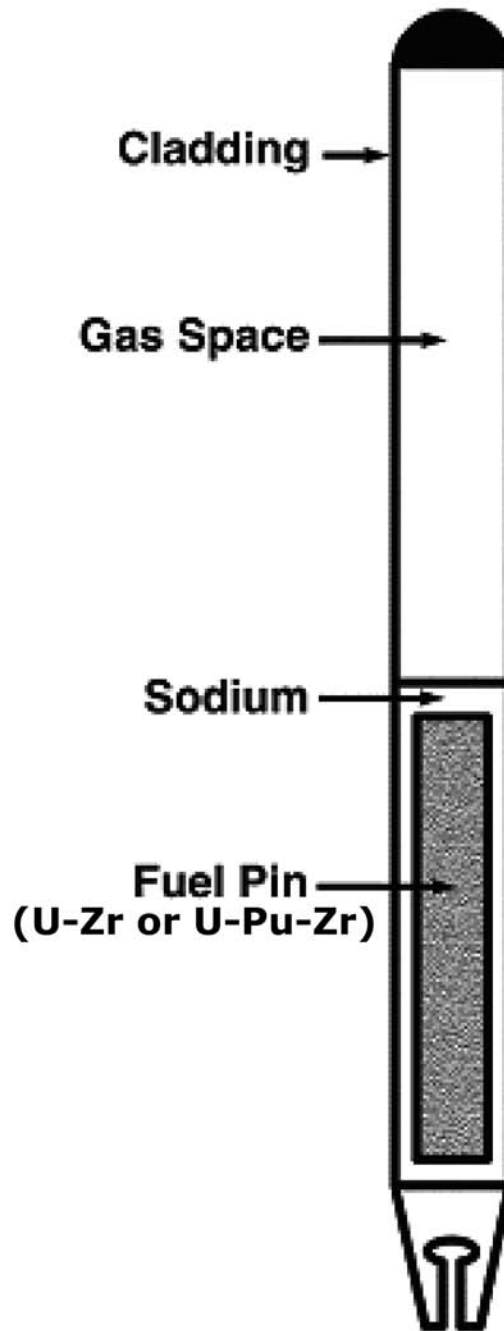
FIG. 25. Principal components of sodium bonded metallic (U-Zr and U-Pu-Zr) fuel pin.

section. The gap is filled with sodium for adequate heat transfer during early stages of irradiation, before the fuel has swelled to contact the cladding. The sodium partially fills the porosity when interconnection occurs. The free plenum above the fuel is sized to keep the hoop stress on the cladding, due to gas pressure from fission gas release, within tolerable limits, to accommodate displaced sodium and also to accommodate axial expansion of fuel rod. The plenum above the fuel is initially filled with helium and a xenon isotope tag gas. The wire wrap around the cladding affords pin to pin separation and uniform flow of the liquid sodium coolant.

Figure 26 shows the flow sheet for preparation of sodium bonded metal fuel pins. The fuel slugs are injection cast in an induction furnace. The electro magnetic field from the copper induction furnace is of dual frequency. At high frequency the field couples with the graphite crucible for heating of the melt while at low frequency the field couples with the melt for a stirring effect.
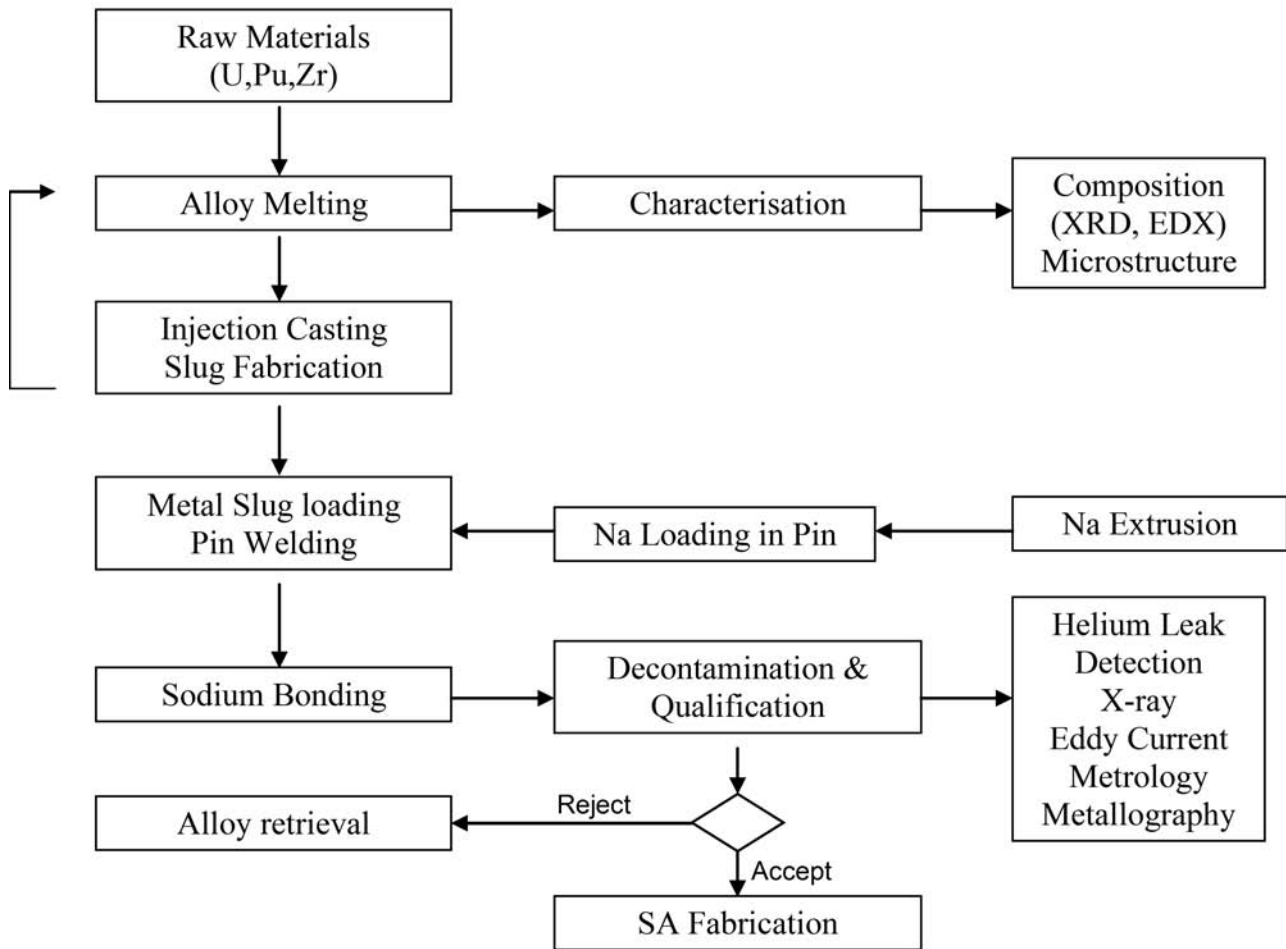
FIG. 26. Flow sheet for fabrication of sodium bonded U-Zr and U-Pu-Zr fuel pins.

The graphite crucibles are coated with alcohol slurry of yttria to prevent the melt from reacting with the crucible. The crucibles are capable of repeated use [60]. The melt is heated to about 1600°C under an argon atmosphere. The furnace is then evacuated and 100 quartz molds, the open end of which, are immersed in the melt. The furnace is immediately pressurized with argon to fill the quartz molds. The pallet that contains the molds is lifted from the melt where the cast fuel immediately solidifies. Figure 27 shows a photograph of the injection casting facility at the Argonne National Laboratory, USA.

The quartz molds are coated with zirconia to prevent the fuel slugs from sticking to the molds. Upon cooling, the fuel slugs are removed from the quartz molds and sheared to length. No grinding of the surface of the slugs is necessary because the diameter of the fuel slugs reflect the precision of the quartz molds. The temperature of the melt cannot exceed 1600°C because the quartz will soften to an unacceptable extent. Thus, the amount of zirconium added to uranium was limited to 10 wt%.

Once injection cast, the fuel slugs are inserted directly into the cladding that contains the sodium bond. Any excess material after cutting the metal fuel slugs is simply put in the next casting rather than directed to the initial steps of a complicated ceramic powder preparation line. Subsequent steps for the loading of the fuel pin are first to put the fuel slug in the cladding jacket and then add the appropriate amount of solid sodium. This is done in a helium glove box for cold fuel. The pins are then heated to liquefy the sodium and xenon tag gas, if desired, is added. An end cap is then welded on the cladding jacket. Bond quality is deduced by measuring the sodium level in the plenum above the fuel with X ray radiography and eddy current testing. All of the above steps lend themselves readily to remote fabrication in a hot cell environment.

FIG. 27. Facilities for injection casting of U-Zr and U-Pu-Zr metallic fuel in ANL, USA.

The casting of the fuel pins is sensitive to a few parameters. The type of defects that would occur in the fuel slugs are porosity, hot tears, and short slugs. The parameters that need to be optimized to avoid these defects are the melt temperature, temperature of the molds prior to injection of the fuel, rate of pressurization, and the quality of the zirconia mold wash.

Improvements in the injection casting process involved the search for better molds to replace the quartz molds and reusable crucibles that would last longer than the graphite crucibles. One method that was successfully used was to cast directly into thin zirconium tubes [61]. The idea was that since the zirconium migrated to the surface of the fuel during irradiation that the performance would not be altered. Both the fuel and the zirconium tube were put in the stainless steel cladding. Beryllia crucibles were successfully used on a limited basis to replace the graphite crucibles used for melting the fuel charge.

Recently, the Central Research Institute of Electric Power Industry (CRIEPI), Japan, has set-up an engineering scale injection casting facility for manufacturing U-10%Zr alloy in batches of 20 kg [62]. Figure 28 shows the outline of the fabrication process of U-10%Zr by injection casting at CRIEPI. Uranium and zirconium metals are melted in a graphite crucible which is inductively heated in a 30 kW furnace at 3 kHz. The graphite crucible is internally coated with yttria to avoid any chemical interaction between the molten metal and graphite. The mold bundle had 38–72 one end closed silica molds coated internally with zirconia. After melting, the crucible is evacuated and the open ends of the silica molds are lowered into the molten metal alloy. The vessel is then refilled with argon in order to inject molten fuel alloy into the silica molds. After cooling, the fuel alloy castings are sheared off at both ends. The cast slugs met the following specifications:

diameter: 5 ± 0.05 mm, length ~400 mm, density: 15.3–16.1 g/cm^3, Zr: 10 ± 1 wt%, total impurity (C, N, O, Si): <2 000 ppm.

A similar facility is being set-up at JAEA under the collaboration between JAEA and CRIEPI for engineering scale experiments with U-Pu-Zr alloys.

In ROK, U-(5, 10, 15) wt%Zr binary alloys and U-10wt%Zr-(2, 4, 6)wt%Ce ternary alloys were cast by vacuum injection casting using an assembly of quartz tube molds. The diameters of U-Zr and U-Zr-Ce rods were in the range of 4–7 mm and the lengths were around 200 mm. Although vacuum injection casting was a proven
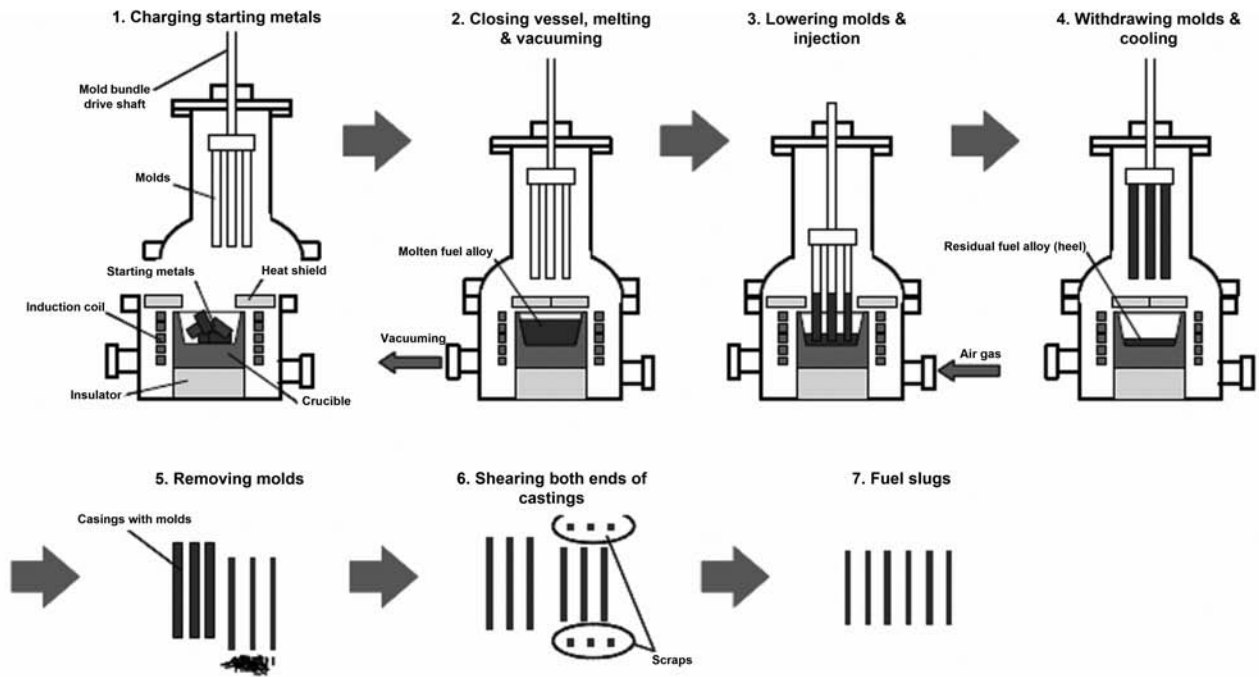
*FIG. 28. Outline of metal fuel fabrication process by injection casting [62].*
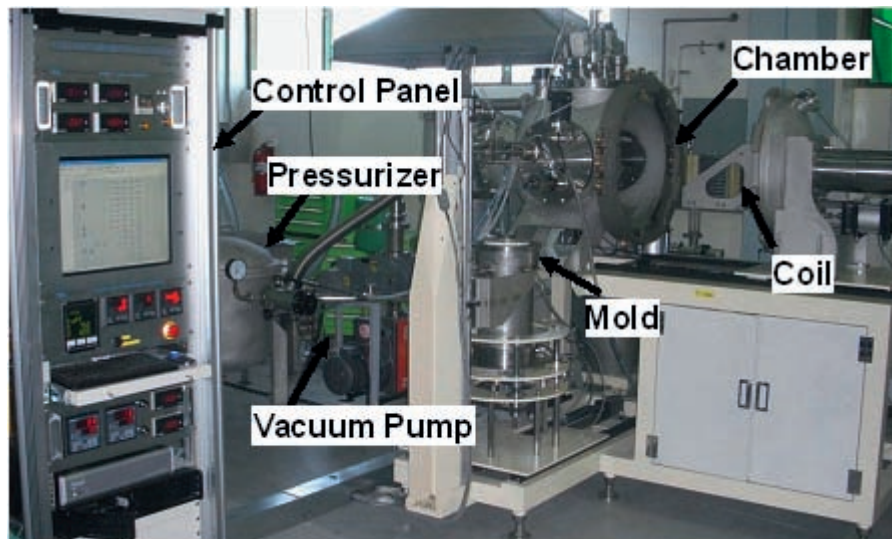
FIG. 29. A vacuum assisted gravity casting system installed in the KAERI metallic fuel research facility.

technology for mass production of metallic fuel pins, further improvements are needed in order to fabricate metallic fuel with minor actinides. High level vacuum on the melt may facilitate evaporation of Am with a high vapour pressure and use of the quartz mold may produce huge volume of long lived radioactive wastes.

A vacuum assisted gravity casting system was designed and installed recently as shown in Fig. 29 in order to reduce the vaporization of Am during the casting process. The upper chamber for a crucible and the lower chamber for a mold were separated to provide a pressure difference between the two chambers. During the casting of U-Zr rod, the crucible chamber was pressurized and the mold chamber was evacuated in order to facilitate an inflow of the melt into the mold assembly. High pressure of the crucible chamber and a crucible cover in this system can reduce the vaporization of Am under an inert atmosphere [63]. Good quality U-(5, 10, 15)wt%Zr and U-10wt%Zr-(2, 4, 6)wt% Ce rods with 6–10 mm in diameter and 300 mm in length were fabricated by the vacuum assisted gravity casting.
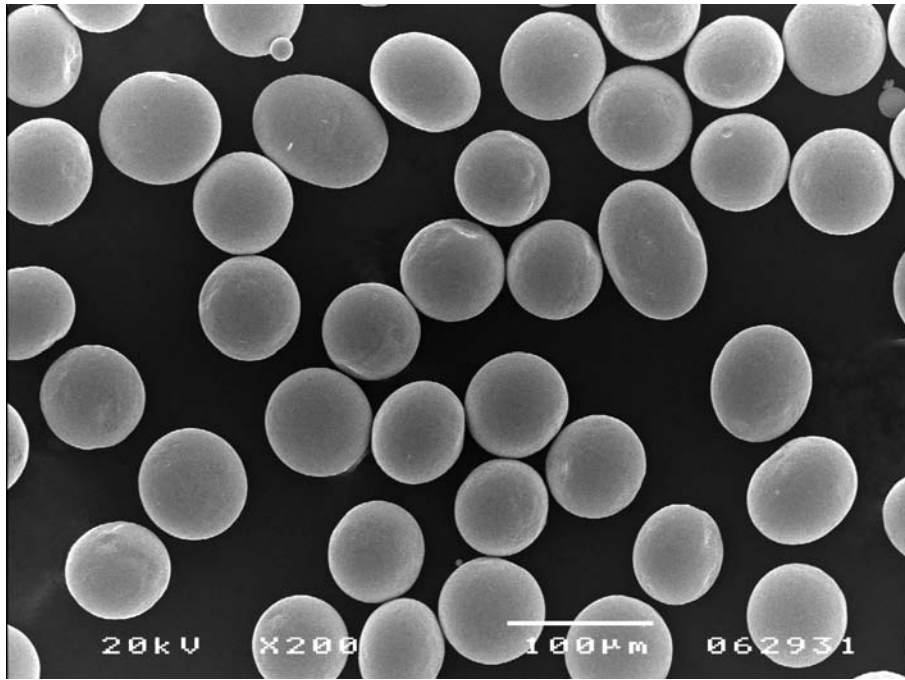
FIG. 30. A scanning electron micrograph showing morphology of U-10wt%Zr powder fabricated by a centrifugal atomization method.
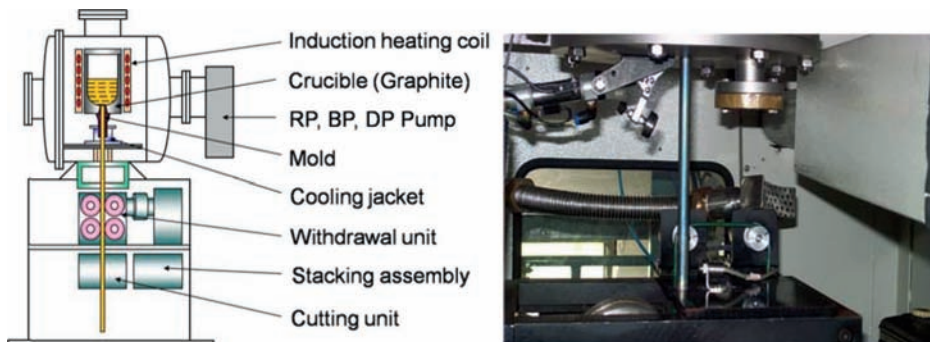

FIG. 31. A conceptual diagram of a continuous casting system and a uranium rod being extracted by continuous casting.

Spherical U-10wt%Zr powder was fabricated by the centrifugal atomization method. When compared with conventionally cast U-Zr, atomized U-Zr has finer grains and lamellar structure. Fine microstructures of metallic fuel would enhance fission gas release rate during irradiation. Metallic fuel pins can be fabricated by vibration packing of spherical U-Zr powder into a stainless steel cladding or a Zr sheath tube. Figure 30 shows the SEM micrograph of U-10% Zr powder.

Continuous casting method can be an appropriate approach for manufacturing metallic fuel because waste mould is not produced as a by-product of the fuel fabrication process. In the continuous casting of uranium, all charged uranium melt in a crucible is extracted completely without any residues and good quality uranium rods were obtained. The fabricated rod had a uniform diameter of 13.7 mm and a length of 2.3 m. Continuous casting of U-Zr alloy for the SFR metallic fuel with a smaller diameter is under development (Fig. 31). It is difficult to optimize the continuous casting conditions for multi-component alloys because their temperature range for solidification is much larger than single component alloys.

India is also pursuing the metallic fuel programme for fast reactors. Engineering scale Injection casting facility is being developed to facilitate fabrication of U-Zr fuel slugs. Experimental metallic fuel pin designs based on sodium bonding and mechanical bonding are being considered for test irradiations in the FBTR [64].
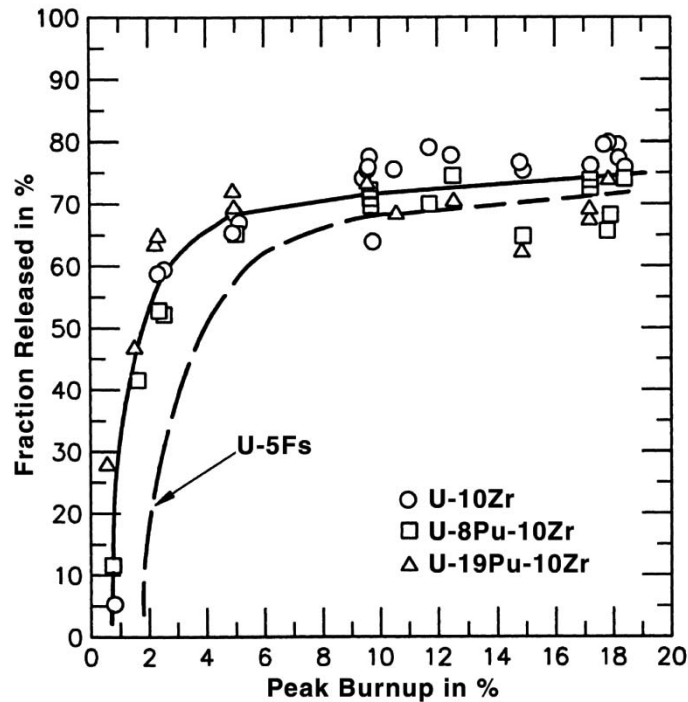
FIG. 32. *The phenomenon of interconnected porosity and gas release for metallic fuels of various compositions.*

5.3. IRRADIATION PERFORMANCE

Early metallic fuel designs, Mark I and Mark IA of EBR II, were not capable of reaching reasonable burnup [65]. These designs attempted to control fuel swelling by heat treatment, alloy additions, and reliance on the cladding strength but all these approaches were only partially successful. The inexorable swelling of the fuel led to breach of the cladding. However, by the late 1960s, a breakthrough was achieved and Mark II fuel design with a larger gap between fuel and cladding and larger gas plenum solved the concern over the burnup capability of metallic fuel. It was found that if the gap between fuel and cladding were made large enough then the fuel could swell unrestricted until the porosity generated by the fission gas bubbles became interconnected and released [66]. This point occurred when the volume swelling reached 30%. The phenomenon of interconnected bubbles and gas release, at the same degree of fuel swelling, was found to be independent of alloy composition as shown in Fig. 32 [67].

An added advantage of metallic fuel with the interconnected porosity was that when a transient occurs, the thermal expansion of the fuel and volume increase due to temperature induced phase transformation would not stress the cladding. Rather the fuel would flow onto itself into the open porosity [6].

A smeared fuel density of about 75% will ensure interconnected bubble formation by the time the fuel reaches the cladding. Results of the irradiation experiments carried out on U-Pu-Zr fuel at smeared densities with 70%, 75% and 85% [72] clearly show a large increase in cladding diameter for the smeared density of 85%. The same effect would materialize should the open porosity close due to solid fission product buildup.

The cladding of Mark II design was changed from 304L to 316 stainless steels annealed and subsequently to cold worked 316 and D 9 in Mark III and IIIA. Initially U-5% Fs was used as the fuel and later it was changed to U-Zr for equal performance without the necessity of the additional alloying elements [70].

Integral fast reactor (IFR) was a metal fuelled breeder concept with an alloy of uranium, plutonium, and zirconium, designated, U-19Pu-10Zr, (where the compositions are given in wt%) as the fuel. The zirconium increases the solidus temperature of the fuel and enhances the compatibility between fuel and cladding. A detailed listing of all the irradiation experiments done on U-Zr and U-Pu-Zr metallic fuel in EBR-II and FFTF are given in reference [73] and summarized in Annex I.

At the conclusion of the IFR programme it was clear that up to 20 at.% burnup was achievable with U-Zr fuel clad in ferritic-martensitic HT-9 (advanced alloys developed in the LMFR programme). Since the D9 austenitic steel swelled more than the ferritic — martensitic HT-9 steel at high burnup, HT-9 was envisaged as the best candidate material for cladding and duct for high burnup [74].

When metal fuel swells, the fuel slug diameter and length increase. The length increase is consistently less than that would be predicted from isotropic swelling. This difference was attributed to the difference in swelling behaviour between the hotter centre of the fuel and the colder periphery [72]. The sodium bonding has a large effect on the thermal conductivity of the fuel pin. Initially, the sodium provides a conduction path across the gap between fuel and cladding. As the porosity forms in the fuel, the thermal conductivity of the fuel decreases until the porosity interconnects and the fission gas is released. The sodium then ingresses into the open porosity and increases the thermal conductivity. This phenomenon was measured with instrumented fuel pins [72].

Irradiated U-Pu-Zr metal fuel exhibits fuel constituent redistribution (to create Zr-depleted zones with attendant lower, local solidus temperatures) as well as fuel/cladding interdiffusion enhanced by lanthanide fission products present in increasing amounts with higher burnup. These two phenomena could lead to formation of lower melting temperature composition regions in the fuel and to effective thinning of the cladding [79]. However, up to a burnup of 20 at% and a peak cladding temperature of 590°C, weakening of the cladding was not observed for U-Pu-Zr fuel clad with HT-9. Recently the constituent redistribution phenomena have been modeled [84]. The Zr-depleted zone formation is more pronounced in U-Pu-Zr than in U-Zr and is temperature dependent (Fig. 33). The low solidus temperature Zr-depleted zone would form in a region of the fuel, where under normal conditions; the temperature would not exceed the local solidus temperature. However, they melted under simulated transient conditions at temperatures as low as 675°C, leading to breach in austenitic stainless steel cladding [78]. The beneficial effects of Zr at the fuel/cladding interface were exhibited in various ways [87]. The zone boundaries vary along the length of the fuel slug as the temperature changes. The formation of the boundaries is time dependent as the alloy constituents rearrange in the radial temperature gradient. The porosity in the zones varies with the composition and crystallographic phases present. The thermal conductivity of the fuel would be difficult to calculate considering the heterogeneity of the fuel. However, the performance parameters of the fuel are satisfactorily determined by the average thermal conductivity of the fuel [72].

5.4. BEHAVIOUR UNDER TRANSIENT CONDITIONS AND AFTER CLAD BREACH

Tests and analyses were carried out on the metallic fuel core to demonstrate safe performance under a range of transient conditions including the ultimate test where the liquid sodium coolant flow of EBR-II was stopped as the reactor was allowed to shut itself down without SCRAM and without human intervention [88, 89]. The driver fuel proved to be extremely robust because after all the upset events, the fuel continued operating to its burnup limit. An important result of the tests was that significant axial expansion of the fuel, inside the cladding, occurred prior to expansion of the clad. Should an overpower transient occur in an operating reactor, this axial expansion would reduce the reactivity and tend to shut the reactor down. The results consistently showed that metallic fuel rods of modern design exhibited failure thresholds around 4 times nominal power (under the relatively fast transient-overpower conditions used in the tests). The data from the transient tests and from a large number of previous metallic fuel transient tests in TREAT were used to develop and validate models of fuel behaviour under transient overpower conditions [29].

One of the concerns of the lanthanide buildup at the fuel-clad interface creates the potential for the formation of a low melting alloy adjacent to the cladding that may cause cladding failure during an over-temperature event. Irradiated fuel pins were heated in-cell to characterize the phenomenon. Even after heating the fuel that has been irradiated to 17 at% burnup up to temperatures of 725^{0}C for 7 hours, no evidence of liquid phase formation was found [72].

Irradiation experiments have also been performed to assess the behaviour of metallic fuel after cladding breach [73]. These experiments were accomplished with U-Zr and U-Pu-Zr fuel clad with 316, D9 and HT-9 steels. At the time of cladding breach, the bond sodium was expelled with fission products, mainly [133]Cs. No further reaction occurred and no fuel was washed out. A summary of all the run-beyond-cladding-breach experiments is given in [6].With the expulsion of the bond sodium the fuel temperature would increase. This increase in temperature accelerated the diffusion of the lanthanide fission products to the cladding interface. The depth of

U-19Pu-10Zr FUEL, L/L₀=.49, 10% BU

FIG. 33. Transverse metallographic section of a U-19Pu-10Zr element at 10 at.% burnup showing radial zone formation.

penetration of the lanthanides into the cladding was larger than that observed on fuel rods that had not breached [72]. Tests in which previously irradiated fuel pins with U-Pu-Zr fuel clad in HT-9 cladding were furnace heated in a hot-cell to simulate loss-of flow events also demonstrated significant safety margin [96, 97, 79].

5.5. METALLIC FUELS WITH MA

Metallic trans uranium — zirconium (TRU-Zr) fuel of composition 40Zr-10Am-10Np-40Pu is being developed at Argonne National Laboratory for use in the proposed subcritical advanced burner reactor (SABR) in the USA. In general, metal fuel has properties that prove favourable for high burnup of TRU, besides high thermal conductivity, the ability to accommodate a high actinide density, and the ability to be directly fed into pyroprocessing and refabrication facilities. Zirconium is selected as the alloying element because Zr containing alloy fuels has been successfully fabricated and reprocessed. The inclusion of zirconium in the metal composition raises the alloy solidus temperature, provides resistance to fuel-clad interactions, provides dimensional stability
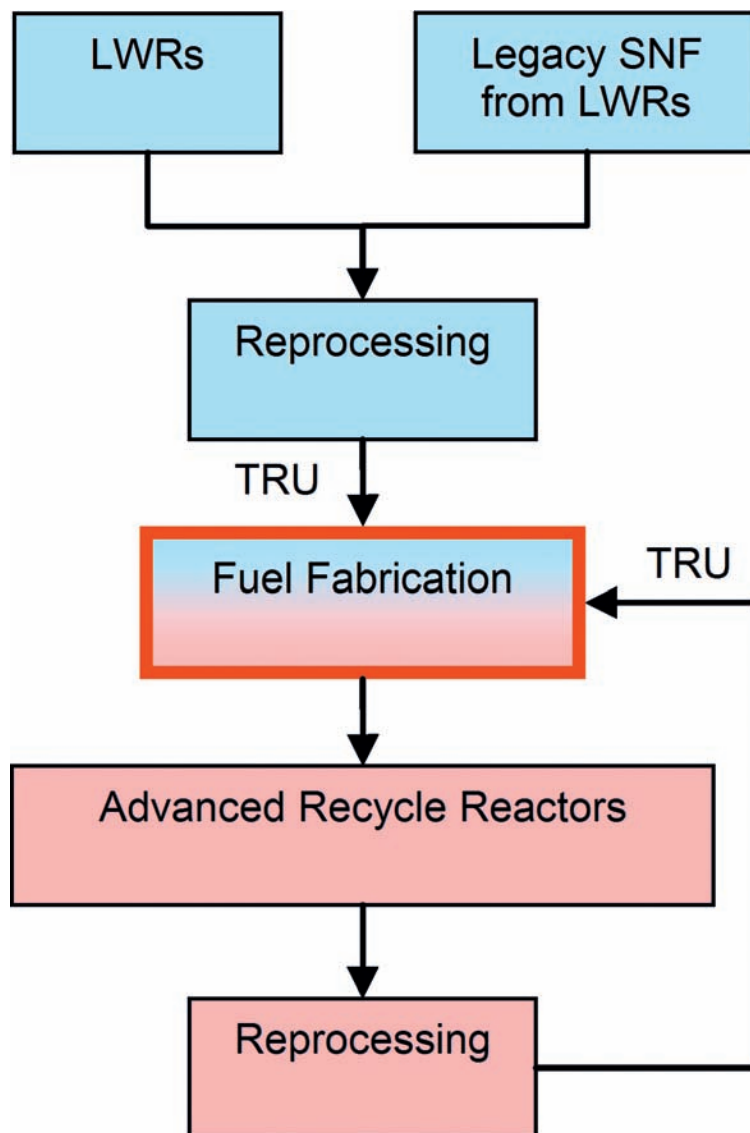
FIG. 34. Nuclear fuel cycle proposed in Global Nuclear Energy Partnership (GNEP).

during irradiation, and provides the possibility of a negative Doppler coefficient in TRU fuel that is free of ^{238}U. In addition, metal fuel dispersed in a zirconium matrix has demonstrated excellent radiation resistance.

Metal fuel with low MA+RE content has been irradiated in PHENIX [98]. Four types of alloys, namely, U-19Pu-10Zr, U-19Pu-10Zr-2MA-2RE, U-19Pu-10Zr-5MA and U-19Pu-10Zr-5MA-5RE, were fabricated by JRC-ITU and encapsulated for irradiation at different burnups. The capsule with low burnup (2.4 at.%) was discharged from the core in August 2004, and subjected to non-destructive post irradiation examination. For SUPERFACT 1, several batches of fuel were fabricated with MA contents of 2%Np, 2%Am, 45%Np and 20%Np + 20%Am. The obtained knowledge is useful for the preliminary evaluation of the above fuels. Investigations of the thermal performance of MA fuels will include power-to-melt tests and the study of the high burnup behaviour.

The technology demonstration element of the US Global Nuclear Energy Partnership (GNEP) programme is aimed at demonstrating the closure of the fuel cycle by transmuting the transuranic elements separated from spent nuclear fuel. As shown in Fig. 34, multiple-pass recycling through fast reactors is envisioned for burning the TRU initially separated from light water reactor spent nuclear fuel. For the initial technology demonstration, it is assumed that SFRs will be used as burner reactors as they represent the most mature fast reactor technology available today.

The US TRU fuel development programme is focused on the fabrication, irradiation, and post-irradiation examination of metallic and oxide fuels designed for sodium cooled fast reactors. Test fuels containing uranium, plutonium, americium, and neptunium are currently being irradiated in the USA (in the advanced test reactor — ATR) and in France (the FUTURIX-FTA test in Phénix). In addition to the development of TRU fuels, the US programme also includes research and development of core materials and startup fuel (containing uranium and plutonium, but no minor actinides) for an initial advanced burner reactor.

The transmutation fuel needed for use in a fast reactor differs from conventional thermal and fast reactor fuels in many ways. Transmutation fuels consist of a blend of five heavy metal elements (U, Pu, Am, Np, Cm) rather than just one or two (U and/or Pu) typical of conventional fuels. The heavy metal elements used in transmutation fuels have thermodynamic properties considerably different from uranium and plutonium and their effect on fuel properties must be factored into the fabrication process. High helium gas generation during irradiation of the americium and curium bearing fuels necessitates a fuel design that limits or accommodates fuel swelling and avoids excessive pressurization of the fuel pins. The final TRU fuel form must accommodate a variable composition in terms of the ratio and content of the heavy metal elements and associated fission product impurities. It is important to note that the compositional and isotopic variability required of the fast reactor transmutation fuel is much wider than the narrow technical specifications used in a conventional fuel obtained from a uniform feedstock.

Considering the differences mentioned above, it is clear that the transmutation fuels of interest are not a simple extension of previously deployed fuels. Therefore, an in-depth research and development programme is required to investigate solutions to the challenges of developing, testing, and ultimately qualifying new transmutation fuels.

Irradiation tests of metallic fuels containing minor actinides are currently in progress in the USA. The compositions of two irradiation experiments are listed in Table 9. The non-fertile fuel compositions in experiment AFC-1B were designed for accelerator based transmutation; the low fertile fuel compositions in experiment AFC-1F were designed for reactor based transmutation. The two experiments were irradiated in ATR at the Idaho National Laboratory in the USA to a burnup level of 4–8 at.%, equivalent to a fission density of $2.7–6.8 \times 10^{20}$ fissions/cm^3. Two companion experiments with the same fuel compositions are also being irradiated in the ATR and are destined for higher burnup, approximately 30–40 at.%.

PIE of AFC-1B and -1F has been performed on the metallic fuel compositions from the low burnup experiments. Fuel performance of the TRU-bearing metallic fuels is best correlated with fission density as a burnup metric rather than atom per cent depletion or GW·d/t, which are typically used as burnup metrics. The burnup metric of atom percent depletion is proportional to the fission density with the proportionality factor dependent on the density of the fissioning constituents. The fissioning constituent density is determined from the fuel compositions and the irradiation system neutron spectrum. In a thermal neutron spectrum, only fissile isotopes such as ^{235}U, ^{239}Pu, and ^{241}Pu are included as fissioning constituents, however in a fast spectrum all the actinides are included as fissioning constituents. The transmutation fuels irradiated in the AFC-1F experiment have a much lower fission density than U-xPu-10Zr fuels at the same atom percent burnup. Using fission density as the burnup metric eliminates the composition dependence in assessing fission damage and provides a standard basis for correlating fuel performance parameters.

TABLE 9. NOMINAL TRU-BEARING FUEL COMPOSITIONS IRRADIATED IN THE USA (ALLOY COMPOSITIONS ARE EXPRESSED IN WEIGHT PERCENT)

Experiment AFC-1B	Experiment AFC-1F
Pu-12Am-40Zr	U-29Pu-4Am-2Np-30Zr
Pu-10Am-10Np-40Zr	U-34Pu-4Am-2Np-20Zr
Pu-40Zr	U-25Pu-3Am-2Np-40Zr
Pu-12Am-40Zr	U-29Pu-4Am-2Np-30Zr
Pu-60Zr	U-28Pu-7Am-30Zr
—	U-25Pu-3Am-2Np-40Zr

Post-irradiation examinations show that fission gas release, radial swelling, and microstructural evolution of the AFC-1F fuel compositions are consistent with U-Pu-Zr fuels. The actinide bearing metallic fuel compositions in experiment AFC-1F exhibited irradiation performance very similar to U-Pu-Zr fuel compositions at equivalent fission densities [99].

A rich database exists on the usage of metallic fuels for fast reactors. Early concerns about the performance of metallic fuels have been resolved. High burnup has been achieved through the application of a simple design change whereby keeping the smear density in the range of 70–75%, interconnected porosity and gas release would occur prior to fuel cladding contact. Extensive compatibility experiments on both irradiated and unirradiated samples have shown that liquid phase penetration of the cladding is not a problem. Burnup of 20 at.% has been achieved on U-Pu-Zr fuel pins without failure. During the course of developing metallic fuels, a number of positive attributes were observed. The entire core of EBR-II, fuelled with U-Zr fuels, was subjected to approximately 60 transients in preparation for tests on advanced ceramic fuels. There was a concern that the relatively high thermal expansion of metallic fuel and phase transformations would cause failure of the cladding. Instead, the fuel plastically flowed into the open porosity rather than stress the cladding. After the transients, the core was operated to the normal burnup limit of the fuel.

Another positive attribute that was completely unexpected was the behaviour of the metallic fuel under severe transients when tested in the TREAT facility. The retained fission gas in the fuel caused the fuel to expand axially prior to cladding failure. This axial expansion results in a strong negative reactivity feedback which would shut the reactor down during an over-power transient event.

Finally, and most importantly, the high thermal conductivity of metallic fuel results in low centerline temperature and thus low stored enthalpy. During a loss of flow event, the temperature rise of the core is minimal and the reactivity increase is terminated due to thermal expansion with no human or mechanical intervention. This behaviour was demonstrated with the primary pumps of EBR-II shutdown with a, SCRAM and the reactor shutdown without intervention.

Most of the development work on metallic fuel in the USA was terminated in 1992. However, development work continued in Japan. More recently, the USA has restarted development studies on metallic fuels within the framework of the Global Nuclear Energy Partnership (GNEP). This programme is considering metallic fuel, along with ceramic fuels, for reactor fuel to burn plutonium and minor actinides. Due to the attributes discussed above, metallic fuel should remain in consideration for future fast reactors. In parallel, because of the ease of remote reprocessing and fabrication, development of pyro-processing should continue. It may be noted that metallic fuel will be the preferred host for minor actinides because of the possibility of co-depositing MA with metallic fuel alloys during pyro-reprocessing. In short, the status of metallic fuel could be summarized as follows:

— **Fabrication**: Metallic fuels are relatively easy and simple to fabricate. However, there is a need to develop remote fabrication capabilities for TRU-bearing metallic fuels. To mitigate Am loss, vacuum assisted gravity casting could be employed. In the first phase, an engineering-scale fabrication facility has to be set-up with batch size of several kilograms of TRU materials. Based on this experience, an industrial scale plant could be set-up in the future.
— **Properties**: The out-of-pile properties and database of metallic fuels is scanty. There is a need to augment the database on the properties of MA-bearing fuels. Likewise, there is a need to develop and share capabilities to characterize and measure properties of irradiated metallic fuels with and without MA.
— **Irradiation testing and qualification**: Fast reactors, irradiation testing facilities and hot cells for post–irradiation examination (PIE) are needed for qualification of metallic fuels for commercial exploitation.

6. THERMOPHYSICAL PROPERTIES

6.1. INTRODUCTION

The performance of nuclear fuel in power reactors is largely dependent on its thermophysical properties and their changes with temperature and irradiation. Experimental data on out-of-pile properties such as melting point, thermal conductivity, thermal expansion are required for fuel design, performance modeling and safety analysis [24]. The variables that influence the out-of-pile properties of fuel are composition, temperature (T), density, microstructure and stoichiometry (O/M, C/M, N/M) of fuels [100]. These properties also change with irradiation. Hence knowledge of these properties and their change with irradiation are essential for fuel design and safety analysis.

Melting point and thermal conductivity of the fuel are needed to evaluate its thermal performance. These two play a crucial role in determining the power to melt of the fuel and decides the operating linear heat rating. Melting point depends on the fuel composition, stoichiometry and burnup. The thermal conductivity of nuclear fuel affects the temperature profile which in turn influences almost all important processes such as fission gas release, swelling, grain growth etc. and limits the linear power [100]. The changes in thermal conductivity occur during irradiation by the formation of fission-gas bubbles, porosities, build-up of fission products and by the change of fuel stoichiometry [101]. Heat capacity of actinide fuels is required in the modeling of heat conduction during normal and under transient conditions and for calculating thermodynamic properties [24].

The coefficient of thermal expansion (CTE) is needed to calculate stresses occurring in the fuel and cladding on change in temperature. If the thermal expansion varies considerably for the fuel and cladding, stresses will be accumulated during the thermal cycling leading to the deformation of the clad [103, 104]. Hence, precise evaluation of CTE data of the fuel is needed. The difference between the coefficients of thermal expansion of the fuel and the cladding determines the status of the fuel-clad gap when the fuel element is brought to power. In safety analysis, the values of thermal expansion data are required in determining the gap conductance and thus the stored energy [101].

6.2. THERMO PHYSICAL AND THERMO MECHANICAL PROPERTIES OF OXIDES

6.2.1. Melting point

The UO_2 melts at a higher temperature than PuO_2. MOX fuel melts at a temperature which lies between that of pure UO_2 and PuO_2. The deviation from the stoichiometry and the burnup lowers the melting temperature. Many authors have measured the melting temperatures of UO_2 and PuO_2 and these show a wide scatter. The IAEA recommended value for the melting temperature of UO_2 and PuO_2 are that of Adamson [105]:

$T_m(UO_2) = 3120 \pm 30$ K

$T_m(PuO_2) = 2701 \pm 35$ K

The uncertainty in the recommended temperature is about 1%.

Recently, Manara et al. [106] have measured the melting temperature of UO_2 and a reported a value of $3\,147 \pm 20$ K. Further, the pressure dependence of melting temperature of UO_2 is reported as:

$T_m(UO_2) = 3147 + 9.29*10^{-2}$ P (MPa)   (6.1)

The above relation is valid in the pressure range of 10–250 MPa.

Effect of plutonium content

Mixed oxide fuel melts incongruently. Solidus /liquidus temperature $(T_S)/(T_L)$ of unirradiated MOX fuel of stoichiometric composition is estimated by the Adamson correlations [105]:

$$T_S \text{ (K)} = 3120.0 - 655.3y + 336.4y^2 - 99.9y^3 \qquad (6.2)$$

$$T_L \text{ (K)} = 3120.0 - 388.1y - 30.4y^2 \qquad (6.3)$$

where y is the PuO_2 content in molar fractions. For PuO_2 mole fraction of 0–0.6 in the fuel, the estimated uncertainties are ±30 K for the solidus temperature and ±55K for the liquidus temperature. For the mole fraction of PuO_2 above 0.6, the estimated uncertainties for the solidus and liquidus temperatures are ±50 K and ±75K, respectively.

Konno et al. [107] have further modified the above values. The solidus and liquidus temperatures of UO_2-PuO_2 binary system obtained by the using the expression given by Adamson and Konno re given in Table 10.

The influence of Am on the melting temperature for fast reactor MOX composition is given by Konno et al [108]. The decrease in the solidus temperature is given by the following relation:

$$\Delta T_s = -(1,206 - 782*y)*X_2 \qquad (6.4)$$

$$\Delta T_L = -(560 - 141*y)*X_2 \qquad (6.5)$$

Where X_2 is Am weight fraction.

TABLE 10. THE SOLIDUS AND LIQUIDUS TEMPERATURE (K) FOR UO_2-PUO_2 BINARY SYSTEM

Pu Fraction	Adamson, 1985		Konno, 2002	
	Solidus (K)	Liquidus (K)	Solidus (K)	Liquidus (K)
0	3120	3120	3138	3138
0.05	3088	3101	3113	3121
0.1	3058	3081	3089	3103
0.15	3029	3061	3065	3085
0.20	3002	3041	3041	3067
0.25	2976	3021	3017	3049
0.30	2951	3001	2994	3030
0.35	2928	2980	2971	3011
0.40	2905	2960	2949	2991
0.45	2884	2939	2926	2971
0.50	2864	2918	2904	2950
0.60	2826	2876	2861	2907

Effect of stoichiometry

The effect stoichiometry on melting temperature has been studied in detail by Konno et al. [107]. The change in solidus and liquidus temperatures as function of O/M ratio and Pu fraction is given by the following relation:

$$\Delta T_s = -(1000–2850y)*(2.00\text{-O/M}) \tag{6.6}$$

$$\Delta T_L = -(280–5000y^3)*(2.00\text{-O/M}) \tag{6.7}$$

Where y is the Pu fraction.
The above relation is valid for an O/M ratio of 1.94 to 2.00.

Effect of burnup

The effect of burnup on the melting temperatures of UO$_2$ and MOX fuel has been investigated by Carbajo et al. [109]. Their data are shown in Fig. 35. They recommended a correction for burnup by decreasing the melting point by 0.5K/MWd/kgHM for both UO$_2$ and MOX fuel.

Konno et al. [107] have measured the melting temperatures of irradiated oxide fuel and the suppression in melting temperature is provided the following correlation:

$$\Delta T_s = -(1.06–1.43y)*Bu + 0.0008[(1.06–1.43y)/0.66]^{1.5})*Bu^2 \tag{6.8}$$

$$\Delta T_L = -(0.50–0.38y)*Bu \tag{6.9}$$

Where y is the Pu fraction (Pu/(U+Pu)), Bu is the burnup in GW·d/t.
A good agreement is observed to MOX fuel having Pu fractions below 0.4 with an uncertainty of ±16.8K.
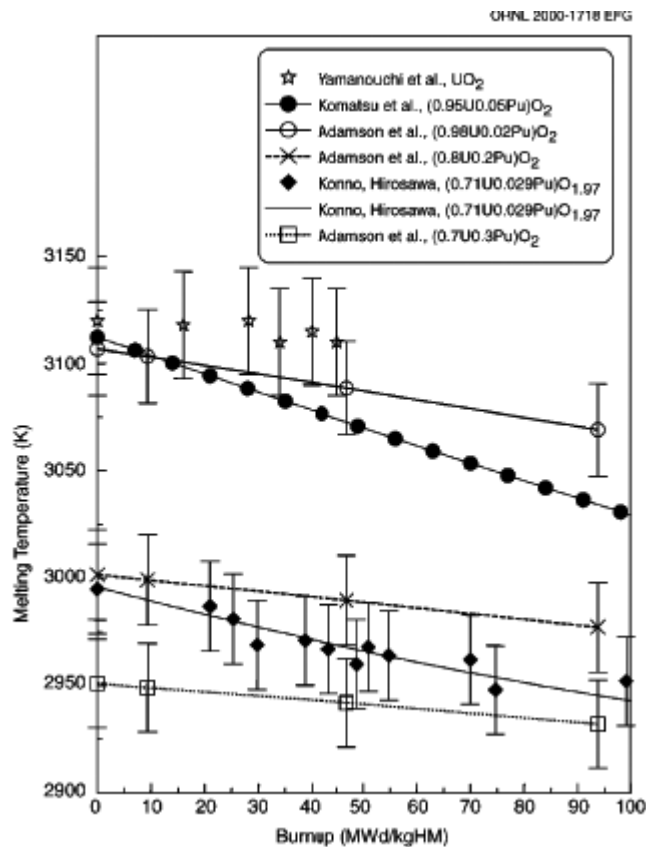
FIG. 35. Effect of burnup on the melting temperature for UO$_2$ and PuO$_2$ fuel with different PuO$_2$ contents [109].

6.2.2. Thermal conductivity

Thermal conductivity measurements

Thermal conductivity of a solid can be measured by two methods:

— By determining the stationary heat flow through the specimen (steady state) which gives k directly;
— By determining the variation of the temperature at a fixed plane, that is a specimen surface, due to an induced non-stationary heat flow (transient) thermal diffusivity, α is obtained.

The thermal conductivity (k) is derived from the measured values of thermal diffusivity data by using the relation:

$$k = \alpha \, \rho \, C_p \tag{6.10}$$

where ρ is the density of the material and C_p its specific heat at constant pressure.

Since the second method is more versatile and requires smaller specimen, it has become a standard method for determining k for T > 600 K. For lower temperatures, the first method is generally adopted.

Effect of temperature

A detailed comparison of stoichiometric oxide fuels shows that the thermal conductivity of both uranium dioxide and mixed dioxide are comparable. Thermal conductivity and melting point are higher at exact stoichiometric composition. Martin [110] recommended the following relation for $(U_{0.8}Pu_{0.2})O_{2-x}$ between temperature (k) and thermal conductivity (W/m.K) as function of x

$$k_{100} = (0.037 + 3.33x + 2.37 * 10^{-4}\,T)^{-1} + 78.9 * 10^{-12}T^3 \tag{6.11}$$

The above equation is valid for the temperature range of 500–2000ºC, over the range $0 < x < 0.1$ and is valid for PuO_2 content of about 20%.

Figure 36 shows the variation of thermal conductivity for 100% dense stoichiometric and hypostoichiometric mixed oxide. The effect of O/M is more prominent at low temperatures (below 1000 K) than at high temperatures of around 3000 K.

Recently, Inoue [111] proposed a new equation for the thermal conductivity of mixed oxide fuel (with Pu content up to 20%) for fast reactors as follows:

$$k_{100} = \{1/[(0.06059 + 0.2754 * (2\text{-O/M})^{0.5} + 2.011 * 10^{-4}\,T)]\} + (4.715 * 10^{9}/T^2)\,\exp(-16361/T) \tag{6.12}$$

where k_{100} is the thermal conductivity of fully dense MOX fuel in W/mK, T the temperature in K. The standard deviation between the data set and the calculated values is 0.20 W/mK (absolute) or 6.2% (relative).

The excellent predictability of the above correlation was validated by comparing the calculated, with measured central temperatures in an instrumented irradiation test in the experimental fast reactor JOYO for low O/M ratio fuel up to 1850 K. This new equation has been shown to predict well and is recommended for fuel pin thermal analysis with typical FR-MOX fuel pellets under beginning of irradiation conditions.

For fully dense MOX fuel, Carbajo et al. [109] have derived the following expression:

$$k_{100}\ (\text{W/mK}) = 1.158[(1/(A + Ct) + (6400/t^{5/2})\,\exp(-16.35/t)] \tag{6.13}$$

Where, A (x) = 2.85x + 0.035 (mK/W), C(x) = (–0.715x + 0.286) (m/W), t = T/1000 (K).
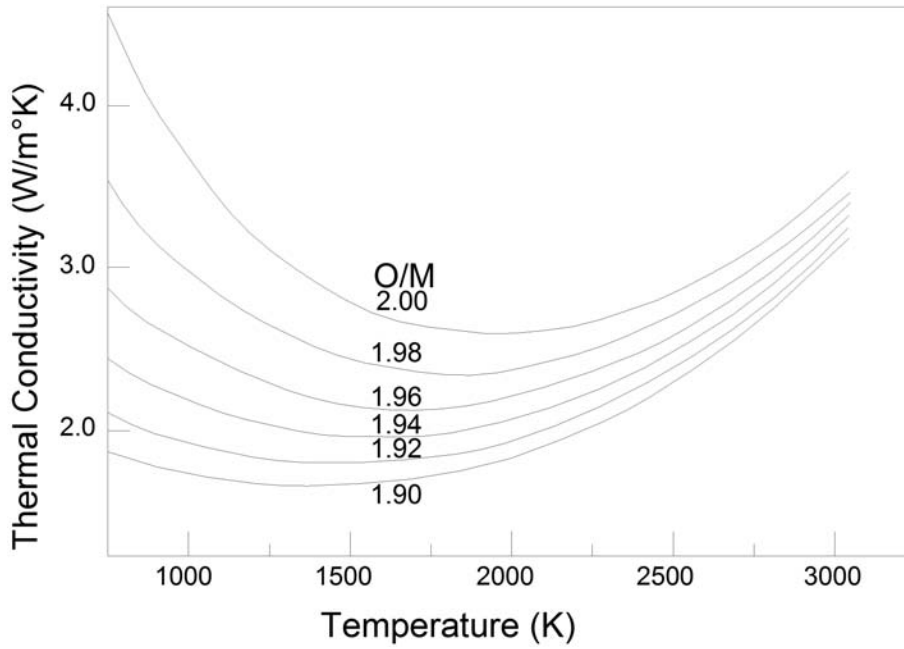
FIG. 36. Thermal conductivity values of 100% dense stoichiometric and hypostoichiometric mixed oxide fuel [110].
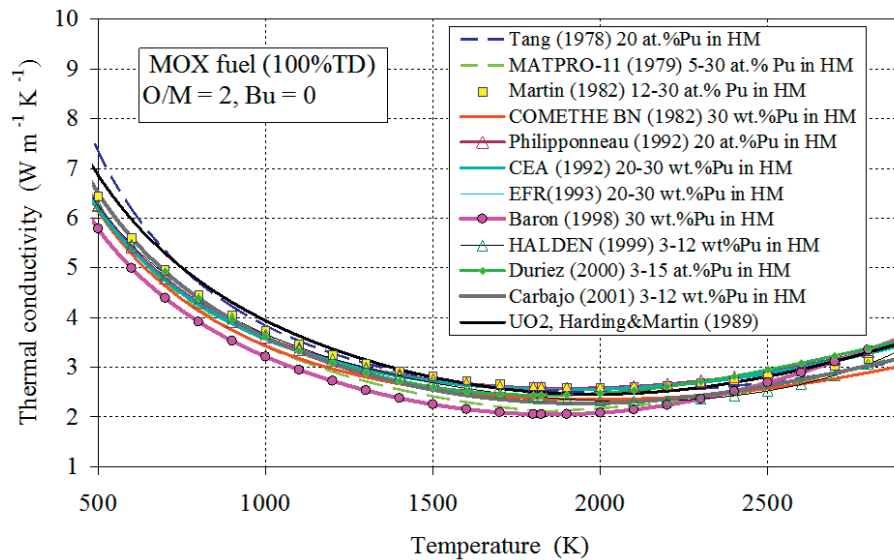
FIG. 37. Thermal conductivity of UO_2 and MOX fuel (up to 30% Pu) reported by various authors plotted against temperature showing scatter [112].

This correlation is valid from 700 to 3 100K, x less than 0.05 and for PuO_2 concentration between 3 and 15%. The uncertainties for the above equation are estimated to be 7% between 700 and 1 800K, increasing to 20% at 3 100K.

The temperature dependence of the thermal conductivity of nearly stoichiometric oxide fuels are shown in Fig. 37. It illustrates that the thermal conductivities measured for FR-MOX by several authors agree fairly well with each other.

Martin [110] recommended the following relation for hyperstoichiometric oxide, $(U_{0.8}Pu_{0.2})O_{2+x}$, between temperature (K) and thermal conductivity (W/m.K) as function of x (0.00 < x < 0.12):

$$k_{100} = (0.037 + 1.67 x + 2.37 * 10^{-4} T)^{-1} + 78.9 * 10^{-12} T^3 \tag{6.14}$$
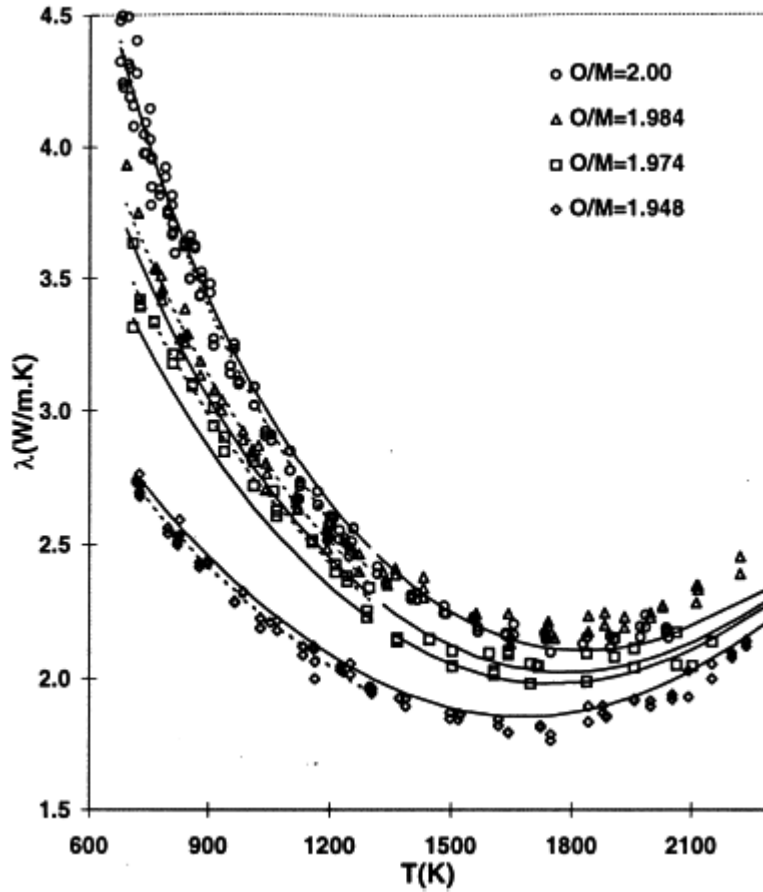
FIG. 38. Shows the variation of thermal conductivity with O/M ratio for different temperatures for UO₂-15%PuO₂ composition [113].

The stoichiometric fuels have the highest thermal conductivity values. It is observed that for the same deviation from the stoichiometry, the thermal conductivity of hyperstoichiometric fuel is lower than that of hypostoichiometric fuel. The conductivity of hyperstoichiometric oxide fuel containing a certain oxygen excess value is approximately equal to that of hypostoichiometric material with a deficiency equal to half this particular value. Figure 38 shows the variation of thermal conductivity with O/M ratio for different temperatures for UO_2-15%PuO_2 composition. This figure shows thermal conductivity variation for UO_2-15%PuO_2 composition for a range of O/M ratio form 1.94 to 2.00.

Effect of Pu addition

Addition of a small amount of PuO_2 to UO_2 decreases the thermal conductivity. However, PuO_2 additions between 3 and 15% does not further decrease the thermal conductivity. If the amount of PuO_2 is increased beyond 15%, then there is an additional decrease in thermal conductivity values of MOX fuel [109]. Washington [114] has recommended that the conductivity of 20% Pu stoichiometric mixed oxide fuel is 5% lower than the corresponding UO_2 fuel. Inoue [111] has reported that 20% plutonium additions to uranium oxide lower the thermal conductivity by 5% to 8%. It can be seen that the effect of PuO_2 additions on thermal conductivity is felt more at low temperatures.

Thermal conductivity of UO_2-21%PuO_2 and UO_2-28%PuO_2 compositions has been determined by Vasudeva Rao et al. [115]. The thermal conductivity data for the above compositions (96%T.D; O/M = 2.00) could be expressed by the following relation:

$$k(UO_2\text{-}21\%PuO_2) = 4.935 + 0.0061\,T - 9.787*10^{-6}\,T^2 + 3.255*10^{-9}\,T^3 \tag{6.15}$$

$$k(UO_2\text{-}28\%PuO_2) = 8.752 - 0.0116\,T + 8.632*10^{-6}\,T^2 - 2.348*10^{-9}\,T^3 \tag{6.16}$$
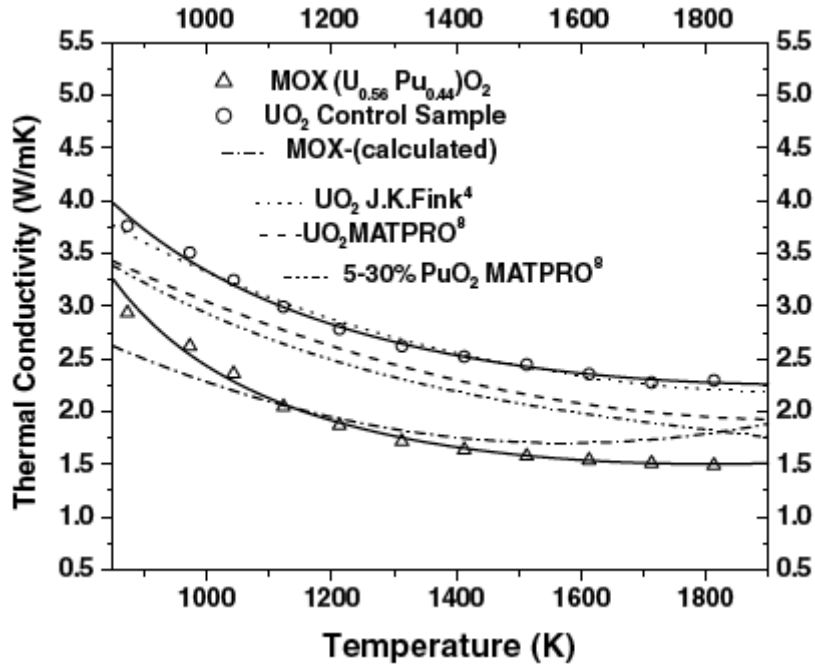
FIG. 39. Thermal conductivity of UO_2-44%PuO_2 pellet as a function of temperature [116].

It is seen from the above study that thermal conductivity is sensitive to Pu content and decreases with increase in the Pu content at a given temperature.

Figure 39 shows the plot of thermal conductivity as a function of temperature for UO_2-44%PuO_2 composition corrected to 95%TD as reported by Sengupta et al. [116]. It was observed that thermal conductivity decreases with increase in temperature and follows a $1/(A + B*T)$ relation. Thermal conductivity of UO_2-44%PuO_2 was found to be 1.80 W/m K while the same for UO_2-30% PuO_2 was 2.33 W/m K at 1000°C. The thermal conductivity data for the above composition could be expressed by the following relation [116]:

$$k = 1/(-0.61 + 1.42 *10^{-3} T - 3.93 *10^{-7}T^2) \tag{6.17}$$

Effect of porosity on thermal conductivity

Pores, like any other defect, scatter phonons and reduce the thermal conductivity. There are many relations in the literature describing the effect of porosity on thermal conductivity. For an exact derivation, the shape and the distribution of porosities must be known. Some of the important relations listed in the literature are given in the annex.

Among these, the following equation proposed by Maxwell-Eucken and also recommended by Carbajo [109] is most commonly used.

$$k_M = [(1 - P)/(1 + \beta P)] \, k_{100} \tag{6.18}$$

where P is the porosity fraction and β is a constant and is 2.

Effect of burnup

For MOX fuel, the thermal conductivity variations with bumup are not significant. Recommendations provided by Martin [110] and Philipponneau [117] as well as previous data obtained by Gibby [118] and Schmidt [52] of unirradiated MOX fuel are shown in Fig. 40. It is found that thermal conductivity of mixed oxide fuel irradiated up to a burnup of 35 GW·d/t is almost in agreement with these recommendations and database for unirradiated fuels. Since the error of this measurement is 10 to 20%, the bumup effect, mainly the effect of fission
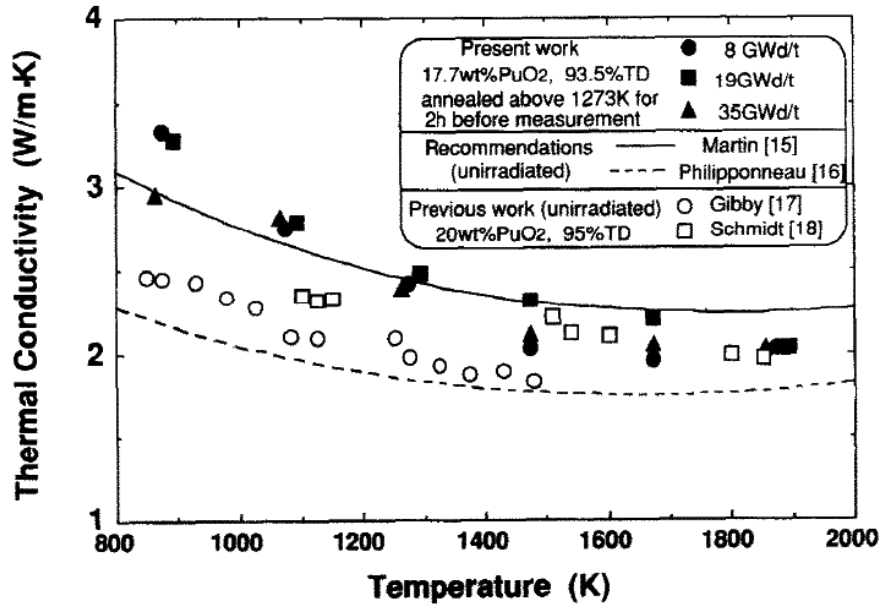
FIG. 40. Thermal conductivity of irradiated MOX fuel [120].

products accumulation, may be hidden by it. Microscopic changes in density and heat capacity during the irradiation can introduce a large error into the measured value. The effect of burnup on thermal conductivity is negligible above 2200 K [119].

6.2.3. Specific heat

For a mixture of UO_2 and PuO_2, the specific heat capacity of the solid is determined by combining the contribution from each constituent in proportion to its weight fraction. For example, the heat capacity for solid MOX $[(U_{1-y}Pu_y)O_2]$ fuel is expressed as

$$C_P (T, MOX) = (1 - y) \, C_P (T, UO_2) + y \, C_P (T, PuO_2) \tag{6.19}$$

where y is the mole fraction of PuO_2.

The specific heat capacity of MOX (or PuO_2) fuel is reported to be slightly larger than the values of UO_2 fuel up to a temperature of 1800 K [119]. The specific heat capacities of pure UO_2, PuO_2 and MOX are shown in Fig. 41. Above 1800 K, the reverse is true: UO_2 fuel has a larger heat capacity than MOX fuel. However, the temperature and the fuel composition are the main variables that influence the heat capacity values. The effect of variation in O/M ratio for MOX fuel may be more significant as indicated in studies by Ogard and Leary [121] and also by Affortit and Marcon [122]. The stoichiometric composition has the lowest heat capacity at all temperatures. Deviations from stoichiometry result in higher heat capacity values. The uncertainty in these specific heat values is ~5%.

Kandan et al. [123] have done calorimetric measurements on Pu rich (U, Pu)O_2 solid solutions. From Fig. 42, it can be seen that the heat capacity values of the solid solutions are in agreement with the computed mole average values using the equations of Carbajo et al. [109] the maximum deviation being 4%. The results indicate that the heat capacities of these plutonium rich $U_{(1-y)}Pu_yO_2$ solid solutions, in the temperature range 298–1800K, obey the Neumann–Kopp's molar additivity rule.

The measured heat capacity of irradiated fuel remains in the band ±10% around the values corresponding to fresh fuel, so that the marked deterioration of the thermal conductivity, k, with burnup is mainly due to a decrease of the thermal diffusivity [109].
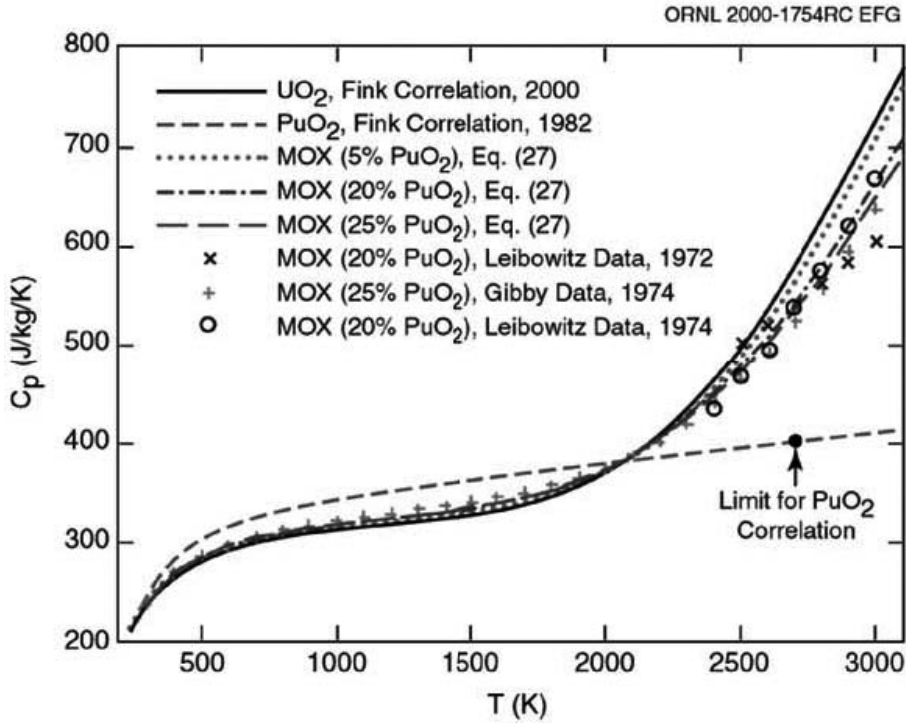
FIG. 41. Specific heat capacity of UO₂, PuO₂ and MOX plotted against temperature [119].
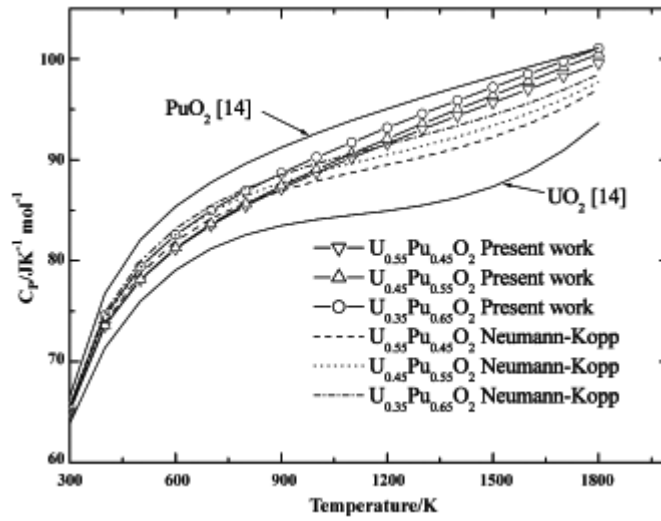
FIG. 42. Comparison of heat capacity data of (U, Pu)O₂ solid solutions calculated from present enthalpy increment measurements with those calculated by Neumann–Kopp's rule [123].

6.2.4. Coefficient of thermal expansion

Both UO₂ and PuO₂ have identical coefficients at low temperature range as shown in Fig. 43. However, at high temperatures (>300ºC) PuO₂ has a higher expansion coefficient.

Existing data on the thermal expansion of UO₂ and (U, Pu)O₂ were reviewed by Martin [124] to establish and recommend a value for reactor usage. He has derived the following expressions for the linear expansion for UO₂ or MOX fuel as a function of temperature.

For 273 K< T < 923 K, the coefficient of thermal expansion ($\alpha(T)$),

$$\alpha(T) \ (1/K) = 9.828 * 10^{-6} - 6.39 * 10^{-10} \ T + 1.33 * 10^{-12}T^2 - 1.757 * 10^{-17} \ T^3 \tag{6.20}$$

61
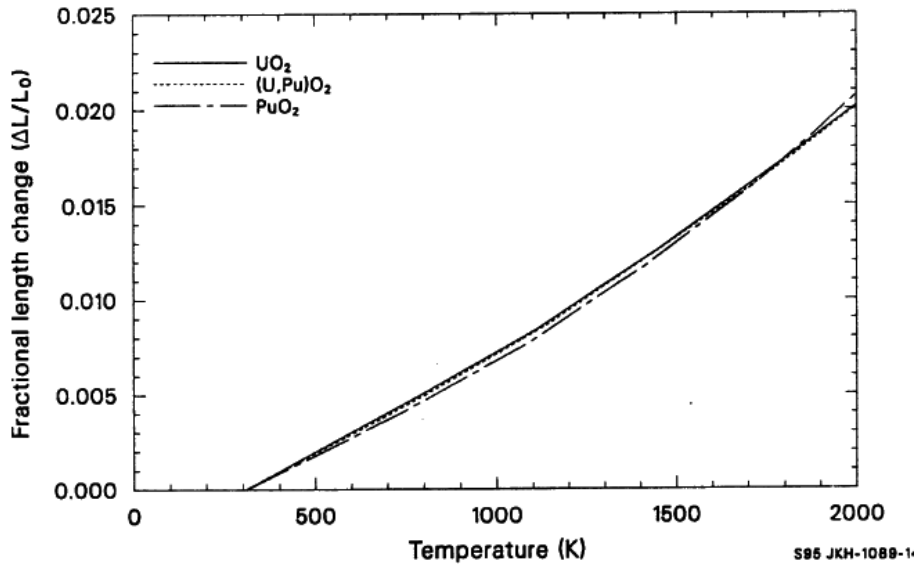
FIG. 43. Thermal-expansion curves for UO_2, PuO_2, and $(U_{0.8}Pu_{0.2})O_{2+x}$ [119].

For 923 K< T <3 120 K

$$\alpha(T)\ (1/K) = 1.1833 * 10^{-5} - 5.013 * 10^{-9}\ T + 3.756 * 10^{-12}T^2 - 6.125 * 10^{-17}\ T^3 \qquad (6.21)$$

Errors in the values of thermal expansion coefficients are $\pm 0.11 * 10^{-6}$, $\pm 0.22 * 10^{-6}$, $\pm 1.1 * 10^{-6}$ (1/K) in the temperature regions of 293–1 273K, 1 273–2 273K, and 2 273–2 929K, respectively [109].

The thermal expansion data for (U, Pu)O_2 lay close to the UO_2 values. The room temperature thermal expansion coefficients for stoichiometric (U, Pu)O_2 and hypostoichiometric (U, Pu)$O_{1.94}$ fuels are approximately $10.5 \times 10^{-6}\ K^{-1}$ and $13 \times 10^{-6}\ K^{-1}$ respectively [103, 125].

The effect of the oxygen-to-metal ratio on the thermal expansion coefficient for (U, Pu)O_{2+x} depends on the deviation from stoichiometric composition according to [24]:

$$\alpha_{(U, Pu)0\ 2+x} = \alpha_0\ (1 - 5.1x) \qquad (6.22)$$

where α_0 is the thermal-expansion coefficient of (U, Pu)O_2 of the same plutonium content. This relation was established only for 20%PuO_2-UO_2 mixture for an O/M ratio of 1.94 < O/M < 2.01 [24].

The coefficient of linear thermal expansion of UO_2-44%PuO_2 was determined using a dilatometer. The Percentage ($\Delta L/L$) could be expressed as a function of temperature by the following relation:

$$(\Delta L/L) * 100 = -0.071 + 0.001 * T - 1.692 * 10^{-7} * T^2 + 2.018 * 10^{-10} * T^3 \qquad (6.23)$$

The uncertainties in the above values are $\pm 6\%$. The average coefficient of linear thermal expansion was found to be $12.52 * 10^{-6}$/K (ambient to 1 000ºC) and the same for MOX containing 30% PuO_2 is $10.65 * 10^{-6}$/K obtained from MATPRO [119].

6.2.5. Density

Densities of pure UO_2 and PuO_2 at 273 K are 10 970 and 11 460 kg/m^3, respectively. The density of UO_2 or MOX as a function of temperature for the temperature range of 273–923 K is given by the following equation [109]:

$$\rho\ (T) = \rho(273)(9.9734 * 10^{-1} + 9.802 * 10^{-6}T - 2.705 * 10^{-10}T^2 + 4.391 * 10^{-13}T^3)^{-3} \qquad (6.24)$$

And the density of UO$_2$ or MOX for the temperature range of 923 K to the melting temperature:

$$\rho (T) = \rho(273)(9.9672*10^{-1} + 1.179*10^{-5}T - 2.429*10^{-9}T^2 + 1.219*10^{-12}T^3)^{-3} \tag{6.25}$$

The density of the solid solution of UO$_2$ and PuO$_2$ changes according to the linear law:

$$\rho \ (kg/m^3) = 10\ 970 + 490y \ (y \text{ is mole fraction of PuO}_2) \text{ at } 273 \text{ K} \tag{6.26}$$

Density of UO$_2$-20%PuO$_2$ fuel is evaluated by the correlation: [126, 127],

$$\rho \ (kg/m^3) = 11080 \ [1 + 2.04 * 10^{-5}(T - 273) + 8.7 * 10^{-9}(T - 273)^2]^{-1} \tag{6.27}$$

Based on the above equation, the density of UO$_2$-20%PuO$_2$ fuel is 9889 kg/m^3 at T$_S$ and 9865 g/m^3 at T$_L$. The recommended uncertainty in the density value is 1% in the entire temperature range [109].

The change in density on melting is of practical concern to the reactor operations since it may contribute to the fuel failure. The accepted value of the density of liquid UO$_2$ at the melting point is 8.74 ± 0.016 g/cm^3. The volume expansion on melting is about 10%. A similar value can be assumed for (U, Pu)O$_2$ [129].

Finally, the burnup also affects the density by the change in the porosity. At low burnup (<15GW·d/t), density increases by the fuel densification process; at the higher burnup, density decreases (porosity increases) due to the fuel swelling [109].

6.2.6. Hot hardness of oxide fuels

Hardness versus temperature plot for UO$_2$-20% PuO$_2$ and UO$_2$-30% PuO$_2$ pellets are shown in Fig. 44. For comparison, the hardness values of pure UO$_2$ are also shown in the same figure. The data points are fitted and used a third degree polynomial of type:

$$H \ (kg/mm^2) = A + BT + CT^2 + DT^3, \tag{6.28}$$
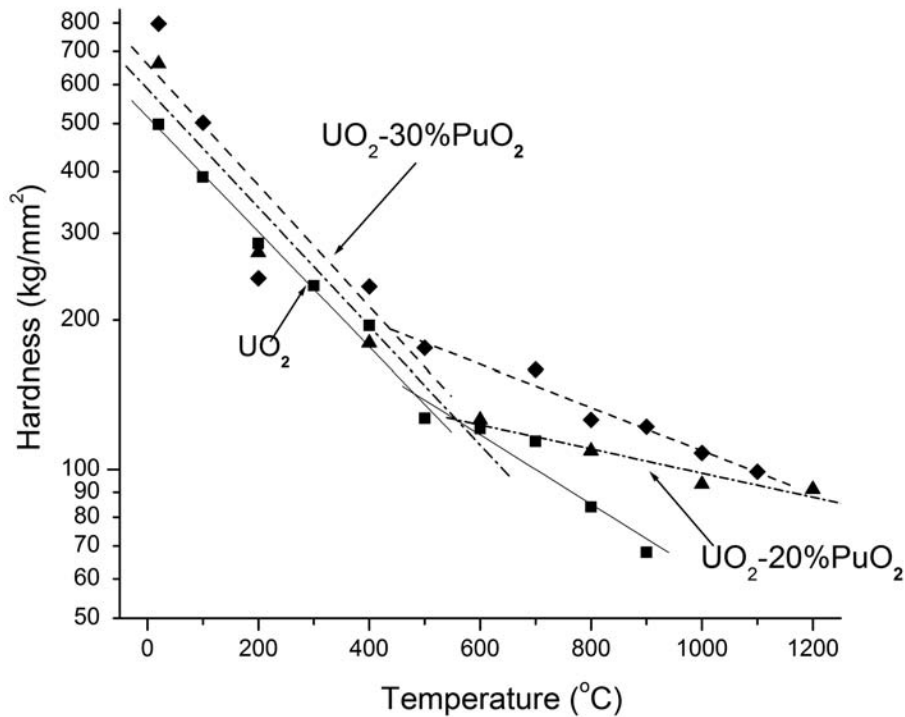
FIG. 44. Hardness versus temperature plot for UO$_2$, UO$_2$-20% PuO$_2$ and UO$_2$-30% PuO$_2$ pellets.

TABLE 11. CONSTANTS OF THE POLYNOMIAL FOR UO$_2$-20% PUO$_2$ AND UO$_2$-30% PUO$_2$ COMPOSITIONS

Composition	A	B	C	D
UO$_2$	522.13	−1.46	0.0018	−8.79 × 10^{-7}
UO$_2$-20%PuO$_2$	683.85	−2.33	0.003	−1.24 × 10^{-6}
UO$_2$-30%PuO$_2$	767.95	−2.65	0.0036	−1.60 × 10^{-6}

Where T is temperature in $^{\circ}$C, and A, B, C and D are constants. The constants of the polynomial for the above compositions are given in Table 11. It can be seen that for the mixed oxide, the hardness values fall sharply up to about 400°C. The fall in hardness values above 400°C is gradual. However, above 600°C, UO$_2$-30% PuO$_2$ and UO$_2$ have the highest and lowest hardness values, respectively.

6.3. THERMO PHYSICAL AND THERMO MECHANICAL PROPERTIES OF CARBIDES AND NITRIDES

Advanced ceramic fuels such as carbides and nitrides have higher thermal conductivities and lower melting points than oxide fuels [10]. The thermal conductivity of mixed carbide fuels increases with temperature, which has a distinct advantage over oxide fuel [10].

6.3.1. Melting point

The melting point of pure UC is given by Matzke [10] as 2780 ± 25 K and Nickerson et al. [130] as 2638 ± 165 K. The melting temperature of PuC is 1875 ± 25 K (PuC decomposes peritectly). The melting temperatures of U$_2$C$_3$ and Pu$_2$C$_3$ are given as 2100 and 2285 K, respectively [32]. The solidus temperature of (U$_{0.8}$Pu$_{0.2}$)C and (U$_{0.8}$Pu$_{0.2}$)$_2$C$_3$ are 2750 ± 30 and 2480 ± 50 K, respectively [32, 10].

The melting temperatures of UN and PuN (under 1 bar N$_2$ pressure) are given as 3035 ± 40 K and 2843 ± 30 K, respectively (PuN decomposes by peritectic reaction). The melting temperature of (U$_{0.8}$Pu$_{0.2}$)N is given as 3053 ± 20 K [35].

Melting point as a function of vapour pressure [Pa] of nitrogen over UN at $10^{-8} \leq P_{N2} \leq 7.5 \times 10^5$ is defined by formula [131]:

$$T_m(K) = 3055 * P_{N2}^{0.02832}. \tag{6.29}$$

Uranium mononitride melts congruently only at high values of partial pressure of nitrogen P_{N2}, at low values of P_{N2} UN decomposes, UN(s) → U(liq) + 0.5 N$_2$(gas).

The solidus temperature for (U$_{0.45}$Pu$_{0.55}$)C fuel was determined in a horizontal dilatometer by heating a pellet up to 2 283 K in flowing Argon gas and monitoring the change in length as a function of temperature. A sudden/abrupt change is slope at 2193 K was observed as shown in Fig. 45 [132]. Beyond this temperature, a high rate of shrinkage was observed which could be attributed to gradual melting of the pellet. This was confirmed by visual and metallographic examination of the sample after cooling to room temperature. Similarly the solidus temperature of (U$_{0.3}$Pu$_{0.7}$)C has been found to be 2148 K.

6.3.2. Thermal conductivity

The cumulative literature on thermal conductivities of UC, PuC, and (U, Pu)C includes several review articles written since 1967 [133]. The thermal conductivity is influenced by several factors such as; fabrication method, impurities, stoichiometry (C/M or N/M), Pu fraction, higher phases, microstructure, irradiation effects, and method of measurement [32].
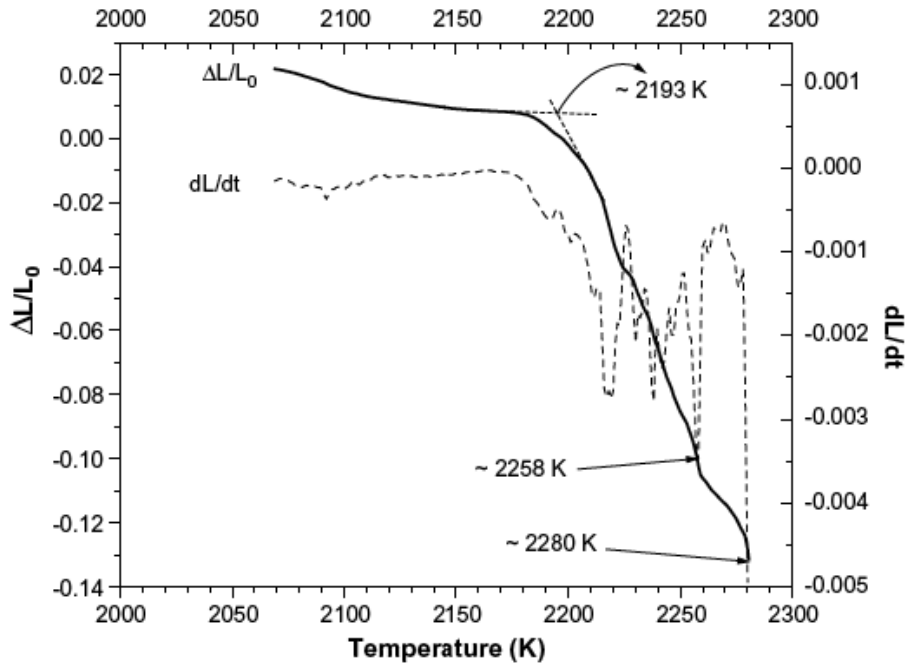
FIG. 45. Determination of the solidus temperature for $(U_{0.45}Pu_{0.55})C$ fuel by a dilatometer [132].
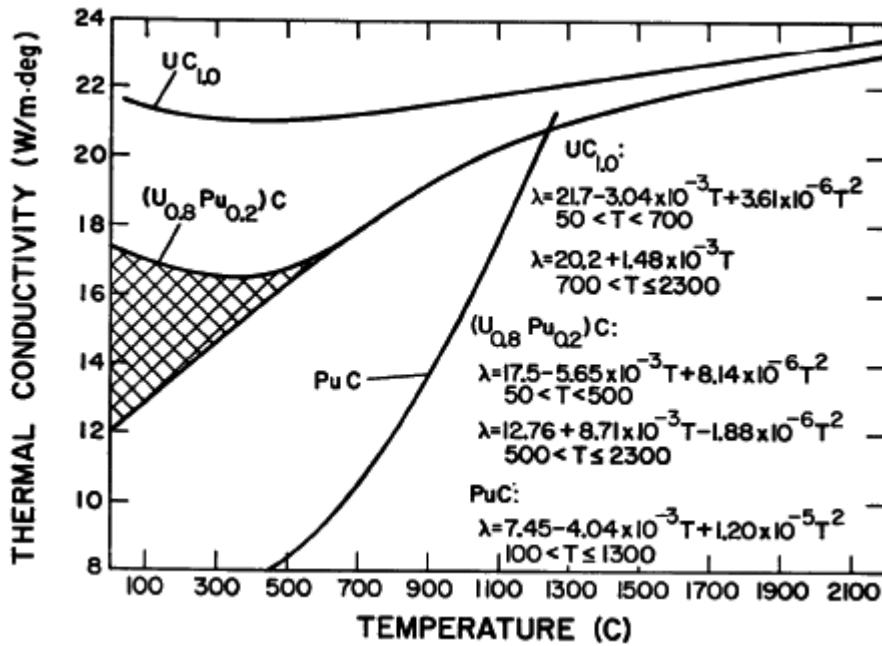
FIG. 46. Suggested thermal conductivity values of UC, PuC and (U, Pu)C [135].

The suggested values of thermal conductivity of UC, PuC and $(U_{0.8}Pu_{0.2})C$ pellets are shown in Fig. 46. For MC, a decrease in conductivity from ambient to about 400°C is illustrated in Fig. 46. However, the uncertainty in conduction mode is illustrated by the cross-hatched area. The values of conductivity of $(U_{0.8}Pu_{0.2})C$ are roughly 20% lower than UC at temperatures below 700°C as indicated by most investigations; a positive temperature dependence above 500°C such that the conductivity approaches that of UC above 2000°C.

Most investigators believe that oxygen concentrations below about 2500 ppm do not significantly affect the thermal conductivity [135]. Bates [136] and Wheeler et al. [137] provide the most comprehensive study for oxygen concentrations in the range 2 at.% (about 0.3 wt%) to 17 at.% (about 2.0 wt%) oxygen. The results of these two

investigations are in reasonable agreement, showing conductivities of about 18 to 19 $Wm^{-1}C^{-1}$ and 12 to 13 $Wm^{-1}C^{-1}$ at 100°C, and 18 to 20 $Wm^{-1}C^{-1}$ and 15 to 18 $Wm^{-1}C^{-1}$ at 1 200°C, respectively, for UC containing about 2 at.% and 17 at.% oxygen. Figure 47 summarizes the thermal conductivity values of UC, PuC and (U, Pu)C containing varying amounts of PuC [10]. The thermal conductivity values decreases with the increase in Pu in the fuel. Storms [138] found that k of MC + M_2C_3 with M = $U_{0.8}Pu_{0.2}$ and low oxygen content changes between 500 K and 1500 K from 17 to 19 $Wm^{-1}K^{-1}$ nearly linearly. This means that the effect of substituting up to 20% of uranium by plutonium is rather strong around 600 K but relatively weak near 1600 K (Fig. 47). The uncertainties of k is ±10% for UC and ±15% for (U, Pu)C for temperatures above ~500°C and still higher for lower temperatures.

Thermal diffusivity of mixed uranium plutonium carbide fuel used in FBTR was measured by transient laser flash method from ambient to 1 773 K in vacuum of 0.133 Pa [132]. The density of MKI $(U_{0.3}Pu_{0.7})$C and MKII $(U_{0.45}Pu_{0.55})$C fuels were 90 ± 1 and 86±2% TD, respectively. The density values were corrected for temperature using the measured average coefficient of linear thermal expansion data, to calculate thermal conductivity at each temperature. Specific heat capacity, C_p of both MKI and MKII fuels were determined by adding the specific heat data available in literature for UC and PuC proportional to the weight fraction present in MC fuels.

It is shown in Fig. 48 that for both fuels, thermal conductivity increases with increase in temperature and thermal conductivity of MKI fuel is almost same as that of MKII up to about 1100 K although density of MKI is higher than that of MKII. Thermal conductivity of mixed carbide fuel decreases with increase in PuC content and increase with increase in temperature and density. The effect of PuC appears more prominent which explains why MKI fuel has lower thermal conductivity (up to a temperature of 1100 K). Beyond a temperature of 1100 K thermal conductivity of MKI is more than that of MKII. This could be attributed to the fact that in MC, PuC is present as a defect structure (PuC_{1-x}) and contributes to electronic transfer of heat which is a function of temperature [139]. This contribution appears to be more for MKI containing 70% PuC than that of MKII containing 55% PuC beyond 1100 K. However, at the average working temperature, both MKI and MKII fuels have almost similar thermal conductivity [140].

For nitrides, the situation is simpler than for carbides because neither oxygen nor large deviations from stoichiometry play an important role [32]. The thermal conductivity values of UN have been determined by different authors [142]. The scatters in the reported results are larger than that for UC [10]. Washinton [114] recommended the following relation for UN:

$$k_{UN} \text{ (W/m/K)} = 10.55 + 0.02T - 5.96 * 10^{-6}T^2 \text{ for } 200 \leq T \leq 1\ 800°C \tag{6.30}$$
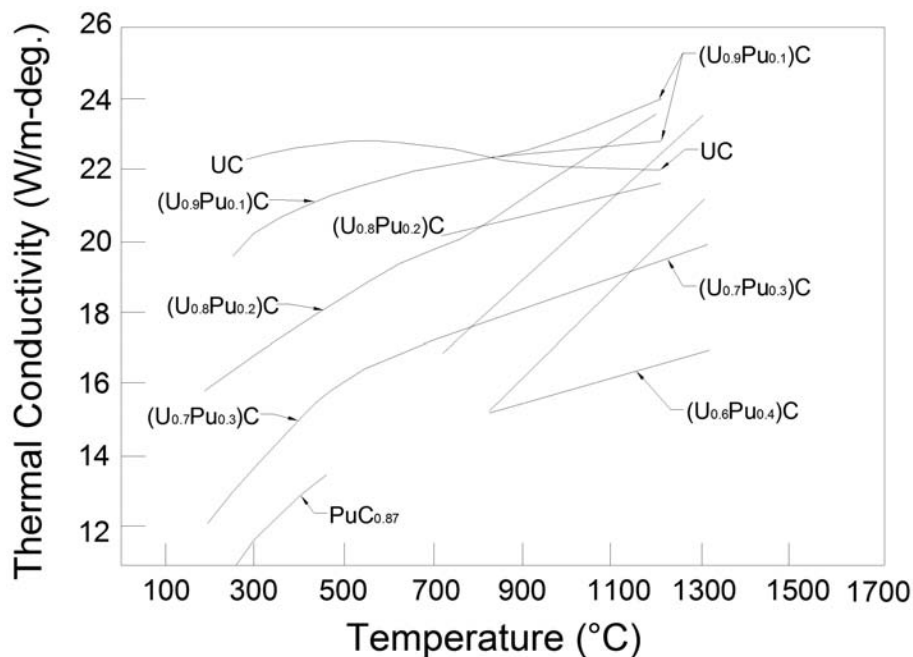
FIG. 47. Thermal conductivity data for UC, PuC and (U, Pu)C containing different amounts of Pu [32].
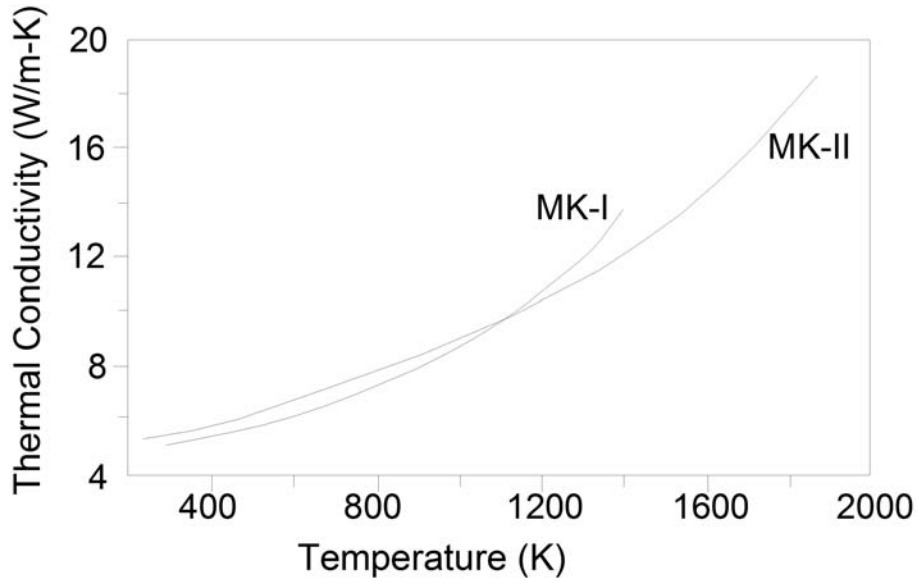
FIG. 48. Thermal conductivity of MKI and MKII FBTR fuels are plotted as a function of temperature [132].
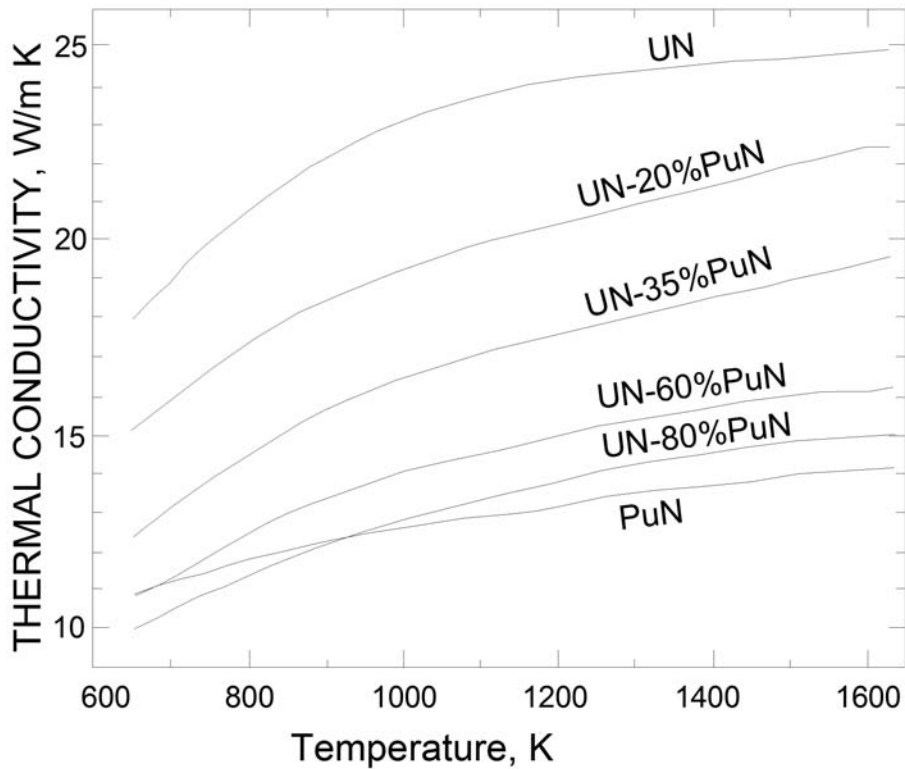
FIG. 49. Temperature dependence of thermal conductivities of (U, Pu)N pellets with varying Pu contents [144].

Thus compared to UC, UN shows a smaller conductivity at low temperatures (<600°C), where as $k_{UN} > k_{UC}$ for T > 1000°C [10].

The effect of alloying UN and PuN appears to be different from the alloying of UC with PuC [32]. In the case of carbides, the effect of alloying on k was stronger at low temperatures than at high temperatures, this is hardly the case if PuN is alloyed with UN (Fig. 49).

The temperature dependence of thermal conductivity of PuN is given by the following relation [10] :

$$K_{PuN} (W/m/K) = 7.73 + 1.34 * 10^{-2}T - 9.5 * 10^{-6}T^2 \text{ for } 200 \leq T \leq 1\,500°C \tag{6.31}$$
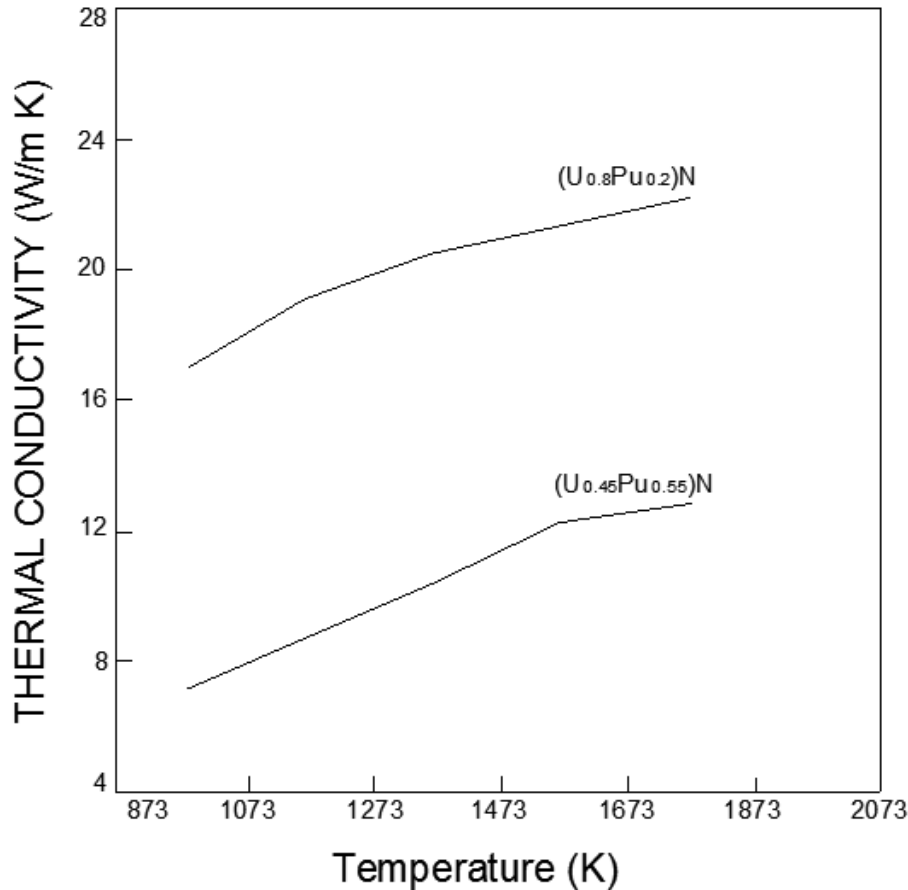
FIG. 50. Thermal conductivities of two promising compositions, UN-55%PuN and UN-20%PuN [150].

The thermal conductivity of (U, Pu)N was found to decrease with increase in Pu content [146, 147]. Thermal conductivity of the pellets containing about 1 wt% oxygen is lower than that of usual nitride pellets containing 0.1–0.2 wt% oxygen by 9–10% and 12–13% at 1000 and 1500 K, respectively. Thermal conductivities of two promising compositions, UN-55%PuN and UN-20%PuN are given in Fig. 50 [147].

The thermal conductivity data on MC and MN fuels may be summarized as follows [32]:

— Thermal conductivity of MC and MN fuels increases with temperature. However, there is significant scatter (±20%) in the reported values;
— Thermal conductivity of MC and MN fuels decreases with increase in plutonium content;
— Thermal conductivity of MC reduces with M_2C_3 and oxygen contents and improves with higher pellet density;
— For (U, Pu)N, a minimal thermal conductivity is reported corresponding to nearly 50% Pu at all temperatures.

6.3.3. Heat capacities of carbides and nitrides

A final assessment of the available thermal and thermodynamic data of the actinide carbide is given by Holley et al. [152]. This contains C_P versus T relation for all actinide carbides, with the exception for U_2C_3. The data for U_2C_3 are those of Oetting et al [153]. In Fig. 51, Cp values of PuC and Pu_2C_3 are plotted together with that of UC for comparison.

C_p versus T relations for nitrides are shown in Fig. 52. C_P (T) relation for UN by Tagawa [154] has been modified recently by Haynes et al. [155]. In Fig. 52, it can be seen that the data for MN lies between that of UN and PuN. On similar ground, one can argue that the value MC should lie between that of UC and PuC.
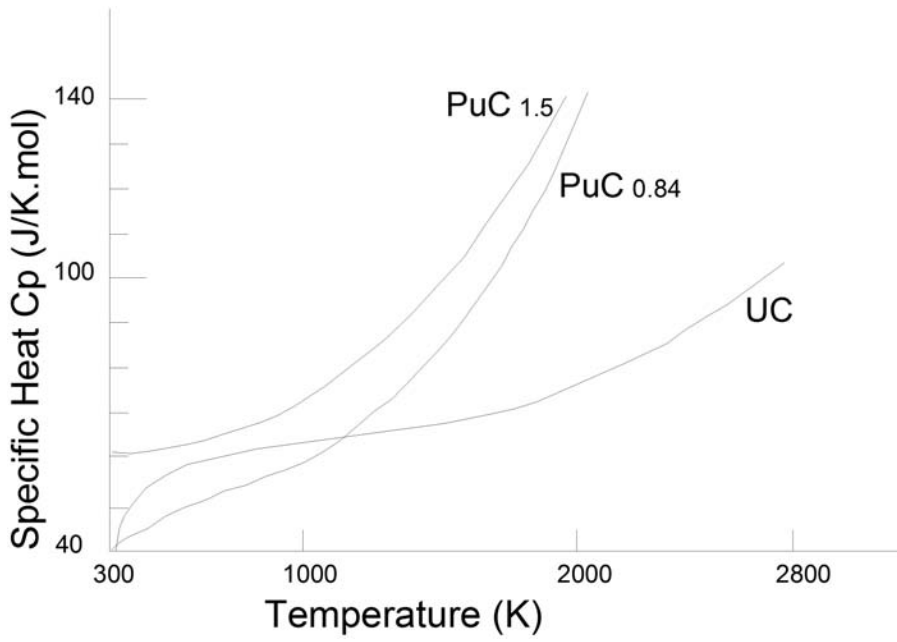
FIG. 51. Heat capacities of UC, PuC and MC pellets [32].
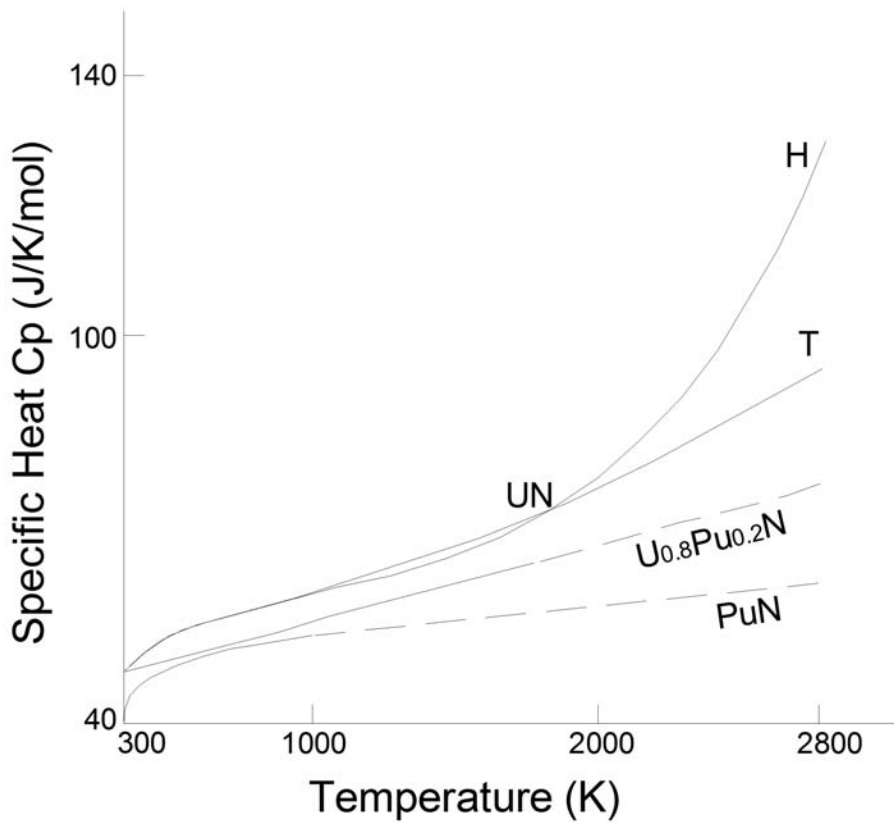
FIG. 52. Heat capacities of PuN and MN pellets. Heat capacity of UN measured by Tagawa [154] and Haynes [155] are also shown [32].

The experimental C_P values are usually represented by 4 or 5 fitting parameters [32]:

$$C_p(J/(mol.K)) = a + bT + cT^2 + dT^3 + e/T^2 \qquad (6.32)$$

The coefficients of the above equation for carbides and nitrides are given in Table 12.

TABLE 12. COEFFICIENTS OF SPECIFIC HEAT RELATION Eq. (6.32) [32]

Fuel	T_{max} (K)	a	b	c	d	e
UC	2780	50.984	2.57×10^{-2}	-1.87×10^{-5}	5.72×10^{-9}	-6.19×10^{5}
U_2C_3	1670	75.354	-2.39×10^{-2}	2.07×10^{-5}	0	-1.45×10^{6}
$PuC_{0.85}$	1875	57.876	-1.45×10^{-2}	7.71×10^{-6}	8.62×10^{-9}	-6.55×10^{5}
Pu_2C_3	2285	78.037	-3.99×10^{-2}	3.52×10^{-5}	0	-1.09×10^{6}
UN	2628	54.15	2.28×10^{-3}	4.37×10^{-6}	0	-6.82×10^{5}
PuN	—	50.2	4.19×10^{-3}	0	0	-8.37×10^{5}
MN	1800	45.38	1.09×10^{-2}	0	0	0

TABLE 13. VALUES OF THE COEFFICIENTS OF THERMAL EXPANSION FOR CARBIDES [10]

Material	CTE $\times 10^{-6}$/°C (at 25°C)	Mean CTE $\times 10^{-6}$/°C (25–1 000°C)
UC	10.1	11.2
PuC	8.5	10.8
(U, Pu)C	8.8	11.9
U_2C_3	10.7	10.6
Pu_2C_3	12.9	14.9
$(U, Pu)_2C_3$	9.6	11.2

6.3.4. Thermal expansion of carbide and nitrides

Most of the carbide data have been determined between 1960+– and 1970 [5]. The expansion coefficients were obtained by dilatometer and X ray diffraction for U_2C_3 and UC respectively. The pronounced difference in expansion between UC and U_2C_3 will lead to considerable internal stresses in UC + U_2C_3 system.

The UC data can be described analytically by the relation [158]:

$$\Delta L/L_0 = -2.01 \times 10^{-4} + 1.004 \times 10^{-5}T + 1.17 \times 10^{-9}T^2 \qquad 20 < T < 2\,000°C \qquad (6.33)$$

Similarly, the data for $PuC_{0.85}$ and U_2C_3 can be described by the following relations [158]:

$PuC_{0.85,}$

$$\Delta L/L_0 = -4.01 \times 10^{-4} + 8.3 \times 10^{-6}T + 3.0 \times 10^{-9}T^2 \qquad 20 < T < 900°C \qquad (6.34)$$

U_2C_3

$$\Delta L /L_0 = 12.6 \times 10^{-4} + 1.077 \times 10^{-5}T - 1.69 \times 10^{-9}T^2 + 1.55 \times 10^{-12}T^3 \qquad 20 < T < 1\,700°C \qquad (6.35)$$

Where L is the length at temperature T (L_T) or at 0°C (L_o), and T is in °C. For UC, the CTE values at 1000 and 2000°C are 11.2×10^{-6} and 12.4×10^{-6}/°C, respectively [32]. For PuC, CTE values at 900°C are 10.9×10^{-6}/°C. The recommended values of CTE for carbide fuels are given in Table 13 [10].

U_2C_3 and UN preferentially remain stoichiometric and do not accept large amounts of oxygen as impurity [32]. Alloying with Pu_2C_3 and PuN, respectively, leads to systematic increase in thermal expansion in mixed M_2C_3 and MN with Pu content. In contrast to U_2C_3 and UN, in UC and in two phase structure MC+ M_2C_3, the effect of Pu is apparently overshadowed by the following factors [32],

(1)   The C deficiency in the alloying component PuC_{1-x};
(2)   Varying amount of dissolved oxygen in the MC phase;
(3)   Varying amount of size distribution of M_2C_3 precipitate in two phase structure MC + M_2C_3.

The thermal expansion was measured from room temperature to 873 K for MKI fuel [$(Pu_{0.7}U_{0.3})C$] under vacuum conditions [132]. The relation between ($\Delta L/L_0$) and T can be expressed by the following equation:

$$\Delta L/L_0 = -16.59 \times 10^{-4} + 4.17 \times 10^{-6}T + 4.60 \times 10^{-9}T^2 \tag{6.36}$$

The percentage thermal expansion [($\Delta L/L_0$) $\times$ 100] at any temperature between 300 and 1800 K can be expressed by

$$\Delta L/L_0 \times 100 = -0.3333 + 7.1528 \times 10^{-4} + 7.6889 \times 10^{-7} T^2 + 2.249 \times 10^{-10}T^3 \tag{6.37}$$

The plot of thermal expansion coefficient versus temperature for MKII [$(Pu_{0.55}U_{0.45})C$] is shown in Fig. 53. An average value of coefficient of thermal expansion between 300 and 1800 K has been calculated as 11.6×10^{-6} K^{-1} for MKII and MKI fuel as 13.8×10^{-6} K^{-1}. So, MKI fuel has higher coefficient of thermal expansion than MKII fuel which is expected due to higher Pu content in the MKI fuel [132].

The situation of nitrides is less complex. Oxygen is hardly soluble in UN and PuN. Sesqui nitride is usually avoided while fabrication of UN. The available experimental data are scarce but relatively consistent [159]. The expansion curve of MN is shown in Fig. 54 along with that of MC (M = $U_{0.8}Pu_{0.2}$). Nitrides have lower expansion coefficient than carbides for the same Pu content [31].

Linear expansion coefficient of UN is calculated by the correlation [131]:

$$\alpha \, (1/K) = 7.096 \times 10^{-6} + 1.409 \times 10^{-9} \, T \quad (298 < T < 2523 \, K) \tag{6.38}$$
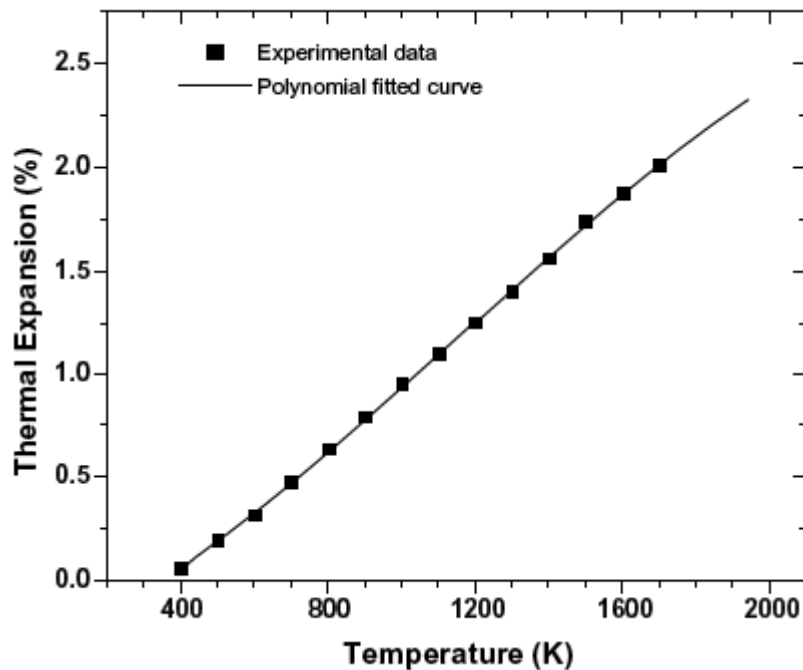

FIG. 53. Thermal expansion as a function of temperature for $(Pu_{0.55}U_{0.45})C$ pellet [132].
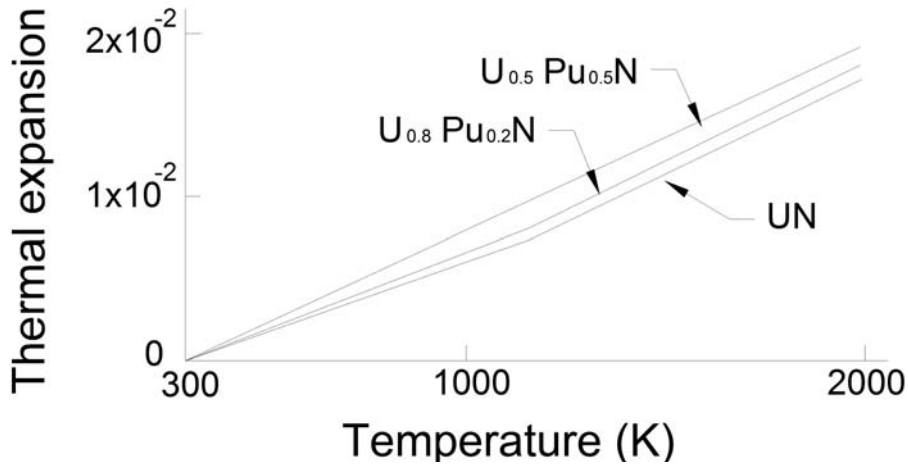
FIG. 54. Expansion curves for UN, PuN and MN pellets [32].

6.3.5. Density

The densities of advanced fuels at high temperature, $\rho(T)$, is given by the following relation:

$$\rho(T) = \rho_0[1 + (\Delta L/L_0)]^{-3} \tag{6.39}$$

where ρ_0 is the density at room temperature.

Density of UC is defined by the following correlation:

$$\rho(T)\ (kg/m^3) = 13630\ (1 - 3.117 \times 10^{-5}T - 3.51 \times 10^{-9}\ T^2) \tag{6.40}$$

where T is temperature, K. This correlation has been derived based on the experimental data in Ref. [161] that were obtained by measurement of linear expansion coefficient in the temperature range from 0 to 2800°C.

The analysis of data in Ref. [163] results in the correlation, which gives more severe decrease of UC density with temperature:

$$\rho\ (kg/m^3) = 13\ 500\ (1 - 2.13 \times 10^{-5}\ T - 2.04 \times 10^{-8}\ T^2) \tag{6.41}$$

Theoretical density of UN at $298 \leq T \leq 2\ 523$ K [131],

$$\rho\ (kg/m^3) = 14420 - 0.2779T - 4.897 \times 10^{-5}T^2. \tag{6.42}$$

The density of $(U_{0.8}Pu_{0.2})C$ and $(U_{0.8}Pu_{0.2})N$ pellets are 13.58 and 14.32 g/cm^3, respectively.

6.3.6. Hot hardness

The hardness of mixed carbides and nitrides has been extensively studied in India [139, 140, 141, 148, 151, 165, 167]. The hardness-temperature plots for FBTR MKI and MKII fuels are shown in Fig. 55. For MKI fuel, the plot clearly shows a change in slope at around 1123 K (0.52 T_m; where Tm is the melting point of the material). The change in slope indicates change in deformation mechanism from simple slip to diffusion controlled processes. For MKII fuel also, hardness decreases with increase in temperature; the decrease being less at lower temperature range (<973 K) than the same at higher temperature. No sharp transition could however be observed in this fuel.

The data generated have been compared with that of Los Alamos [168] who had reported data from experimental measurements for mixed carbide containing 21% and 69% PuC. The data generated at Los Alamos [168] for 69% PuC are in close agreement with those of the data containing 70% PuC (MKI) up to 1100 K. The
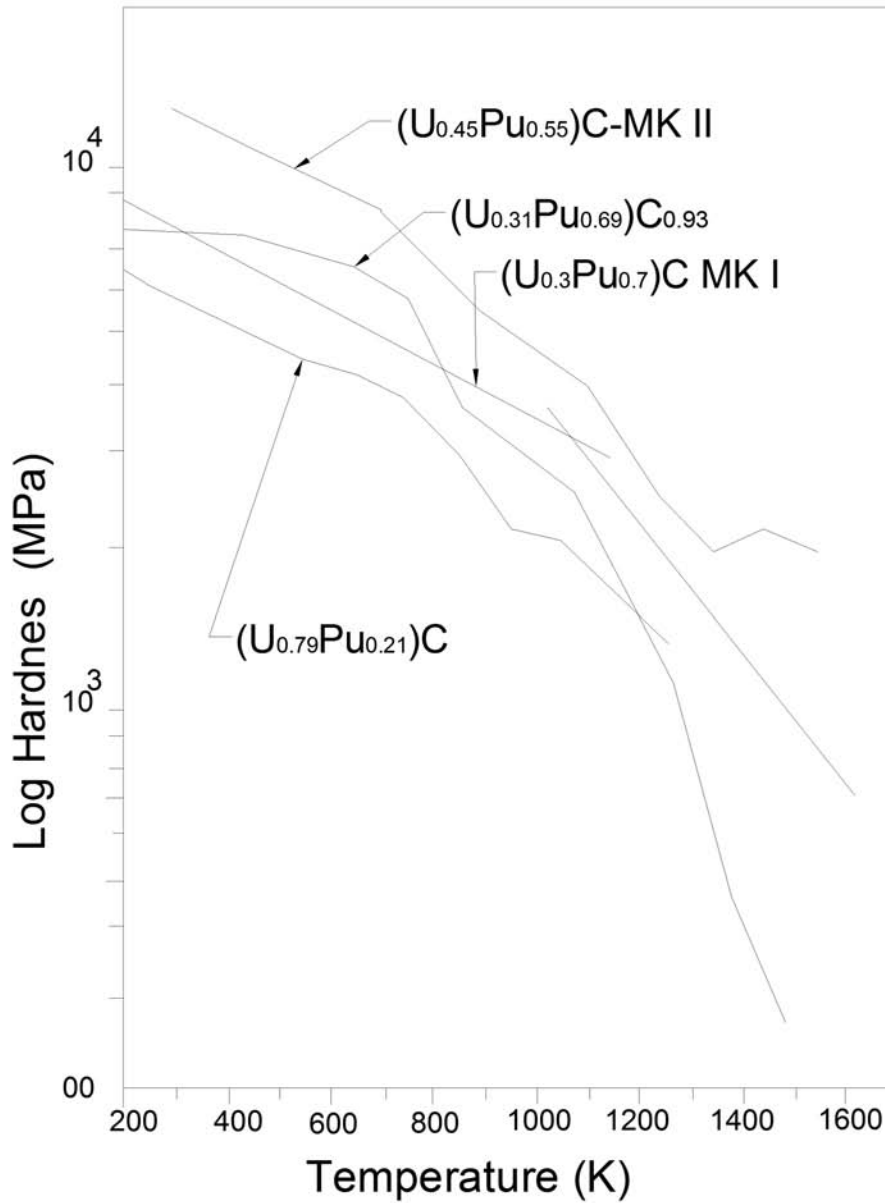
FIG. 55. Variation of hardness with temperature for MKI and MKII fuels [165].

small variation in the hardness could be attributed to difference in composition, second phase sesquicarbide and porosity between the samples. Hardness data of MKII fuel is higher than that of MKI fuel at all temperatures. This could be attributed to higher melting point of MKII fuel compared to MKI, which has a direct bearing on hardness. Higher hardness of MKII fuel than either MKI containing 70% PuC or that containing 20% PuC could also be due to solid solution hardening. An increase in hardness beyond 1300 K could be due to either or combined effects of micro structural changes and oxidation at higher temperature. The hot-hardness data for UN, PuN and $(U_{0.7}Pu_{0.3})N$ are shown in Fig. 56.
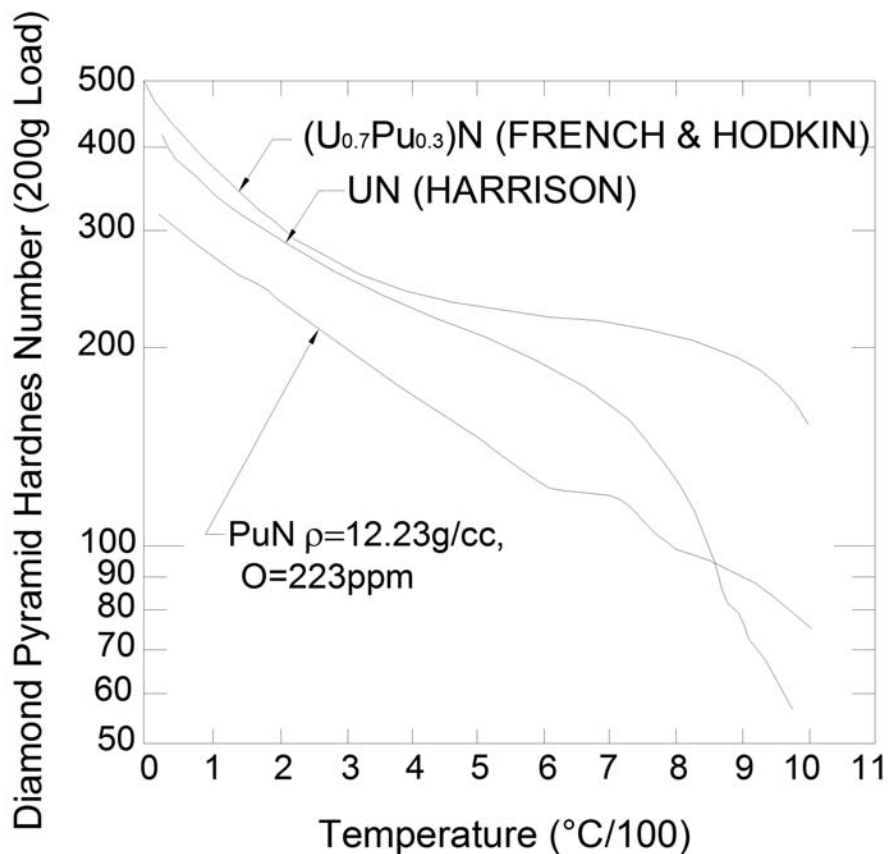
FIG. 56. Hardness-temperature plots for UN, PuN and MN pellets [168].

TABLE 14. PROPERTIES OF U-Pu-Zr ALLOYS [171]

Property	U		U		U		U	
	Pu	Zr	Pu	Zr	Pu	Zr	Pu	Zr
Nominal composition: wt%	11.1	6.3	15	6.8	15	10	18.5	14.1
At %	10	15	13.6	14.3	12.9	22.5	15	30
Approx. Liquidus temperature (^{o}C)	1200		1240		1250		1290	
Approx. solidus temperature (^{o}C)	1120		1105		1155		1170	
Hardness at 25 ^{o}C as cast (DPH)*	470		440		540		410	

* Diamond pyramid hardness.

6.4. THERMOPHYSICAL AND THERMO MECHANICAL PROPERTIES OF METAL FUELS

6.4.1. Melting temperature

Plutonium is the lowest melting element among Th, U, Pu, Am, Np at 640°C (913K), with Np close at 645°C (618K). The melting temperature of pure U is 1 405K. For U-15 wt% Pu [169, 170], solidus temperature and liquidus temperatures are 1249 K and 1335 K, respectively. The solidus and liquidus temperatures of some important U-Pu-Zr alloys are shown in Table 14. The solidus temperature of fuel increases by ~13°C for each per cent of zirconium present for a U-20% Pu alloy [171]. The solidus and liquidus temperatures of U-Pu and U-Pu-Fs alloys are given in Table 15.

TABLE 15. PROPERTIES OF URANIUM-PLUTONIUM-FISSIUM[#] ALLOYS [171]

Property	U	U	Pu	U	Pu	Fz	U	Pu	Fz	U	Pu	Fz
Composition: wt%		90	10	80	10	10	75	15	10	60	20	10
At %		90	10	69.9	8.7	21.4	65.5	13.1	21.4	61.1	17.5	21.4
Liquidus temp (°C)	1133	1060			1010			1000			990	
Solidus temp (°C)	1133	1025			910			865			820	
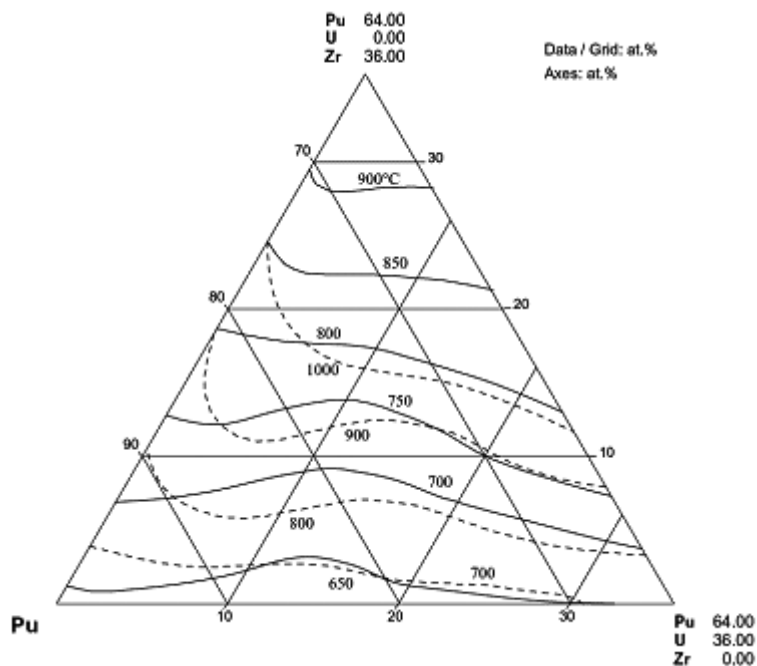
FIG. 57. *Liquidus (dashed lines) and solidus (solid lines) temperature in the Pu rich corner of Pu-U-Zr ternary system [172, 173].*

In the U-Pu system, both the solidus and liquidus temperatures increase with the addition of Zr as shown in Fig. 57 based on work by Farkas et al. [172, 173].

6.4.2. Thermal conductivity

Thermal conductivity of pure uranium in the range of 293−1405 K is estimated using the correlation given below to an accuracy of ±10% [174]:

$$k(W/m/K) = 22 + 0.023(T - 273) \tag{6.43}$$

The thermal conductivities of U-Zr alloys were determined by Takahashi et al. [175] at temperatures from 300 to 1000 K. The thermal conductivities were calculated by the additivity law using heat capacity values estimated from those of uranium and zirconium. Figure 58 shows the thermal conductivities in the temperature region from 300 to 1400 K, together with those of metallic uranium and zirconium [176]. Both the thermal diffusivities and the thermal conductivities of U-Zr alloys exhibited minimum values in the δ-phase alloy having a composition of U-72.4 at% Zr.

A correlation to predict the thermal conductivity of U-Zr alloys for U-rich (U > 50 wt%) cases has been developed at ANL [176]. This includes the U-Zr data from Touloukian et al. [177], Takahashi et al. [175], and the Zr data from Fink et al. [178].
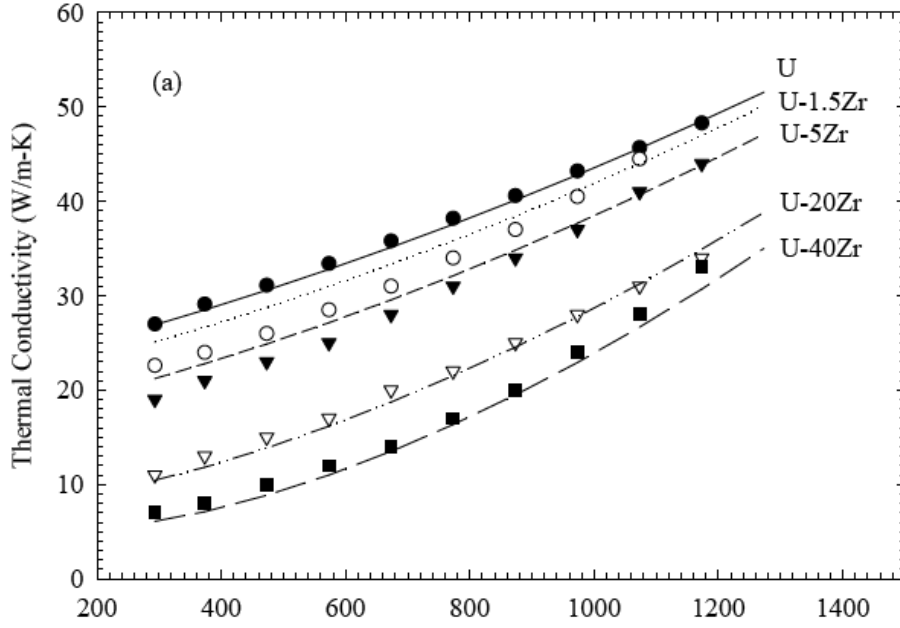
FIG. 58. Thermal conductivity of U-Zr alloys plotted against temperature [176].

$$k_{Zr-U} = [1 - (1 - x_{Zr})^{0.5}]k_{Zr} + (1 - x_{Zr})^{0.5} [x_{Zr} k_{c,U} + (1 - x_{Zr})k_U] \qquad (6.44)$$

where is the x_{Zr} weight fraction of Zr, k_U is the thermal conductivity of uranium, k_{Zr} the thermal conductivity of Zr, and $k_{c,U}$ is a thermal conductivity correction due to the alloying effect.

Thermal conductivity data on U-Pu-Zr alloys are scanty. The thermal conductivity of U-15%Pu-15%Zr and U-15%Pu-25%Zr (at %) has been determined by Farkas et al. [179] in the temperature range 100–900°C and is shown in Fig. 59. Thermal conductivity of U-15%Pu-15%Zr is 11.1 W/m/°C at 100°C and rises to 30.1 W/m/°C at 900°C. Similarly, for U-15%Pu-25%Zr alloy, it rises from 9.2 W/m/°C at 100°C to 26.01 W/m/°C at 900°C. The thermal conductivity of the extruded specimen of U-15%Pu-6.8%Zr was measured from 110–892°C. The thermal conductivity increased from 12.7 to 31.7 W/m/°C. Above the transition temperatures, the material became sufficiently soft and deformation occurred. Measurements in this temperature range were adjusted to reflect the magnitude of this deformation. Ogata [180] has given the following relation for the thermal conductivity of U-Pu-Zr fuel.

$$k \ (W/m/K) = 16.309 + 0.02713 \ T - 46.279C_z + 22.985C_z^2 - 53.545C_p \qquad (6.45)$$

$(T < 1173K, C_p < 0.16, C_z < 0.72)$

Where C_p, C_z is the atom fraction of Pu and Zr, respectively, T in Temperature K.
The thermal conductivity of U-Pu-Zr alloy can also be represented by the following relation [181]:

$$k(\ W/m/K) = a + bT + cT^2 \qquad (6.46)$$

Where, $a = 17.5*((1 - 2.23*W_{zr})/(1 + 1.61*W_{zr}) - 2.62*W_{Pu})$

$b = 0.0154*((1 + 0.061*W_{zr})/(1 + 1.61*W_{zr}) + 0.9*W_{Pu})$

$c = 9.38*10^{-6}*(1 - 2.7*W_{Pu})$

where W_U, W_{Pu} and W_{Zr} are the weight fractions of U, Pu and Zr, respectively.
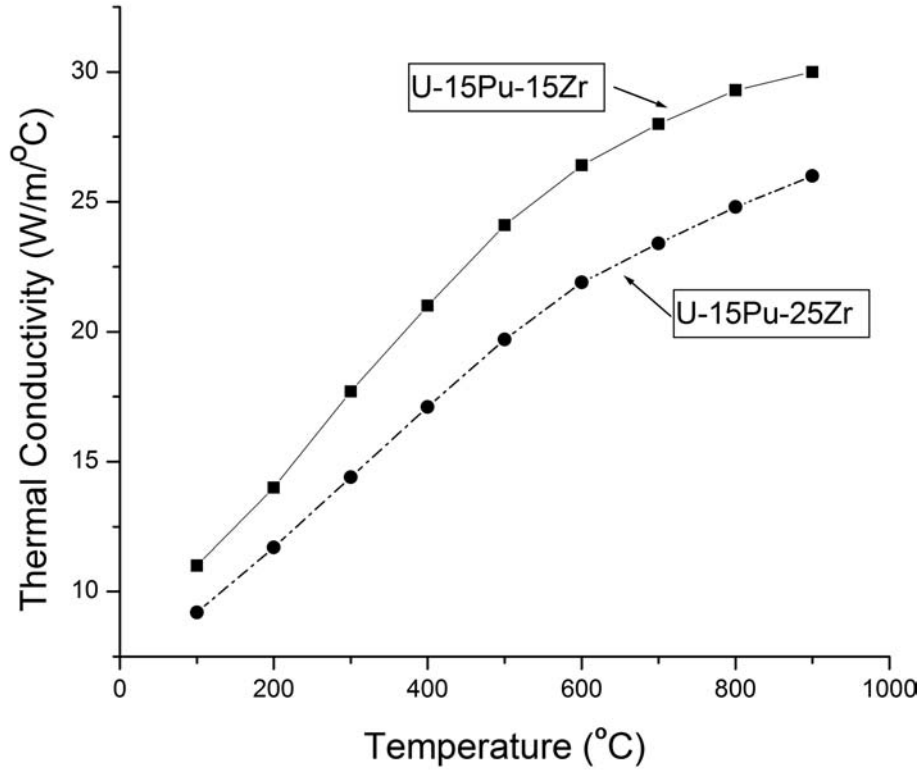
FIG. 59. Thermal conductivities of U-Pu-Zr alloys at different temperatures [179].

For U-15%Pu, the above equation becomes:

$$k(T) = 10.6225 + 0.17479\ T + 5.5811 * 10^{-6}\ T^2\ (W/m/K) \tag{6.47}$$

Where T is in K.
For fuel containing porosity, the following correction factor is employed:

$$f(p) = (1 - p)/(1 + 2.5p) \tag{6.48}$$

where p is the porosity fraction, and

$$k(T,p) = f(p) * k(T, 100\% TD) \tag{6.49}$$

6.4.3. Specific heat of metallic fuels

Heat capacity of uranium in the range of 293−942 K is calculated by expression in Ref. [174]:

$$Cp\ [J/(kg.K)] = 104.82 + 5.3686 \times 10^{-3}\ T + 10.1823 \times 10^{-5}\ T^2. \tag{6.50}$$

$$At\ 942 \leq T \leq 1049\ K\ Cp = 176.4\ J/(kg.K); \tag{6.51}$$

$$At\ 1\ 049 \leq T \leq 1405\ K\ Cp = 156.8\ J/(kg.K)\ [182] \tag{6.52}$$

Heat capacities of U-Zr alloys have been determined by laser-flash calorimetry from 300 to 1100 K [183]. The measured specific heat for the un-irradiated fuel is representative and consistent with the values estimated from the Neumann–Kopp rule. The heat capacities of uranium rich alloys show the normal temperature dependence up to 870 K, while those of zirconium-rich alloys have a small hump above 650 K. The heat capacity anomalies were

observed between 870 and 970 K, which correspond with the predicted phase transitions of the alloys. At temperatures above the phase transitions, heat capacities of U(γ)Zr(β) phase were determined to be 31–36 J/mol/K and have a very small temperature dependence up to 1100 K [183].

Limited amount of thermodynamic data is available on ternary U-Pu-Zr alloys. Farkas et al. [184] have determined the heat capacity of U-12.23%Pu-21.8%Zr (at.%) from 25°C–1150°C. They gave the following relations:

For temperature range of 25°C–650°C, for the two phase alloy of α(U) + (U,Zr),

$$\Delta H \, (T) \, (J/mol/K) = -6833.1 + 18.76 \, T + 0.0129T^2 \tag{6.53}$$

$$C_p(T) \, (J/mol/K) = 18.76 + 0.0258T \tag{6.54}$$

For temperature range of 25°C to 650°C, for the two phase alloy of α(U) + γ(U),

$$\Delta H \, (T) \, (J/mol/K) = 8560.1 + 14.15 \, T + 0.01265T^2 \tag{6.55}$$

$$C_p(T) \, (J/mol/K) = 14.15 + 0.0253T \tag{6.56}$$

The specific heat of U-15%Pu-10%Zr (composition in wt%) is given as a function of temperature by Savage [185] as:

$$C_p(T) \, (cal/g.atom.^{\circ}C) = 6.36 + 0.00636T \, (25–600^{\circ}C) \tag{6.57}$$

$$C_p(T) \, (cal/g.atom.^{\circ}C) = 3.79 + 0.00623T \, (650–l \, 150^{\circ}C) \tag{6.58}$$

The specific heat of U-10%Pu-10% Fs (composition in wt%) is given as a function of temperature as [185]:

$$C_p(T) \, (cal/g.atom.^{\circ}C) = 2.69 + 0.0131T \, (100–500^{\circ}C) \tag{6.59}$$

$$C_p(T) \, (cal/g.atom.^{\circ}C) = -3.52 + 0.0176T \, (600–800^{\circ}C) \tag{6.60}$$

And the specific heat of U-10%Pu (composition in wt%) is given as [185]:

$$C_p(T) \, (cal/g.atom.^{\circ}C) = 4.40 + 0.0117T \, (100–550^{\circ}C) \tag{6.61}$$

$$C_p(T) \, (cal/g.atom.^{\circ}C) = -58.3 + 0.0100T \, (600–700^{\circ}C). \tag{6.62}$$

6.4.4. Thermal expansion of metallic fuels

Metal fuels have large expansion coefficients compared to oxides or carbides. The linear expansion versus temperature (T in $^{\circ}$C) for alpha uranium without texture is given by:

$$L(T) = L_o(1 + 14.8.10^{-6}T + 5.5.10^{-9}T^2) \tag{6.63}$$

The expansion values of ternary U-Pu-Zr are shown in Table 16 [186]. It can be seen that metallic fuels have comparatively high CTE values. The CTE values above the transformation temperature are about 25% higher than that at low temperature.

The coefficients of thermal expansion for U-Pu-Zr alloys as a function of the composition are given by the following relation:

$$\alpha_{fuel}*10^{-6} \, (K^{-1}) = 19.41 + 12.67*C_{Pu} - 13.37*C_{zr} \tag{6.64}$$

Where, C_{Pu} and C_{Zr} are the concentration of Pu and Zr in atom fractions, respectively.

TABLE 16. THERMAL EXPANSION COEFFICIENTS OF U-Pu-Zr ALLOYS

Composition (wt%)	U-17.2Pu-14.1Zr
Expansion coefficient $\times 10^{-6}$/°C (ambient to transformation)	18.2
Transformation range, °C	596 to 665
Expansion dl (%)	0.58
Expansion coefficient $\times 10^{-6}$/°C (transformation to 950 °C)	22.3

Using the above relation, the coefficients of thermal expansion for U-15%Pu is given by:

$$\alpha_{fuel} *10^{-6} \ (K^{-1}) = 21.3 \tag{6.65}$$

The thermal expansion coefficient for U–15Pu–10Zr is $17.6 * 10^{-6}$ K^{-1} for $298 < T < 900$ K, and $20.1 * 10^{-6}$ K^{-1} for $T > 900$ K [171, 187].

6.4.5. Density

The density of uranium as a function of temperature is given by the following relations [174, 188]:

$$\rho \ (kg/m^3) = 19.36 \times 103 - 1.03347 \ T \ \text{at} \ 273 \leq T \leq 942 \ \text{K} \ (\alpha \ \text{phase}), \tag{6.66}$$

$$\rho \ (kg/m^3) = 19.092 \times 103 - 0.9807 \ T \ \text{at} \ 942 \leq T \leq 1049 \ \text{K} \ (\beta \ \text{phase}), \tag{6.67}$$

$$\rho \ (kg/m^3) = 18.447 \times 103 - 0.5166 \ T \ \text{at} \ 1049 \leq T \leq 1405 \ \text{K} \ (\gamma \ \text{phase}). \tag{6.68}$$

The density of liquid uranium at 0.1 MPa and at $1405 \leq T \leq 2100$ K [189, 190]

$$\rho \ (kg/m^3) = 20332 - 2.146T \tag{6.69}$$

Density of liquid plutonium at the melting point is [191] = $16\ 500 \pm 80$ (kg/m³). In the temperature range t = 650–950°C, density is given by the following relation:

$$\rho \ (kg/m^3) = 17567 - 1.451 \ t. \tag{6.70}$$

The densities of U-Pu-Zr and U-Pu-Fs alloys as a function of composition are given in Tables 17 and 18, respectively.

TABLE 17. PROPERTIES OF U-Pu-Zr ALLOYS

Property	U		U		U		U	
	Pu	Zr	Pu	Zr	Pu	Zr	Pu	Zr
Nominal composition: wt%	11.1	6.3	15	6.8	15	10	18.5	14.1
At.%	10	15	13.6	14.3	12.9	22.5	15	30
Density at 25 °C as cast (g/cm³)	16.8		16.6		15.8		14.8	

TABLE 18. PROPERTIES OF URANIUM-PLUTONIUM-FISSIUM ALLOYS:

Property	U	U	Pu	U	Pu	Fz	U	Pu	Fz	U	Pu	Fz
Composition: wt%		90	10	80	10	10	75	15	10	60	20	10
At.%		90	10	69.9	8.7	21.4	65.5	13.1	21.4	61.1	17.5	21.4
Density at 25°C (g/cm³)	19.1	18.7		16.8			16.5			16.8		

Density of U-15Pu-10Zr (wt%) as a function of temperature is given by the following relation [192]:

$$\rho \ (g/cm^3) = 15.8/[1.0 + 0.000018(T - 298)]^3 \text{ for } 298 < T < 868K \tag{6.71}$$

$$\rho \ (g/cm^3) = 15.3235/[1.0 + 0.000074(T - 868)]^3 \text{ for } 868 < T < 938K \tag{6.72}$$

$$\rho \ (g/cm^3) = 15.0/[1.0 + 0.000020(T - 938)]^3 \text{ for } 938K < T \tag{6.73}$$

6.4.6. Hot hardness

Figure 60 shows the hardness versus temperature plot for pure U, U-10%Zr and U-Pu-Zr alloys. Hardness data of some common cladding materials are also shown in the same figure. Among the fuels, pure U showed the lowest hardness values in the low temperature range up to 600°C. However, in the temperature range of 650–700°C, the hardness of U showed a considerable increase. This is clearly shown in Fig. 60. The sudden increase in hardness is due to the formation of β phase. On heating further, the hardness falls steeply with the formation of γ phase. The γ phase was found to be very soft with hardness values falling to about 1 kg/mm². On addition of 10% Zr to U, the hardness value increases by about 20%. The hot hardness behaviour of ternary of U-15%Pu-7%Zr was studied by Tokar [193]. These values are also shown in Fig. 60. The hardness values for the ternary alloys are higher than that of U and U-10%Zr alloy up to 500°C. However, above 600°C, the above composition has the lowest hardness.

It can be seen that hardness of austenitic steel is the least at all temperatures covered in this study. The hardness of ferritic martensitic steel like HT-9 is about 30% higher than that of D-9. Among the cladding materials, the highest hardness values were shown by nickel based alloy, Inconel 718.

Figure 60 shows that for the temperature range covered in this study, the hardness of nickel based alloy is higher than the fuels, viz., U, U-10%Zr and U-Pu-Zr alloys. This indicates that the chances of clad failure due to FCMI is very little since fuel can easily creep on contact with the clad rather than rupturing it. Generally, creep rate is inversely proportional to the hardness, which means that the higher the hardness the lower the creep rate. The hardness values of the clad and fuel at the reactor operating temperature of 600°C is 360 kg/mm² and that of U-15%Pu-7%Zr is only 40 kg/mm². This means that the fuel can easily creep on contact with clad without damaging the clad.

For ferritic martensitic alloy like HT-9, the clad is softer than the fuel compositions in the low temperature range. However, above 500°C, HT-9 is stronger than the fuel compositions covered in this study. At 600°C, the hardness of HT-9 is 130 kg/mm² while that of U-10%Zr and U-15%Pu-7%Zr alloy are 45 and 40 kg/mm², respectively. This again indicates that there is a sufficient margin in the hardness values to avoid FCMI. D-9 clad is the softest among the cladding materials covered in this study [195, 196]. It is softer than U-10%Zr and U-15%Pu-7%Zr alloys up to 550°C. On comparing the hardness values at 600°C, it can be seen that the hardness of D-9 is only marginally higher than the fuel compositions [194].

6.5. THERMO PHYSICAL PROPERTIES OF FUELS CONTAINING MA

6.5.1. Oxides containing MA

Fast reactors in advanced burner mode could also utilize minor actinide elements together with uranium and plutonium as fuel. There is also R&D experience on minor actinide based fuels and targets for ADS. Several MA
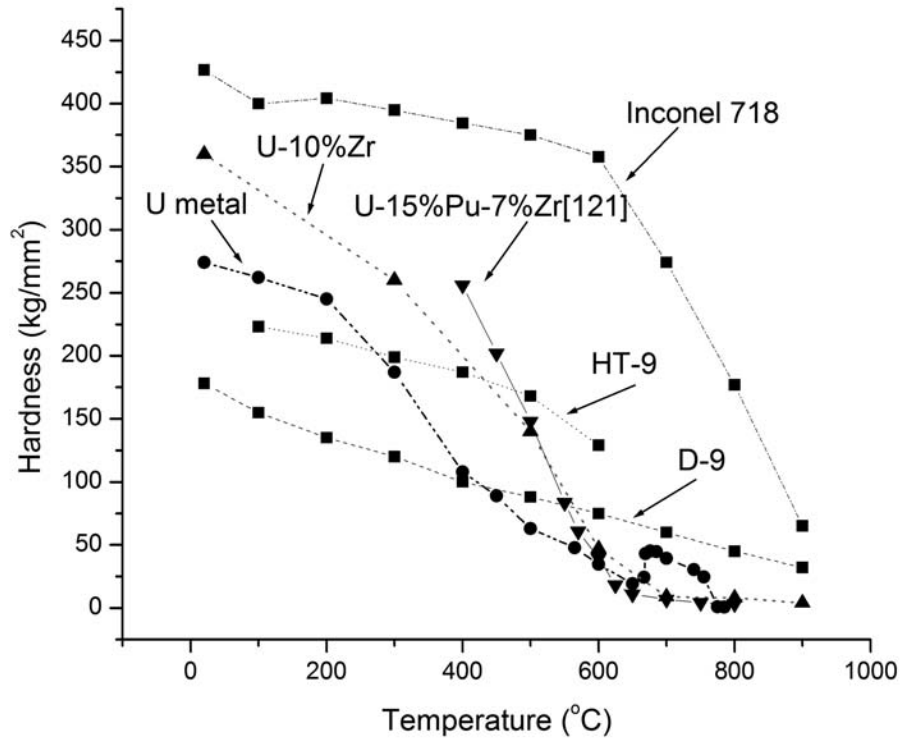
FIG. 60. Hardness versus temperature plot for U, U-10% Zr, U-15%Pu-7%Zr alloys. Hardness data of D-9, HT-9, Inconel 718 are also shown in the figure [194].
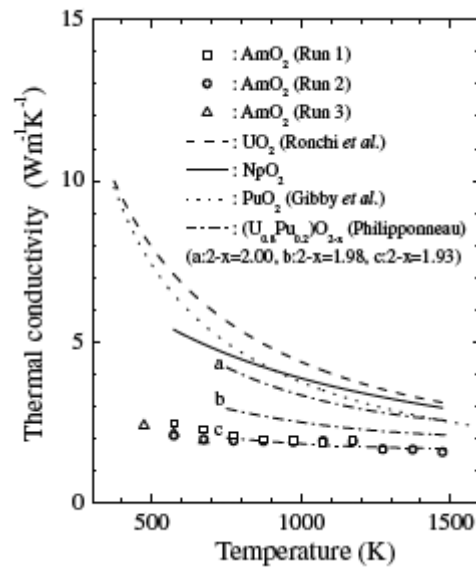
FIG. 61. Temperature dependence of thermal conductivity of AmO_{2-x} and NpO_2, together with those of UO_2, PuO_2 and $(U_{0.8}Pu_{0.2})O_{2-x}$ [197].

which has a half-life of 14.4 years, is generated. Consequently, its daughter nuclide [241]Am builds up in the MOX fuel with time. Hence, it is essential that one must know the thermal behaviour of minor actinides.

The thermal conductivities of AmO_{2-x} and NpO_2, together with those of UO_2, PuO_2 and $(U_{0.8}Pu_{0.2})O_{2-x}$ for comparison, are shown in Fig. 61. The thermal conductivity of NpO_2 from 873 to 1 473 K lay between those of UO_2 and PuO_2. The thermal conductivities of AmO_{2-x} and NpO_2 decreased with increasing temperature in the temperature range investigated. This temperature dependence of the thermal conductivities of AmO_{2-x} and NpO_2 was similar to that of UO_2, PuO_2 and $(U_{0.8}Pu_{0.2})O_{2-x}$ [197, 198]. The thermal conductivities of MOX containing Np- and Am-oxides (Am-MOX and Np-MOX) were measured by the laser flash method in the temperature range from 900 to 1 770 K. The obtained conductivities were normalized to those of 100% and are shown in Fig. 62 [199].
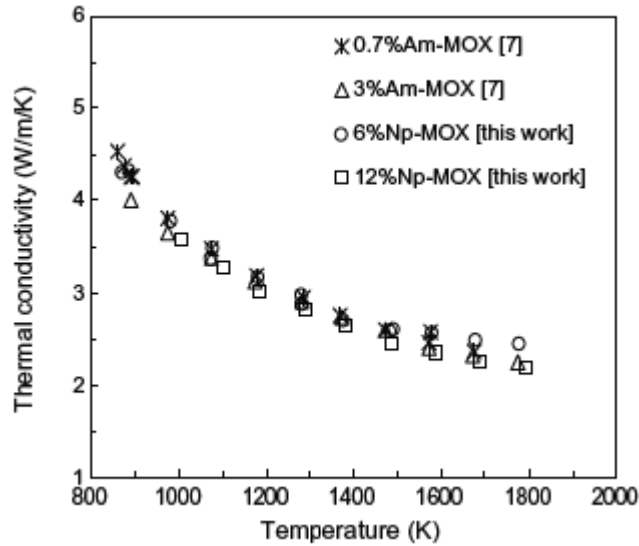
FIG. 62. The thermal conductivities of (U, Pu,Np)O₂ and (U, Pu,Am)O₂ solid solutions at temperatures from 900 to1770 K [199].
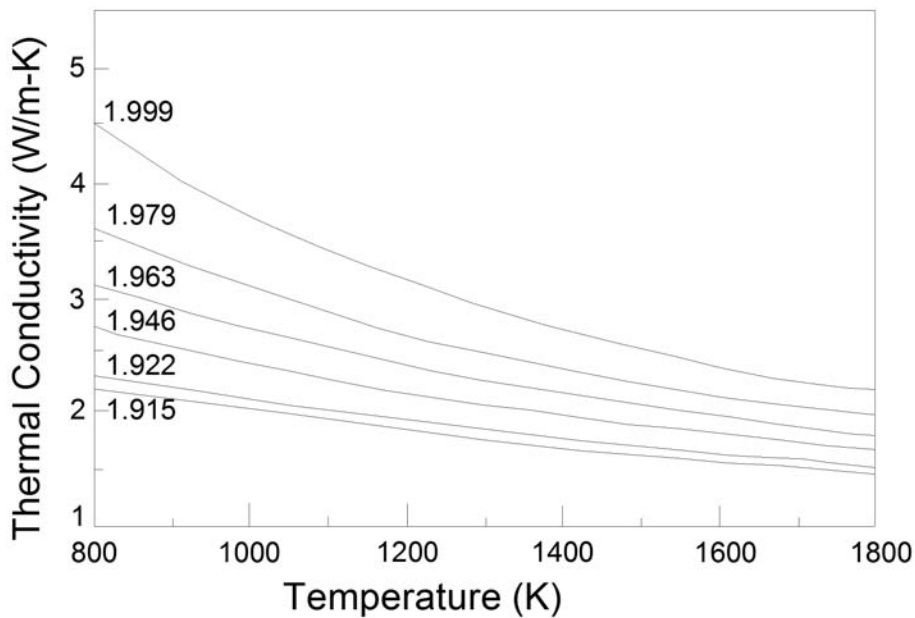
FIG. 63. Thermal conductivities of $(U_{0.68}Pu_{0.30}Am_{0.02})O_{2-x}$ as a function of temperature for different O/M ratios [200].

The thermal conductivities of 2%Am–MOX having a different O/M ratio are shown in Fig. 63 as a function of temperature [200]. The thermal conductivities data were normalized to 100% of the theoretical density by using the modified Maxwell–Eucken relationship. This figure indicates that the thermal conductivities of 2%Am–MOX decrease with increasing temperature and larger deviations of O/M ratios from 2.00. The effect of O/M ratio on the thermal conductivity is large and is significant especially in the low temperature region.

The heat capacity of NpO_2 was determined by drop calorimetry and was found slightly larger than that of UO_2 and about 7% smaller than that of PuO_2 [199] (see Fig. 64).

6.5.2. MN fuels with MAs

Nitride is a candidate material of advanced fuels for fast reactors and for transmutation of minor actinide elements such as Np, Am and Cm [54] because of its advantageous thermal and neutronic properties [53, 201, 202].
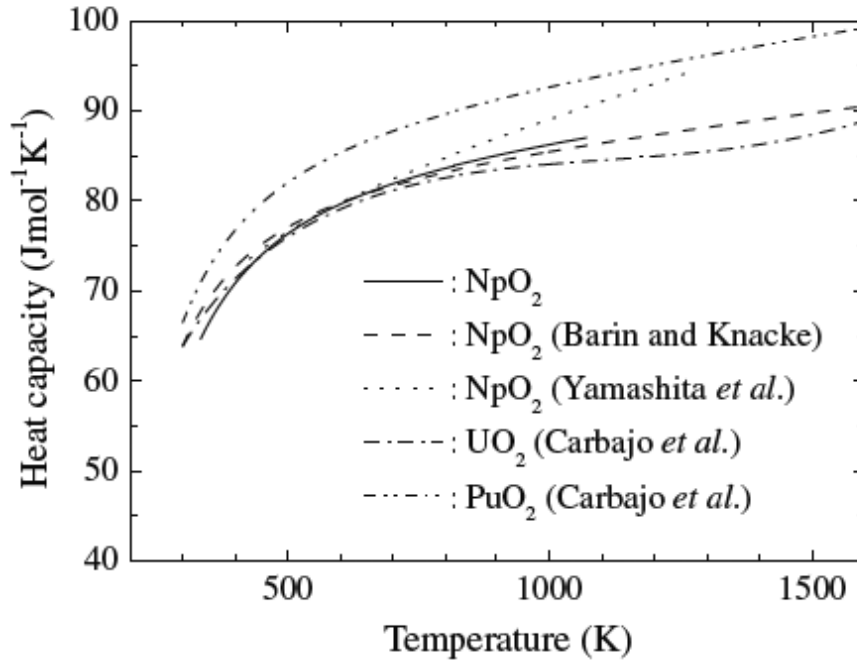
FIG. 64. *Heat capacity of NpO$_2$, together with those of UO$_2$ and PuO$_2$ as a function of temperature [199].*

The thermo physical and thermodynamic properties of actinide mononitrides; i.e., UN, NpN, PuN and AmN, are essential in fuel designs and evaluation of fuel behaviour. The thermal conductivities of UN, NpN and PuN are found to have a tendency to increase gradually with temperature [197], while to decrease with the atomic number of the actinide element component because of the decrease of electronic contribution (see Fig. 65). The solid solutions of the mononitrides show temperature dependence similar to those of two component nitrides each and possess intermediate thermal conductivity values.

Thermal conductivities ZrN, PuN and (Pu,Zr)N with varying amount of Zr contents is given in Fig. 66 [176]. The thermal expansions of UN, NpN, PuN and AmN are shown in Fig. 67. The thermal expansions of AmN and PuN were found to be close to each other and larger than that of UN, whereas the thermal expansion of NpN was nearly the same as that of UN [197]. The heat capacities of AmN and NpN obtained, together with those of UN and PuN, are shown in Fig. 68. The heat capacity of AmN was found to be slightly smaller than those of UN, NpN and PuN.

6.5.3. Metal fuels with MA

The US fast reactor fuel programme demonstrated the use of americium bearing fuel in the early 1990s [203]. The X501 experiment was conducted in EBR-II as part of the IFR programme to demonstrate MA burning through the use of a homogeneous recycle scheme. The nominal fuel composition used in the X501 experiment was U-20.3%Pu-l0.0%Zr-2.1%Am-1.3%Np and is based on a concept where the standard IFR fuel is fabricated with Pu extracted from spent LWR fuel which has cooled 10 years Limited post-irradiation examination results from the X501 experiment indicate that the addition of 1.2 wt.% of americium did not alter the behaviour of metallic U-Pu-Zr fuel. Metallic fuel is being considered as the transmutation fuel for the HYPER (hybrid power extraction reactor) in the Republic of Korea [204]. U-TRU-Zr is being considered for the alloy fuel slug, and the cladding material is HT9.

The thermal conductivity of the unirradiated U-TRU-Zr alloy, $k_{100,}$ can be expressed as the function of the temperature and alloy composition [181].

$$k_{100} = 17.5[(1 - 2.23\ Wz)/(1 + 1.61\ Wz) - 2.62\ W_P] + 1.54*10^{-2}[(1 + 0.061\ Wz)/$$
$$(1 + 1.61\ Wz) + 0.9\ Wp)]T + 9.38*10^{-6}(1 - 2.7\ Wp)T^2 \qquad (6.74)$$
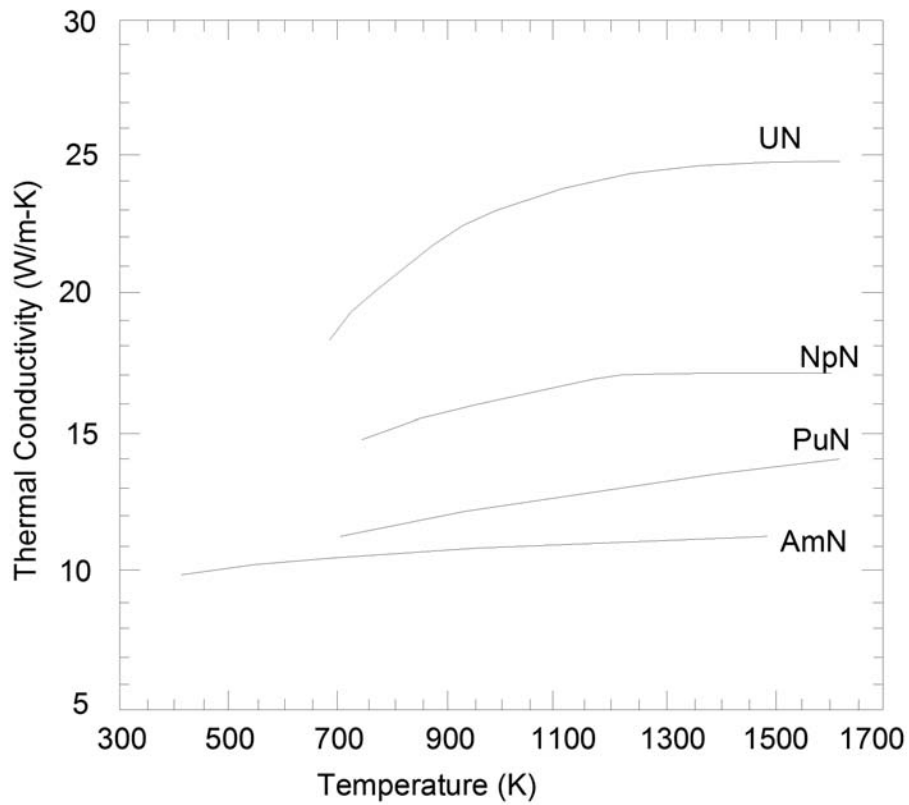
FIG. 65. The thermal conductivity values of UN, NpN, PuN and AmN [197].
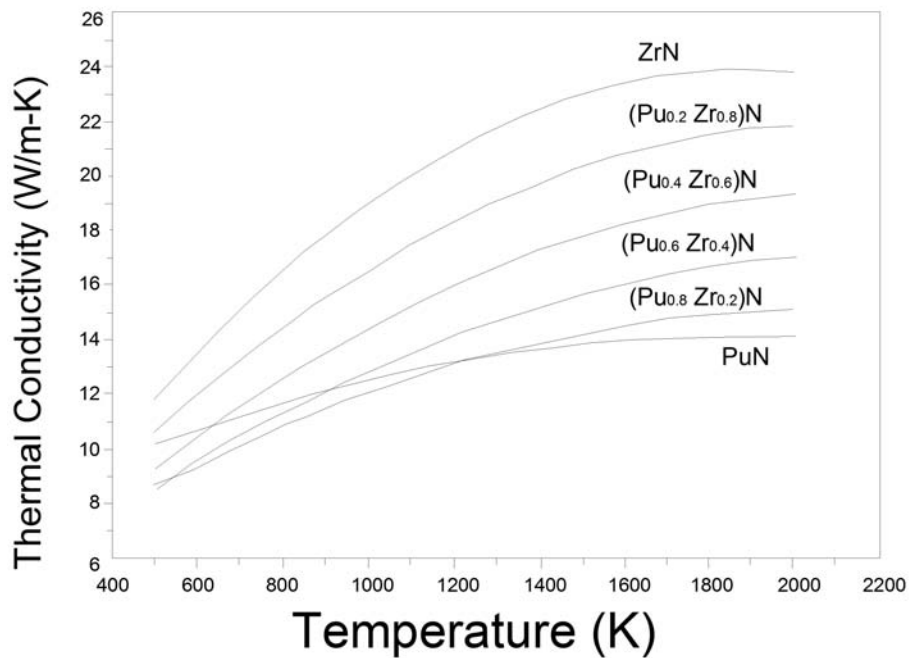
FIG. 66. The thermal conductivity values of ZrN, PuN and (Zr,Pu)N [176].
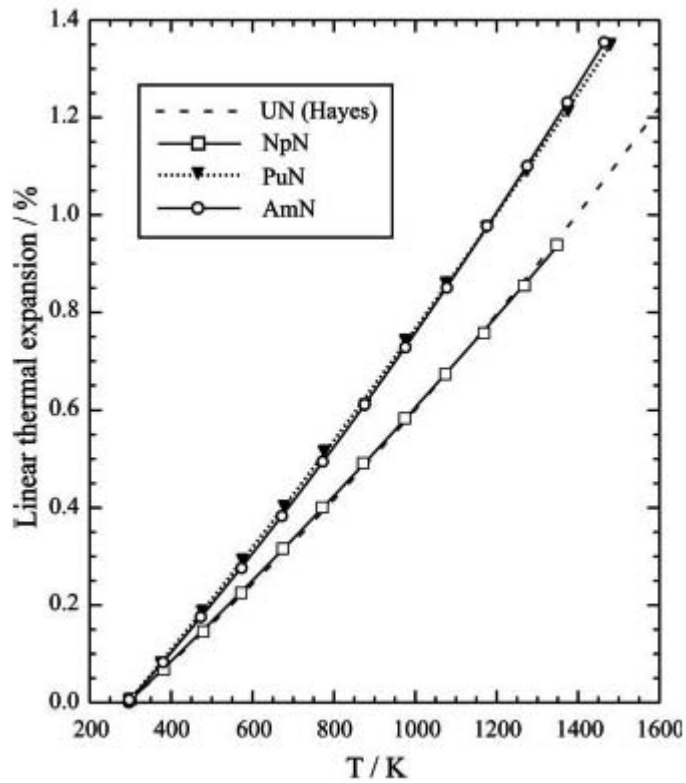
FIG. 67. Linear expansion coefficients for UN, NpN, PuN, AmN [197].
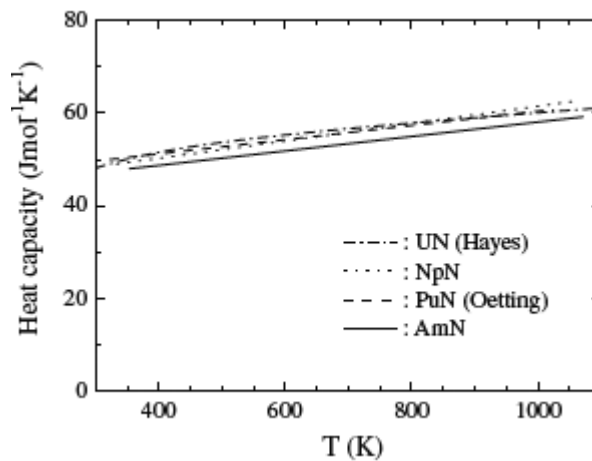
FIG. 68. Specific heat values UN, NpN, PuN, AmN [197].

where, T is the temperature in Kelvin and W_z, W_P are the weight fraction of zirconium and TRU, respectively.

Figure 69 shows the thermal conductivity values U-Zr alloys along with that of Pu-12Am-40Zr and U-29Pu-4Am-30Zr alloys [175, 205]. Figure 70 compares the thermal conductivity values U, Pu, Np, Am, Cm. Their thermal expansion values are compared in Fig. 71.
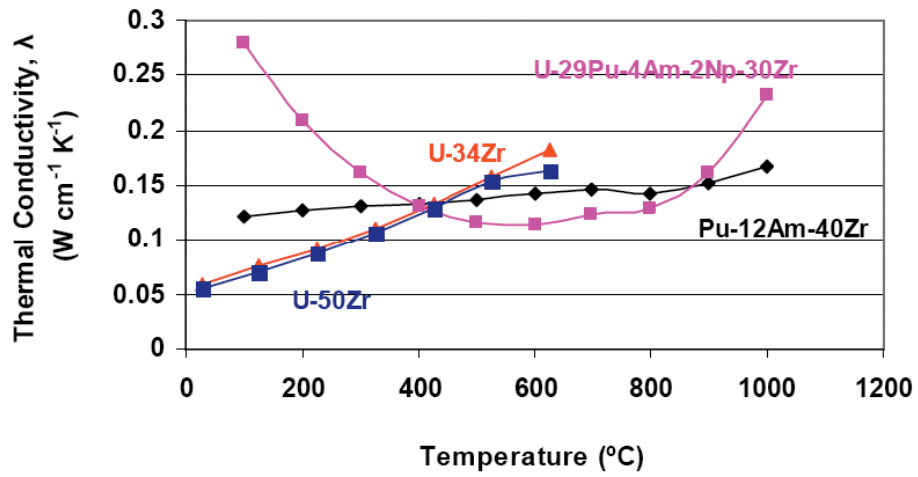
FIG. 69. Thermal conductivity values U-Zr alloys along with that of Pu-12Am-40Zr and U-29Pu-4Am-30Zr alloys [175, 205].
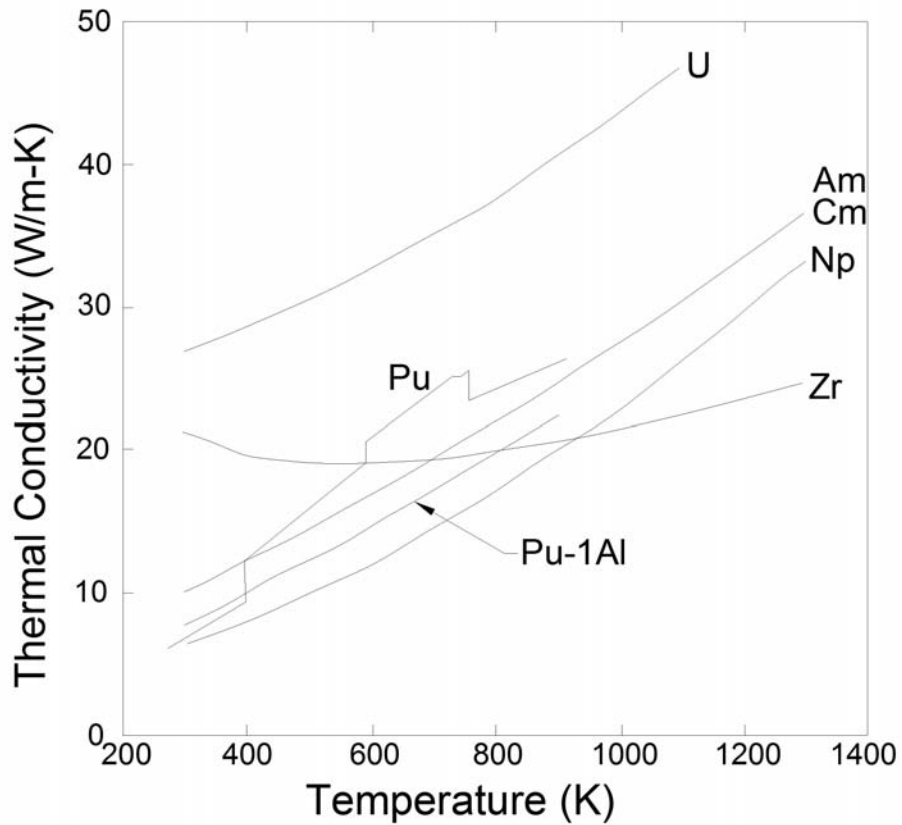
FIG. 70. Comparison of the thermal conductivity values U, Pu, Np, Am, Cm [176].
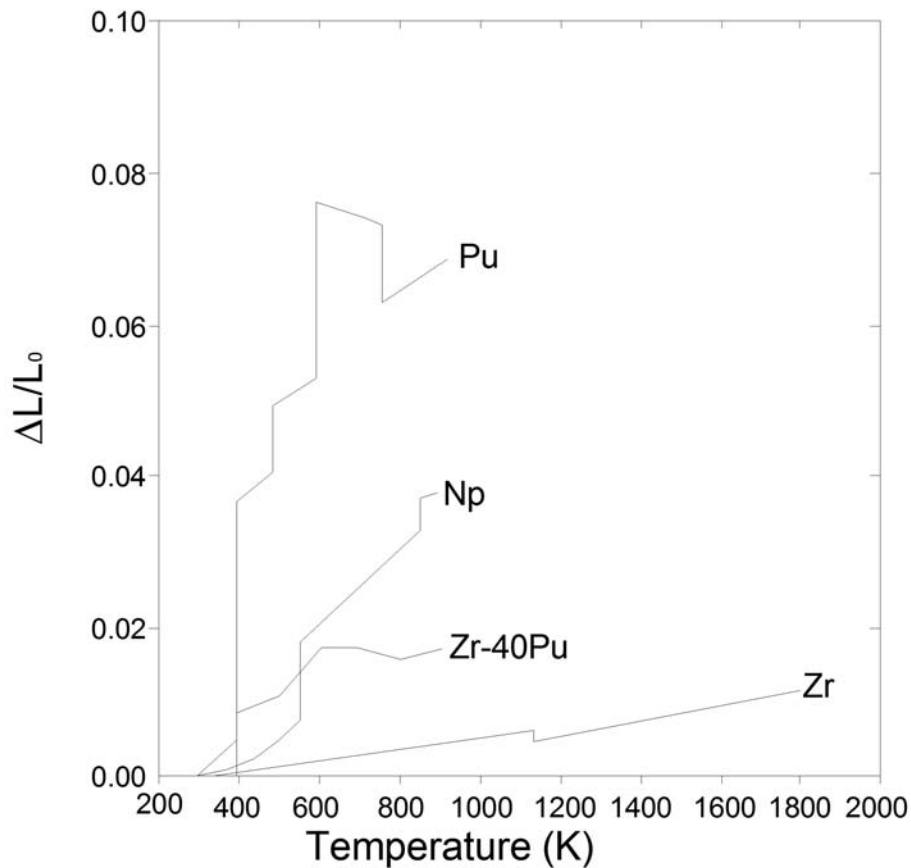
FIG. 71. Thermal expansion values of Pu, Np, Zr, Zr-40%Pu [176].

7. SUMMARY AND RECOMMENDATIONS

The present generation of nuclear power reactors in the world are mostly thermal reactors. The LWRs account for more than 85% of these reactors followed by the PHWRs, which contribute to some 6% of the reactors. The water cooled reactors are likely to dominate the nuclear power programme worldwide up to the middle of this century and beyond. The LWRs and PHWRs use low enriched uranium containing <5% ^{235}U and natural uranium (99.3% ^{238}U + 0.7% ^{235}U), respectively, as fuel in the form of high density uranium oxide pellets, which are stacked and encapsulated in zirconium alloy cladding tubes. These reactors mostly use the fuel in 'once-through' mode. In such 'open' fuel cycle, <1% of the uranium that is mined and used in reactors as fuel is utilized and most of the ^{238}U is locked either in the tailings of the ^{235}U enrichment plant or in spent fuel. It is universally agreed that the natural uranium utilization could be increased by a factor of 60 or more by reprocessing the spent fuel and recycling the plutonium, transmuted from uranium 238, in a fast reactor. Thus fast reactors and multiple recycling of plutonium in 'closed' fuel cycle ensure most efficient utilization of natural uranium resources. The main mission of fast reactor, either as breeder or as burner or both, is to generate nuclear electricity economically and safely in a sustainable manner on a long term basis, while managing the high level waste and protecting the environment and ensuring proliferation–resistance of fissile materials. Sodium is the proven and accepted coolant for fast reactor and several test, prototype and commercial sodium cooled fast reactors (SFR) have demonstrated satisfactory performance in the last 50 years (reactor year experience). One of the key issues to the commercial success of the SFR is to develop plutonium based fuels, with or without minor actinides, that will perform satisfactorily to high burnup (present target: 20 at.% or ~200 GW·d/t HM) and also develop cladding, duct and other structural materials for fuel assembly that would not fail due to radiation damage up to 200 dpa. The early fuels were capable of only

1–3 at.% burnup. In the initial phase of the SFR fuel development, a great deal of emphasis was placed on developing individual fuel pins that could achieve high burnup. However, no fast reactor fuel system has been able to take advantage of the high burnup capability of individual fuel pins. The interaction of fuel pins within the fuel bundle, the interaction of the fuel bundle with the duct, and the bow and swelling of the duct are equally important as the burnup capability of individual fuel pins. In fact, the exposure capability of all past and existing fast reactor fuel systems has been limited by distortion of the duct when excessive fuel handling forces are needed. During the last five decades, many hurdles had to be overcome, not the least of which was the fast neutron irradiation damage of cladding and duct materials. Development of high performance cladding and duct materials was truly an international effort.

The SFR should offer very high flexibility to enable operation of the reactor in plutonium and minor actinide burning mode or to sustain and increase the plutonium inventory by breeding. Arising out of the results obtained from experiments with MOX fuel, it is currently believed that the target burners for future large commercial fast reactors of about 200 GW·d/(t HM) can be achieved if improvements in fuel assembly and rod structural materials are incorporated. In addition to this, SFRs because of its flexibility in accommodating different fuel types and compositions, could contribute to the burning and reduction of the amount of minor actinides. One of the important concerns for plutonium management is the protection of plutonium from unauthorized diversion while at the same time allowing the sustainable use of nuclear power. SFRs and closed fuel cycle with co-location of fuel fabrication, reactor and reprocessing plants facilitate proliferation resistance. The neutron and gamma emitting isotopes of plutonium namely ^{238}Pu, ^{240}Pu, ^{241}Pu and ^{242}Pu act as effective barriers and provide proliferation resistance.

Based on the experience in the last five decades, the following conclusions are drawn on the status and further development of SFR fuels:

— Mixed uranium plutonium oxide (MOX) is the reference fuel for SFR. The mixed oxide or MOX fuel has attained maturity in France, the UK,and Japan, where: (a) industrial scale fabrication, (b) large irradiation database both as driver fuel and as experimental fuel pins to high burnup and (c) industrial scale reprocessing have been demonstrated. In fact, fabrication of MOX fuel is virtually an extension of UO_2 (HEU or Nat. U) fuel fabrication because UO_2 and PuO_2 are isostructural, completely solid soluble and have very similar thermodynamic and thermo physical properties. However, MOX fuel fabrication is done in shielded glove boxes, with remote and automated operations because of the high radio toxicity of plutonium. MIMAS (Belgo-nuclear) and SBR (UK) are still the reference methods of production of MOX fuel, though these are associated with 'radiotoxic dust hazard'. The DDP process developed at RIAR, based on vibro-compaction of MOX granules obtained by pyro-chemical processing of spent MOX fuel is an advanced technique for the fabrication of MOX fuel pins for fast reactor. Similar to DDP, the DOVITA process has been developed for fabrication of MOX fuel with minor actinides. Dust free Vibro-sol and SGMP process are other advanced techniques for fabrication of MOX fuel. The SGMP process is a hybrid of sol-gel and conventional pelletization process. It is dust free, amenable to automation and remotization, ensures excellent micro homogeneity and could be tailored to produce MOX pellets of controlled density and microstructure.
— Mixed uranium plutonium monocarbide and mononitride fall in the same category of non-oxide advanced ceramic fuels for SFRs. Mixed carbide has demonstrated high burnup (160 GW·d/t HM) as driver fuel in FBTR, India. The MC and MN fuels are however more difficult and expensive to manufacture and are associated with the challenges of pyrophoricity, reprocessing and C-14 in case of MN fuel.
— Metallic fuel is an advanced fuel for SFR and is very efficient from the point of view of high breeding ratio and low doubling time. Metallic fuel, in combination with pyro-electrolytic reprocessing and injection casting is very promising for IFR with co-location of reactor, fuel fabrication and reprocessing facility. Metallic fuels are easy to manufacture remotely on an industrial scale. The IFR initiative allowed metal fuel to be the center-piece of fuel development for the USDOE throughout the 1980s and well into the 1990s. Metal fuel, along with the high burnup capability, has the highest fissile density for breeding and lends itself to the proliferation resistance and remote pyro-reprocessing. Tests in EBR-II, that extrapolate to large pool-type sodium cooled reactors, demonstrated that a metal fueled core could sustain a loss of coolant flow and a loss of heat sink, without SCRAM, and shut itself down, with no core damage. This inherent safety feature is due to the high thermal conductivity of metal fuel, in contrast to the low thermal conductivity and high fuel temperature of mixed oxide fuel. However, the experience on metallic fuel is restricted to the USA mainly, though R&D efforts are underway in Japan, the ROK and India.

— One of the objectives of SFRs will also be to burn MA. It is possible to introduce small amounts (1–5%) of MA in MOX, MC, MN and metallic fuels without much difficulty and without affecting the properties and performance significantly. However, remote, automated and heavily shielded facilities are needed for handling MA bearing fuels. The details of MA bearing fuels are being covered in a separate IAEA publication.

— The radiation damage of fuel structural materials is a major challenge of high burnup SFR fuels. Several sections of this report showed the progression in improvement of fuel performance as the cladding and duct materials changed from the austenitic alloys (304, 316, 316CW, 316CW-Ti modified) to the very low swelling martensitic alloy HT-9. Further improvement is underway with oxide dispersion strengthened (ODS) alloy. If one single effort were to be chosen that contributed to the successful development of fast reactor fuels, it would be the cladding and duct development programmes from several nations. The details of the SFR fuel structural materials have been covered in a recent IAEA publication.

— There is a need for international database and collaborative research on out-of-pile and in-pile property evaluation and irradiation-testing of MOX, MC, MN and metallic fuels and fuel structural materials like modified austenitic steel, ferritic-martensitic alloys including HT-9 and ODS steels. International collaboration is also needed for effective utilization of the very few SFRs that will be in operation in the world, namely, BOR 60, BN-600, JOYO, Monju and FBTR for development of advanced fuels and fuel assembly structural materials. The IAEA could play a pivotal role in facilitating this.

REFERENCES

[1] INTERNATIONAL ATOMIC ENERGY AGENCY, Fast Reactor Database; 2006 Update, IAEA-TECDOC-1531, IAEA, Vienna (2006).

[2] INTERNATIONAL ATOMIC ENERGY AGENCY, Status of Liquid Metal Cooled Fast Reactor Technology, IAEA-TECDOC-1083, IAEA, Vienna (1999).

[3] Advanced LMFBR fuels, ERDA 4455, Proc. Topical Meeting on Advanced LMFBR Fuels, 10-13 Oct.1977, Tucson, Arizona (1977).

[4] Fuel and Fuel Elements for Fast Reactors, Proc. of IAEA conference, Vol I & II (1974) 04

[5] RUSSELL, L.E., (Ed.), Carbides in Nuclear Energy, McMillan, London **1, 2** (1963).

[6] WALTERS, L.C., SEIDEL, B.R., KITTEL, J.H., Performance of Metallic Fuels and Blankets in Liquid-Metal Fast Breeder Reactors, Nucl. Technol. **65** (1984) 179–231.

[7] CHANG, Y., Technical rationale for metal fuels in fast reactors, Nucl. Eng. Des. 39 (2007) 161–170.

[8] HOFMAN, G.L., WALTERS, L.C., "Metallic Fuels for Fast Reactors", Materials Science and Technology, A Comprehensive Treatment (CAHN, R.W., HAASEN, P., KRAMER, E.J., Eds) **10A** (1994).

[9] FERNANDEZ, A, MCGINLEY, J., SOMERS, J., WALTER, M.,"Overview of past and current activities on fuels for fast reactors at the Institute for Transuranium Elements", J. Nucl. Mater. **392** (2009) 133–138.

[10] MATZKE, Hj., Science Of Advanced LMFBR Fuels, Chapter 4, North-Holland (1986) 176.

[11] Reliable Fuels for Liquid Metal Reactors, Proc. Conf., Tucson, 1986, Am. Nucl. Soc. (1986).

[12] INTERNATIONAL ATOMIC ENERGY AGENCY Advanced Fuel for Fast Breeder Reactors — Fabrication and Properties and their Optimization, IAEA-TECDOC-466, IAEA, Vienna (1988).

[13] Fast Reactors and Related Fuel Cycles, FR-91, Proc. Int. Conf., Kyoto, 1991, JNC (1991).

[14] Long Term Use of Nuclear Power in Japan and the Nuclear Fuel Cycle, Power Line Japan, The Federation of Electric Power Companies of Japan **31** (February 2008) 2.

[15] INTERNATIONAL ATOMIC ENERGY AGENCY, Utilization of particle fuels in different reactor concepts, IAEA-TECDOC-286, IAEA, Vienna (1983).

[16] GANGULY, C., Sol-gel microsphere pelletization for the fabrication of conventional and advanced fuels, Metals, Mat. Processes **1** 4 (1990) 253.

[17] Proc. of IAEA Panel on Sol-gel Process for Fuel Fabrication, IAEA-161 (1974).

[18] LEDERGERBER, G., INGRID, F., STRATTON, R.W., Trans. FNC-86 Conf. Geneva (1986) 225–232.

[19] SWANSON, K.M., STRASS, W., BATEY, W., ERDA 4455, Am. Nucl. Soc. (1977) 95–109.

[20] GRACHEV, A.F, et.al., Experience and prospects of using fuel elements based on vibrocompacted oxide fuel, International Scientific and Technical Conference, Nuclear Power and Fuel Cycles(NFEC-1), Summaries of Reports, Moscow-Dimitrovgrad (2003) 35–37.

[21] GANGULY, C., LINKE, U., KAISER, F, Characterization of $(U,Ce)O_2$ prepared by sol-gel microsphere pelletization process, Metallograph **20** (1987) 1.

[22] BYCHKOV, A.V., et al., "Overview of RIAR activity on pyro-process development and application to oxide fuel and plans in coming decade", Proc. of the workshop on Pyrochemical separation, Avignon, France, 14-16, March 2000, OECD-NEA pp. 37–46.

[23] INTERNATIONAL ATOMIC ENERGY AGENCY, Status and Advances in MOX Fuel Technology, IAEA-TRS-415, IAEA, Vienna (2003).

[24] OLANDER, D.R., Fundamental Aspects of Nuclear Reactor Fuel Elements, TID-26711-P1, USDOE (1976) 145.

[25] LEGGETT, R.D., HECK, E.N., LEVINE, P.J., HILBERT, R.F., "Steady State Irradiation Behaviour of Mixed oxide Fuel Pins Irradiated in EBR-II," Proc. Int'l Conf. on Fast Breeder Reactor Fuel Performance, Monterey, CA, March 5–8, paper obtainable as U.S. DOE report no. HEDL SA-1683 FP.

[26] LAWRENCE, L.A., et al., Performance of Advanced Oxide Fuel Pins in EBR-II, Proceedings of the International Conference on Reliable Fuels for Liquid Metal Reactors, Tucson, AZ, September 7–11, 1986, Am. Nucl. Soc., La Grange Park, IL, 3–62–3–74.

[27] ALDERMAN, C.J. PITNER, A.L, Transient Testing of Long-Lifetime Mixed-Oxide Liquid-Metal Reactor Fuel, Trans. Amer. Nucl. Soc. **56** (1988) 382–383.

[28] BAUER, T.H., HOLLAND, J.W. WRIGHT, A.E., Late-Stage Accident Behaviour of a Highly Disrupted LMR Oxide Fuel Bundle, Trans. Amer. Nucl. Soc. **66** (1992) 317–318.

[29] WRIGHT, A.E., DUTT, D.S., HARRISON, L.J., Fast Reactor Safety Testing in TREAT in the 1990s, Proc. Int'l Fast Reactor Safety Mtg, Snowbird, Utah, 1990, Amer. Nucl. Soc., La Grange Park, IL, 233–243.

[30] UKAI, S., FUJIWARA, M., "Perspective of ODS alloys application in nuclear environments", J. Nucl. Mater. 307–311 (2002) 749–757.

[31] CRAWFORD, D.C., PORTER, D.L., HAYES, S.L., "Fuels for sodium cooled fast reactors: US perspective", J. Nucl. Mater. 371 (2007) 202–231.

[32]   BLANK, H., "Nonoxide Ceramic Nuclear Fuels", from Nuclear Materials, Part I Volume 10 A (FROST, B. R. T., Ed.), appearing in Mater. Sci. and Techn., A Comprehensive Treatment (CAHN, R.W., HAASEN, P, KRAMER, E.J., Eds) VCH Verlagsgesellschaft mbH (1994) 191–357.

[33]   LEARY, J., KITTLE, H. (Eds), Advanced LMFBR Fuels, Proc. Tech. Mtg, Tucson, ERDA 4455, Amer. Nucl. Soc. (1977).

[34]   SINHA, R.K., KAKODKAR, A., Nucl. Eng. Des. **236** (2006) 683.

[35]   GANGULY, C., et. al., Development and Fabrication of 70% PuC – 30 % UC fuel for the Fast Breeder Test Reactor in India, Nucl. Technol. 72 (1986) 59.

[36]   GANGULY C., HEGDE, P.V., JAIN, G.C., Fabrication of (Pu0.55 U0.45)C fuel pellets for the second core of the Fast Breeder Test Reactor in India, Nucl. Technol. 105 (1994) 346.

[37]   RESHETNIKOV, F.G., et al., "Studies of Methods for Manufacturing Meats of Uranium Monocarbide, Mononitride and Carbonitride for Fuel Elements of Fast-Neutron Reactors", Fuel and Fuel Elements for Fast Reactors (Proc. Symp.), IAEA, Vienna (1973) 25.

[38]   RICHTER, K., Nuclear Energy Maturity, "Progress in Nuclear Energy Series", Edn. Pergamon, Oxford, (1976) 7, 20.

[39]   ROGOZKIN B.D., et al., "Mononitride mixed fuel for fast reactors", (Proc. Tech. Comm. Mtg Obninsk, 1994), IAEA-TECDOC-840, IAEA, Vienna (1995) 229–236.

[40]   GANGULY, C., PhD thesis , Calcutta University (1980).

[41]   GANGULY, C, ROY, P.R., "Fabrication of Advanced LMFBR Fuels at BARC", Fast Reactor Fuel Cycles, BNES, London (1982).

[42]   RICHTER, K., et al., Direct pressing: A new method of fabricating MX fuel pellets, Nucl. Technol. (1985) 70.

[43]   GANGULY, C., HEGDE, P.V., J. Sol Gel Sci. Technol. 9 (1997) 285–294.

[44]   MASON, R.E., HOTH, C.W., STRATTON, R.W., BOTTA, F., Irradiation and Examination Results of the AC-3 Mixed Carbide Test, Trans. Am. Nucl. Soc. 66 (1992) 215–217.

[45]   LEGGETT III, W.D., LEGGETT, R.D., "A Decade of Progress in Fast Reactor Fuel," in LMR: A Decade of LMR Progress and Promise, Washington, D.C, Nov 11–15, 1990, Am. Nucl. Soc., La Grange Park, IL, (1990) 138–143.

[46]   STRATTON, R.W., et al., Fabrication Processes, Design and Experimental Conditions for the Joint U.S.-Swiss Mixed Carbide Test in FFTF (AC-3 Test), J. Nucl. Mater. 204 (1993) 39–49.

[47]   NEUHOLD, R.J., WALTERS, L.C., LEGGETT, R.D., MATTHEWS, R.B., "High Reliabilty Fuel in the US", Proc. of the Int'l Conf. on Reliable Fuels for Liquid Metal Reactors, Tucson, AZ, September 7–11, 1986, Am. Nucl. Soc., La Grange Park, IL, 1-16–1-29.

[48]   LYON, W.F., BAKER, R.B., LEGGETT, R.D., "Performance Analysis of a Mixed Nitride Fuel System for an Advanced Liquid Metal Reactor", Proc. LMR: A Decade of LMR Progress and Promise, Washington, D.C, Nov 11–15, 1990, Am. Nucl. Soc., La Grange Park, IL, 236–241.

[49]   BAUER, A.A., CYBULSKIS, P., GREEN, J.L., "Mixed-Nitride Fuel Performance in EBR-II", Proc. of the Symp. on Advanced LMFBR Fuels, Tucson, AZ, Oct. 10–13, 1977, pp. 299–312.

[50]   BALDEV RAJ, An overview of R&D on fast reactor fuel cycle, Proc. of INSAC-2003, IT-5.

[51]   BALDEV RAJ., et al. "Post-irradiation examination of mixed (Pu, U) C fuels irradiated in fast breeder reactor", (Proc. Tech. Comm. Mtg Obninsk, 1997,), IAEA-TECDOC-1039, IAEA, Vienna (1998).

[52]   SCHMIDT, H.E., Proc., 4th Journe´es d' Actinides, Harwell, UK (June 26, 1974), Atomic Energy Research Establishment Report AERE-R-7961 (1975).

[53]   SUZUKI, Y., ARAI,Y., J. Alloy. Compds. 271–73 (1998) 577–582.

[54]   INTERNATIONAL ATOMIC ENERGY AGENCY, Validity of Inert Matrix Fuel in Reducing Pu Amounts in Reactors, IAEA-TECDOC-1516, IAEA, Vienna (2006) 55.

[55]   MINATO, K., et al., Fabrication of nitride fuels for transmutation of minor actinides, J. Nucl. Mater. 320 (2003) 18–24.

[56]   ARAI, Y., Okamoto, Y., Suzuki, Y., Thermal conductivity of NpN from 740 to 1600K, J. Nucl. Mater. 211 (1994) 248.

[57]   WALTERS, L.C., "Thirty years of fuels and materials information from EBR-II", J. Nucl. Mater. 270 (1999) 39–48.

[58]   TILL, C.E., CHANG, Y.I., HANNUM, W.I., "The Integral Fact Reactor — An Overview," Progress In Nuclear Energy 31 (1997) 3–11.

[59]   SACKETT, J.I., "Operating and Test Experience with EBR-II, The IFR Prototype", Progress in Nuclear Energy 31 No. ½ (1997) 111–129.

[60]   DOUGLAS E. et al., A US perspective on fast reactor fuel fabrication technology and experience Part I: Metal fuels, J. Nucl. Mater. 389 (2009) 458–469.

[61]   CRAWFORD, D.C., LAHM, C.E., TSAI, H., PAHL, R.G., Performance of U-Pu-Zr Fuel Cast into Zirconium Molds, J. Nucl. Mater. 204 (1993) 157–164.

[62]   INOUE, T., TANAKA, H., "Recycling of actinides produced in LWR and FBR fuel cycles by applying pyrometallurgical process", Proc. GLOBAL-1997, Yokohama, Oct. 1997 (1997) 646–652,.

[63]   HUANG, W, NAM, C., BYRUN, T.S., KIM, Y.C., Nucl. Techn. 123(2002) 130.

[64]   BALDEV RAJ, Presented in the Technical meeting: Characterization and Quality Control of Nuclear Fuels (CQCNF-2009), Hyderabad, Feb. (2009).

[65]   WALTER, C.M., OLSON, N.J., HOFMAN, G.L., EBR-II Driver –Fuel Qualification and Performance, J. Nucl. Metall. 19 (1973) 181–202.

[66]   BARNES, R.S., A Theory of Swelling and Gas Release for Reactor Materials, J. Nucl. Mater. 11 (1964) 135.

[67]   HOFMAN, G.L., WALTERS, L.C., "Metallic Fast Reactor Fuels," from Nuclear Materials, Part I Volume 10 A (FROST, B.R.T., Ed.), appearing in Materials Science and Technology, A Comprehensive Treatment (CAHN, R.W., HAASEN, P., KRAMER, E.J., Eds), VCH Verlagsgesellschaft mbH (1994) 1–43.

[68]   WALTERS, L.C., KITTEL, J.H., "Development and Performance of Metal fuel Elements for Fast Breeder Reactors", J. Nucl. Techn. 48 (1980) 273.

[69]   EINZIGER, R.E., SEIDEL, B.R., "Irradiation Performance of Metallic Driver Fuel in Experimental Breeder Reactor II to High Burnup", J. Nucl. Technol. 50 (1980) 25–39.

[70]   LAHM, C.E., et al., Experience with Advanced Driver Fuels in EBR-II, J. Nucl. Mater. 204 (1993) 119–123.

[71]   GOLDEN, G.H., PLANCHON, H.P., SACKETT, J.I., SINGER, R.M., Evolution of Thermal-Hydraulics Testing in EBR-II, Nucl. Eng. Des. 101 (1987) 3–12.

[72]   HOFMAN, G.L., WALTERS, L.C., BAUER, T.H., "Metallic Fast Reactor Fuels," Progress in Nuclear Energy 31 (1997) 83–110.

[73]   CRAWFORD, D.C., et al., J. Nucl. Mater. 371 (2007) 232–242.

[74]   GARNER, F.A., "Irradiation Performance of Cladding and Structural Steel in Liquid Metal Reactors", Part I Volume 10 A (FROST, B.R.T., Ed.), appearing in Mater. Sci. and Techn., A Comprehensive Treatment (CAHN, R.W., HAASEN, P, KRAMER, E.J., Eds), VCH Verlagsgesellschaft mbH (1994) 419–543.

[75]   LEGGETT, R.D., WALTERS, L.C., "Status of LMR Fuel Development in the United States of America", J. Nucl. Mater. 204 (1993) 23–32.

[76]   POWELL, R.W., JOHNSON, G.D., HAMILTON, M.L., GARNER, F.A., "LMR Cladding and Duct Materials Development", Proc. Int. Conf. on Reliable Fuels for Liquid Metal Reactors, Tucson, AZ, September 7–11, 1986, Ameri. Nucl. Soc., La Grange Park, IL, 4-17–4-29.

[77]   PITNER, A.L., BAKER, R.B., "Metal Fuel Test Programme in the FFTF", J. Nucl. Mater. 204 (1993) 124–130.

[78]   BATTE, G.L., HOFMAN, G.L., "Run-Beyond-Cladding-Breach (RBCB) Test Results for the Integral Fast Reactor (IFR) Metallic Fuels Programme", Proc. Int. Fast Reactor Safety Mtg, Snowbird, Utah, 1990, Ameri. Nucl. Soc., La Grange Park, IL, 207–221.

[79]   HOFMAN, G.L., PAHL, R.G., LAHM, C.E., PORTER, D.L., Swelling Behaviour of U-Pu-Zr Fuel, Metallurgical Transactions A 21A (1990) 517–528.

[80]   PORTER, D.L., LAHM, C.E., PAHL, R.G., Fuel Constituent Redistribution During the Early Stages of U-Pu-Zr Irradiation, Metallurgical Transactions A 21A (1990) 1871–1876.

[81]   HOFMAN, G.L., HAYES, S.L., PETRI, M.C., "Temperature Gradient Driven Constituent Redistribution in U-Zr Alloys," J. Nucl. Mater. 227 (1996) 277–286.

[82]   KEISER, D.D., PETRI, M.C., Interdiffusion Behaviour in U-Pu-Zr Fuel versus Stainless Steel Couples, J. Nucl. Mater. 240 (1996) 51–61.

[83]   COHEN, A.B., TSAI, H., NEIMARK, L.A., Fuel/Cladding Compatibility in U-19Pu-10Zr/HT9-Clad Fuel at Elevated Temperatures, J. Nucl. Mater. 204 (1993) 244–251.

[84]   KIM, Y.S., HOFMAN, G.L., YACOUT, A.M., J. Nucl. Mater. (2009) (in press).

[85]   TSAI, H., NEIMARK, L.A., ASAGA, T., SHIKAKURA, S., "Behaviour of Mixed-Oxide Fuel Elements During an Overpower Transient", J. Nucl. Mater. 204 (1993) 217–227.

[86]   CHANG, L. K., KOENIG, J. F., PORTER, D. L., Whole-Core Damage Analysis of EBR-II Driver Fuel Elements Following SHRT Programme, Nucl. Eng. Des. 101 (1987) 67–74.

[87]   Safety Analysis and Technical Basis for Establishing an Interim Burnup Limit for Mark-V and Mark VA Fueled Subassemblies in EBR-II, compiled by L. L. Briggs, L. K. Chang and D. J. Hill, Argonne National Laboratory (1995).

[88]   SEIDEL, B.R., BATTE, L., HOFMAN, G.L., "Off-Normal Performance of EBR-II Driver Fuel", Proc. Int. Conf., on Reliable Fuels for Liquid Metal Reactors, Tucson, AZ, September 7–11, 1986, Ameri. Nucl. Soc., La Grange Park, IL, 6-48–6-66.

[89]   WALTER, C.M., GOLDEN, G.H., OLSON, N.J., "U-Pu-Zr Metal Alloy: A Potential Fuel for LMFBRs", ANL-76-28, Argonne National Laboratory (1975).

[90]   LAHM, C.E., et al., EBR-II Driver Fuel Qualification for Loss-of-Flow and Loss-of-Heat-Sink Test without SCRAM, Nucl. Eng. Des. 101 (1987) 25–34.

[91]   LAHM, C.E., KOENIG, J.F., SEIDEL, B.R., "Consequences of Metallic Fuel cladding Liquid Phase Attack During Over-Temperature Transient on Fuel Element Lifetime", Proceedings of International Fast Reactor Safety Meeting, Snowbird, Utah, 1990, Amer. Nucl. Soc., La Grange Park, IL, 139–143.

[92]   KRAMER, J.M., BAUER, T.H., "Fuel Damage During Off-Normal Transients in Metal-Fueled Fast Reactors", Proc. Int. Fast Reactor Safety Mtg, Snowbird, Utah, 1990, Amer. Nucl. Soc., La Grange Park, IL, 145–154.

[93]   BAUER, T.H., et al., Behaviour of Modern Metallic Fuel in TREAT Transient Overpower Tests, Nucl. Techn. 92 (1990) 325–352.

[94]   MILES, K.J., "Metal Fuel Safety Performance", Proc. Int'l Topical Mtg in Safety of Next Generation Fast Reactors, Seattle, WA, May 1–5, 1988, Amer. Nucl. Soc., La Grange Park, IL, 119–124.

[95]   SOFU, T., KRAMER, J.M., CAHALAN, J.E., SASSYS/SAS4A-FPIN2 Liquid-Metal Reactor Transient Analysis Code System for Mechanical Analysis of Metallic Fuel Elements, Nucl. Techn. 113 (1996) 268–279.

[96] LIU, Y.Y., et al., Behaviour of EBR-II Mk-V-Type Fuel Elements in Simulated Loss-of-Flow Tests, J. Nucl. Mater. 204 (1993) 194–202.

[97] KRAMER, M., LIU, Y.Y., BILLONE, M.C., TSAI, H.C., Modeling the Behaviour of Metallic Fast Reactor Fuels During Extended Transients, J. Nucl. Mater. 204 (1993) 203–211.

[98] MIZUNO, T., NIWA, H., Advanced MOX Core Design Study of Sodium Cooled Reactors in Current Feasibility Study on Commercialized FR cycle Systems in Japan Nucl. Techn. 146 (2004) 155–163,

[99] MACLEAN, H.J., HAYES, S.L., INL/CON-07-12159 (Global-2007).

[100] LEMEHOV, S.E., Sobolev, V., Van Uffelen, P, J. Nucl. Mater. 320 (2003) 66.

[101] MASSIH, A.R., Swedish Nuclear Power Inspectorate Report, SKI report 2006:10 (2006).

[102] POPOV, S.G., CARBAJO, J.J., IVANOV, V.K., YODER, G.L., ORNL/TM-2000/351.

[103] OGGIANU, S.M., KAZIMI, M.S., MIT report MIT-NFC-TR-021 (2000).

[104] KUTTY, T.R.G., GANGULY, C., SASTRY, D.H., J. Nucl. Mater. 226 (1995)197.

[105] ADAMSON, M.G., AITKEN, E.A., CAPUTI, R.W., J. Nucl. Mater. 130 (1985) 349.

[106] MANARA, D., et al., J. Nucl. Mater. 342 (2005) 148–163.

[107] KONNO, J., HIROSAWA, T., Nucl. Sci. Techn. 39 (2002) 771–777.

[108] KONNO, J., Nucl. Sci. Techn. 39 (2002) 1299–1302.

[109] CARBAJO, J.J., YODER, G.L., POPOV, S.G, IVANOV, V.K., A review of thermophysical properties of MOX and UO2 fuel, J. Nucl. Mater. 299 (2001) 181—198.

[110] MARTIN, D.G., A re-appraisal of thermal conductivity of UO2 and mixed (U, Pu) mixed oxide, J. Nucl. Mater. 110 (1982) 73.

[111] INOUE, M., Thermal conductivity of uranium-plutonium oxide fuel for fast reactors, J. Nucl. Mater. 282 (2000) 186–195.

[112] SOBOLEV, V., ARIEN, B., ip-eurotrans, dmi-wp1.5 meeting, lyon, oct 10–11, 2006.

[113] DURIEZ, C., Alessandri, J-P., Gervais, T., Philipponneau, Y., Thermal conductivity of hypostoichiometric low Pu content (U, Pu)O2-x mixed oxide, J. Nucl. Mater. 277 (2000) 143–158

[114] WASHINGTON, A.B.J., UKAEA report TRG-R-2236 (1973).

[115] VASUDEVA RAO, P.R., ANTHONYSAMY, S., KRISHNAIAH, M.V., CHANDRAMOULI, V., J. Nucl. Mater. 348 (2006) 329–334.

[116] SENGUPTA, A.K., et al., J. Nucl. Mater. 385 (2009) 173–177.

[117] PHILIPPONNEAU, Y., J. Nucl. Mater. 188 (1992) 194–197.

[118] GIBBY, R.L., "The Effect of Plutonium Content on the Thermal Conductivity of (U, Pu)O2 Solid Solutions," J. Nucl. Mater. 38 (1971) 163–177

[119] SCDAP/RELAP5/MOD 3.2 Code Manual, Volume IV: MATPRO – A Library of Materials Properties for Light Water Reactor Accident Analysis, NUREG/CR-6150, Vol. IV (INEL-96/0422), Rev. 1 (1997).

[120] YAMAMOTO, K., et al., Melting temperature and thermal conductivity of irradiated mixed oxide fuel, J. Nucl. Mater. 204 (1993) 85–92.

[121] INTERNATIONAL ATOMIC ENERGY AGENCY, Thermodynamics of Nuclear Materials, IAEA, Vienna (1968) 651.

[122] AFFORTIT, MARCON, J., "Chaleur Specifique a Haute Temperature des Oxydes D'Uranium et dePlutonium", Revue Internationale des Hautes Temperatures et des Refractaires 7 (1970) 236–241.

[123] KANDAN, R., BABU, R., NAGARAJAN, K., VASUDEVA RAO, P.R., Thermochimica Acta 472 (2008) 46–49.

[124] MARTIN, D.G., J. Nucl. Mater., 152,(1988) 94.

[125] TERENTYEV, D., GOVERS, K., SOBOLEV, V., LEMEHOV, S., Proc. Global 2005, paper no. 74.

[126] DHARMADURAI, G, On Estimation of Critical Temperatures of Fast Reactor Fuels, Nucl. Eng. Des. 73 3 (1982) 287−291.

[127] CHAWLA, T.C., et al., Thermophysical Properties of Mixed Oxide Fuel and Stainless Steel Type 316 for Use in Transition Phase Analysis, Nucl. Eng. Des. 67 1 (1981) 57–54.

[128] INTERNATIONAL ATOMIC ENERGY AGENCY, Thermophysical Properties of Materials for Nuclear Engineering, IAEA-THPH, IAEA, Vienna (2008) 36.

[129] BREITUNG, W., REIL, K.O., The Density and Compressibility of Liquid (U, Pu)-mixed oxide, Nucl. Sci. Eng. 105 3 (1990) 205−217.

[130] NICKERSON, G.M., KASTENBERG, W.E., Preliminary Assessments of Carbide Fuel Pins During Mild Overpower Transients in LMFBRs, Nucl. Eng. Des. 36 (1976) 209.

[131] HAYES, S.L., Material Property Correlations for Uranium Mononitride. I. Physical Properties, J. Nucl. Mater. 171 2−3 (1990) 262−270.

[132] MAJUMDAR, S., SENGUPTA, A.K., KAMATH, H.S., Fabrication, characterization and property evaluation of mixed carbide fuels for a test Fast Breeder Reactor, J. Nucl. Mater. 352 (2006) 165–173.

[133] MENSHIKOVA, T.S., Atomic Energy Vol. 31 (1971).

[134] SHETH, A., LEIBOWITZ, L., "Thermal Conductivity Values for Advanced Fuels," Interim Report, Argonne National Laboratory report ANL-AFP-3 (Nov. 1974).

[135] LEWIS, H. D., KERRISK, J.F., Los Alamos Report, LA-6096 (1976).

[136] BATES, J.L., "Thermal Conductivity and Electrical Resistivity of Uranium Oxycarbide," Battelle Memorial Institute report BNWL-989 (1969).

[137] WHEELER, M.J., KING, E., MANFORD, C., HEDGER J., Thermal Diffusivity of Uranium and Uranium-Plutonium Carbides, J. Brit. Nucl. Ener. Sot. 10 1 (1971) 55–64.

[138] STORMS, E.K., Los Alamos Report LA-9524 (1982).

[139] SENGUPTA, A.K., et al., Am. Ceram. Soc. Bull. 65 (1986) 1057.

[140] SENGUPTA, A.K., et al., Nucl. Technol. 12 (2003) 260.

[141] SENGUPTA, A.K., et. al., "Important out-of-pile thermophysical properties of uranium-plutonium mixed carbide fuels for a fast breeder test reactor", Studies on Fuels with Low Fission Gas Release, IAEA-TECDOC-970, IAEA, Vienna (1997) 125.

[142] HAYES, S.L., THOMAS, J., REDDICORD, K., Material Property Correlations forUranium Mononitride. J. Nucl. Mat. 171 (1990) 262

[143] ROSS, S., GENK, E., Thermal conductivity correction for uranium nitride fuel between 10 and 1923 K, J. Nucl. Mater. 151 (1988) 313.

[144] ARAI, Y., SUZUKI, Y., IWAI, T., OHMICHI, T., "Dependence of the thermal conductivity of (U, Pu)N on porosity and plutonium content", J. Nucl. Mater. 195 (1992) 37.

[145] KELLER, D.L., Uranium-Plutonium Nitride Fuels for LMFBR Applications, US report BMI 1837 and 1845 (1968).

[146] ARAI, Y., MORIHIRA, M., OHMICHI, T., "The effect of oxygen impurity on the characteristics of uranium and uranium-plutonium mixed nitride fuels", J. Nucl. Mater. 202 (1993) 70–78.

[147] MATSUI, T., OHSE, R., Thermodynamic Properties of Uranium Nitride, Plutonium Nitride, Uranium-Plutonium Mixed Nitride. High Temperature-High Pressures 19 (1987) 1.

[148] GANGULY, C., HEGDE, P.V., SENGUPTA, A.K., "Status of (U, Pu)N fuel development in BARC", Advanced Fuel for Fast Breeder Reactors: Fabrication and Properties and Their Optimization, IAEA-TECDOC-466, IAEA, Vienna (1988) 7.

[149] GANGULY, C., HEGDE, P.V., SENGUPTA, A.K., Preparation, characterisation and of evaluation of out-of pile properties of (U, Pu)N fuel pellets, J. Nucl. Mater. 178 (1991) 234–241.

[150] GANGULY, C., ROY, P.R. SEAL, A.K., Trans. Powder Metall. Association of India 7 (1980) 22.

[151] GANGULY, C., et al., Nucl. Technol. 72 (1986) 59.

[152] HOLLEY, Jr, C.E., RAND M.H., STORMS, E.K., Chemical Thermodynamics, Part 6, The Actinide Carbide, IAEA, Vienna (1984).

[153] OETTING, F.L., NAVARATIL, J.D., STORMS, E.K., J. Nucl. Mater. 45 (1973) 271.

[154] TAGAWA, H., J. Nucl. Mater. 51 (1974) 78.

[155] HAYES, S., THOMAS, J., REDDICORD, K. "Material Property Correlations for Uranium Mononitride", J. Nucl. Mat. 171 (1990) 300.

[156] SHETH, A., LEIBOWITZ, L., Argonne National Laboratory report ANL-AFP-11 (1975).

[157] STAHL, D., STRSSSER, A., "Properties of solid Solution Uranium-Plutonium Carbides, " in Carbides in Nuclear Energy (RUSSELL, L.E., et al., Eds), Proc. of Symposium held at Harwell, England, November 1963, Vol. 1, pp. 373–391.

[158] ANDREW, J.F., LATIMER, T.W., Los Alamos Report LA-6037-MS (1975).

[159] BENZ, R., J. Nucl. Mat. 31 (1969) 93.

[160] BENZ, R., HUTCHINSON,W., J. Nucl. Mat. 36 (1970) 135.

[161] KOTELNIKOV, R.B. et al. High Temperature Nuclear Fuel/2nd Edition, Atomizdat (1978) (in Russian).

[162] PREUSSER, T., Modeling of Carbide Fuel Rod, Nucl. Techn. 57 (1982) 343−371.

[163] NICOLAS, R. URAN/Ch.2 "Materials for Nuclear Engineering" (MCINTOSH, A.B., HEAL, T.J., Eds), Temple Press Ltd, London (1960).

[164] SAMSONOV, G.V., VINNITSKY, I.N., Refractory Compounds/Handbook, Metallurgiia (1976) (in Russian).

[165] MAJUMDAR, S., SENGUPTA, A.K., KAMATH, H.S., J. Nucl. Mater. 352 (2006) 165–173.

[166] GANGULY, C., HEGDE, P. V., SENGUPTA, A. K., J. Nucl. Mater. 178 (1991) 234–241.

[167] SENGUPTA, A.K., BASAK,U., GANGULY C., J. Mater. Sci. Lett. 6 (1987) 20.

[168] TOKAR, M., "High Temperature Compressive Creep and Hot Hardness of Uranium-Plutonium Carbides", Los Alamos Scientific Laboratory report LA-4704 (July 1971).

[169] MASSALASKI, T.B., Binary phase diagrams, ASM, Material park 1990.

[170] PAHL, R.G., PORTER, D.L., LAHM, C.E.,HOFMAN, G.L., "Experimental Studies Of U-Pu-Zr Fast Reactor Fuel Pins In EBR-II", CONF-8809202-2.

[171] KITTEL, J. H., et al., Plutonium And Plutonium Alloys As Nuclear Fuel Materials, Nucl. Eng. Des. 15 (1971) 373–440.

[172] FARKAS, M.S., et al., Reactor Mater. 10(4) (1968) 203–216.

[173] FARKAS, M.S., et al., Reactor Mater. 11(2) (1968) 81–92.

[174] INTERNATIONAL ATOMIC ENERGY AGENCY, Thermo physical Properties of Materials for Water Cooled Reactors, IAEA-TECDOC-949, IAEA, Vienna (1997).

[175] TAKAHASHI, Y., YAMAWAKl, M., YAMAMOTO, K., J. Nucl. Mater. 154 (1988) 141.

[176] KIM, Y.S., HOFMAN, G.L., AAA FUELS HANDBOOK, Argonne National Laboratory.

[177] TOULOUKIAN, Y.S., et al., Thermo physical Properties of Matter, FI/Plenum, New York 1 (1970).

[178] FINK, J. K., LEIBOWITZ, L., J. Nucl. Mater. 226 44 (1995).

[179] FARKAS, M.S., et.al, Reactor Mater. 9(3) (1966) 151–165.

[180] OGATA, T., J. Nucl Sci Techn. Supplement 3 (2002) 675–681.

[181] BILLIONE, M.C., et al., "Status of Fuel Element Modeling Codes for Metallic Fuels", Proc. ANS Conf. Reliable Fuels for LMRs, Tucson, 1986.

[182] RAHN, F.J., ADAMANTIADES, A.G., KENTON, J.E., BRAUN, C.A., Guide to Nuclear Power Technology, John Wiley & Sons, N.Y. (1984).

[183] MATSUI, T., NATSUME, T., NAITO, K., J. Nucl. Mater. 167 (1989) 152.

[184] FARKAS, M.S., STORHOK, V.W., et.al, Reactor Mater. 10(2) (1967) 69–82.

[185] SAVAGE, J. Nucl. Mater. 25, (1968) 249.

[186] FARKAS, M.S., et.al, Reactor Mater. 8(3) (1965) 119–134.

[187] CAHALAN, J.E., SEVY, R.H., SU, S.F., CONF-850410-3, Argonne National Laboratory (1985).

[188] FINK, J.K., PETRI, M.C., Thermo physical Properties of Uranium Dioxide/Report ANL/Re-97/2.-Argonne: Argonne National Laboratory (1997).

[189] SHPILRAIN, E.E., FOMIN, V.A., KACHALOV, V.V., Density and Surface Tension of Liquid Uranium, Teplofizika Vysokikh Temperatur 26 5 (1988) 892−900 (in Russian).

[190] MULFORD, R.N.R., SHELDON, R.I., Density and Capacity of Liquid Uranium at High Temperatures, J. Nucl. Mater. **154** (1998) 268−275.

[191] EMELIANOV, V.S., EVTYUKHIN, A.I., Metallurgy of Nuclear Fuel. Properties and Manufacturing Science of Uranium, Thorium and Plutonium/2nd rev. and enl. ed., Atomizdat (1968) (in Russian).

[192] HIRANO, G., IWASAKI, T., HRAKAWA, N., Nucl. Sci. Techn. 37 (2000) 237–243.

[193] TOKAR, M., Los Alamos Report, LA-4284 (1969).

[194] KUTTY, T.R.G, SENGUPTA, A.K.,, ARUN KUMAR,, KAMATH, H.S., Proc. Theme Meeting on Modern Developments and practices in mechanical testing of structural materials (MDPMT-2007), BRNS (DAE) (2007) 203.

[195] KUTTY, T.R.G., GANGULY, C., J. Nucl. Mater. 182 (1991) 258.

[196] KUTTY, T.R.G., JARVIS, T., GANGULY, C., J. Nucl. Mater. 246 (1997) 189.

[197] MINATO, K., et al., J. Nucl. Mater. 389 (2009) 23.

[198] NISHI, T., et al., J. Nucl. Mater. 373 (2008) 295.

[199] MORMOTO, K., KATO, M., OGASAWARA, M., KASHIMURA, M., J. Nucl. Mater. 389 (2009) 179.

[200] MORMOTO, K., KATO, M., OGASAWARA, M., KASHIMURA, M., J. Nucl. Mater. 374 (2008) 378.

[201] MUKAIYAMA, T., et al., Int. Conf. on Evaluation of Emerging Nuclear Fuel Cycle Systems (GLOBAL '95), Versailles, France (1995) 110.

[202] THETFORD, R.,MIGNANELLI, M., J. Nucl. Mater. 320 (2003) 44–53.

[203] MEYER, M.K., HAYES, S.L., CARMACK, W.J., TSAI, H., J. Nucl. Mater. (2009) (in press).

[204] LEE, B.O., "Analysis on the Temperature Profile and the Thermal Conductivities of the Metallic and the Dispersion Fuel Rods for HYPER", Proc. KNS, May 2001.

[205] KENNEDY, Jr., et al., J. Nucl. Mater. 294 (1/2) (2001) 93.

[206] INTERNATIONAL ATOMIC ENERGY AGENCY, Advanced Fuel Technology and Performance: Current Status and Trends, IAEA-TECDOC-577, IAEA, Vienna (1990).

ANNEX

TABLE A–I. SUMMARY OF SELECTED METALLIC FUEL IRRADIATION EXPERIMENTS IN EBR-II AND FFTF

Experiment ID	Fuel composition	Cladding material	Number of rods in ass'y	Smeared density (%)	Cladding OD (cm)	Wall thickness (cm)	Plenum-to-fuel volume ratio	Peak power (kW/m) (beginning of life)	Peak cladding temp (°C) (beginning of life)	Peak burnup (at.%)	Fast fluence × 10^{22} n/cm² (E>0.1MeV)	Breached rod information
X419 Prototype and fuel behaviour	U-10Zr, U-8Pu-10Zr, U-19Pu-10Zr	D9	61	75	0.584	0.038	1	39.4	560	11.9	12	
X420 Prototype, fuel behaviour, failure mode, RBCB	U-10Zr, U-8Pu-10Zr, U-19Pu-10Zr	D9	61	75	0.584	0.038	1	36.1	590	18.4	18.5	1 breach @ 16.4 at.% burnup; 530°C at breach
X421 Prototype, fuel behaviour, failure mode	U-10Zr, U-8Pu-10Zr, U-19Pu-10Zr	D9	61	75	0.584	0.038	1	39.4	560	17.1	19.6	
X423 Fuel swelling and restructuring	U-10Zr, U-3Pu-10Zr, U-8Pu-10Zr, U-19Pu-10Zr, U-22Pu-10Zr, U-26Pu-10Zr	316	37	75	0.737		1	42.7	522	4.9	8.07	
X425 (X425A/B/C) Lead IFR	U-10Zr, U-8Pu-10Zr, U-19Pu-10Zr	HT-9	61	75	0.584	0.038	1	48.2	590	3, 11, 16.2, 19.3	20.6	
X429 (X429A/B) Fabrication variables and strain prediction	U-10Zr, U-8Pu-10Zr, U-19Pu-10Zr	HT-9 316SS	61	75	0.584	0.038	1	42.7	600	7.7, 10.6, 14.4	13.8	1 breach ea. @ 6.5 and 10 at.% burnup

TABLE A–I. SUMMARY OF SELECTED METALLIC FUEL IRRADIATION EXPERIMENTS IN EBR-II AND FFTF (cont.)

Experiment ID	Fuel composition	Cladding material	Number of rods in ass'y	Smeared density (%)	Cladding OD (cm)	Wall thickness (cm)	Plenum-to-fuel volume ratio	Peak power (kW/m) (beginning of life)	Peak cladding temp (°C) (beginning of life)	Peak burnup (at.%)	Fast fluence $\times 10^{22}$ n/cm^2 (E>0.1MeV)	Breached rod information
X430 (X430A/B) HT-9, peak cladding temp., large diameter, compatibility	U-10Zr, U-19Pu-10Zr, U-22Pu-10Zr, U-26Pu-10Zr	HT-9	37	75	0.737	0.041	1.4	49.2	540	11.5	20.6	
X431 (X431A) Blanket safety	U-2Zr, U-6Zr, U-10Zr	HT-9	19	85	0.940	0.038-0.051	1.8	39.4	507	3.9	15.4	
X432 (X432A) Blanket safety	U-2Zr, U-6Zr, U-10Zr	HT-9	19	85	0.940	0.038-0.051	1.8	39.4	507	4.5	16.6	
X435 (X435A) Mk-III qual	U-10Zr	D9	61	75	0.584	0.038	1.4	49.2	591	19.8	22.8	
X436 Mk-III quall	U-10Zr	D9	61	75	0.584	0.038	1.4	34.4	596		8.45	
X437 Mk-III quall	U-10Zr	D9	61	75	0.584	0.038	1.4	37.7	597		10	
X438 Mk-III quall	U-10Zr	D9	61	75	0.584	0.038	1.4	32.8	623		9.45	
X441 (X441A) FCMI test and LIFE-METAL benchmark	U-19Pu-6Zr, U-19Pu-10Zr, U-19Pu-12Zr	HT-9 D9	61	70-85	0.584	0.038	1.1–2.1	45.9	600	12.7	10.1	
X447 (X447A) U-Zr high-temp.	U-10Zr	HT-9	49	75	0.584	0.046	1.4	36.1	660	10	9.17	1 breach @ 9.5 at.% burnup; 630°C at breach

TABLE A–I. SUMMARY OF SELECTED METALLIC FUEL IRRADIATION EXPERIMENTS IN EBR-II AND FFTF (cont.)

Experiment ID	Fuel composition	Cladding material	Number of rods in ass'y	Smeared density (%)	Cladding OD (cm)	Wall thickness (cm)	Plenum-to-fuel volume ratio	Peak power (kW/m) (beginning of life)	Peak cladding temp (°C) (beginning of life)	Peak burnup (at.%)	Fast fluence $\times 10^{22}$n/cm^2 (E>0.1MeV)	Breached rod information
X448 (X448A) Mk-IV qual.	U-10Zr	HT-9	61	75	0.584	0.046	1.4	45.9	552	14.6	14.9	
X449 Mk-IV qual.	U-10Zr	HT-9	61	75	0.584	0.046	1.4	29.5	578	11.3	17.7	
X450 Mk-IV qual.		HT-9	61	75	0.584	0.046	1.4	36.1	576	10.2	13.1	
X451 (X451A) Mk-IV qual.	U-10Zr	HT-9	61	75	0.584	0.046	1.4	32.8	623	13.7	13.7	
X452 Fuel Impurities	U-10Zr	D9	61	75	0.584	0.038		34.4	596	6.1	5.38	
X453 Fuel impurities	U-10Zr	D9	61	75	0.584	0.038		34.4	596	8.5	8.45	
X454 Fuel impurities	U-10Zr	D9	61	75	0.584	0.038		49.2	547	8.3	9.12	
X455 Fuel impurities	U-10Zr	D9	61	75	0.584	0.038		49.2	547	10.3	9.16	
X481 Mk-III design with Pu	U-19Pu-10Zr	D9	61	75	0.584	0.038	1.4	49.2	579	10	11.3	
X483 (X483A) Mk-IIIA, reference 316SS qual.	U-10Zr	316	61	75	0.584	0.038	1.4	49.9	552	14.8	15.7	

TABLE A–I. SUMMARY OF SELECTED METALLIC FUEL IRRADIATION EXPERIMENTS IN EBR-II AND FFTF (cont.)

Experiment ID	Fuel composition	Cladding material	Number of rods in ass'y	Smeared density (%)	Cladding OD (cm)	Wall thickness (cm)	Plenum-to-fuel volume ratio	Peak power (kW/m) (beginning of life)	Peak cladding temp (°C) (beginning of life)	Peak burnup (at.%)	Fast fluence $\times 10^{22} \text{n/cm}^2$ (E>0.1MeV)	Breached rod information
X484 Mk-IIIA, reference 316SS qual.	U-10Zr	316	61	75	0.584	0.038	1.4	36.1	576	11.7	11.9	
X485 Mk-IIIA, reference 316SS qual.	U-10Zr	316	61	75	0.584	0.038	1.4	39.7	576	10.5	10.7	
X486 Mk-IIIA, reference 316SS qual.	U-10Zr	316	61	75	0.584	0.038	1.4	37.1	623	13.9	13.9	
X489 High-Pu for PRISM design	U-19Pu-10Zr, U-28Pu-10Zr	HT-9 HT-9M	61	75	0.584	0.046	1.4	36.1	606	5.4	4.83	
X492 (X492A/B) Zr-sheathed fuel	U-3Zr, U-20.5Pu-3Zr	HT-9 HT-9M	61	75	0.584	0.038	1.4	41.0	551	10.5	11.1	
X496 Long lifetime	U-10Zr	HT-9	37	59	0.686	0.056	3	63.3	536	8.3	6.9	
X501 Minor-actinide-bearing fuel	U-20.2Pu-10Zr -1.3Np-1.2Am, U-10Zr	HT-9	2 + 59	75	0.584	0.046	1.4	44.9	≤540	7.6	14.2	
IFR-1 Fuel column length effects	U-10Zr, U-8Pu-10Zr, U-19Pu-10Zr	D9	169	75	0.686	0.056	1.2	49.2	615(604)	94 GWd/MTHM	15.4	

TABLE A–I. SUMMARY OF SELECTED METALLIC FUEL IRRADIATION EXPERIMENTS IN EBR-II AND FFTF (cont.)

Experiment ID	Fuel composition	Cladding material	Number of rods in ass'y	Smeared density (%)	Cladding OD (cm)	Wall thickness (cm)	Plenum-to-fuel volume ratio	Peak power (kW/m) (beginning of life)	Peak cladding temp (°C) (beginning of life)	Peak burnup (at.%)	Fast fluence $\times 10^{22} n/cm^2$ (E>0.1MeV)	Breached rod information
MFF1A FFTF Lead Metal Fuel Test	U-10Zr	HT-9	8	75	0.686	0.056	1.2	42.7	577	38 GWd/MTHM	5.6	
MFF-1 FFTF Lead Metal Fuel Test	U-10Zr	HT-9	5	75	0.686	0.056	1.2	43.0	577	95 GWd/MTHM	17.3	
MFF-2 FFTF Metal Prototype	U-10Zr	HT-9	169	75	0.686	0.056	1.3	54.1	618	143 GWd/MTHM	19.9	
MFF-3 FFTF Metal Prototype	U-10Zr	HT-9	169	75	0.686	0.056	1.3	59.1	643	138 GWd/MTHM	19.2	
MFF-4 FFTF Series III.b qualification	U-10Zr	HT-9	169	75	0.686	0.056	1.5	56.8	618	135 GWd/MTHM	19	
MFF-5 FFTF Series III.b qualification	U-10Zr	HT-9	169	75	0.686	0.056	1.5	55.8	651	101 GWd/MTHM	14	
MFF-6 FFTF Series III.b qualification	U-10Zr	HT-9	169	75	0.686	0.056	1.5	55.8	588	141 GWd/MTHM	12.8	

A–II. THERMAL CONDUCTIVITY OF NUCLEAR FUELS

In normal conditions, thermal conductivity and linear power determine the peak fuel operating temperature. Under the accident conditions, the thermal conductivity of the fuel determines the maximum permissible linear rating, χ_{max}, if central melting is to be avoided [A–1, A–2]. The thermal conductivity, k, allows the determination of centre temperature of fuel T_c, when the surface temperature T_s, is known by using the conductivity integral,

$$\chi = 4\pi \int_{T_s}^{T_c} kdT \tag{A–1}$$

where χ is the linear rating.

In actinide oxides, the deviation from stoichiometry and the presence of foreign atoms or porosity results in lower values of k. In general, phonon–phonon scattering and phonon–impurity scattering are the dominant mechanisms of the thermal conductivity in ceramics. Klemens [A–3] has proposed a heat conduction model in materials where the phonon–phonon (Umklapp) scattering and the phonon–impurity scattering occur simultaneously. Theoretically the phonon component the thermal conductivity k may be written as:

$$k = (A + BT)^{-1} \tag{A–2}$$

where A and B are constants and T is the absolute temperature.

Thermal resistivity (R), which is the reciprocal of thermal conductivity (k), of the above oxides, can be described by the following equation:

$$R = 1/k = A + BT \tag{A–3}$$

The parameter A represents the influence of phonon scattering by lattice imperfections and the parameter B describes the influence of phonon-phonon scattering [A–4]. The influence of substituted impurities on the thermal conductivity is described by the increase of the parameter A, while parameter B remains nearly constant by substitution. The parameter A also depends on the difference in mass and radius between the substituted atom and the host atom [A–4, A–5]. The constants A and B can be obtained from the least squares fitting of the experimental data.

A–III. EFFECT OF POROSITY ON THERMAL CONDUCTIVITY

Pores, like any other defect, scatter phonons and reduce the thermal conductivity. There are many relations in the literature describing the effect of porosity on thermal conductivity. For an exact derivation, the shape and the distribution of porosities must be known. Some of the important relations listed in the literature are given below [A–1, A–6–A–11]:

1. Loeb: $\quad k_M=(1 - P)k_{TD}$ $\hspace{4cm}$ (A–4a)

2. Modfied Loeb $\quad k_M= (1 - \alpha P)k_{TD}$, where $2 < \alpha < 5$ $\hspace{3cm}$ (A–4b)

3. Kampf & Karsten $\quad k_M= (1 - P^{2/3})k_{TD}$ $\hspace{4cm}$ (A–4c)

4. Biancharia $\quad k_M= (1 - P)/(1 - (\beta - 1)P)k_{TD}$, $\beta = 1.5$ for spherical pores $\hspace{1cm}$ (A–4d)

5. Maxwell-Eucken $\quad k_M= [(1 - P)/(1 + \beta P)]k_{TD}$ $\hspace{4cm}$ (A–4e)

6. Bauer $k_M = [(1 + 0.5P)/(1 - P)]k_{TD}$ (A–4f)

7. Steinbock $k_M = (1 - P)^{3/2} k_{TD}$ (A–5g)

Among the above, Eq. (A–4a) under predicts the data and equations (A–4d) and (A–4e) account for the shape of the pores. IAEA recommends the value of α as 2.5 for UO_2 and mixed oxide. It is found that values for 100% dense (k_{TD}) materials can vary considerably depending upon the type of correction employed. Since there are so many relations available in the literature, either a directly measured data are needed for the actual fuel, or else porosity corrections should be made for a small variations in porosity only.

A–IV. THERMAL CONDUCTIVITY OF ACTINIDE OXIDES

The analysis of the lattice defect thermal resistivity and the evaluation of phonon scattering by the various defect scattering centres in pure and mixed actinide oxides have been carried out by several authors [A–1, A–2, A–5, A–6, A–12–A–15] Accordingly, A of Eq. (A–2) can be given as:

$$A = C(\Gamma_u + \Gamma_o) \tag{A–6}$$

Where $C = (\pi^2 V\theta)/(3hv^2)$ and V, θ, h and v denote the average atomic volume, Debye temperature, Planck's constant and phonon velocity, respectively. Γ_u is the scattering cross section arising from Pu substitution and Γ_o is that from all other native defects present in the sample[A–1]. The scattering cross-section Γ_u can be expressed in terms of the mass and size difference of the substituted atom over that of the host:

$$\Gamma_u = (1 - x)x[(\Delta M/M)^2 + \varepsilon (\Delta r/r)^2] \tag{A–7}$$

Where x is atomic fraction of Pu, ΔM and Δr are the mass and radius difference between U and Pu atom respectively, M and r average mass and radius of the substituted atom and ε is an adjustable parameter. From the above, it is clear that scattering cross section depend up on the following viz:

— mass difference between U and Pu atoms;
— size difference between U and Pu atoms;
— charge of U ion;
— microstructure.

The mass differences between U and Pu atoms are less than 3%, and hence its contribution to thermal resistivity can be neglected. The difference between their sizes is not appreciable and hence its contribution to thermal resistivity may also be neglected. The charge of the U ion depends up on the O/M ratio of the pellet. This means that at higher O/M, some of U^{+4} ions are converted to U^{+5} or U^{+6} ions. This suggests that O/M ratio is the most important factor controlling the thermal conductivity of mixed oxide fuels.

The parameter B is given by the following relation [A1],

$$B = B_0\{[a_0/ (a_0)_{UO2}]^2 [(T_M)_{UO2}/T_M]^{3/2}\} \tag{A–8}$$

where, B_0 is the value for pure UO_2, a_0 is the lattice constant, T_M is the melting point of the mixed stoichiometric oxide, and $(a_0)_{UO2}$ and $(T_M)_{UO2}$ are the same properties for pure UO_2.

Thermal conductivity studies on oxide fuel constitute an area of work which was particularly active in the 1960s, and a number of reviews were published during that period [A–16–A–20]. Every parameter affecting thermal conductivity was widely studied and reported in the literature. The thermal conductivity of fully dense oxide fuel (k_s) in the as-fabricated condition is normally described by:

$$k_s = k_{Phonon} + k_{Electron} \tag{A–9}$$
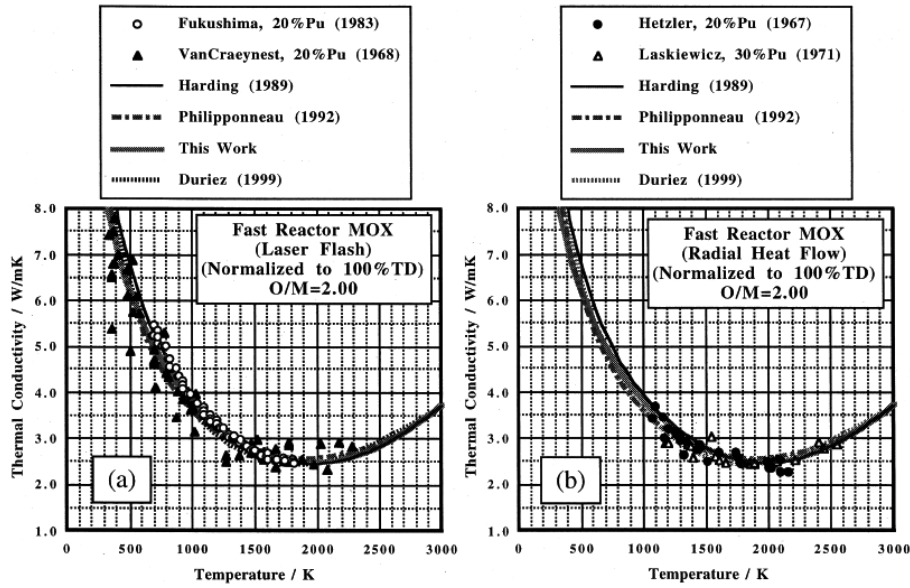
FIG. A–I. Thermal conductivity of MOX fuel is plotted against temperature showing scatter [A–24].

which is the sum of the contributions by phonon (k_{Phonon}) and electron ($k_{Electron}$) conduction. The above equation can be rewritten as [A–1]:

$$k_s = [1/(A + BT)] + [(C/T^2) \exp(-D/T)] \tag{A–10}$$

where T is the temperature, and A, B, C, and D are constants. Below 2 000 K phonon conduction is dominant whereas at higher temperatures electron conduction becomes dominant. The temperature dependence of the thermal conductivity of stoichiometric oxide fuels, measured by laser flash and radial heat flow techniques, are shown in Fig. A–1. The scatter in values of thermal conductivities is with in 5%.

The effect of Pu on thermal conductivity of MOX fuel for various temperatures is shown in Figs A–II and A–III shows the variation of thermal conductivity with O/M ratio for different temperatures for UO_2-20%PuO_2 composition. Gibby [A–21–A–23] has reported that the ΔA values that best fit his measured thermal conductivities were proportional to the nonstoichiometry parameter x:

$$\Delta A/x \sim 400 \tag{A–11}$$

Substituting the above values in equation (A–11),

$$k = 1/[A_0 + 400x + B(x,q)T] \tag{A–12}$$

As the temperature is increased, the O/M effect becomes less pronounced because the last term in the denominator of Eq. (A–12) dominates the middle term.

A–V. SPECIFIC HEAT

Fuel enthalpy and its temperature derivative, heat capacity, are important for fuel behaviour during normal and transient conditions. Accurate knowledge of the specific heat of the fuel material is needed for assessment of reactor behaviour under transient conditions, where the thermal diffusivity, $k/\rho C_P$, determines the time dependence of the temperature [A–1, A–25]. Finally, fuel heat capacity and thermal conductivity together determines the fuel time constant, which is a key parameter in fuel stability analysis.
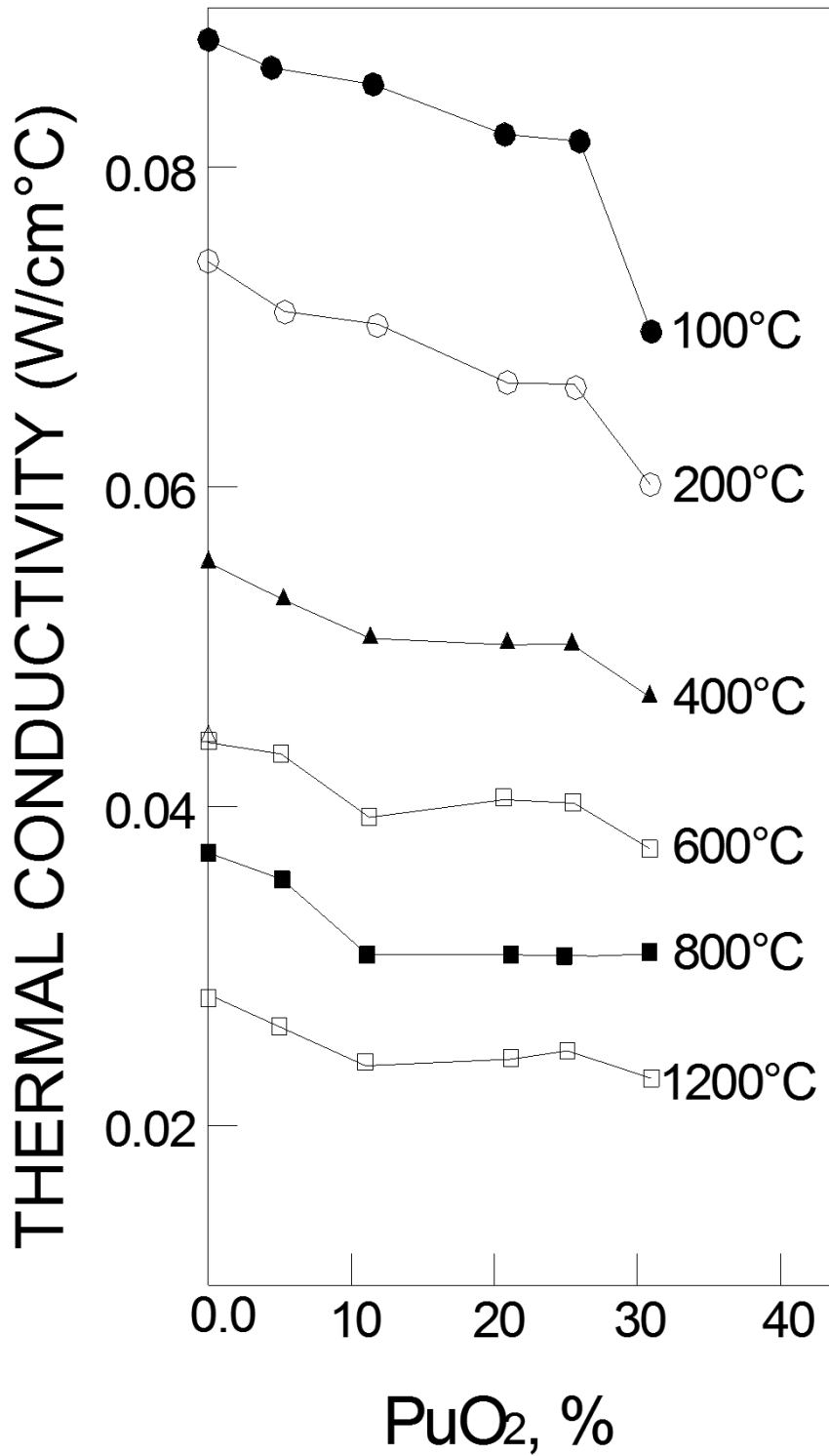
FIG. A–II. Effect of Pu content on thermal conductivity of MOX fuel [A–1].

The enthalpy and heat capacity for actinide fuels are functions of the following [A–25]:

— Temperature,
— Fuel composition,
— O/M ratio,
— Fuel burnup.
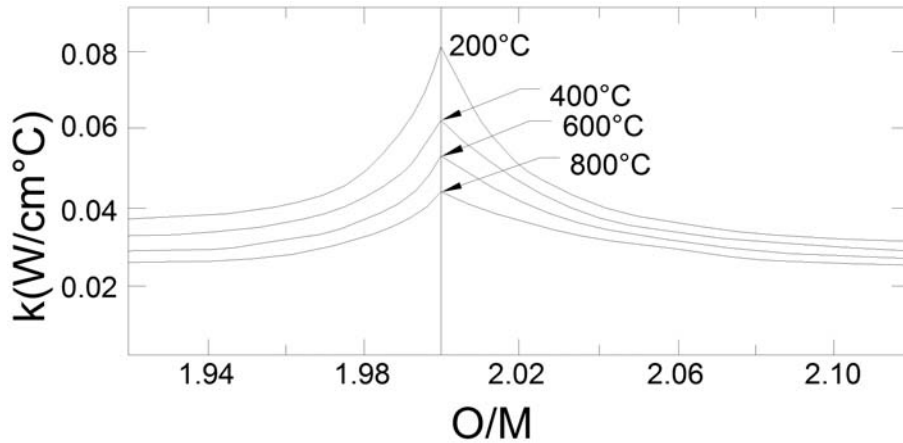
FIG. A.III. Shows the variation of thermal conductivity with O/M ratio for different temperatures for UO$_2$-20%PuO$_2$ composition [A–1].
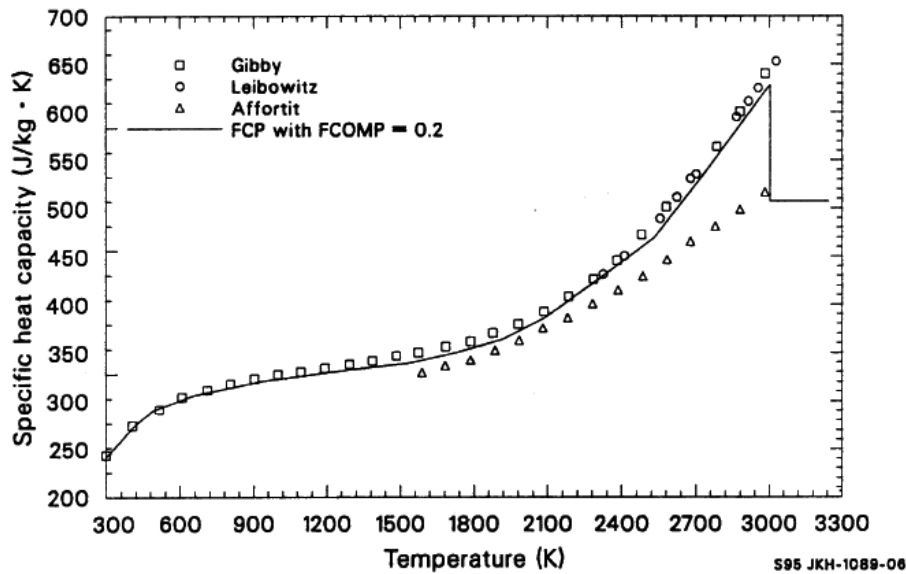

FIG. A–IV. Specific heat capacity of (U$_{0.8}$Pu$_{0.2}$)O$_2$ from three different experiments plotted against temperature [A–25].

The most common technique of determining specific heat capacity is to measure the enthalpy of a sample by a drop calorimeter or by a differential scanning calorimeter (DSC) and deduce the heat capacity by finding the rate of enthalpy change with temperature. Generally, the enthalpy data are fitted using an empirical function, often a simple polynomial equation.

The effect of O/M ratio and burnup on heat capacity is small. Their effect is to increase the heat capacity slightly. In UO$_2$, Hiernaut et al. [A–28] have observed a λ shaped phase transition at 2670 ± 30 K prior to melting. At this transition, the heat capacity increases very sharply in a narrow temperature interval. A similar kind of phase transition is expected in MOX fuel [A–26–A–27]. The MATPRO data of specific heat capacity of (U$_{0.8}$Pu$_{0.2}$)O$_2$ from three different experiments plotted against temperature and is shown in Fig. A–4 [A–25]. Figure A–5 shows the effect of O/M ratio on specific heat for (U$_{0.8}$Pu$_{0.2}$)O$_{2+x}$.

A–VI. HOT HARDNESS

Hardness is an easily measured mechanical property that can provide insight into the strength of the fuel. Since hardness is related to yield stress, U.T.S, stress exponent and other mechanical properties by simple empirical
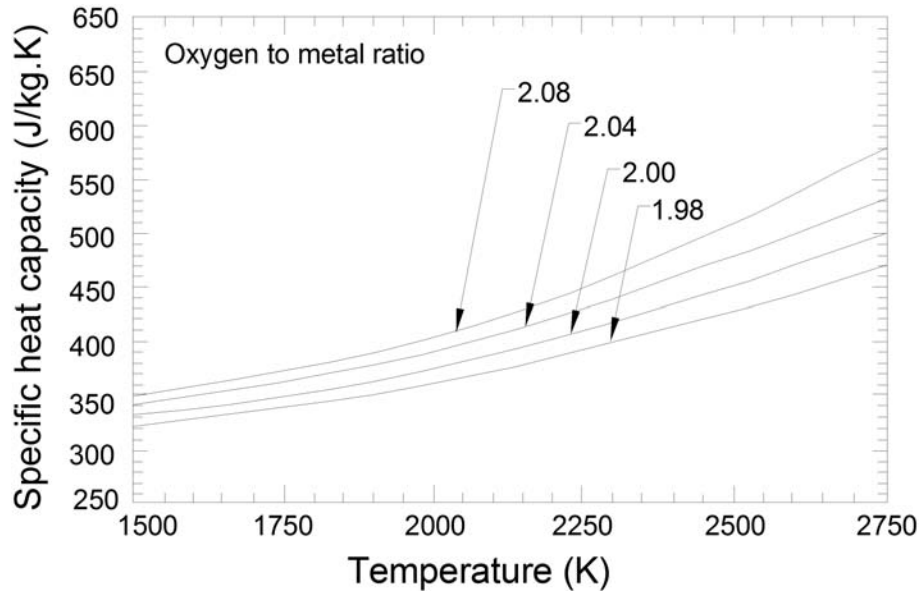
FIG. A–V. Specific heat capacity as a function of temperature and O/M ratio for $(U_{0.8}Pu_{0.2})O_2$ [A–25].

relations, prediction of these mechanical properties from hardness data will be very useful for radiotoxic materials where conventional testing is very difficult to perform [A–29]. The hot hardness data further give information on softening behaviour [A–30] and can be correlated to the Larson-Miller and Sherby-Dorn parameters to predict the long term rupture and creep properties. The basis of the hardness testing is the assumption that hardness is independent of the loading time. If the indenter is sinking into the specimen after attaining the full load, the solid is said to exhibit indentation creep. Walker [A–31] has defined indentation creep as a time dependent motion of hard indenter into a solid under a constant load [A–32–A–33]. During the indentation creep, the indenter maintains its load over a period of time under well-controlled conditions and changes in the indentation size are monitored [A–33]. Indentation creep is influenced by a large number of variables such as material's plastic deformation properties, diffusion constants, the normal acting load on indenter, duration of indentation etc.

It is widely recognized that the flow stress, σ of any metal consists of two components [A–34–A–35]:

$$\sigma = \sigma^*(\dot{\varepsilon},T) + \sigma_I(\varepsilon) \tag{A–13}$$

where σ^* is called the frictional stress which depends on temperature and strain rate but not on the level of work hardening. σ^* becomes negligible at intermediate and high temperatures. In contrast, σ_I, the athermal stress, depend on temperature only through the temperature dependence of shear modulus [A–34]. σ^* is associated with the stress required in order to permit the glide dislocations to overcome the short-range barriers by thermal activation where as σ_I is associated with the long-range elastic interaction of dislocations. Since hardness and flow stress are intimately related, H can be separated into rate dependent and rate independent components as:

$$H = H^*((\dot{\varepsilon},T) + H_I(\varepsilon) \tag{A–14}$$

where H^* represents the frictional component of hardness and H_I represents an athermal component, the latter dependent on temperature through the temperature dependence of shear modulus. It is reported that the hardness and elastic properties of metals and alloys are closely related. Young's modulus of steel decreases by about 1/3 on heating up to 1 073 K but a proportional reduction in hardness is of the order of 90% [A–35]. This indicates that softening is associated with the reduction of modulus. To account for this, H-T data are to be treated after correcting for the temperature variation of modulus. The data can then be represented by the relation:

$$H/G = A_1 \exp(-B_1 T/T_m) \tag{A–15}$$

107

The correction for shear modulus variation with temperature is made by computing the shear modulus at any temperature from

$$G_T = G_0 \ [1 + (T - 300)/T_m)](T_m/G_0 \times dG/dT) \tag{A–16}$$

where G_0 and G_T are the shear modulus at room temperature and at temperature T, respectively.

Hot hardness measurements are carried out with the help of a hot hardness tester. The indenters are generally made of sapphire, cubic boron nitride (CBN) or diamond. For testing, metallographically polished sample was loaded into the specimen holder. Care was taken to maintain the sample surface perpendicular to the microscope axis. The load was applied at a rate of 0.2 mm/min. The instrument is calibrated using a standard (Cu: SRM; National Bureau of Standards, USA) sample. Hot hardness measurements are generally carried out in vacuum (0.1Pa) from room temperature to the required temperature at every 100°C interval or any suitable interval using a dwell time of 5 s. The sample temperature is kept constant within ±1°C and that of the indenter was kept within ±3°C. Hot harness measurements were carried out judiciously selecting representative areas. At each temperature, three indentations are made and their average value is reported. For indentation creep experiments, at each temperature, the hardness was measured as a function of dwell time.

A–VII. THERMAL CONDUCTIVITY RELATIONS FOR UC AND MC

The thermo physical properties of UC and UN are affected by the following factors [A–12, A–36]:

— Effect of excess carbon in carbides;
— Amount of PuC and PuN present in mixed carbides and nitrides, respectively;
— Effect of oxygen as residual impurity from fabrication in UC and in UN;
— Effect of porosity for both carbide and nitride;
— Effect of metallic impurities within and beyond their solubility limits, especially with regard to fission products.

Lewis and Kerrisk [A–37] reviewed thermal conductivity studies carried by various authors of carbides and recommended the following equations for UC for 100% T.D.:

$$k \ (Wm^{-1}C^{-1}) = 21.7 - 3.04 * 10^{-3} \ T + 3.61 * 10^{-6}T^2 \qquad 50 < T < 700°C \tag{A–17}$$

$$k \ (Wm^{-1}C^{-1}) = 20.2 + 1.48 * 10^{-3}T \qquad 700 < T < 2\ 300°C \tag{A–18}$$

The recommended equation for PuC (100%T.D.) is as given below [A37]:

$$k \ (Wm^{-1}C^{-1}) = 7.45 - 4.04 * 10^{-3} \ T + 1.20 * 10^{-5}T^2 \qquad 50 < T < 1\ 300°C \tag{A–19}$$

Matzke [A12] has given the following relations of $k \ (Wm^{-1}C^{-1})$ of $(U_{0.8}Pu_{0.2})C$ between 50°C and 2 300°C for fully dense material,

$$k = 17.5 - 5.65 * 10^{-3} \ T + 8.14 * 10^{-6}T^2 \qquad 50 < T < 500°C \tag{A–20}$$

$$k = 12.76 + 8.71 * 10^{-3} \ T - 1.88 * 10^{-6}T^2 \qquad 500 < T < 2\ 300°C \tag{A–21}$$

REFERENCES TO THE ANNEX

[A–1] OLANDER, D.R., Fundamental Aspects of Nuclear Reactor Fuel Elements, TID-26711-P1, US Department of Energy (1976) 145.

[A–2] OGGIANU, S.M. and KAZIMI, M.S., MIT report MIT-NFC-TR-021 (2000).

[A–3] KLEMENS, P.G., High Temp. High Press. 17 (1985) 41.

[A–4] BAKKER, K., CORDFUNKE, E.H.P., KONINGS, R.J.M., SCHRAM, R.P.C., J. Nucl. Mater. 250 (1997) 1.

[A–5] POPOV, S.G., CARBAJO, J.J., IVANOV, V.K., YODER, G.L., ORNL/TM-2000/351.

[A–6] MARINO, G.P., J. Nucl. Mater. 38 (1971) 178.

[A–7] LOEB, A.L., J.Am. Ceram. Soc. 37 (1954) 96–99.

[A–8] MACEWAN, J.R., STOUTE, R.L., NOTLEY, M.F., Effect of Porosity on the Thermal Conductivity of UO_2, J. Nucl. Mater. 24 (1967) 109–112.

[A–9] BIANCHERIA, A., The Effect of Porosity on Thermal Conductivity of Ceramic Bodies, Trans. Am. Nucl. Soc. 9 (1966) 15.

[A–10] ONDRACEK, G., SCHULZ, B., The Porosity Dependence of the Thermal Conductivity for Nuclear Fuels, J. Nucl. Mater. 46 (1973) 253–258.

[A–11] VANCRAEYNEST, J.C., STORA, J.P., "Effect de la Porosite sur la Variation de Conductubilite Thermique du Bioxyde d'Uranium en Fonction de la Temperature," J. Nucl. Mater. 37 (1970) 153–158.

[A–12] MATZKE, Hj., Science Of Advanced LMFBR Fuels, Chapter 4, North-Holland (1986) 176.

[A–13] RICHTER, J., SCHMIDT, H.E., TASMAN, H.A., Report EUR-5119e (1974).

[A–14] LEMEHOV, S.E., SOBOLEV, V., VAN UFFELEN, P, J. Nucl. Mater. 320 (2003) 66.

[A–15] YOUNG, R.A., J. Nucl. Mater. 87 (1979) 283.

[A–16] MARTIN, D.G., J. Nucl. Mater. 110 (1982) 73.

[A–17] PHILIPPONNEAU, Y., J. Nucl. Mater. 188 (1992) 194–197.

[A–18] DURIEZ, C., ALESSANDRI, J-P., GERVAIS, T., PHILIPPONNEAU, Y., Thermal conductivity of hypostoichiometric low Pu content (U, Pu)O2-x mixed oxide, J. Nucl. Mater. 277 (2000) 143–158.

[A–19] CARBAJO, J.J., YODER., G.L., POPOV, S.G., IVANOV, V.K., "A review of thermophysical properties of MOX and UO2 fuel", J. Nucl. Mater., 299 (2001) 181–198.

[A–20] Washington, A.B.J., UKAEA report TRG-R-2236 (1973).

[A–21] GIBBY, R.L., The Effect of Plutonium Content on the Thermal Conductivity of (U, Pu)O_2 Solid Solutions, J. Nucl. Mater. 38 (1971) 163–177.

[A–22] GIBBY, R.L., "The Thermal Diffusivity and Thermal Conductivity of Stoichiometric, $(U_{0.8} Pu_{0.2})O_2$",BNWL-704 (1968).

[A–23] GIBBY, R.L., The Effect of Oxygen Stoichiometry on the Thermal Diffusivity and Conductivity of $(U_{0.75}Pu_{0.25})O_{2-x}$, BNWL-927 (Jan. 1969).

[A–24] INOUE, M., Thermal conductivity of uranium-plutonium oxide fuel for fast reactors, J. Nucl. Mater. 282 (2000) 186–195.

[A–25] SCDAP/RELAP5/MOD 3.2 Code Manual, Volume IV: MATPRO – A Library of Materials Properties for Light Water Reactor Accident Analysis, NUREG/CR-6150, Vol. IV (INEL-96/0422), Rev. 1 (1997).

[A–26] CARBAJO, J.J., YODER, G.L., POPOV, S.G., IVANOV, V.K., A review of thermophysical properties of MOX and UO_2 fuel, J. Nucl. Mater., 299 (2001) 181-198.

[A–27] CHASANOV, M.G., LEIBOWITZ, L. AND GABELNICK, S.D., J. Nucl. Mater. 49(1973/74) 129–135.

[A–28] HIERNAUT, J.P., Int. J. Thermophys. 14 (1993) 259.

[A–29] KUTTY, T.R.G., RAVI, K., GANGULY, C., J. Nucl. Mater. 265 (1999) 91.

[A–30] TABOR, D., Micro indentation Techniques in Material Science and Engineering (BLAU, P.J., LAWN, B.R., Eds), ASTM-STP-889, ASTM, Philadelphia (1985) 129.

[A–31] WLAKER, W.W., The Science of Hardness Testing and its Research Application, (WESTBROOK, J.H., CONARD, H., Eds), ASM, Metals Park, Ohio (1971), p 258.

[A–32] LI, W.B. and WARREN, R., Acta Metall.Mater. **41**, 3065 (1993).

[A–33] LI, W.B., HENSHALL, J.L., HOOPER, R.M. and EASTERLING, K.E., Acta Metall. Mater. **39**, 3099 (1991).

[A–34] STONE, D.S., YODER, K.B., J. Mater. Res. 9 (1994) 2524.

[A–35] TAYLOR, G., Prog. Mater. Sci. 36 (1992) 29.

[A–36] BLANK, H., "Nonoxide Ceramic Nuclear Fuels", in Materials Science and Technology (Cahn, R.W., Haasen, P., Kramer, E.J., Eds), Weinheim-New York-Basel-Cambridge-Tokyo **10 A** (1994) 191–357.

[A–37] LEWIS, H.D., KERRISK, J.F., Los Alamos Report, LA-6096 (1976).

CONTRIBUTORS TO DRAFTING AND REVIEW

Baldev, R.	Indira Gandhi Centre for Atomic Research, India
Basak, U.	Bhabha Atomic Research Centre, India
Bibilashvili, Y.K.	Bochvar Institute of Inorganic Materials, Russian Federation
Bryusov, A.N.	Institute for Physics and Power Engineering, Russian Federation
Busurin, Y.	International Atomic Energy Agency
Bychkov,A.V.	Research Institute of Atomic Reactors, Russian Federation
Depisch, F.	International Atomic Energy Agency
Dyneko, I.	Economy of Obninsk City Admin., Russian Federation.
Filatova, E.	Institute of Nuclear Materials, Russian Federation.
Fromont, M.	CEA/CEN-Cadarache, France
Ganguly, C.	International Atomic Energy Agency
Inozemtsev, V.	Bochvar Institute of Inorganic Materials, Russian Federation
Itoh, K.	Nuclear Development Corporation, Japan
Jung, I.H.	Korea Atomic Energy Research Institute, Republic of Korea
Kamath, H.S.	Bhabha Atomic Research Centre, India
Kormilitsyn, M.	Research Institute of Atomic Reactors, Russian Federation
Koyama, T.	Japan Atomic Energy Agency, Japan
Kutty, T.R.G.	Bhabha Atomic Research Centre, India
Mason , M.	CEA/CEN-Marcoule, France
Mathonniere, G.	CEA-Saclay, France
Mizuno, T.	Japan Atomic Energy Agency, Japan
Nawada, H.P.	International Atomic Energy Agency
Poplavskiy, V.M.	Institute for Physics and Power Engineering, Russian Federation
Rouault, J.	CEA/CEN-Cadarache, France
Ryu, H. Y.	
Sinelnikov, L.P.	Institute of Nuclear Materials, Russian Federation
Stanculescu, A.	International Atomic Energy Agency

Uchiyama, G.	JNC, Japan
Vasudeva Rao, P.R.	Indira Gandhi Centre for Atomic Research, India
Walters, L.	Private consultant, United States of America
XU, M.	China Atomic Energy Institute, China

Consultants Meetings

Dimitrovgrad, Russian Federation: 11–13 May 2005
Vienna, Austria: 17–19 December, 2007
Kalpakkam, India: 25–29 May 2009

Technical Meeting

Obninsk, Russian Federation: 21–23 November 2005

Structure of the IAEA Nuclear Energy Series

Nuclear Energy Basic Principles
NE-BP

Nuclear General Objectives
NG-O

1. Management Systems
NG-G-1.#
NG-T-1.#

2. Human Resources
NG-G-2.#
NG-T-2.#

3. Nuclear Infrastructure and Planning
NG-G-3.#
NG-T-3.#

4. Economics
NG-G-4.#
NG-T-4.#

5. Energy System Analysis
NG-G-5.#
NG-T-5.#

6. Knowledge Management
NG-G-6.#
NG-T-6.#

Nuclear Power Objectives
NP-O

1. Technology Development
NP-G-1.#
NP-T-1.#

2. Design and Construction of Nuclear Power Plants
NP-G-2.#
NP-T-2.#

3. Operation of Nuclear Power Plants
NP-G-3.#
NP-T-3.#

4. Non-Electrical Applications
NP-G-4.#
NP-T-4.#

5. Research Reactors
NP-G-5.#
NP-T-5.#

Nuclear Fuel Cycle Objectives
NF-O

1. Resources
NF-G-1.#
NF-T-1.#

2. Fuel Engineering and Performance
NF-G-2.#
NF-T-2.#

3. Spent Fuel Management and Reprocessing
NF-G-3.#
NF-T-3.#

4. Fuel Cycles
NF-G-4.#
NF-T-4.#

5. Research Reactors — Nuclear Fuel Cycle
NF-G-5.#
NF-T-5.#

Radioactive Waste Management and Decommissioning Objectives
NW-O

1. Radioactive Waste Management
NW-G-1.#
NW-T-1.#

2. Decommissioning of Nuclear Facilities
NW-G-2.#
NW-T-2.#

3. Site Remediation
NW-G-3.#
NW-T-3.#

Key
BP: Basic Principles
O: Objectives
G: Guides
T: Technical Reports
Nos. 1-6: Topic designations
#: Guide or Report number (1, 2, 3, 4, etc.)

Examples
NG-G-3.1: Nuclear General (**NG**), Guide, Nuclear Infrastructure and Planning (topic **3**), **#1**
NP-T-5.4: Nuclear Power (**NP**), Report (**T**), Research Reactors (topic **5**), **#4**
NF-T-3.6: Nuclear Fuel (**NF**), Report (**T**), Spent Fuel Management and Reprocessing, **#6**
NW-G-1.1: Radioactive Waste Management and Decommissioning (**NW**), Guide,
Radioactive Waste (topic **1**), **#1**

IAEA
International Atomic Energy Agency

Where to order IAEA publications

In the following countries IAEA publications may be purchased from the sources listed below,
or from major local booksellers. Payment may be made in local currency or with UNESCO coupons.

AUSTRALIA
DA Information Services, 648 Whitehorse Road, MITCHAM 3132
Telephone: +61 3 9210 7777 • Fax: +61 3 9210 7788
Email: service@dadirect.com.au • Web site: http://www.dadirect.com.au

BELGIUM
Jean de Lannoy, avenue du Roi 202, B-1190 Brussels
Telephone: +32 2 538 43 08 • Fax: +32 2 538 08 41
Email: jean.de.lannoy@infoboard.be • Web site: http://www.jean-de-lannoy.be

CANADA
Bernan Associates, 4501 Forbes Blvd, Suite 200, Lanham, MD 20706-4346, USA
Telephone: 1-800-865-3457 • Fax: 1-800-865-3450
Email: customercare@bernan.com • Web site: http://www.bernan.com

Renouf Publishing Company Ltd., 1-5369 Canotek Rd., Ottawa, Ontario, K1J 9J3
Telephone: +613 745 2665 • Fax: +613 745 7660
Email: order.dept@renoufbooks.com • Web site: http://www.renoufbooks.com

CHINA
IAEA Publications in Chinese: China Nuclear Energy Industry Corporation, Translation Section, P.O. Box 2103, Beijing

CZECH REPUBLIC
Suweco CZ, S.R.O., Klecakova 347, 180 21 Praha 9
Telephone: +420 26603 5364 • Fax: +420 28482 1646
Email: nakup@suweco.cz • Web site: http://www.suweco.cz

FINLAND
Akateeminen Kirjakauppa, PO BOX 128 (Keskuskatu 1), FIN-00101 Helsinki
Telephone: +358 9 121 41 • Fax: +358 9 121 4450
Email: akatilaus@akateeminen.com • Web site: http://www.akateeminen.com

FRANCE
Form-Edit, 5, rue Janssen, P.O. Box 25, F-75921 Paris Cedex 19
Telephone: +33 1 42 01 49 49 • Fax: +33 1 42 01 90 90
Email: formedit@formedit.fr • Web site: http://www. formedit.fr

Lavoisier SAS, 145 rue de Provigny, 94236 Cachan Cedex
Telephone: + 33 1 47 40 67 02 • Fax +33 1 47 40 67 02
Email: romuald.verrier@lavoisier.fr • Web site: http://www.lavoisier.fr

GERMANY
UNO-Verlag, Vertriebs- und Verlags GmbH, Am Hofgarten 10, D-53113 Bonn
Telephone: + 49 228 94 90 20 • Fax: +49 228 94 90 20 or +49 228 94 90 222
Email: bestellung@uno-verlag.de • Web site: http://www.uno-verlag.de

HUNGARY
Librotrade Ltd., Book Import, P.O. Box 126, H-1656 Budapest
Telephone: +36 1 257 7777 • Fax: +36 1 257 7472 • Email: books@librotrade.hu

INDIA
Allied Publishers Group, 1st Floor, Dubash House, 15, J. N. Heredia Marg, Ballard Estate, Mumbai 400 001,
Telephone: +91 22 22617926/27 • Fax: +91 22 22617928
Email: alliedpl@vsnl.com • Web site: http://www.alliedpublishers.com

Bookwell, 2/72, Nirankari Colony, Delhi 110009
Telephone: +91 11 23268786, +91 11 23257264 • Fax: +91 11 23281315
Email: bookwell@vsnl.net

ITALY
Libreria Scientifica Dott. Lucio di Biasio "AEIOU", Via Coronelli 6, I-20146 Milan
Telephone: +39 02 48 95 45 52 or 48 95 45 62 • Fax: +39 02 48 95 45 48
Email: info@libreriaaeiou.eu • Website: www.libreriaaeiou.eu

JAPAN
Maruzen Company, Ltd., 13-6 Nihonbashi, 3 chome, Chuo-ku, Tokyo 103-0027
Telephone: +81 3 3275 8582 • Fax: +81 3 3275 9072
Email: journal@maruzen.co.jp • Web site: http://www.maruzen.co.jp

REPUBLIC OF KOREA
KINS Inc., Information Business Dept. Samho Bldg. 2nd Floor, 275-1 Yang Jae-dong SeoCho-G, Seoul 137-130
Telephone: +02 589 1740 • Fax: +02 589 1746 • Web site: http://www.kins.re.kr

NETHERLANDS
De Lindeboom Internationale Publicaties B.V., M.A. de Ruyterstraat 20A, NL-7482 BZ Haaksbergen
Telephone: +31 (0) 53 5740004 • Fax: +31 (0) 53 5729296
Email: books@delindeboom.com • Web site: http://www.delindeboom.com

Martinus Nijhoff International, Koraalrood 50, P.O. Box 1853, 2700 CZ Zoetermeer
Telephone: +31 793 684 400 • Fax: +31 793 615 698
Email: info@nijhoff.nl • Web site: http://www.nijhoff.nl

Swets and Zeitlinger b.v., P.O. Box 830, 2160 SZ Lisse
Telephone: +31 252 435 111 • Fax: +31 252 415 888
Email: infoho@swets.nl • Web site: http://www.swets.nl

NEW ZEALAND
DA Information Services, 648 Whitehorse Road, MITCHAM 3132, Australia
Telephone: +61 3 9210 7777 • Fax: +61 3 9210 7788
Email: service@dadirect.com.au • Web site: http://www.dadirect.com.au

SLOVENIA
Cankarjeva Zalozba d.d., Kopitarjeva 2, SI-1512 Ljubljana
Telephone: +386 1 432 31 44 • Fax: +386 1 230 14 35
Email: import.books@cankarjeva-z.si • Web site: http://www.cankarjeva-z.si/uvoz

SPAIN
Díaz de Santos, S.A., c/ Juan Bravo, 3A, E-28006 Madrid
Telephone: +34 91 781 94 80 • Fax: +34 91 575 55 63
Email: compras@diazdesantos.es, carmela@diazdesantos.es, barcelona@diazdesantos.es, julio@diazdesantos.es
Web site: http://www.diazdesantos.es

UNITED KINGDOM
The Stationery Office Ltd, International Sales Agency, PO Box 29, Norwich, NR3 1 GN
Telephone (orders): +44 870 600 5552 • (enquiries): +44 207 873 8372 • Fax: +44 207 873 8203
Email (orders): book.orders@tso.co.uk • (enquiries): book.enquiries@tso.co.uk • Web site: http://www.tso.co.uk

On-line orders
DELTA Int. Book Wholesalers Ltd., 39 Alexandra Road, Addlestone, Surrey, KT15 2PQ
Email: info@profbooks.com • Web site: http://www.profbooks.com

Books on the Environment
Earthprint Ltd., P.O. Box 119, Stevenage SG1 4TP
Telephone: +44 1438748111 • Fax: +44 1438748844
Email: orders@earthprint.com • Web site: http://www.earthprint.com

UNITED NATIONS
Dept. I004, Room DC2-0853, First Avenue at 46th Street, New York, N.Y. 10017, USA
(UN) Telephone: +800 253-9646 or +212 963-8302 • Fax: +212 963-3489
Email: publications@un.org • Web site: http://www.un.org

UNITED STATES OF AMERICA
Bernan Associates, 4501 Forbes Blvd., Suite 200, Lanham, MD 20706-4346
Telephone: 1-800-865-3457 • Fax: 1-800-865-3450
Email: customercare@bernan.com · Web site: http://www.bernan.com

Renouf Publishing Company Ltd., 812 Proctor Ave., Ogdensburg, NY, 13669
Telephone: +888 551 7470 (toll-free) • Fax: +888 568 8546 (toll-free)
Email: order.dept@renoufbooks.com • Web site: http://www.renoufbooks.com

Orders and requests for information may also be addressed directly to:

Marketing and Sales Unit, International Atomic Energy Agency
Vienna International Centre, PO Box 100, 1400 Vienna, Austria
Telephone: +43 1 2600 22529 (or 22530) • Fax: +43 1 2600 29302
Email: sales.publications@iaea.org • Web site: http://www.iaea.org/books